

**IMPLICATIONS OF THE DIAGENETIC HISTORY ON POLYMER FLOODING
PERFORMANCE FOR THE BEN NEVIS FORMATION, HEBRON FIELD, JEANNE D'ARC
BASIN, OFFSHORE NEWFOUNDLAND, CANADA**

by © Luis E. Valencia, B.Eng.

A Thesis submitted to the School of Graduate Studies
in partial fulfillment of the
requirements for the degree of

Master of Science in Earth Sciences (Geology)
Department of Earth Sciences
Memorial University of Newfoundland

May 2017

St. John's Newfoundland and Labrador

ABSTRACT

The Hebron Project is the fourth major offshore development in Newfoundland and Labrador with more than 700 MBO recoverable. This research focuses on the Ben Nevis Formation (Pool 1) polymer flooding experimental evaluation based on its diagenetic history, reservoir characterization, and the recovery mechanism interactions. The reservoir properties were studied before and after the application of polymer flooding at laboratory scale using optical petrographic and SEM-MLA analyses, showing an increase of calcite cement and fines to Pool 1 top, diminishing the reservoir properties and establishing them as potentially the most critical diagenetic features to influence the EOR performance. Three polymers were tested at Pool 1 reservoir conditions, and core flooding experiments showed an additional oil recovery increase (3-6 %) after water flooding with FLOOPAM-5115. Polymer flooding, as the secondary method, consistently showed a higher increase in oil recovery than standard water flooding stage; thus applying polymer flooding in an early stage of the field development would be beneficial.

Keywords: Polymer flooding, Hebron Field, Ben Nevis Formation.

ACKNOWLEDGEMENTS

First and foremost, my thanks go to the Sacred Heart of Jesus for the guidance and blessings in my life.

I want to express my appreciation to Dr. Lesley A. James and Dr. Karem Azmy, for their continued support and advice throughout the entire M.Sc. program.

Also, I am grateful for the financial support provided to this project by Hibernia Management and Development Company (HMDC), Chevron Canada, the Natural Sciences and Engineering Research Council of Canada (NSERC), the Canada Foundation for Innovation (CFI), Research and Development Corporation (RDC), Petroleum Exploration Enhancement Program (PEEP), through Dr. James and Dr. Azmy grants. Special thank goes to RDC for the Ocean Industries Student Research Award (OISRA), its financial support allowed me to participate in different technical conferences to promote Newfoundland research.

Big thanks go to all my friends of Hibernia Enhanced Oil Recovery lab, especially to Mahsa Moayedi and Edison Sripal for their support during my experimental setup, and my great friend Norah Hyndman for the manuscript reviews.

Finally, from the bottom of my heart thanks to my family (mom, dad, brothers, aunts) and Sepideh for their love and support during this step of my journey.

TABLE OF CONTENTS

CHAPTER 1. INTRODUCTION AND OVERVIEW	1
1.1. Background.....	1
1.2. Objectives and methods	3
1. 3. Geological Overview	3
1.3.1. Hebron Field Structural Geology.....	3
1.3.2. Hebron Field Stratigraphy.....	4
1.3.3. Ben Nevis Sandstone Diagenesis.....	5
1.4. Enhanced Oil Recovery (EOR) Overview	6
1.4.1. Principles.....	6
1.4.2. Polymer Flooding.....	7
1.5. Thesis Organization	8
1.6. Co-authorship statement	11
CHAPTER 2. LABORATORY SCALE CHARACTERIZATION METHODOLOGY FOR OFFSHORE POLYMER FLOODING PROJECT: HEBRON FIELD, EASTERN CANADA	13
2.1. Abstract.....	13
2.2. Introduction.....	14
2.3. Methodology.....	16
2.3.1. EOR techniques screening in Ben Nevis Formation reservoir (Pool 1).....	16
2.3.2. Analog fields comparison	18

2.3.3. Polymers screening experiments: materials and experimental methodology	20
2.4. Results and discussion	24
2.4.1. Polymer solution concentrations definition	24
2.4.2. Polymer solutions viscosity as a function of salinity	28
2.4.3. Temperature control on polymer viscosity	29
2.4.4. Polymer solutions stability through time	30
2.4.5. Polymer Viscoelastic Properties Evaluation	33
2.4.6. Core flooding experiments using standard cores	40
2.5. Conclusions.....	46
2.6. Acknowledgements.....	47
2.7. References.....	47
CHAPTER 3. IMPLICATIONS OF THE DIAGENETIC HISTORY ON POLYMER FLOODING	
PERFORMANCE FOR THE BEN NEVIS FORMATION, HEBRON FIELD, OFFSHORE	
NEWFOUNDLAND, CANADA	
3.1. Abstract.....	53
3.2. Introduction.....	54
3.3. Geological Settings	55
3.4. Methodology	58
3.4.1. Reservoir Characterization.....	58
3.4.2. Core Flooding Experiments	59
3.5. Results.....	65
3.5.1. Reservoir characterization.....	65

3.5.2. Polymer Flooding Experiments	69
3.6. Conclusions.....	77
3.7. Acknowledgements.....	78
4.8. References.....	78
CHAPTER 4. IMAGE ANALYSIS OF PORE NETWORK EVOLUTION OF BEN NEVIS FORMATION SANDSTONES UNDER EXPERIMENTAL POLYMER FLOODING	82
4.1. Abstract.....	82
4.2 Introduction.....	83
4.3 Geological Settings	85
4.3.1. Regional Tectonic History	85
4.3.2. Hebron Field Structural Geology	87
4.3.3. Hebron Field Stratigraphy.....	88
4.4. Materials and Methods.....	88
4.4.1. Core Plug Samples	88
4.4.2. Rock Mineralogy and Textures.....	90
4.4.3. Digital Image Analysis (DIA).....	90
4.4.4. Polymer Flooding Experiments	93
4.5. Results and Discussion	94
4.5.1. Standard Mineralogical Study.....	94
4.5.2. Porosity Network Changes.....	98
4.5.3. Pores Shape Characterization.....	101
4.6. Conclusions.....	105

4.7. Acknowledgements.....	106
4.8. References.....	106
CHAPTER 5. SUMMARY.....	109
5.1. Conclusions.....	109
5.2. Directions for future research	110
REFERENCES	111
APPENDICES	120
APPENDIX A: Error Analysis	120
A.1. Reading Errors	120
A.2. Mean Value and Standard Deviation:	120
A.3. Propagation of Errors:	121
APPENDIX B: Rheology Experiments Raw Data.....	122
B.1. Evaluation of viscosity variation of FP-3430S polymer solution at different concentrations, shear rates, and reservoir temperature 62°C.	122
B.2. Polymer solutions viscosity in seawater (injection water) at different polymer concentrations, at 10 s ⁻¹ shear rate and reservoir temperature 62°C	148
B.3. Polymer solutions viscosity in synthetic formation water at different polymer concentrations, at 10 s ⁻¹ shear rate and reservoir temperature 62°C	149
B.4. Salinity effect in the polymers solution viscosity in different brines at 2000 mg/L, 10 s ⁻¹ shear rate, and reservoir temperature 62°C	150
B.5. Polymer performance vs. temperature for defined concentrations at 10 s ⁻¹	159
B.6. Thermal stability at 62°C and 10 s ⁻¹ shear rate of polymers in SW and FW brines	159

B.7. Polymers viscoelasticity evaluation	160
APPENDIX C: Reservoir Characterization	171
C.1. Detailed mineralogical composition using MLA	171
C.2. General thin sections	173
C.3. Core plugs selections from Hebron exploration cores (core slabs)	174
APPENDIX D: Digital Image Analysis (DIA)	175
APPENDIX E: Synthetic Oil Viscosity Measurement	178
E.1. Oil mix calculation following Shu’s correlation	178
APPENDIX F: Porosity and Absolute Permeability Measurement.....	183
F.1. Porosity Measurement and Pore Volume Calculation	183
F.2. Absolute Permeability Calculation	184
APPENDIX G: Core flooding experiments raw data	185
G.1 Standard Cores	185
G.2. Hebron Well Cores.....	197
APPENDIX H: Core flooding Material Balance Calculation.....	217
H.1.1. Primary waterflooding (formation water)	218
H.1.2. Oil flooding until no more water production	218
H.1.3. Secondary waterflooding (2 PV of injection water (seawater))	219
H.1.4. Polymer flooding (2 PV).....	220
H.1.5. Tertiary waterflooding (1 PV).....	220
APPENDIX H: Experimental set-up images	221

LIST OF TABLES

Table 2.1. Ben Nevis Formation (Pool 1) reservoir properties.....	17
Table 2.2. Ben Nevis Formation (Pool 1) EOR techniques screening.....	17
Table 2.3. Brine compositions.....	21
Table 2.4. Standard cores properties.....	22
Table 2.5. Viscosity reduction as a function of temperature.....	29
Table 2.6. Relaxation times (λ) for polymers at different conditions.....	35
Table 2.7. Errors in core flooding experiments.....	41
Table 2.8. Core flooding experiments results.....	44
Table 2.9. Average pressures during core flooding experiments.....	45
Table 3.1. Brines composition.....	60
Table 3.2. Pool 1 composite cores properties.....	62
Table 3.3. Polymer flooding experiment variables.....	65
Table 3.4. Core flooding experiments results.....	71
Table 4.1. Mineralogical composition difference in polymer flooding experiments.....	97
Table 4.2. Total porosity values comparison after applying polymer flooding in Pool 1 composite cores.....	99
Table 4.3. Total porosity percentile distribution obtained from S-curves.....	101

Table 4.4. Pore geometric equivalent forms.....	101
-------------------------------------------------	-----

LIST OF FIGURES

Figure 1.1. Hebron Field structural section.....	4
Figure 1.2 EOR methods.....	6
Figure 1.3 Staged process for polymer flood project evaluation.....	8
Figure 2.1 Average reservoir properties comparison in offshore polymer flooding projects.....	19
Figure 2.2. Water salinity comparison across offshore polymer flooding projects.....	19
Figure 2.3. Core flooding apparatus scheme.....	23
Figure 2.4. Viscosity of FP-3430S polymer at 62°C in different brines.....	26
Figure 2.5. Concentrations of polymer required to obtain a 10 s ⁻¹ shear rate at 62°C.....	27
Figure 2.6. Salinity effect in the polymers solution viscosity in different brines at 2000 mg/L.....	28
Figure 2.7. Polymer performance vs. temperature for defined concentrations at 10 s ⁻¹	30
Figure 2.8. Polymer solutions thermal stability at 62°C and 10 s ⁻¹ shear rate.....	32
Figure 2.9. Comparison of viscoelastic moduli, elastic storage modulus (G') and viscous loss modulus (G'') as of function of angular frequency for FP-3430S.....	36
Figure 2.10. Comparison of viscoelastic moduli, elastic storage modulus (G') and viscous loss modulus (G'') as of function of angular frequency for FP-5115.....	36
Figure 2.11. Cox-Merz rule comparison at different brines salinity for FP-3430S.....	38
Figure 2.12. Cox-Merz rule comparison at different brines salinity for FP-5115.....	38

Figure 2.13. Extensional viscosity comparison at different brines salinity and temperature for FP-3430S.....	39
Figure 2.14. Extensional viscosity comparison at different brines salinity and temperature for FP-5115.....	40
Figure 2.15. Effect of core and polymer type on total oil recovery factor.....	42
Figure 2.16. Pressure profile during flooding sequence.....	46
Figure 3.1. Hebron Field location at Jeanne D’Arc.....	56
Figure 3.2. Hebron Field structural section.....	58
Figure 3.3. Composite cores sample locations.....	62
Figure 3.4. Core flooding apparatus scheme.....	64
Figure 3.5. Mineralogical profile at Pool 1 reservoir.....	66
Figure 3.6. Siderite cement.....	66
Figure 3.7. Lithic fragments (red arrow) with matrix (green arrow) of fine grains.....	67
Figure 3.8. Sandstone classification.....	67
Figure 3.9. Proposed diagenetic model at Ben Nevis Formation (Pool 1).....	69
Figure 3.10. Total oil recovery in high permeability cores.....	72
Figure 3.11. Total oil recovery in low permeability cores.....	73
Figure 3.12. Proposed fluid-rock mechanism interaction model.....	74

Figure 3.13. Influence of experimental variables on Total oil recovery difference between pair of experiments.....	76
Figure 3.14. Pressure profile during flooding sequence.....	77
Figure 4.1. Hebron Field location at Jeanne D’Arc Basin.....	86
Figure 4.2. Hebron Field structural section.....	87
Figure 4.3. Composite core sample locations.....	89
Figure 4.4. Composite core after polymer flooding.....	89
Figure 4.5. Image selection pattern.....	91
Figure 4.6. Object extraction by gray intensity threshold.....	93
Figure 4.7. Mineral and textural changes observed in the high permeability Pool 1 sandstones.....	95
Figure 4.8. Mineral and textural changes observed in the low permeability Pool 1 sandstones.....	96
Figure 4.9. Porosity probability S-curves.....	100
Figure 4.10. Pore shape proportions before and after polymer flooding injection in low permeability sandstones.....	103
Figure 4.11. Pore shape proportions before and after polymer flooding injection in high permeability sandstones.....	103
Figure 4.12. Pore shapes proportions dispersion before and after polymer flooding injection in Pool 1 cores samples.....	104
Figure 4.13. SEM-MLA images comparison used to define pore shape and mineral relationship.....	105

LIST OF ABBREVIATIONS

API	American Petroleum Institute gravity
ATBS	Acrylamide tert-butylsulfonic acid
BEN	Bentheimer cores
BSE	Backscattered electron
C₆H₇NaO₆	Sodium isoascorbate
C-NLOPB	Canada-Newfoundland and Labrador offshore petroleum board
CO₂	Carbon dioxide
DIA	Digital image analysis
DW	Deionized water
EDTA	Ethylenediaminetetraacetic acid
EDX	Energy dispersive X-ray
EOR	Enhanced oil recovery
FW	Synthetic formation water
H₂S	Hydrogen sulfide
HC WAG	Hydrocarbon water alternative gas
HPAM	Partially hydrolyzed polyacrylamides
MLA	Mineral liberation analyzer
N₂	Nitrogen
NaHCO₃	Sodium bicarbonate
O₂	Oxygen
QC	Quality control
SCAL	Special core analysis
SEM	Scanning electron microscopy
SW	Seawater
UGB	Upper Gray Berea

LIST OF VARIABLES, PARAMETERS AND UNITS

A	Area (cm ²)
cm	Centimeter
cP	Centipoise
dP	Differential pressure (psi)
ft/day	Foot per day
G'	Elastic storage modulus
G''	Viscous loss modulus
K	Permeability (mD)
L	Length (cm)
M	Mobility ratio
MBO	Million barrels oil
mm	Millimeter
mD	Millidarcy
mPa.S	Milli pascal second
m/s	Meter per second
N₁	First normal stress difference
K_o	Oil permeability
K_w	Water permeability
OD	Outside diameter (in)
OOIP	Original oil in place (cm ³)
psi	Pound per square inch
PV	Pore volume (cm ³)
Q	Flow rate (cm ³ /s)
R	Principal radius
ROIP	Residual oil in place (cm ³)
SAOS	Small Amplitude Oscillatory Shear
S_{wc}	Connate water saturation (%)

S_{or}	Residual oil saturation (%)
TDS	Total dissolved solids (ppm)
ω	Angular frequency
λ	Relaxation time ($1/\omega$)
λ_w	Water mobility (mD)
λ_o	Oil mobility (mD)
μ_w	Water viscosity (cP)
μ_o	Oil viscosity the mobility ratio (cP)

CHAPTER 1. INTRODUCTION AND OVERVIEW

1.1. Background

The ongoing increasing demand for oil generates a critical challenge for the oil industry to procure new oil resources. Adding new oil reserves can be achieved by finding new discoveries or by optimizing oil production from current resources. The cost associated with the first option is significant since new resources are expected to occur in challenging environments. Therefore, upgrading the current reserves by applying enhanced oil recovery (EOR) techniques is a more likely strategy to meet the demand (Manrique et al. 2010; Saaborian-Jooybari et al. 2016).

Reservoir characterization for EOR requires an understanding of the origin, timing, trend, and magnitude of geologic events that affected the reservoir anatomy (internal structure and composition of the rock). Specially, small-scale heterogeneities, not always critical to primary and secondary recovery, may affect sweep and displacement efficiencies in EOR operations significantly. Dickey (1979) stated that the most common cause of EOR projects failure was heterogeneity of the reservoir.

This research project is focused on the Ben Nevis Formation, which is considered the main reservoir of Hebron Field, offshore Newfoundland, Canada. The Ben Nevis Formation reservoir consists of fine-grained sandstone deposited in a marine shoreface depositional environment, and it is anticipated to produce approximately 70 percent of the Hebron Project's crude oil (ExxonMobil, 2011).

Normore (2006) evaluated the origin, distribution and paragenetic sequence of carbonate cements in the Ben Nevis Formation at White Rose Field located in Jeanne d'Arc Basin, 46 Km Northwest to Hebron Field. Some highlighted findings in his research are that calcite cemented concretions are the dominant authigenic cement found in the Ben Nevis Formation at the White Rose Field. Normore (2006) considered that the higher density of concretionary cemented intervals is located at the base of the formation but cementation intensity increases upsection, thus leading to potential reservoir permeability stratification.

This characteristic would adversely affect the performance of EOR methods as chemical flood according to Szpakiewicz et al. (1987).

The purpose of this research is to experimentally examine potential EOR methods in the Ben Nevis Formation based on its diagenetic history, reservoir characterisation, and the recovery mechanism interactions. The EOR method screening performed in this research, considering the oil and reservoir properties in Pool 1, and limited gas supply in the Hebron Field, led us to consider polymer flooding as a possible EOR method to be evaluated for Pool 1, Hebron Field; this will be discussed in more detail in further chapters. Polymer flooding is a well-known technology for onshore oil fields where polymer is mixed in the injected water to increase the water viscosity. This reduces fingering of the injected water through viscous oil and reduces the adverse effects of heterogeneities in the reservoir, thereby improving the sweep, reducing water production and increasing the recovery of oil (Selle et al., 2013).

A potential disadvantage to the application of polymer flooding in Pool 1 could be that the average permeability ranges from 300 to 500 mD in some areas, which is considered relatively low compared with reservoirs where this technique has been successfully applied.

On the other hand, formation water salinity in the Pool 1 (> 60,000 ppm) is higher than the offshore field analogues used for the EOR screening. Previous studies consider that polymers solutions at high salt concentrations experience repulsion between the polymer backbone charges and the local double layer formed by the small electrolyte species, and consequently the viscosity is lower. The effect of divalent ions is even more significant than that of monovalent species (Sorbie, 1991; Sheng, et al. 2015). Therefore, a suitable polymer is required to minimize the salinity effect on polymer solution viscosity. High temperature and shear rate could also generate polymer degradation.

Providing a foundation to understand the fluid-rock interactions during the application of polymer flooding in the Ben Nevis Formation will lead to improve the subsurface assessment of the Hebron Field, and potentially reduce uncertainties in designing and implementing EOR in the future.

1.2. Objectives and methods

In order to have a better knowledge of the Pool 1 reservoir heterogeneities and the polymer solutions interactions, different objectives are defined through this research:

- Perform an EOR screening evaluation at Ben Nevis Formation (Pool 1), Hebron Field considering its reservoir and fluids properties; through the use of published screening methodologies and offshore analogs fields.
- Establish the potential diagenetic features of Pool 1 that could impact the EOR techniques performance, taking into consideration rock type description before and after polymer flooding through optical microscopy, scanning electron microscopy (SEM) and mineral liberation analyzer (MLA).
- Define polymer solution concentrations to achieve a favorable mobility ratio at Pool 1 reservoir conditions, considering their viscosity variations as a function of salinity, temperature, stability and viscoelastic properties; through rheological experiments.
- Perform digital image analysis (DIA) studies to identify rock textural changes before and after polymer flooding application; through J MicroVision 1.2.7 software using SEM images in selected Hebron cores.
- Validate incremental oil recovery via core flooding studies; using standard (Berea and Bentheimer cores) and Hebron Field cores.

1.3. Geological Overview

1.3.1. Hebron Field Structural Geology

The Hebron Field lies on a horst block with a graben to the southwest and to the northeast (Figure 1.1). The horst block is part of the north-south trending and north-plunging Terra Nova anticline and the fault-bound basin-dividing northwest-southeast “trans-basin” trend. The trapping configuration for the Ben Nevis and

Hibernia Reservoirs on the horst block is fault dependent three ways. The Jeanne d’Arc Reservoir has a combination of structural and stratigraphic trap configuration (Shannon et al., 1995).

The fault setting is comprised of NW-SE striking faults in the field-range from less than 0.5 km to 4.5 km in length dipping predominantly to the northeast between 55 and 60 degrees. The exception to this is the Hebron Fault, which dips between 55 and 60 degrees to the southwest and created the Hebron horst fault block. The pools are in structural traps defined by the major faults creating the fault blocks. The oil-water contacts are determined by spill-points between the fault blocks (ExxonMobil, 2011).

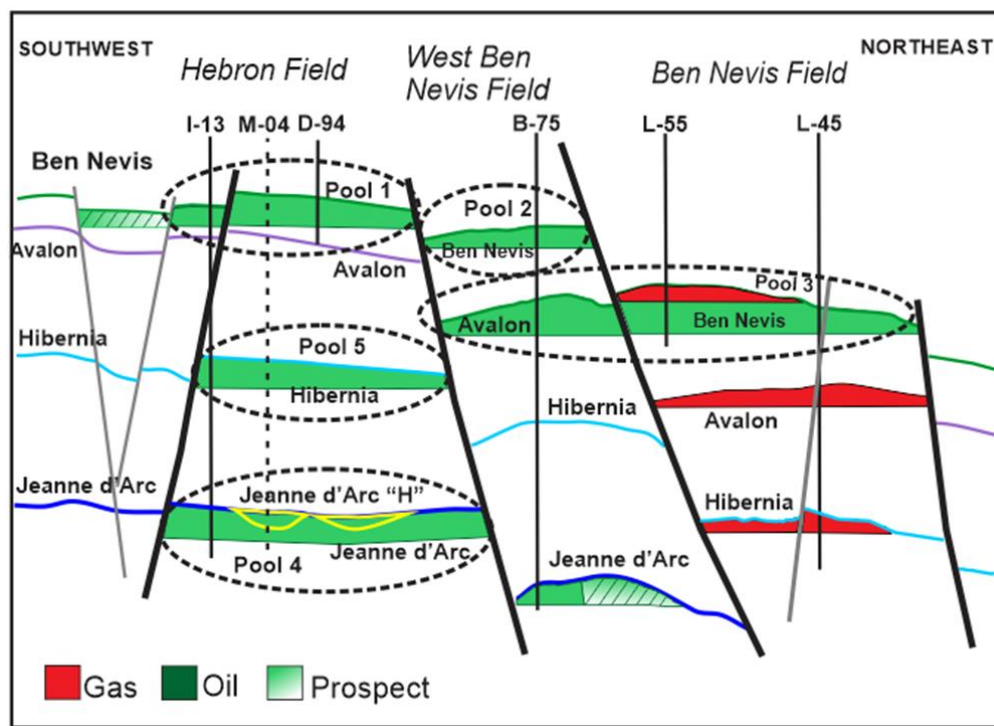


Figure 1.1. Hebron Field structural section (modified after ExxonMobil, 2011).

1.3.2. Hebron Field Stratigraphy

The three main reservoirs for the Hebron field are the Ben Nevis, Hibernia, and Jeanne d’Arc Formations. The Ben Nevis Formation (Upper Aptian to Albian), unconformably overlies the Avalon Formation. It consists of 125 to 500 m thick succession of upward fining of fine to very fine grained calcareous sandstone

with interbedded thin layers of sandy limestone grading upward into glauconitic siltstone and shale (Shannon et al., 1995).

The depositional environment is primarily lower to upper shoreface, with subtle facies changes, highly correlative, and a very high net-to-gross ratio. On a more detailed scale, the depositional environment and stratigraphy are more complicated. The cores show many cycles of wave-dominated marine depositional events that encompass a range of facies (upper shoreface to offshore marine). Individual cycles are thin (tens of centimetres), and are interpreted to be laterally extensive (one to tens of kilometres). The dominant environment of deposition on the horst block of the Hebron Field is proximal lower shoreface. The reservoir package has occasional coquinas, made of shallow marine shell debris, and rare shales (ExxonMobil, 2011).

1.3.3. Ben Nevis Sandstone Diagenesis

Abid (1988) assessed the relative timing of calcite cementation in four reservoir sandstones of the Hibernia Field on the basis of petrography and oxygen carbon isotopes.

Normore (2006) evaluated the origin, distribution, and paragenetic sequence of carbonate cements in the Ben Nevis Formation at the White Rose Field located in the Jeanne d'Arc Basin, 46 km northwest of the Hebron Field. He found that calcite cemented concretions are the dominant authigenic cement found in the Ben Nevis Formation at the White Rose Field. While there is no compartmentalization of the Ben Nevis Formation, the increased volume of calcite cement may reduce the total volume of oil and gas initially in place as well as reducing the recoverable oil and gas.

According to the Hebron Development Plan, several scenarios for predictive models have been used to estimate the distribution of calcite cementation in the Ben Nevis Reservoir. The distribution and lateral extent of calcite cemented sandstones are not well established in the literature so predictive modeling was used. Nevertheless, it is unlikely that the cement zone is laterally continuous across the whole Hebron Field.

It is unreasonable for all the points to coalesce in one impermeable sheet because of its multi-point source genesis (ExxonMobil, 2011).

1.4. Enhanced Oil Recovery (EOR) Overview

1.4.1. Principles

Enhanced oil recovery (EOR) is the recovery of oil by injection of a fluid that is not native to the reservoir. EOR is a means to extend the productive life of an otherwise depleted and uneconomic oil field. It is usually practiced after recovery by other, less risky and more conventional methods, such as pressure depletion and water flooding, have been exhausted (Lake and Walsh, 2008). In general, EOR methods increase the oil recovery by reducing the mobility ratio and/or increasing the capillary number. EOR methods should be tailored to the specific reservoir characteristics, as can be seen in Figure 1.2, there are different methods divided at high level in thermal (heat source involved), gas injection (consider the injection of a gas that is not native in the reservoir), and chemical & others, that involve mainly chemical additives to alter rock wettability, mobility ratio, etc.

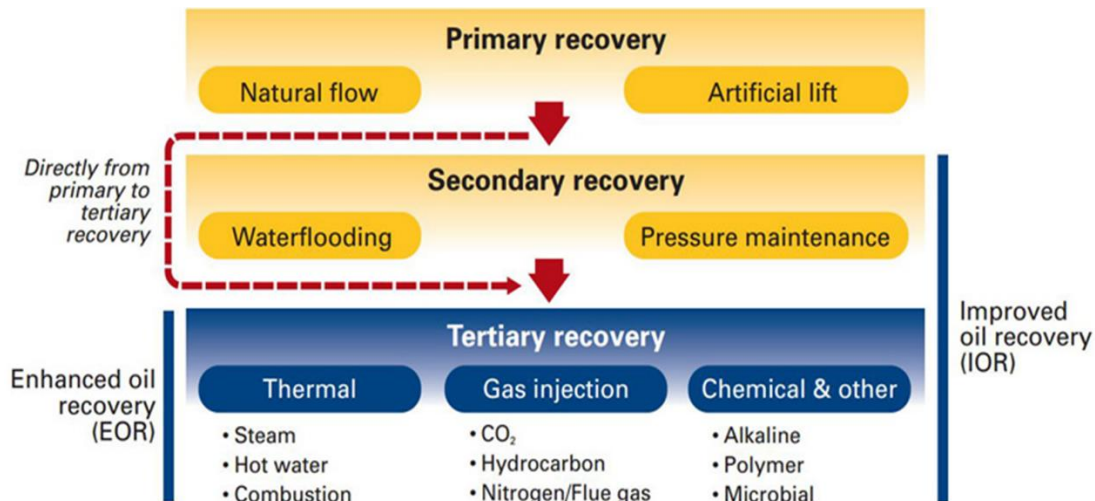


Figure 1.2. EOR methods (source www.slb.com)

1.4.2. Polymer Flooding

Adding polymer to the injection water basically increases the injection water viscosity, reduces the water-oil mobility ratio, then improves the vertical and aerial sweep efficiency (Wang et al. 2013). As shown in equation 1, where λ_w is the water mobility, λ_o is the oil mobility, K_w is the effective water permeability, K_o is the effective oil permeability, μ_w is the water viscosity and μ_o is the oil viscosity, the mobility ratio (M) is inversely proportional to the water viscosity. Increasing the water viscosity, reduces the mobility ratio, thereby increasing the sweep efficiency, and, as a consequence, oil recovery is enhanced.

$$M = \frac{\lambda_w}{\lambda_o} = \frac{K_w/\mu_w}{K_o/\mu_o} = \frac{K_w\mu_o}{K_o\mu_w} \quad (1)$$

Many factors are important during polymer flooding. During the design of a polymer flood, critical reservoir factors that traditionally receive consideration are the reservoir lithology, stratigraphy, important heterogeneities (such as fractures), oil viscosity, distribution of remaining oil, well pattern, and well distance. Critical polymer properties include cost effectiveness (e.g., cost per unit of viscosity, resistance to degradation (mechanical/shear, oxidative, thermal, microbial), tolerance of reservoir salinity and hardness, retention by rock, inaccessible pore volume, permeability dependence of performance, rheology, and compatibility with other chemicals that might be used. Issues long recognized as important for polymer-bank design include bank size (volume), polymer concentration and salinity (affecting bank viscosity and mobility), and whether (and how) to grade polymer concentrations in the chase water (Seright, 2010).

Kaminsky et al. (2007), proposed a staged process (Figure 1.3) that reflects experiences from ExxonMobil's own studies and applications of polymer floods as well as the published experiences of others; suggesting eleven areas to be evaluated: analogs, reservoir modeling, polymer selection, solution rheology, polymer retention, polymer stability, injectant preparation, injectivity, facilities, quality assurance and economics; focusing the staged process on reservoir engineering.

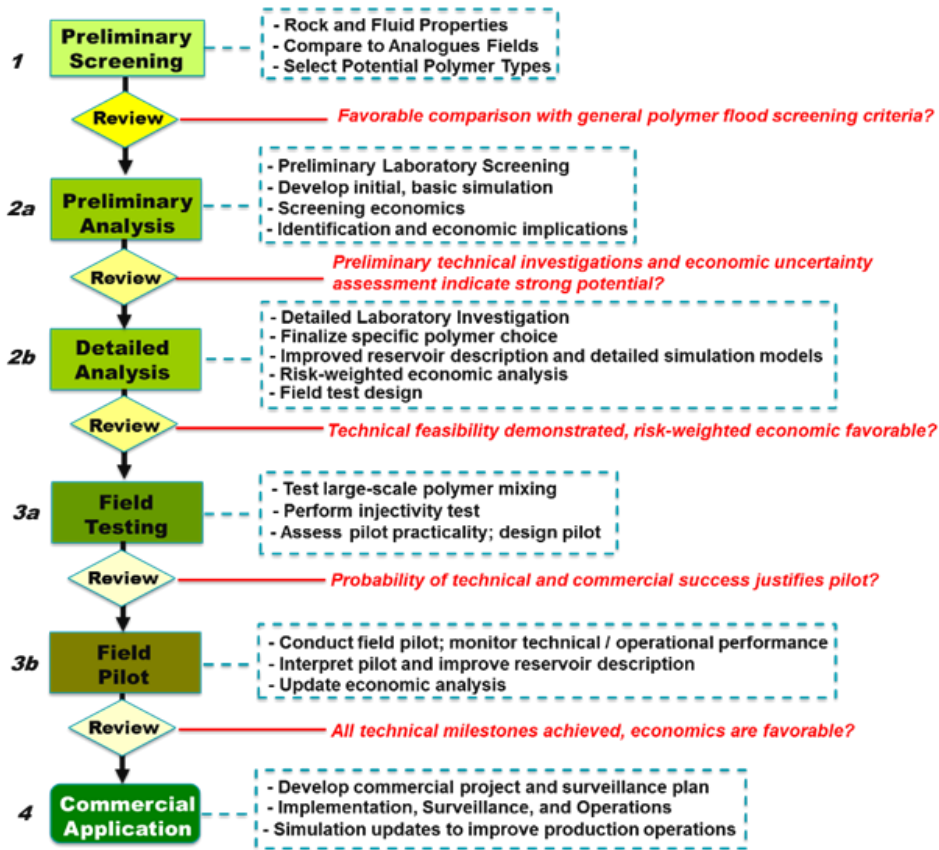


Figure 1.3 Staged process for polymer flood project evaluation (modified after Kaminsky et al. 2007).

1.5. Thesis Organization

This thesis is presented in manuscript format. Chapter 1 serves as an introduction to the project and an overview of the regional geology, as well as an introduction of polymer flooding as EOR technique. Chapters 2, 3 and 4 are manuscripts for peer-reviewed articles that will be submitted as papers as follows:

- **Chapter 2:** *Laboratory Scale Characterization Methodology for Offshore Polymer Flooding Project: Hebron Field, Eastern Canada*, this paper will be submitted to *Journal of Petroleum Science and Engineering*.

Abstract: The Ben Nevis Formation (Pool 1) at the Hebron Field consists of fine-grained sandstone of a marine shoreface environment. It is anticipated to produce approximately 70% of the Hebron Project's recoverable crude oil, the fourth major offshore development in Newfoundland and Labrador. Hebron crude oil is heavy with an API gravity of 17 – 24° API and the preliminary enhanced oil recovery (EOR) screening, considering the oil and reservoir properties, coupled with the difficulty in sourcing potential injection gas, led to the investigation of polymer flooding. Once the potential EOR technology has been selected, reservoir properties were evaluated in the laboratory. The applied characterization methodology included the validation of reservoir properties for EOR methods screening and comprehensive polymer solution evaluation conducted at reservoir conditions, considering rheological behaviour and the effects of salinity and temperature. Polymer screening experiments suggest that FP-3430S and FP-5115 polymers are more stable than Guar Gum at Pool 1 reservoir conditions. Core flooding experiments using standard cores show 59.8 (± 0.3) % and 55.5 (± 0.4) % of oil recovery in high and low permeability cores, respectively. Laboratory methodology error associated to the experimental setup indicates reproducibility conditions. The EOR investment decisions are heavily impacted by the timing involved in the project planning. This study illustrates the importance of early investigation to provide better understanding of the field conditions and reduce uncertainties to accelerate the EOR project cycle time.

- **Chapter 3:** *Implications of the diagenetic history on enhanced oil recovery performance for the Ben Nevis Formation, Hebron Field, Offshore Newfoundland, Canada.* This paper will be submitted to *SPE Reservoir Evaluation and Engineering*.

Abstract: The Hebron Project is the fourth major offshore development in Newfoundland and Labrador with an estimated 2620 MBO in place and more than 700 MBO recoverable. This research focuses on the Ben Nevis Formation reservoir (Pool 1) which is anticipated to produce 70% of the Hebron Project's crude oil. In comparison with the density of crude oil from nearby offshore fields, Hebron crude oil is considered heavy with an API gravity of 17 – 24° API. The first oil is expected

in 2017, and the current best estimate for recovery factor is 30%. Applying enhanced oil recovery (EOR) methods could increase this recovery factor; however, the effectiveness of these methods will depend on the nature of the reservoir. Considering these premises, the purpose of this research is to experimentally examine potential EOR methods to apply to the Ben Nevis Fm. (Hebron Field) based on its diagenetic history and the recovery mechanism interactions. Preliminary enhanced oil recovery (EOR) screening, considering the oil and reservoir properties, coupled with difficulties in sourcing potential injection gas, led to the investigation of polymer flooding. The reservoir mineralogy and texture were studied before and after the application of experimental polymer flooding. Pre-flooding investigation showed calcite cement and fine grains (clays) increasing upward the formation (at Pool 1), with the associated diminishment of reservoir properties. This establishes the calcite and clay content as potentially the most critical diagenetic features to influence the EOR performance in Pool 1. Core flooding experiments showed an additional oil recovery increase in the range of 3-6% after water flooding, with FLOOPAM-5115 being the most effective polymer at the reservoir conditions evaluated. Polymer flooding, as a secondary method, consistently showed a higher increase in oil recovery. This final paper includes the experimental results of the proposed laboratory methodology applied to Hebron cores, as well as the oil recovery results after applying polymer flooding considering the reservoir nature.

- **Chapter 4: *Image Analysis of Pore Network Evolution of Ben Nevis Formation Sandstones under Experimental Polymer Flooding.*** This paper will be submitted to *Bulletin of Canadian Petroleum Geology*.

Abstract: Digital image analysis (DIA), along with microscopic petrographic analysis, can be applied to improve pore system characterization in sedimentary rocks. The current study focuses on the application of these techniques to study the evolution of rock pore networks in Ben Nevis Formation sandstones from the Hebron Field, offshore Newfoundland, which were subjected to experimental polymer flooding injection. DIA protocol can be summarized in the following stages: (i) detailed pre- and post-injection description of mineralogy and texture seen in thin sections using

optical and scanning electron microscopy - mineral liberation analysis (SEM-MLA) technique; (ii) adjustment and calibration of DIA tools; (iii) data acquisition protocol; and (iv) study and quantification of porosity by DIA. The DIA results highlight the petrographic changes observed in the investigated samples. Polymer flooding injection in high permeability sandstones resulted in a relative porosity increase, whereas the low permeability sandstones showed the opposite. Other minor changes, such as variations in the roughness and roundness of pore edges were observed.

Raw data and detailed calculations are included in appendixes listed as follow:

- A. Error Analysis
- B. Rheology Experiments Raw Data
- C. Reservoir Characterization
- D. Digital Image Analysis (DIA)
- E. Synthetic Oil Viscosity Measurement
- F. Porosity and Absolute Permeability Measurement
- G. Core flooding experiments raw data
- H. Core flooding Material Balance Calculation
- I. Experimental set-up images

1.6. Co-authorship statement

Luis E. Valencia, I carried out all the sample preparation for both polymer solutions as well as cores used in the core flooding experiments. This involved preparing solutions using different polymers at different concentrations with different salinities, then analysing them with a rheometer in order to understand their rheological characteristics. I assembled the core flooding set up considering the reservoir pressure and temperature conditions following Hibernia EOR lab lessons learned. Additionally, I performed the digital image analysis of the selected SEM images. Finally, all the core flooding experiments were carried out by

myself, considering the required data quality (QC). The manuscript was written by myself and then passed onto co-authors accordingly. The interpretations and conclusions presented benefited from continuous discussion with Dr. Lesley A. James and Dr. Karem Azmy at all stages of the project. Co-authors reviewed the manuscripts and helped to improve it.

Dr. Lesley A. James, Lesley provided the design and helped the implementation of the M.Sc. project. She assisted with the core sample collection and provided help during the experimental variables definition and guidance throughout the project. Lesley provided criticism and discussion during preparation of the manuscript.

Dr. Karem Azmy, Karem provided the design and helped the implementation of the M.Sc. project. He provided geological support for the rock samples thin sections analysis. He also contributed significantly to the discussion and editing the manuscript during preparation.

CHAPTER 2. LABORATORY SCALE CHARACTERIZATION METHODOLOGY FOR OFFSHORE POLYMER FLOODING PROJECT: HEBRON FIELD, EASTERN CANADA

To be submitted to *Journal of Petroleum Science and Engineering*.

Luis E. Valencia, Lesley A. James*, Karem Azmy

Memorial University of Newfoundland, St. John's, Canada

* Corresponding author e-mail: ljames@mun.ca

Keywords: Enhanced Oil Recovery, Polymer Flooding, Ben Nevis Formation, Hebron Field, Screening.

2.1. Abstract

The Ben Nevis Formation (Pool 1) at the Hebron Field consists of fine-grained sandstone of a marine shoreface environment. It is anticipated to produce approximately 70% of the Hebron Project's recoverable crude oil, the fourth major offshore development in Newfoundland and Labrador. Hebron crude oil is heavy with an API gravity of 17 – 24° API and the preliminary enhanced oil recovery (EOR) screening, considering the oil and reservoir properties, coupled with the difficulty in sourcing potential injection gas, led to the investigation of polymer flooding. Once the potential EOR technology has been selected, reservoir properties were evaluated in the laboratory. The applied characterization methodology included the validation of reservoir properties for EOR methods screening and comprehensive polymer solution evaluation conducted at reservoir conditions, considering rheological behaviour and the effects of salinity and temperature. Polymer screening experiments suggest that FP-3430S and FP-5115 polymers are more stable than Guar Gum at Pool 1 reservoir conditions. Core flooding experiments using standard cores show 59.8 (± 0.5) % and 55.5 (± 0.5) % of oil recovery in high and low permeability cores, respectively. Laboratory methodology error associated to the experimental setup indicates reproducibility conditions. The EOR investment decisions are heavily impacted by the timing involved in the project planning. This

study illustrates the importance of early investigation to provide better understanding of the field conditions and reduce uncertainties to accelerate the EOR project cycle time.

2.2. Introduction

Enhanced-oil-recovery (EOR) implementation is complex and successful application requires that the methodology be tailored to the specific reservoir. Therefore, a systematic staged evaluation and development processes are required to screen, evaluate, pilot test, and apply EOR processes for particular applications (Teletzke et al., 2010). Applying an effective EOR road map reduces reservoir uncertainties and economic risk (Al Mjeni et al., 2011). At any stage, if the project does not meet the company's technical and financial criteria for that stage, it does not proceed further. Therefore, there are two key features in the preliminary stages that determine the fate of the research project either to continue or abandon; one is repeating the early stages to find more suitable solutions, and the other is establishing the correct timing to perform any EOR road map stage based on the information gathered (Kaminsky et al., 2007).

The Hebron Field is the fourth major offshore development in Newfoundland and Labrador with first oil expected in 2017. Hebron crude oil in the Ben Nevis Formation reservoir (Pool 1) is of lower API gravity (17-24°) compared with those from other nearby offshore fields in the area (ExxonMobil, 2011).

The available information provided in the Hebron Development Plan (ExxonMobil, 2011) was reviewed and compared to EOR screening guidelines published in the literature (Taber et al., 1997a; Taber et al., 1997b, Al Adasani and Bai, 2011; Alvarado and Manrique, 2013). The result of this comparison coupled with the challenge of sourcing an injection gas, led to consider polymer flooding as a suitable alternative for Pool 1.

Polymer flooding involves the addition of polymer to the injected water to increase the viscosity of the injected fluid (water) to improve sweep efficiency, reduce oil bypassing and viscous fingering, and to

increase oil recovery (Maia et al., 2009). Kaminsky et al. (2007) considered the complexity of polymer EOR evaluation and design and proceeded to identify several important factors to determine the suitability of a polymer flood for a chosen field. The authors considered that oil viscosity, mobile oil saturation, ability for the polymer to propagate through the reservoir, compatibility of the polymer with the reservoir rock and fluids at in situ conditions, reservoir heterogeneity, as the most important factors to consider during the evaluation of polymer flooding application in a field.

The ideal properties for polymers as mobility control agents can be summarized as follows: low cost or high effectiveness, high injectivity, efficiency when mixed with reservoir brines (up to 20% total dissolved solids), resistant to mechanical degradation (up to 1000 m³/m²/d flux when entering porous rock), 5 to 10 years stability at reservoir temperature (up to 200 °C), resistant to microbial degradation, low retention (e.g., adsorption) in porous rock, effective in the presence of oil or gas, and not sensitive to O₂, H₂S, pH or oilfield chemicals (Seright et al., 2009).

In spite of the great number of polymers documented in the literature, only two types are actually used for mobility control in polymer injection processes in the oil industry: a synthetic polymer family classified as partially hydrolyzed polyacrylamides and a biological polymer known as xanthan gum (de Melo et al., 2002; Seright et al., 2009).

Xanthan gum is well known to have excellent performance in high salinity brines; however, it is highly susceptible to bacterial degradation and expensive. Polyacrylamide performance depends on its molecular weight and degree of hydrolysis. Partially hydrolyzed polyacrylamides (HPAMs), which is one of the polyacrylamide groups, has the shape of a straight chain of acrylamide monomers in which some of monomers have been hydrolyzed. HPAM is the most often utilized polymer in EOR applications due to its relatively low price and good viscosifying properties. Nevertheless, some HPAMs have no resistance to thermal degradation and their carboxyl groups are screened by positive ions, leading to reduced viscosity and limited application in wells with high temperature and salinity (Maia et al., 2009; Abidin et al., 2012).

Thus, laboratory experiments that evaluate the effect of water salinity, temperature, mechanical degradation are crucial to find the most suitable polymer for specific reservoir conditions.

The laboratory scale characterization represents a relatively inexpensive evaluation and provides a valuable approach to reservoir uncertainties at the pore and core scale. In the current study, a series of experiments were conducted to investigate the effect of several design parameters on the performance of polymer flooding under Ben Nevis Formation reservoir (Pool 1) conditions at the Hebron Field. We investigated how concentration, salinity and reservoir temperature affected the polymer viscosity, viscoelastic properties, and stability. The focus is the relevance of laboratory scale characterization to reduce uncertainties in an EOR project, using the Hebron Field, offshore Newfoundland as a case of study.

2.3. Methodology

2.3.1. EOR techniques screening in Ben Nevis Formation reservoir (Pool 1)

Ben Nevis Formation reservoir (Pool 1) properties (Table 2.1), as reported in the Hebron Development Plan (ExxonMobil, 2011) were compared with the preferential range of reservoir properties proposed in the screening guidelines of Taber et al. (1997a), Taber et al. (1997b), Al Adasani and Bai (2011), and Alvarado and Manrique (2013) for different EOR techniques based on successful EOR projects worldwide. An arbitrary scale was used in the current work to assess the different techniques and establish the most suitable for the currently investigated reservoir, where: (3) corresponds to a property in the average or best value, (1) corresponds to a property in the value range, (0) is assigned when there is no data available, and (-5) corresponds to a property outside of the value range. A higher total value was considered the best option, as shown in Table 2.2.

Table 2.1. Ben Nevis Formation (Pool 1) reservoir properties (ExxonMobil, 2011)

Reservoir	Fluid Properties		
Ben Nevis Formation (Pool 1)	Oil Gravity (API)	Oil Viscosity (mPa.s)	Formation Water Salinity (ppm)
	17 - 24	6.1 - 27	> 60,000
	Rock Properties		
	Rock Type	Porosity (%)	Permeability (mD)
	Sandstone	14 - 27	5 - >1000
	Net Reservoir Thickness (m)	Depth TVD (m)	Temperature (°C)
	100 - 130	1828 - 1929	54 - 64

Table 2.2. Ben Nevis Formation (Pool 1) EOR Techniques Screening

EOR Technique	Oil Gravity	Viscosity (mPa.s)	Rock Type	Porosity (%)	Permeability (mD)	Net Res	Depth (m)	Temperature (°C)	Total Sum
Miscible Gas Injection									
CO ₂	-5	1	3	1	1	0	3	3	7
HC WAG	-5	1	3	1	1	-5	1	1	-2
Immiscible Gas Injection									
Nitrogen	1	1	3	1	1	0	1	1	9
CO ₂	3	1	3	1	1	0	1	1	11
HC WAG	1	1	3	3	1	0	1	1	11
Chemical									
Polymer	1	1	3	3	1	0	1	1	11
ASP	-5	-5	3	1	-5	0	-5	1	-15
Thermal									
Combustion	1	1	1	3	1	0	1	1	9
Steam	1	-5	3	1	1	0	1	1	3

Legend: (3) corresponds to a property in the average or best value, (1) corresponds to a property in the value range, (0) is assigned when there is no data available, and (-5) corresponds to a property outside of the value range. Value ranges corresponds to the screening guidelines.

Table 2.2 shows that immiscible gas injection (CO₂, HC WAG) appears like a possible EOR technique in Pool; however, due to a lack of potential CO₂ sources in the province, lack of infrastructure to transport any offshore gas to a 350 Km offshore facility, and hydrocarbon gas volumes expected to be produced at Hebron Field are thought not be sufficient for gas based EOR techniques (ExxonMobil, 2011; Mahdavi, et al.,

2014). Hence, polymer flooding becomes a suitable candidate for Pool 1 based on the performed reservoir properties screening and the considered operational constraints. Specific screening guidelines for polymer flooding in heavy oil field proposed by Saboorian-Jooybary et al. (2016) were also considered. Nevertheless, their study is constrained to heavy oil with a viscosity more than 100 mPa.s, and mainly onshore fields, which is not the case of Hebron Field.

2.3.2. Analog fields comparison

Offshore analog fields at different development stages of polymer flooding were identified to compare with the Hebron Field (Pool 1) settings. The fields were: Dalia, Angola (Morel et al., 2012); SZ36-1, China (Han et al., 2006); Heidrun, Norway (Reid et al., 1996); Captain, UK (Osterloh and Law, 1998); and Mariner, UK (Berg et al., 2013). The presence of low permeability facies (5 - 220 mD) and high salinity formation water (> 60,000 ppm TDS) are the main Pool 1 reservoir properties that slightly differ from the analog fields reservoir properties general trend, as shown in Fig. 2.1 and Fig. 2.2.

As can be seen in Fig. 2.2., a potential use of desulfated seawater for polymer flooding solution preparation as Dalia Field, could be beneficial to reduce the original formation water salinity at Pool 1, instead of using standard seawater. However; economic evaluations and water compatibility studies are required to evaluate the proposal feasibility.

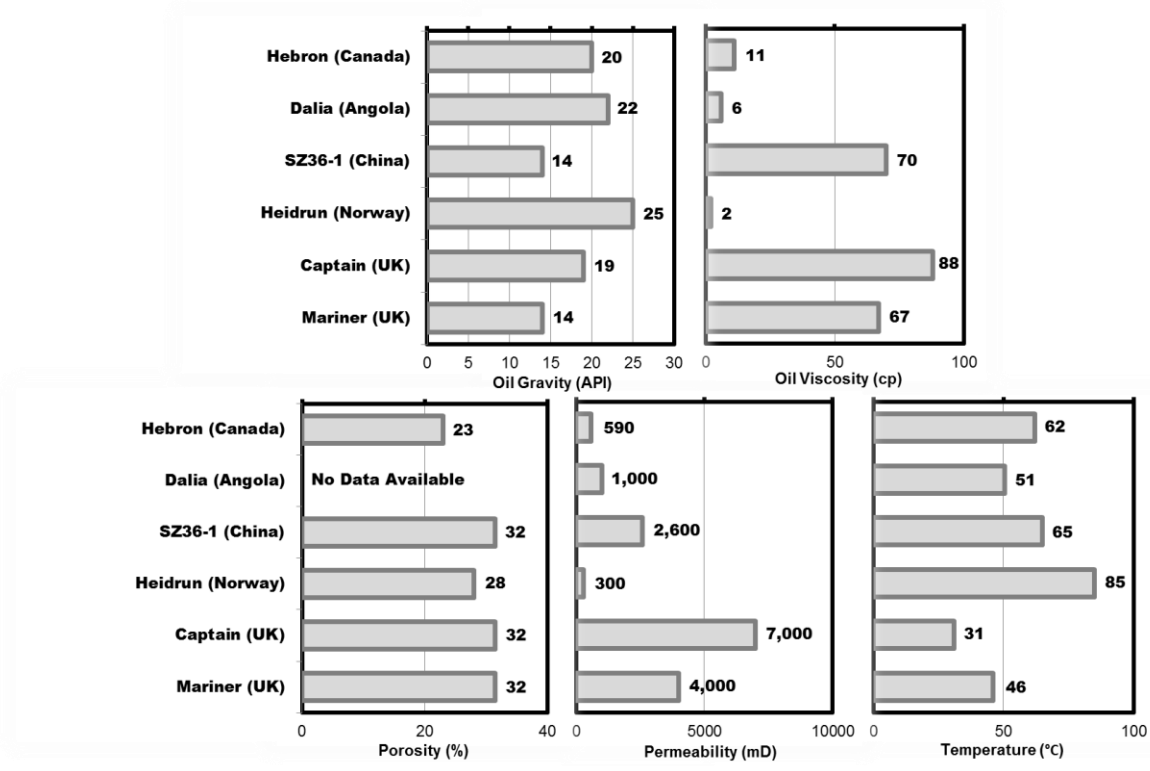


Figure 2.1 Average reservoir properties comparison in offshore polymer flooding projects. Data from Morel et al., 2012, Han et al., 2006, Reid et al., 1996, Osterloh and Law, 1998, Berg et al., 2013.

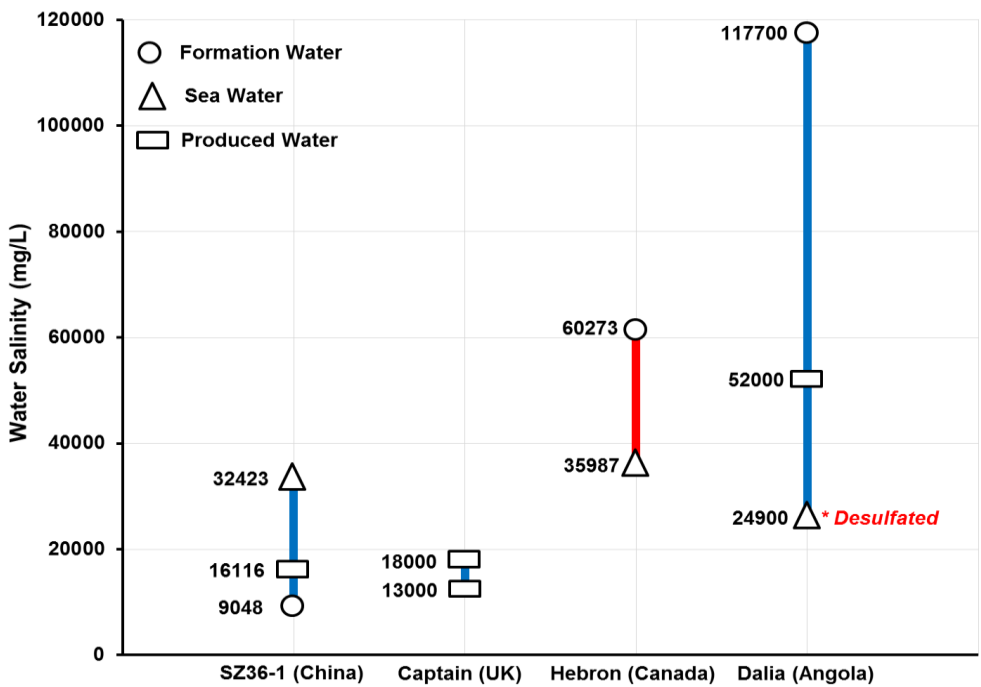


Figure 2.2. Water salinity comparison across offshore polymer flooding projects. Data from Han et al., 2006, Osterloh and Law, 1998, ExxonMobil, 2011, and Morel et al., 2012.

2.3.3. Polymers screening experiments: materials and experimental methodology

2.3.3.1. Polymers

The polymers used in the experiments are divided in two groups: a) straight-chain partially hydrolyzed polyacrylamides (HPAM) and b) biopolymers. The two HPAMs, provided in the powder-form by SNF Floerger, were FLOPAAM 3430S, Lot GH1381 (copolymer of acrylamide and acrylic acid, approximately 25 - 30% anionicity, stated molecular weight 11-14 million Daltons) and FLOPAAM 5115, Lot RG2639/4-6 (sulfonated terpolymer, medium in acrylamide tert-butylsulfonic acid, approximately 25% anionicity, stated molecular weight 8-12 million Daltons). Hereafter, these polymers will be identified as FP-3430S and FP-5115, respectively.

The biopolymer, Guar Gum, was a galactomannan, primarily the ground endosperm of guar beans. Guar Gum, is used principally as a viscous slugging fluid, pumped at connections to ensure that all cuttings are removed from the annulus while drilling surface holes with water. It could be particularly useful offshore, as it can be added directly to seawater. This is significant as one of the principal ideas of this work is to try to reduce operational constraints associated with offshore development. The powder-form was provided by M-I SWACO.

2.3.3.2. Brines

Two kinds of brines were used in the experiments. One is simulated to represent the formation water (FW) of Pool 1 with total dissolved solids (TDS) of 60,273 mg/L (ExxonMobil, 2011). The second brine is seawater from the Grand Banks area, offshore Newfoundland (SW), with 36,155 mg/L TDS, which is the current injection water used for water flooding operations in the nearby offshore fields. Prior to conducting the experiments, each brine solution was filtered under vacuum through 0.22 μm Millipore™ to eliminate any dust and/or insoluble particles. The detailed compositions are listed in Table 2.3.

Table 2.3. Brine compositions (mg/L)

Ions	Grand Banks Seawater (SW)	Synthetic Formation Water (FW)
Na ⁺	10,887	21,058
Ca ²⁺	379	1401
Mg ²⁺	1,323	391
SO ₄ ²⁻	3,248	86
Cl ⁻	20,186	39,440
HCO ₃ ⁻	132	348
TDS	36,155	62,724

2.3.3.3. *Experimental oil*

The simulated oil used in the displacement experiment was compounded by mixing a light crude oil sampled from offshore Newfoundland with Athabasca bitumen, in a proportion of 14:1. The oil was degassed and dehydrated, and the measured viscosity was 10.9 cP at 62 °C, 2775 psi, which represents Pool 1 reservoir conditions. Shu (1984) oil mixing criteria was followed to reach a similar Hebron Field Pool 1 oil viscosity. Detailed information regarding the synthetic oil preparation and viscosity measurement could be found at Appendix E.

2.3.3.4. *Reducing agents*

Following the procedure outlined by Levitt et al. (2011) and Seright and Skejvrak (2015), a solution of 4% sodium bicarbonate (NaHCO₃), 1% EDTA and 1% sodium isoascorbate (C₆H₇NaO₆) was used to flood the cores prior to the experiment in order to remove any excess iron produced due to oxidation and assure that cores were in a reduced state, similar to subsurface conditions. Additionally, 1000 mg/L of C₆H₇NaO₆

solution was added to the polymer solutions and brines, before flooding experiments to avoid oxidation effects.

2.3.3.5. Standard cores

Bentheimer (BEN) and Upper Gray Berea (UGB) sandstone cores were used to evaluate the polymers behavior in core flooding experiments at Pool 1 reservoir conditions. The objective of using standard cores for the polymer flooding experiments, it is to optimize the laboratory methodology and evaluate the associated error and reproducibility prior to use the actual Hebron cores. These sandstone standard cores were selected mainly based on their permeability and porosity range, which is similar to Hebron Field exploration wells core plugs (K : 60 - 1400 mD ; Φ : 23%); more detail about Hebron cores mineralogical composition and reservoir characterization could be found in Chapters 3 and 4. Composite cores with two cylindrical pieces of 1.5 inches diameter and 3 inches length were prepared to perform the core flooding experiments. This core arrangement was used to replicate the conditions for core flooding experiments using actual Pool 1 core plugs. Core properties are shown in Table 2.4.

Table 2.4 Standard cores properties

Core	Bentheimer (BEN)	Upper Gray Berea (UGB)
Brine Perm (mD)	1300	105
Gas Perm (mD)	2000	280 - 350
Porosity (%)	24	18
UCS (psi)	4000	6000 - 8000
Dimensions (in)	1.5 diameter 6 length	1.5 diameter 6 length

2.3.3.6. Polymer solutions bulk viscosity measurements

Polymer solutions were prepared following the procedures described in API RP63 (1990) using a mechanical stirrer. Initial stock polymer solutions (5000 mg/L) were diluted in three solution sets using SW, FW, and deionized water (DW). All polymer solutions were filtered by gravity through 4-7 μm

Whatman™ filters, and degassed in a N₂-purged environment to control oxygen concentration. Polymer solution viscosities were measured using the Anton-Paar Modular Compact Rheometer 300, considering a shear rate interval of 0.1 s⁻¹ to 1000 s⁻¹, and using dual gap geometry.

2.3.3.7. Core flooding apparatus

The core flood apparatus was set up to conduct flood experiments at Hebron Pool 1 reservoir conditions, 62 °C, 2800 psi back pressure, and 3500 psi overburden pressure. Figure 2.3 shows a schematic diagram of the apparatus, which consists of a high pressure Quizix pump QX-20K (1) to inject distilled water at desired flow rate or pressure to the bottom part of the custom made floating piston accumulators. The top half of the accumulators (2) are filled with the reservoir fluids (formation brine, seawater, polymers, and oil) to be injected into the core held in a Vinci TRC core holder (4). High pressure Swagelok stainless steel tubing 316/316L (1/8" OD) and Swagelok fittings were used. The constant overburden pressure (3500 psi) was maintained by an Enerpac P-392 hand pump (9). The produced fluids flow through a backpressure regulator Equilibar rating 10000 psig to be collected in a burette (7). The inlet and outlet pressure were measured using two PARO 9000-10K-101 high pressure transducers (3). The entire apparatus was set in an oven Despatch model RFD2-35-2E (10) to maintain the reservoir temperature.

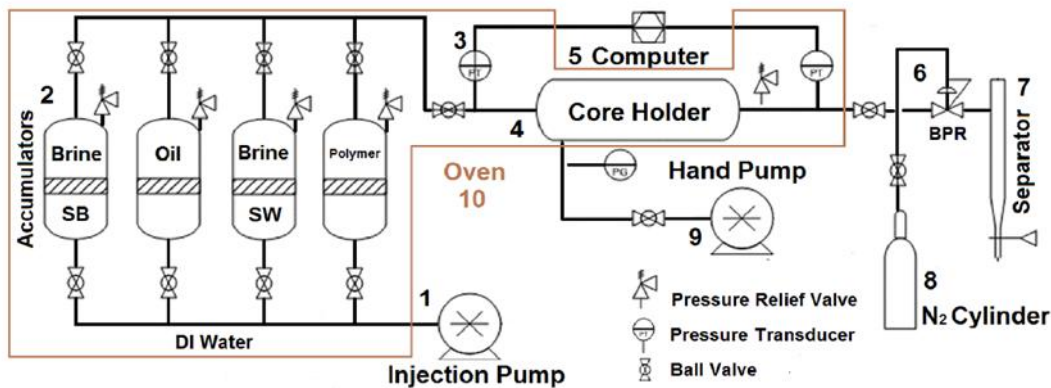


Figure 2.3. Core flooding apparatus scheme.

2.3.3.8. Core flooding

Prior to performing the core flooding oil displacement experiments, the core samples were flooded with a solution of 4% NaHCO₃, 1% EDTA, and 1% C₆H₇NaO₆ at a flow rate of 0.28 mL/min, previously filtered and degassed, until the iron concentration in the effluent was less than 1 ppm; then the cores were dried in 100 °C oven until constant weight, then vacuum saturated with the synthetic formation water (FW) until constant weight. All brines and polymer solutions were deaerated under vacuum and kept under N₂ bubbling to remove dissolved oxygen and prevents bubble formation during injection. The core flooding procedure is briefly described as follows: (i) formation water (FW) saturated core was placed in the setup and flooded with FW to measure the effective permeability at different flow rates; (ii) the core was saturated with oil at 0.28 mL/min to establish the irreducible water saturation; (iii) the core was aged for one day; (iv) two pore volumes (PV) of seawater (SW) were injected into the core at 0.28 mL/min; (v) two PV of polymer solution, at specific concentration according to the polymer type, were injected at 0.06 mL/min; (vi) one PV of seawater (SW) was injected; and (vii) the core and polymer solutions were changed and process repeated from (i) to (vi). Additional experimental set-up pictures could be found in appendix H.

2.4. Results and discussion

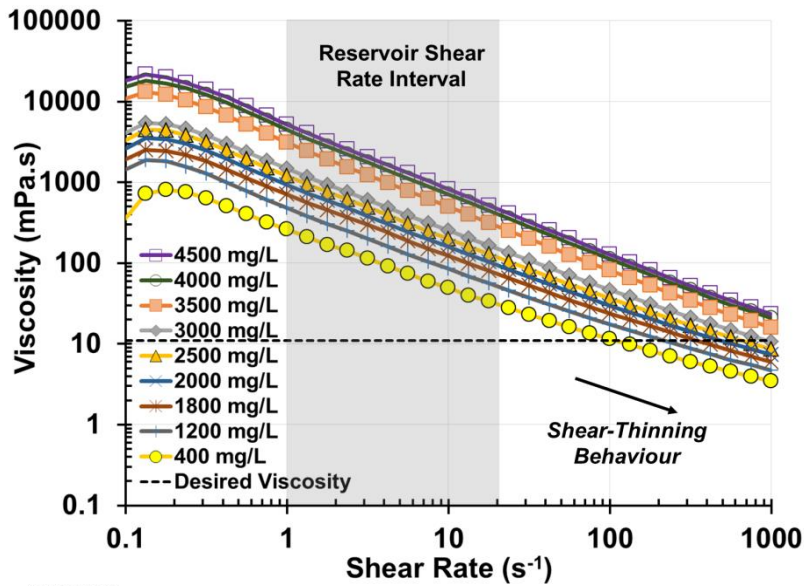
2.4.1. Polymer solution concentrations definition

Polymer solution concentrations were established considering the average live oil viscosity (11 mPa.s), and reservoir temperature (62°C) (ExxonMobil, 2011). The stock polymer solution (5000 mg/L) of each polymer evaluated (FP-3430S, FP-5115, Guar Gum) was diluted in three sets using deionized water (DW), seawater (SW), and formation water (FW) as solvents, in a 400 - 4500 mg/L concentration range. Rheological experimental raw data is listed in appendix B.

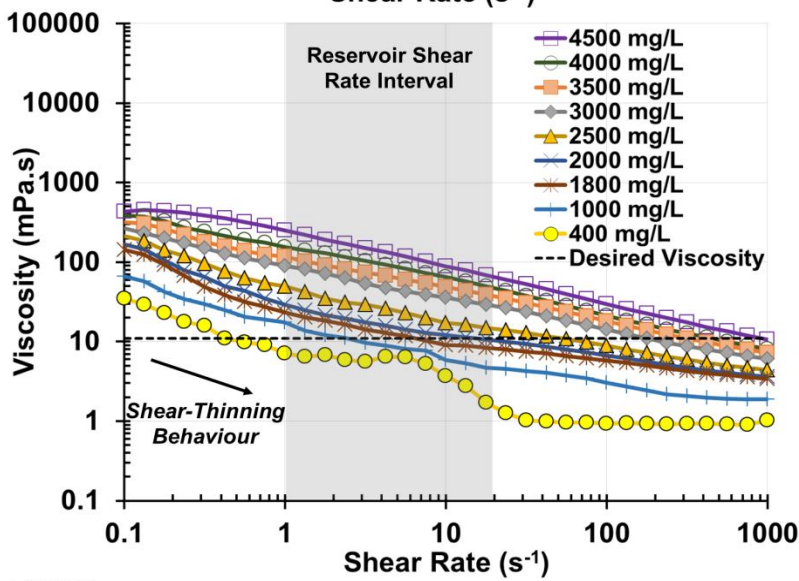
All polymers showed a shear thinning viscosity behaviour, which means that the viscosity decreased as the shear rate increased. The results of FP-3430S are shown in Figure 2.4 as an example.

In order to evaluate the polymer solution concentration, viscosity measurements were compared at a specific shear rate of 10 s^{-1} , a typical shear rate in oil reservoirs according to Rothstein (2013) and considering a polymer solution viscosity at least $11 \text{ mPa}\cdot\text{s}$. The desired viscosity of $11 \text{ mPa}\cdot\text{s}$ was required to reach a 1:1 viscosity ratio, between Pool 1 oil viscosity and the polymer solutions to be tested.

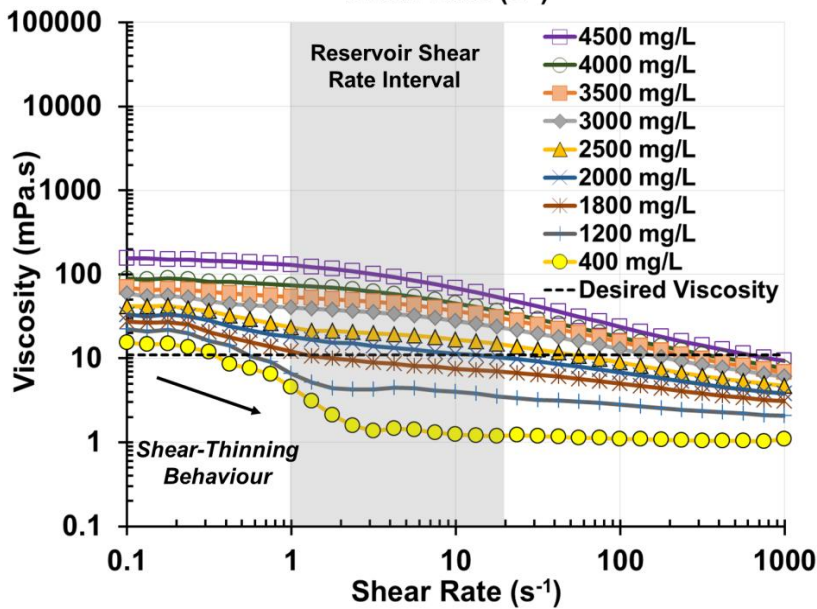
As can be seen in Fig.2.4, there is a high viscosity drop when the salinity of the solvent increase from deionized water to formation water, especially at lower shear rate. This effect has higher impact at low polymer concentration (i.e. 400 mg/L) as can be seen in fig. 2.4b and fig. 2.4c, where the viscosity drop break point is achieved at 7 s^{-1} and 1 s^{-1} , respectively. On the other hand, it could be observed that polymer solutions at higher shear rate tend to a steady viscosity trend; this could be explained as the maximum degradation point where the macromolecules could be break down.



a) Viscosity variations of FP-3430S polymer solutions prepared in deionized water at 62°C

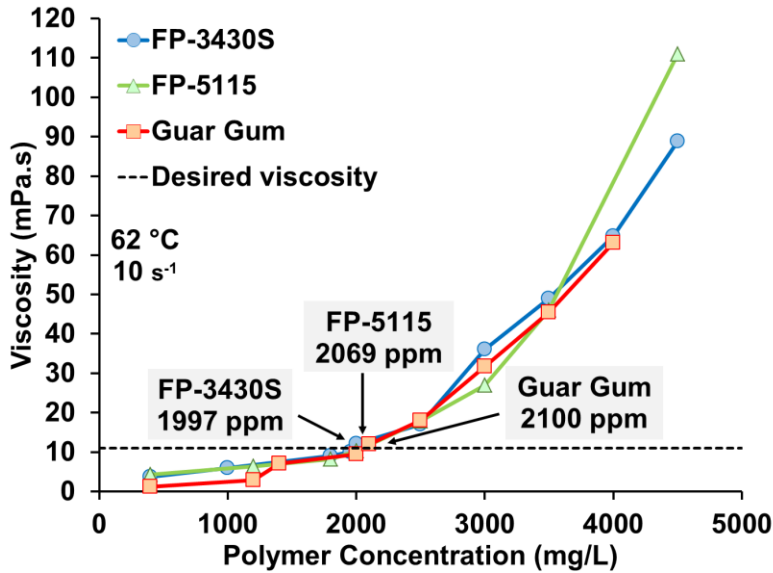


b) Viscosity variations of FP-3430S polymer solutions prepared in seawater at 62°C

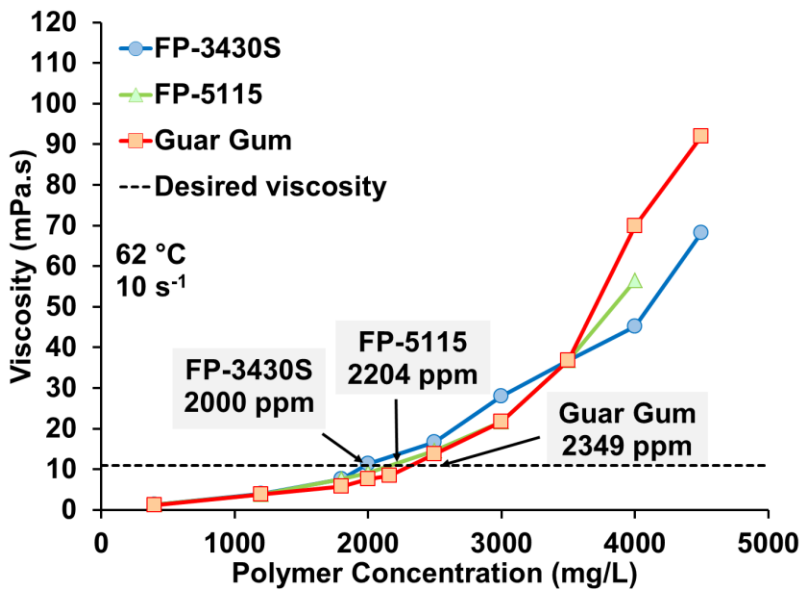


c) Viscosity variations of FP-3430S polymer solutions prepared in formation water at 62°C

Figure 2.4. Viscosity of FP-3430S polymer at 62°C



a) Polymer concentration required to achieve the desired viscosity in polymer solutions prepared in seawater at 62°C



b) Polymer concentration required to achieve the desired viscosity in polymer solutions prepared in formation water at 62°C

Figure 2.5. Concentrations of polymer required to obtain the desired viscosity (11 mPa.s) at 10 s^{-1} shear rate, and 62°C.

Figures 2.5a and 2.5b indicate the minimum concentration of polymer required to achieve the desired viscosity (11 mPa.s) at standard reservoir shear rate (10 s^{-1}). FP-3430S required a lower concentration, both in seawater (SW) and formation water (FW), compared with the other polymers tested, potentially due to its higher molecular weight.

2.4.2. Polymer solutions viscosity as a function of salinity

The FP-3430S and FP-5115 solutions, prepared with seawater (SW) and formation water (FW), showed similar viscosity reductions from their initial viscosity in a solution prepared with deionized water (DW) with the same concentration (2000 mg/L) (Fig.2.6). Viscosity reductions for the HPAMs were on the order of 95%, whereas the Guar Gum counterparts were 34% in SW and 46% in FW, respectively. The lower viscosity reductions observed by the Guar Gum could indicate a higher salinity tolerance than those of the others. However, the initial viscosity of Guar Gum in deionized water (14 mPa.s) (Fig. 2.6, using a 2000 ppm polymer solution and 10 s^{-1} as referenced) is substantially lower than that of the HPAMs (255 mPa.s) and thus the viscosity reductions percentage of HPAMs are higher.

FP-3430S, at a lower concentration, showed limited variation (0.2%) from SW (1997 mg/L) to FW (2000 mg/L) compared with FP-5115 (7%) and Guar Gum (12%). The results indicate that FP-3430S is more resistant to high salinity, possibly due to its higher molecular weight and anionicity. Detailed raw data is found at appendix B.

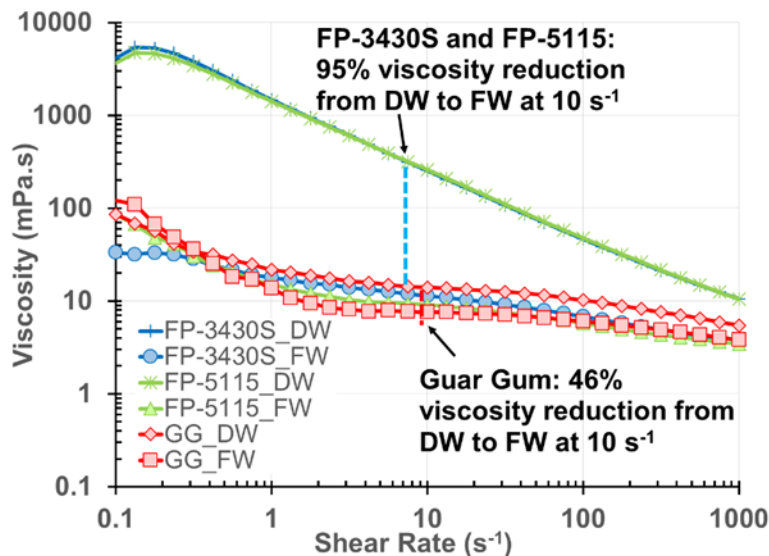


Figure 2.6. Salinity effect in the polymers solution viscosity in different brines at 2000 mg/L.
Note: DW (deionized water); FW (formation water); GG (guar gum)

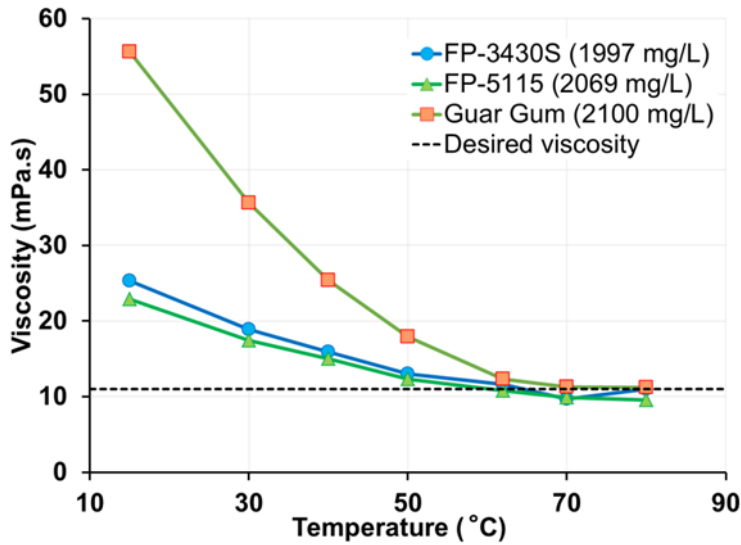
2.4.3. Temperature control on polymer viscosity

The polymer viscosity, as a function of temperature, was investigated and the results are shown in Table 2.5 and plotted in Fig. 2.7. As expected, the relative viscosity reduction decreased as temperature and shear rate increased in all cases except for the Guar Gum in seawater (SW). This could be due to the fact that polymers at those conditions are closer to their maximum degradation point. The FP-3430S and FP-5115 polymers showed a similar trend in relative viscosity reductions at different temperatures regardless of the shear rate and brine salinity. At the same conditions, Guar Gum showed a higher viscosity reduction. Nevertheless, Guar Gum showed a higher viscosity at low temperature compared with the HPAMs for the polymer concentrations used in this study, as can be seen in Fig. 2.7.

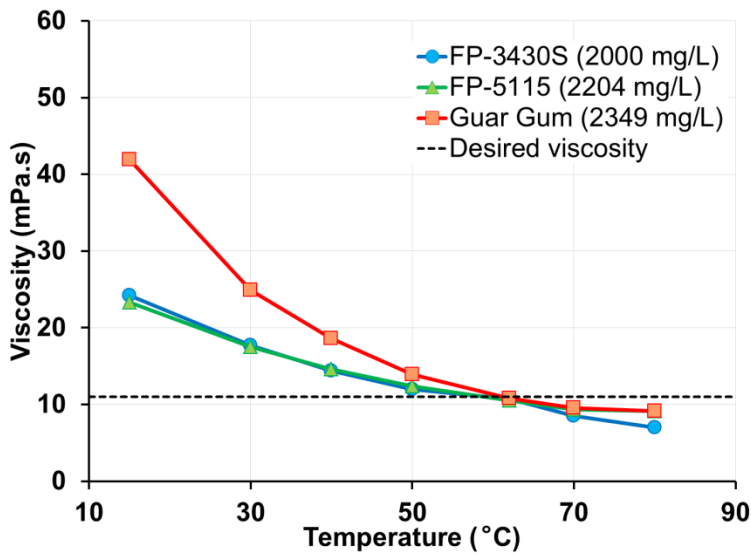
Table 2.5 Viscosity reductions as a function of temperature

Polymer	Water Type	Low Shear Rates (0.1 - 10 s ⁻¹)			High Shear Rates (10 - 1000 s ⁻¹)		
		15-40 °C	40-62 °C	62-80 °C	15-40 °C	40-62 °C	62-80 °C
FP-3430S	Sea (SW)	23%	19%	10%	18%	14%	10%
	Formation (FW)	26%	19%	12%	20%	15%	12%
FP-5115	Sea (SW)	21%	16%	8%	17%	14%	10%
	Formation (FW)	27%	18%	11%	18%	14%	8%
Guar Gum	Sea (SW)	32%	35%	ND	24%	24%	ND
	Formation (FW)	41%	26%	8%	24%	19%	13%

Legend: (ND) no reproducible data available



a) Performance of Polymer solutions prepared in sea water vs. temperature at 10 s⁻¹



b) Performance of Polymer solutions prepared in formation water vs. temperature at 10 s⁻¹

Figure 2.7. Polymer performance vs. temperature for defined concentrations at 10 s⁻¹

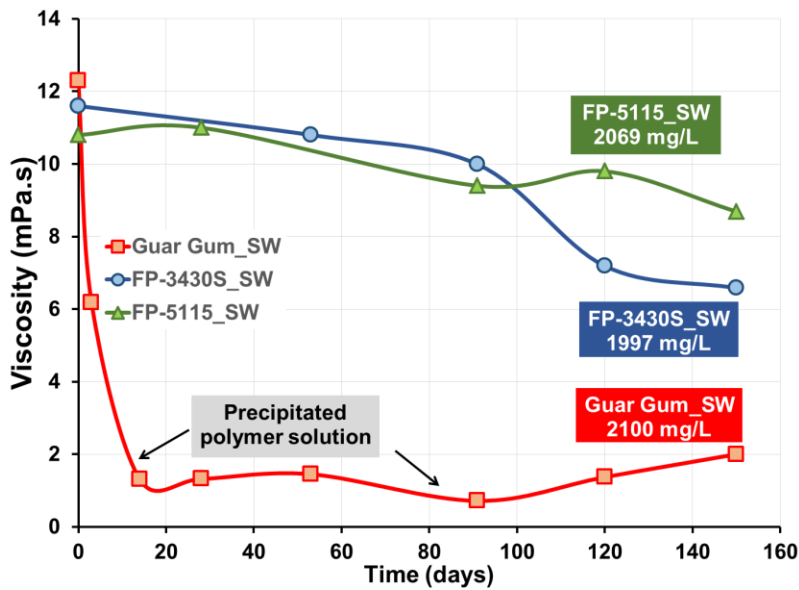
2.4.4. Polymer solutions stability through time

The thermal aging study was designed to verify that the polymers do not degrade significantly at reservoir temperature over time. This was a long term test of 5 months duration, using polymer solutions dissolved in seawater and synthetic formation water. During solution preparation, oxygen was reduced to a minimum by bubbling the solution with nitrogen, creating an anaerobic environment in order to avoid polymer degradation by oxidation.

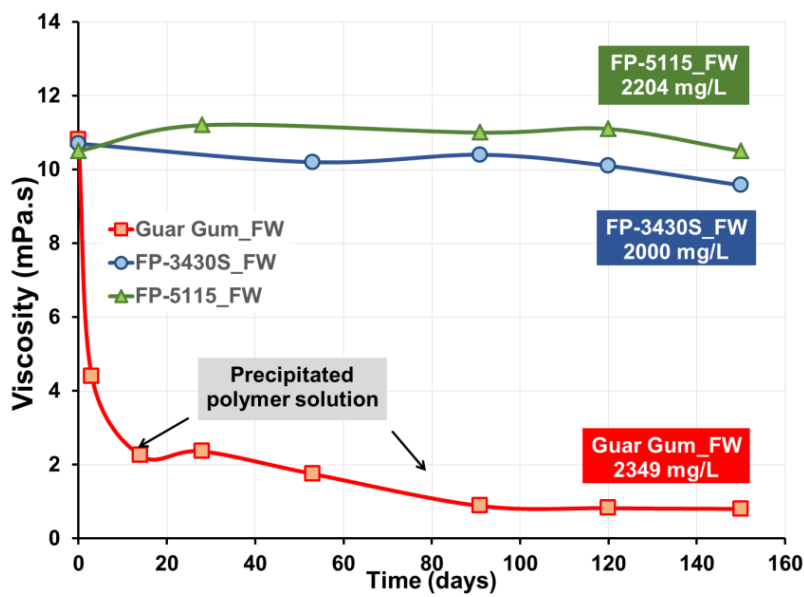
For each set condition (polymer type-brine vs time tested), two amber well-sealed bottles were prepared for testing after 30, 50, 90, 120 and 150 days, in order to assure data reproducibility. At the scheduled time, the fluids were removed from the oven at reservoir temperature (62°C) to measure the viscosity in the rheometer at 10 s⁻¹ shear rate and 62°C. Guar Gum solutions showed a highly-reduced viscosity after thirty days, therefore an additional shorter duration test was designed (at 3 and 15 days) to evaluate the viscosity drop in more detail.

The HPAMs polymers in both brines presented similar behavior after 90 days of aging time, with a maximum viscosity drop of 5% (Fig. 2.8). After that time, FP-3430S (especially in seawater (SW) solution) experienced a higher viscosity drop of 40%. This drop could potentially be related to the lower polymer concentration solution, oxidation issues and/or polymer chemical composition. FP-5115 in both brines showed a higher thermal stability behavior over the aging time likely due to the presence of acrylamide tert-butylsulfonic acid (ATBS) in its composition. According to Fink (2015), ATBS are larger in size and provide a significant chain rigidity and hence a better shear stability. Gaillard et al. (2014), also showed, from similar aging and core flooding experiments, that polymers with ATBS in specific amount improve thermal and salt stability, and suggested that some of them may withstand harsh reservoir conditions with little loss of viscosity for at least one year.

Guar Gum solutions showed a high viscosity reduction after three days (55% drop) and fifteen days (85%). Also, polymer precipitation was noticed in the solutions after fifteen days at 62°C, potentially related to the hydrolysis nature of Guar Gum. Based on these results, Guar Gum was screened out of additional evaluation for use in EOR applications at Pool 1 reservoir conditions, due to its poor resistance to high temperature and high salinity environments over the time.



a) Thermal stability at 62°C and 10 s⁻¹ shear rate of HPAMs and Guar Gum polymer solutions prepared in seawater (SW)



b) Thermal stability at 62°C and 10 s⁻¹ shear rate of HPAMs and Guar Gum polymer solutions prepared in formation water (FW)

Figure 2.8. Polymer solutions thermal stability at 62°C and 10 s⁻¹ shear rate.

2.4.5. Polymer Viscoelastic Properties Evaluation

During porous media flow, polymer chains are pulled and contracted due to the different changes in pore sizes, this often leads the polymers to exhibit elastic behaviour. As the polymer solution flows through a series of pore bodies and pore throats in a porous medium, the fluid may experience elongational or extensional behaviour (Vermolen et al., 2014). Galindo-Rosales et al. (2012) refer to a coexistence of shear and elongational components to describe polymers behaviour; this is mainly due to the flow path complexity. The shear components will come from the viscous polymer behaviour and the elongational or shear thickening response will come from the elastic polymer behaviour (Gogarty et al. 1972, Jones and Walters 1989). Flow difficulties in porous media can be identified by evaluating the flow response of polymers from their viscous and elastic behaviour.

Field applications and evaluation has demonstrated the possible effect of the polymer viscoelastic behaviour. Wang et al. (2001), Xia et al. (2004) and Wang et al. (2007) for instance, attributed the increase in recovery factor of up to 12% in the Daqing Field to this polymer phenomenon. Additional research like the one presented by Vermolen et al. (2014) demonstrated that the residual oil saturation is reduced due to the elastic effect of the polymers, rather than due to the viscous stripping

In order to obtain further insights for the presented work, a comprehensive evaluation of the polymer viscoelastic behaviour was performed. The evaluation is based on Oscillatory and Normal stress measurements. A rheological viscoelastic characterization was performed for the FP-3430S and FP-5115 polymer solutions of the current study. Oscillatory tests were carried out to measure polymer elastic properties at rest (Hincapie and Ganzer 2015), with the use of a coaxial cylinders (cup and bob). On the other hand, First normal stress difference (N_1), as a quantitative measurement of elasticity during flow, using a cone and plate geometry, was measured for the mentioned samples. The N_1 measurements became a challenge, possible due to similar reasons like the ones presented by Ewoldt et al. (2015) and Makosco (1994), it is difficult to obtain representatives N_1 results due to: 1) mechanical artifacts of the geometry

affected by the high temperatures, 2) instable solutions due to the high salinity of the make-up water and 3) fading response of the polymer due to the very low of very high shear rates.

The main evaluation focused into determine the validity of the Cox-Merz rule in order to ensure comparable data and to link the rheological data, collected in the steady-state shear experiment, to those in dynamic oscillatory experiments for entangled polymer liquids. Cox and Merz (1958) noticed that the complex viscosity is nearly equal to the steady shear viscosity when the shear rate and frequency are equal. Simply stated, the steady state shear viscosity (bulk viscosity) at a given shear rate is equal to the dynamic viscosity at the same frequency. By including the Cox-Merz evaluation, we enable the understanding and clarification of the rheological data presented and the reliability of the results in shear and oscillatory approaches.

2.4.5.1 Small Amplitude Oscillatory Shear (SAOS) Comparison

Oscillatory measurements have been used to define the polymer elastic properties. This type of measurements is often divided into two, amplitude sweep and frequency sweep, the second one dependent on the other. Amplitude sweep measurements were performed at constant frequency and temperature with variations in shear stress, in an attempt to define the linear viscoelastic region and torque levels (Makosco, 1994). Data gathered from the amplitude sweep measurements were utilized to run frequency measurements, thus enable determining the cross over point, frequency at which the elastic storage modulus (G') is equal to the viscous loss modulus (G'') (Ewoldt et al., 2015). The inverse of the frequency at which occurs the cross over is a measure of the longest relaxation time of the polymer and it is expressed in radians per second. This express the time when the polymer becomes more viscous than elastic dominated (Makosco, 1994). In other words, the characteristic relaxation time (λ) can be determined as the inverse of the angular frequency (ω) at the cross over point of the moduli (G' and G'') (Kim et al., 2010). Thus, relaxation time will be the reciprocal of angular frequency ($1/\omega$). The relaxation time is widely used in the literature to define the Deborah number (Delshad et al., 2008, Xia et al. 2004 and Wang et al. 2007) - the material fluidity at defined flow conditions - and to determine the degree of elasticity for each polymer

solution. The downside of the SAOS measurements is that it depicts the viscoelastic behaviour of the polymer at rest, thus only provides an idea how elastic a polymer may be (Hincapie et al., 2015). Therefore, the SAOS outcome when analyzing the flow through porous media, one can argue is not representative, but still highly useful.

Table 2.6 summarize the SAOS data gathered for the polymer solutions discussed in this work. It clearly depicted that the salinity and temperature will cause an effect in polymer elastic behavior, e.g. going from 413s for DW to 0.28s for SW at 22°C. and Fig. 2.9 show that the FP-3430S polymer depicted a potential increasing trend in the cross over frequency as the salinity and temperature increased, and thus diminishing the relaxation time and the elasticity response. The FP-5115 polymer exhibits a higher increase in the cross over frequency with temperature and salinity changes than the FP-3430S counterpart; this is attributed to their prevalence of viscous behaviour rather than elastic. Detailed experimental raw data could be found in appendix B.

Table 2.6. Relaxation times (λ) for polymers at different conditions

Polymer	Concentration (mg/L)	Temp (°C)	Brine	G'/G'' (Pa)	Frequency (Hz)	ω (rad/s)	λ (s)
FP-3430S	1997	22	DW	0.41	0.0024	0.015	413
			SW	0.42	3.6	22	0.28
		62	DW	0.42	0.011	0.070	89
			SW	0.10	4.5	29	0.22
FP-5115	2069	22	DW	0.33	0.011	0.069	91
			SW	0.34	7.1	45	0.14
		62	DW	0.30	0.049	0.31	20
			SW	0.50	11	71	0.09

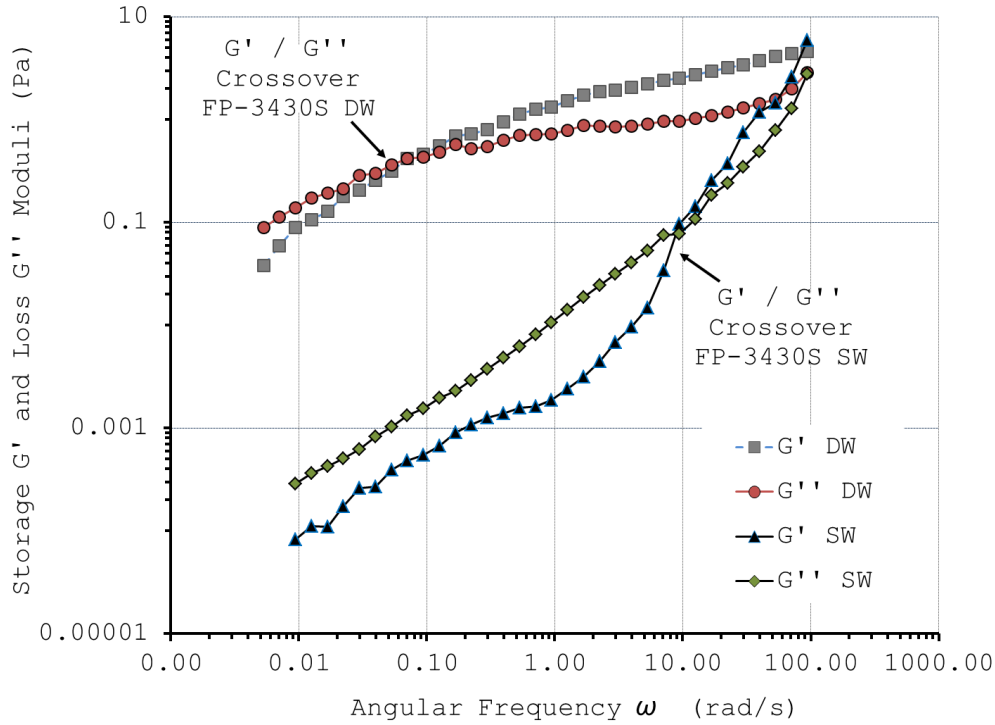


Figure 2.9. Comparison parameters obtained from SAOS measurements. Viscoelastic moduli: elastic storage modulus (G') and viscous loss modulus (G'') as of function of angular frequency for FP-3430S, 1997 mg/L, 62° C, dissolved in different brines.

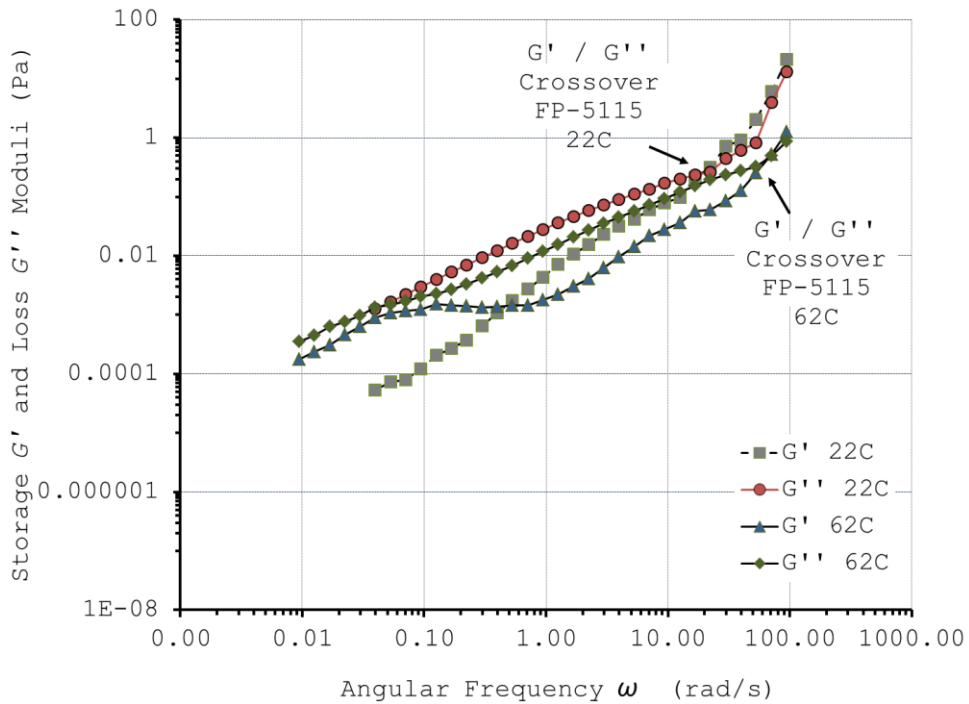


Figure 2.10. Comparison parameters obtained from SAOS measurements. Viscoelastic moduli: elastic storage modulus (G') and viscous loss modulus (G'') as of function of angular frequency for FP-5115, 2069 mg/L, SW brine, at different temperatures

2.4.5.2. *Cox-Merz Rule Validation*

Data obtained from rotational and oscillatory measurements was compared by the application of the Cox-Merz rule. Results can be observed in figures 2.11 and 2.12, the evaluation showed similarities when comparing the shear-rate dependence of the steady-state viscosity and the frequency dependence of the complex viscosity for both polymers at different brine. FP-5115 showed a higher correlation at Pool 1 injection water salinity (SW). Changes in the correlation can be explained by the salinity impact on the polymer viscoelasticity properties, as well as measurement artefacts.. It can be seen that for FP-3430S polymer the viscosity measured by SAOS and rotation depicts a match, which implies the Cox-Merz rule holds for this solution. A different behaviour was observed for the FP-5115 polymer where a match is not observed. In both cases as well, the salinity depicted a strong impact in the solution, seen by the mismatch of the data. This could be explained by 1) the salinity effect in the polymer viscoelastic properties, as described by Hincapie and Ganzer (2015) and 2) by possible measurement errors due to the solutions instability, caused by the temperature and salinity. Note that the measurement were performed three times, and values reported refers to those obtained with errors margins below 3%. Detailed raw data is listed in appendix B.

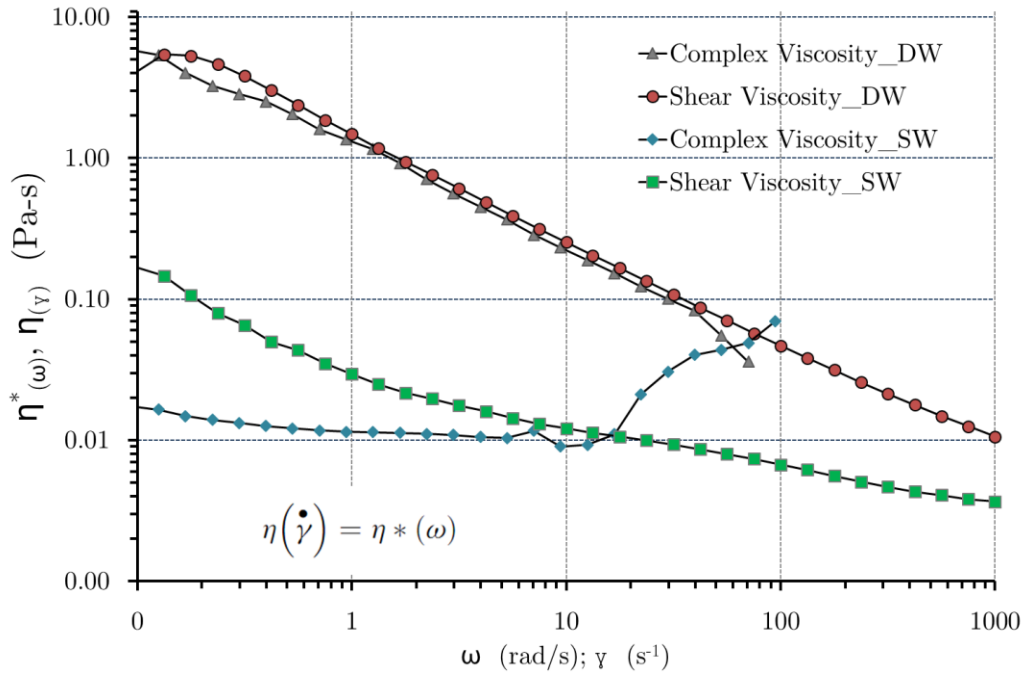


Figure 2.11. Cox-Merz rule evaluation for the polymers considered during this work comparison at different brines salinity. FP-3430S polymer (1997 mg/L) 22°C

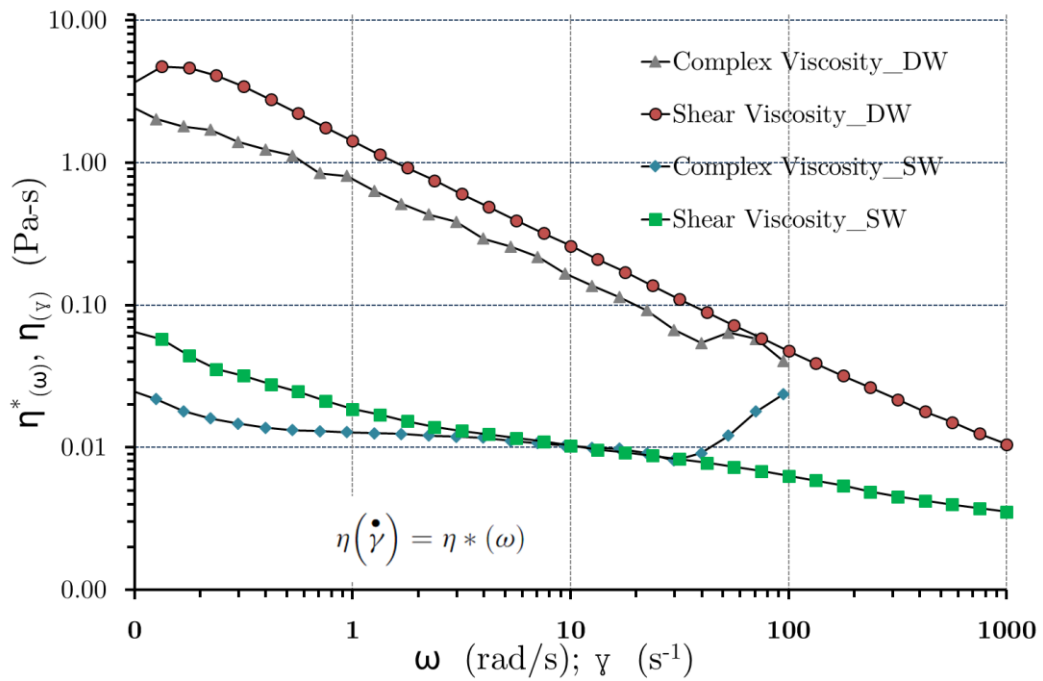


Figure 2.12. Cox-Merz rule evaluation for the polymers considered during this work comparison at different brines salinity. FP-5115 polymer (2069 mg/L)

2.4.5.3. Extensional Viscosity

It can be observed from figures 2.13 and 2.14 the elongational behaviour depicted for the solutions considered in this study. FP-3430S shows an expected viscosity reduction once salinity and temperature is increased. Nevertheless, all the FP-3430S solutions, regardless of salinity or temperature, have a viscosity increase as the apparent extensional rate increases. Extensional viscosity raw data is listed in appendix B.

Based on the extensional viscosity analyses, FP-5115 exhibits a higher relative salinity stability compared with FP-3430S (Fig. 2.13 and 2.14). However, higher viscosity values were recorded at reservoir temperature (62 °C) in a different trend (viscosity decrease at higher extensional rate) as compared with other solutions, these could be artefact.

Overall, the combination of complementary rheological techniques to optimize and define the polymer solutions did not show considerable elastic behaviour and thus, elasticity does not play a major role in the experimental design.

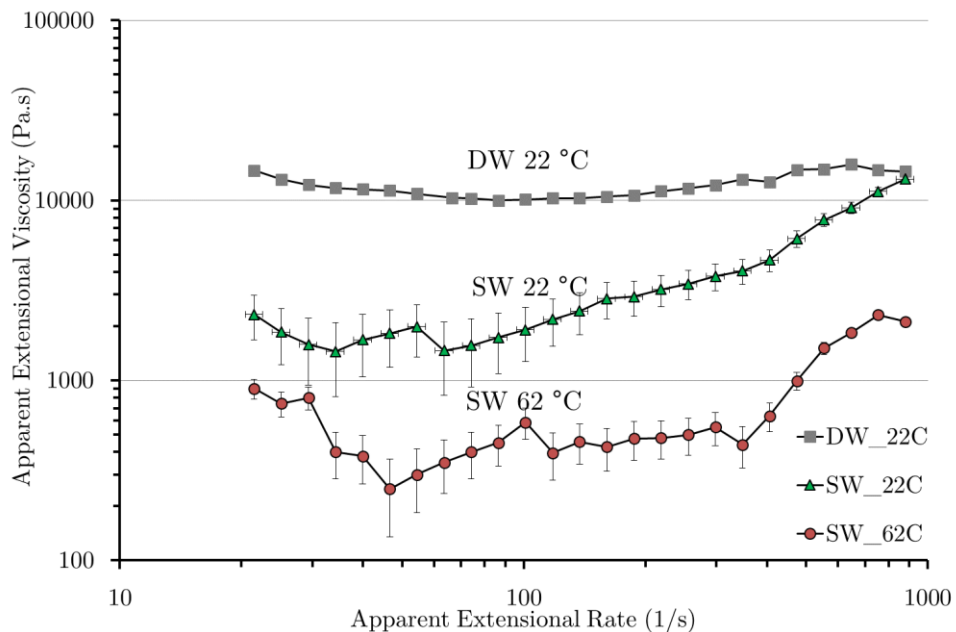


Figure 2.13. Extensional viscosity comparison at different brines salinity and temperature FP-3430S polymer (1997 mg/L)

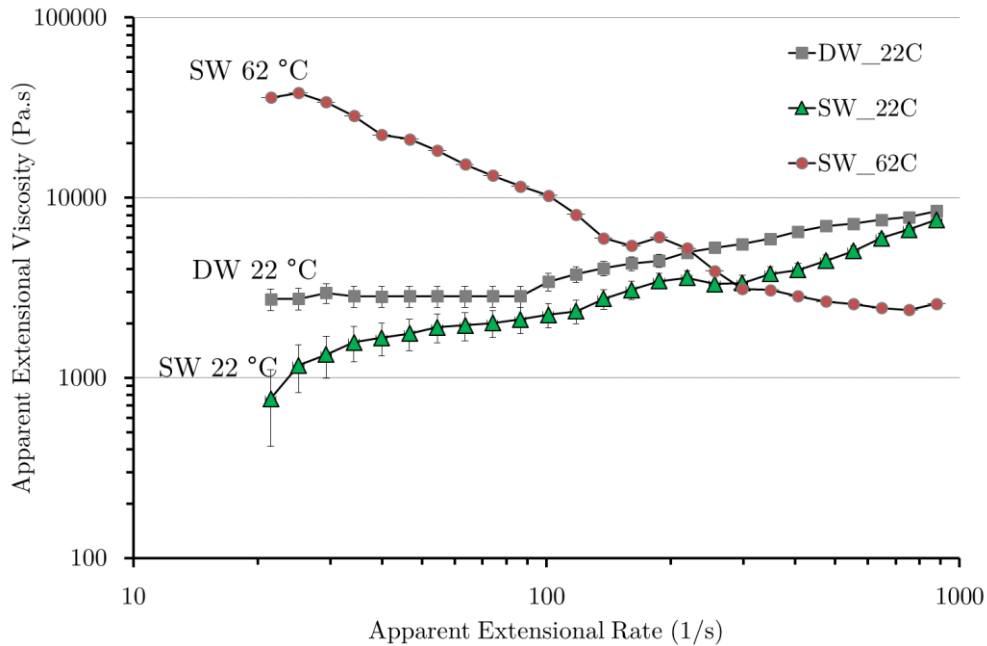


Figure 2.14. Extensional viscosity comparison at different brines salinity and temperature FP-5115 polymer (2069 mg/L)

2.4.6. Core flooding experiments using standard cores

Bentheimer (BEN) and Upper Gray Berea (UGB) sandstone composite cores were used to perform core flooding experiments under Pool 1 reservoir conditions; with oil recovery factor and the experimental error associated to the methodology as the key parameters to be evaluated.

2.4.6.1. Experimental methodology error

The use of standard cores (same type of core for pair of experiments) in this study allowed us to evaluate the reproducibility of experimental conditions, errors related to the core flooding apparatus set-up, and polymer solution behavior in oil recovery. This is used as an initial step to optimise the core flooding setup and perfect techniques prior to using core plugs from the exploration wells which are limited and introduce the influence of heterogeneity on the analyses results.

All core flooding experiments followed a similar flooding sequence, as described in section 2.2.3.8. The FP-5115 polymer solution (2069 mg/L) diluted in seawater (SW) was selected to evaluate the low

permeability cores (Upper Gray Berea Sandstone, considering UGB-1 similar to UGB-2), and FP-3430S polymer solution (1997 mg/L) diluted in seawater (SW) for the high permeability cores (Bentheimer, considering BEN-1 similar to BEN-2). Guar Gum was screened out in prior tests, and was therefore not considered for core flooding experiments. Polymer-core type runs were established based on the stability test results, and time constraints to evaluate all the variables. Error parameters are shown in Table 2.7., and calculations considerations are described in appendixes A, G and H.

Table 2.7 Errors in core flooding experiments

Exp #	Core	Permeability (mD)	Porosity (%)	Polymer Type	Flooding Sequence (PVI)			Total Recovery (%)	Avg. (%)	Std. Dev. (+/-)
					2nd WF	PF	3rd WF			
1	BEN-1	1000	24	FP-3430S	2	2	1	60.0	59.8	0.2
2	BEN-2							59.5	59.8	0.2
3	UGB-1	105	18	FP-5115	2	2	1	55.1	55.5	0.2
4	UGB-2							55.8	55.5	0.2

Table 2.7 shows a poor variation ($STDev \pm 0.2 \%$) respect to the average value obtained between the oil recovery values for similar pair of experiments 1-2 ($59.8 \pm 0.2 \%$) and 3-4 ($55.5 \pm 0.2 \%$); these results confirm a considerable reproducibility in the experimental conditions and setup established, which allows future studies to quantify the effect of reservoir heterogeneity in oil recovery at Pool 1. The dispersion values ($STDev$) obtained in table 2.7 reflects the variation respect the total oil recovery (%) obtained from similar pair of experiments; nevertheless, value dispersion associated to the error propagation as part of every measure performed in the experimental sequence is shown in the next section, and the calculation explained in detail in Appendixes A, G and H.

2.4.6.2. Oil recovery results

Table 2.8 summarizes the results of core flooding runs. Experiment # 1 has the higher oil recovery followed by experiment #2. These results are mainly influenced by the better reservoir properties (higher permeability and porosity) of Bentheimer (BEN) cores compared with those of the Upper Gray Berea (UGB) cores used in the experiments #3 and #4. Additionally, Fig. 2.15 exhibits a faster oil recovery with less pore volume of injection water for the BEN core experiments compared with the UGB core. Therefore, a lower resistance to the water flooding is expected offered by the pore media in BEN cores due to their higher permeability compared with UGB cores.

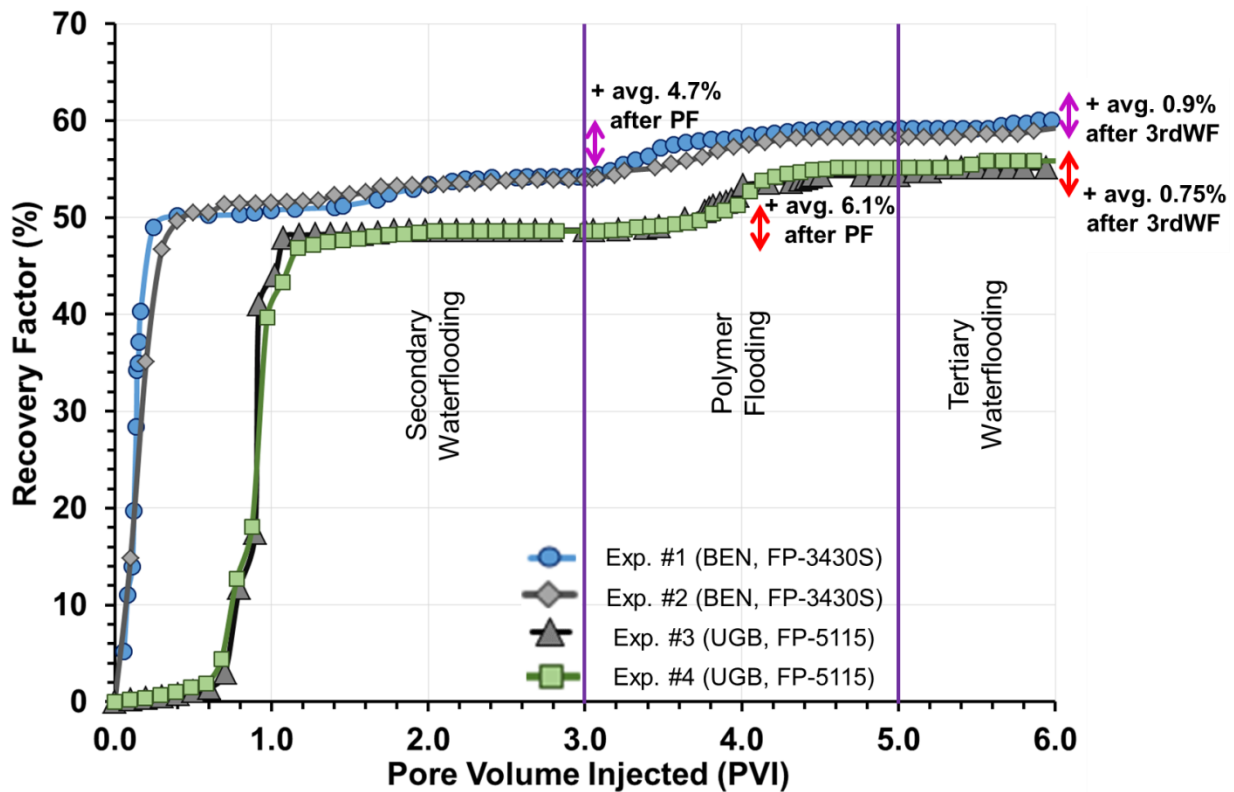


Figure 2.15. Effect of core and polymer type on total oil recovery factor.

The oil recovery values from experiments #3 and #4 (5.7 % and 6.5 %, respectively) were higher during the polymer flooding phase despite the lower permeability compared with experiments # 1 and #2 (4.9 % and 4.4 %, respectively) (Table 2.8). This is likely attributed to the FP-5115 chemical structure, which

includes ATBS monomers adding more stability to high salinity and high shear conditions. On the other hand, FP-5115 has a lower molecular weight than FP-3430S allowing propagating effectively through smaller pore-throats that are common in low permeability porous media. Nevertheless, the oil recovery incremental due to polymer flooding after secondary waterflooding for the high permeability cores (exp. #1 and #2) was reached at lower PV injected, approximately 0.5 PV of polymer flood compared with the low permeability cores (exp. #3 and #4) that required almost 1 PV of polymer flood until the incremental was reached.

A tertiary waterflooding stage (1 PV of seawater injection) was considered in the flooding sequence of this research as recommended practice in the procedures described in API RP63 (1990), in order to obtain steady state conditions and determine the post-polymer flow permeability in future studies. However, an additional oil recovery was also observed in this phase in both pair of experiments (~ 1%).

For all core or polymer types, there is a general trend in the optimum number of pore volume injected to obtain oil recovery (Fig. 2.15); shown as inflexion points in the cumulative curves slope. In the case of the secondary water flooding phase, 1.5 PVI seems to reflect the point where additional water injection does not represent a higher increase in oil recovery. Similarly, 1 PV and 0.5 PV, are the inflexion points for the polymer flooding and tertiary water flooding phases, respectively. Thus, an experiment optimization could be performed for future core flooding experiments at pool 1 reservoir conditions.

Table 2.8 shows a summary of the core flooding experiments results using the standard cores, and considering the error propagation associated to the measures; however, the final standard deviation is ± 0.5 % for all the experiments which is relatively low considering all the steps involved in the experimental flooding sequence. Detailed information about error propagation calculation could be found in appendices A, G and H.

Table 2.8. Core flooding experiments results

Experiment #	Polymer Type	Composite Core	Swc	Sor 2 nd WF	2 nd Waterflooding Recovery (%OOIP)	Sor PF	Polymer Flooding Recovery (%OOIP)	Sor 3 rd WF	3 rd Waterflooding Recovery (%OOIP)	Total Recovery (%OOIP)
1	FP-3430S	BEN-1	0.339 ± 0.004	0.303 ± 0.004	54.2 ± 0.4	0.270 ± 0.005	4.9 ± 0.6	0.264 ± 0.005	0.9 ± 0.6	60.0 ± 0.5
2	FP-3430S	BEN--2	0.342 ± 0.004	0.301 ± 0.004	54.2 ± 0.4	0.273 ± 0.005	4.4 ± 0.6	0.267 ± 0.005	0.9 ± 0.6	59.5 ± 0.5
3	FP-5115	UGB--1	0.434 ± 0.004	0.290 ± 0.004	48.7 ± 0.4	0.258 ± 0.005	5.7 ± 0.6	0.254 ± 0.005	0.8 ± 0.6	55.1 ± 0.5
4	FP-5115	UGB-2	0.405 ± 0.004	0.306 ± 0.004	48.6 ± 0.4	0.268 ± 0.005	6.5 ± 0.6	0.263 ± 0.005	0.7 ± 0.6	55.8 ± 0.5

Legend: Swc (connate water saturation), Sor 2nd WF (residual oil saturation after 2nd water flooding), Sor PF (residual oil saturation after polymer flooding), Sor 3rd WF (residual oil saturation after 3rd water flooding).

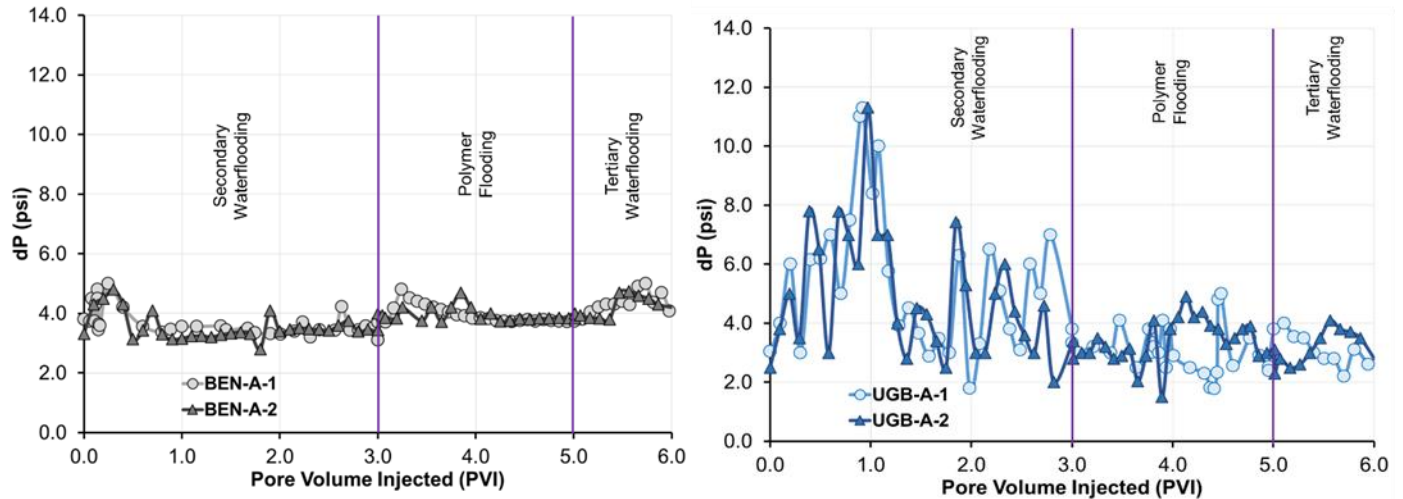
Table 2.9. Average pressures during core flooding experiments

Exp #	Core	2nd WF		PF		3rd WF	
		Pin (psia)	Pout (psia)	Pin (psia)	Pout (psia)	Pin (psia)	Pout (psia)
1	BEN-A-1	2837 ± 90	2833 ± 90	2799 ± 104	2795 ± 104	2840 ± 47	2835 ± 47
2	BEN-A-2	2845 ± 95	2841 ± 95	2814 ± 101	2810 ± 101	2848 ± 44	2844 ± 44
3	UGB-A-1	2834 ± 137	2826 ± 135	2780 ± 123	2775 ± 124	2838 ± 18	2831 ± 18
4	UGB-A-2	2830 ± 130	2822 ± 141	2773 ± 120	2765 ± 120	2839 ± 20	2833 ± 21

Legend: Pin (inlet pressure), Pout (outlet pressure), 2nd WF (secondary waterflooding), PF (polymer flooding), 3rd WF (tertiary waterflooding).

As can be seen in table 2.9, there is a variation in the average inlet and outlet pressure during the different stages of the coreflooding experiments, being lower during the polymer flooding stage in general. This could be attributed to the flow rate used during the experiments, being higher in the secondary and tertiary waterflooding stages, 0.28 cm³/min (5 ft/day) compared with the flow rate used during the polymer flooding stage, 0.06 cm³/min (1 ft/day). The pressure in the tertiary waterflooding stage is relatively higher compared with the secondary waterflooding, potentially due to the presence of a potential mechanical entrapment of polymers in a previous phase; however, more studies are required to support this hypothesis.

Fig. 2.16 illustrates the pressure drop along the core as a function of the pore volume injected. As expected, the pressure differential rate (dP) varies more in the experiments performed in low permeability cores (UGB) than high permeability cores (BEN). The injected fluid (seawater and polymer solutions) experiences a high pressure drop during flow through smaller pores and pore throats. An additional observation from these experiments is the correlation between the higher pressure drop and higher oil production for all the flooding sequence phases, as can be seen in Fig. 2.15 and Fig. 2.16.



A) High Permeability Cores

B) Low Permeability Cores

Figure 2.16. Pressure profile during flooding sequence.

2.5. Conclusions

EOR screening guidelines published in the literature were used to evaluate potential EOR techniques application at Hebron Field Pool 1, based on its reservoir and fluid properties. Polymer flooding was considered as potential option; therefore, through a laboratory scale characterization the performance of this technique at Pool 1 reservoir conditions was investigated. Three polymers were used in the study to investigate how the concentration, salinity and reservoir temperature affected the polymer viscosity, viscoelastic properties and stability.

The effects of the aforementioned parameters on oil recovery at Pool 1 are as follow:

- Both tested HPAM polymers (FP-3430S and FP-5115) showed similar viscosity responses to salinity and temperature changes compared with the biopolymer (Guar Gum) counterpart.
- Guar Gum was found to be highly unstable at the reservoir conditions over time, and did not meet polymer screening criteria of providing the required viscosity in brines at reservoir temperatures for prolonged time.

- FP-3430S showed a higher viscosifying power, requiring less polymer to reach the same viscosity values at different brine salinities.
- Polymer viscoelastic evaluation suggests that the elasticity of the polymers do not play an important role in this experimental design.
- FP-5115 systematically showed a higher stability character, and is thus considered the most suitable polymer for application in the reservoir studied.
- Core flooding experiments using standard cores show 59.8 (± 0.5) % and 55.5 (± 0.5) % of oil recovery in high and low permeability cores, respectively. Polymer flooding stage generates an average 4.7% oil recovery in high permeability cores, and average 6.1% in low permeability cores; this is likely attributed to the type of polymer (FP-5115) used in each experiment.
- Applying a systematic laboratory characterization methodology could lead to reduced field uncertainties at early stage of the field at relatively low cost.

2.6. Acknowledgements

Thanks to Hibernia EOR lab staff for their support during the experimental work. Special thanks to Dr. Anand Yethiraj for the use of his rheology laboratory, and Dr. Rafael Hincapie for providing his support during polymer rheological experiments design. Thanks to SNF Floerger and MI-Swaco Atlantic Canada for providing graciously the HPAMs and Guar Gum polymers samples, respectively. This work was supported generously and graciously by Hibernia Management and Development Company (HMDC), Chevron Canada, the Natural Sciences and Engineering Research Council of Canada (NSERC), the Canada Foundation for Innovation (CFI), Research and Development Corporation of Newfoundland (RDC), and the Petroleum Exploration Enhancement Program (PEEP).

2.7. References

Abidin, A.Z., Puspasari, T., Nugroho, W.A., 2012. Polymers for enhanced oil recovery technology. *Procedia Chemistry* 4 (2012) 11-16.

Al Adasani, A. and Bai, B., 2011. Analysis of EOR projects and updated screening criteria. *J. Petrol. Sci. Eng.* 79 (2011) 10-24.

Al Mjeni, R., Arora, S., Cherukupalli, P., van Wunnik, J., Edwards, J., Felber, B.J., Gurpinar, O., Hirasaki, G., Miller, C., Jackson, C., Kristensen, M., Lim, F., Ramamoorthy, R., 2011. Has the time come for EOR? *Schlumberger Oilfield Review*. 22 (4) 16-35.

Alvarado, V. and Manrique, E. 2013. Engineering design challenges and opportunities beyond water flooding in offshore reservoirs. Paper OTC 24105 presented at the 2013 Offshore Technology Conference, Houston, U.S.A., 6-9 May.

API, 1990. API Recommended practice 63 (RP63). Recommended practices for evaluation of polymers used in enhanced oil recovery operations.

Berg, E.A., Silcock, S., Ostbo-Bjastad, B., 2013. Next step in offshore heavy oil - Mariner reservoir development. Paper SPE 166575 presented at the 2013 SPE Offshore Europe Oil and Gas Conference and Exhibition, Aberdeen, U.K., 3-6 September.

Cox, W. P. and Merz, E.H. 1958. Correlation of dynamic steady flow viscosities. *J. Polymer Sci.* (28) 619-622.

de Melo, M.A, Da Silva, I.P.G, de Godoy, G.M.R., Sanmartim, A.N., 2002. Polymer injection projects in Brazil: dimensioning, field application and evaluation. Paper SPE 75194 presented at the 2002 SPE/DOE Improved Oil Recovery Symposium, Tulsa, U.S.A., 13-17 April.

Delshad, M., Kim, D.H., Magbagbeola, O.A., Huh, C., Pope, G.A., Tarahhom, F., 2008. Mechanistic interpretation and utilization of viscoelastic behaviour of polymer solutions for improved polymer-flood efficiency. Paper SPE-113620-MS presented at the 2008 SPE/DOE Symposium on Improved Oil Recovery, Tulsa, USA, 20-23 April.

Ewoldt, R.H., Johnston, M.T., Caretta, L.M. 2015. Experimental challenges of shear rheology: how to avoid bad data, in complex fluids in biological systems: experiment, theory, and computation, E.S. Spagnolie, Editor. Springer New York: New York, NY. p. 207-241

ExxonMobil, 2011. Hebron Project Development Plan. <http://www.cnlopb.ca/pdfs/conhebdevplan.pdf>

Fink, J. 2015. Petroleum engineer's guide to oil field chemicals and fluids. Elsevier p. 825.

Gaillard, N., Giovannetti, B., Favero, C., Caritey, J.P., Dupuis, G., Zaitoun, A. 2014. New water soluble anionic NVP acrylamide terpolymers for use in harsh EOR conditions. Paper SPE 169108 presented at the 2014 SPE Improved Oil Recovery Symposium, Tulsa, U.S.A, 12-16 April.

Galindo-Rosales, F.J., Campo-Deaño, L., Pinho, F. T., Bokhorst, E., Hamersma, P. J., Oliveira, M. S. N., Alves, M. A. 2011. Microfluidic systems for the analysis of viscoelastic fluid flow phenomena in porous media. *Microfluidics and Nanofluidics*. 12(1) 485-498.

Gogarty, W.B., Levy, G. L., Fox, V. G. 1972. Viscoelastic effects in polymer flow through porous media. Paper SPE 4025-MS, San Antonio, Texas.

Han, M., Xiang, W., Zhang, J., Jiang, W., Sun, F., 2006. Application of EOR technology by means of polymer flooding in Bohai oil fields. Paper SPE 104432 presented at the 2006 SPE International Oil & Gas Conference and Exhibition, Beijing, China, 5-7 December.

Hincapie, R.E., Duffy, J., O'Grady, C., Ganzer, L., 2015. An approach to determine polymer viscoelasticity under flow through porous media by combining complimentary rheological techniques. Paper SPE-174689-MS presented at the 2015 SPE Enhanced Oil Recovery Conference, Kuala Lumpur, Malaysia, 11-13 August.

Hincapie, R., Ganzer, L. 2015. Assessment of polymer injectivity with regards to viscoelasticity: lab evaluations towards better field operations. Paper SPE-174346-MS presented at the EUROPEC 2015. Madrid, Spain, 1-4 June.

Jones, D.M., Walters, K. 1989. The behaviour of polymer solutions in extension-dominated flows, with applications to enhanced oil recovery. *Rheologica Acta*, 28(6) 482-498.

Kaminsky, R.D., Wattenbarger, R.C, Szafranski, R.C., Coutee, A.S., 2007. Guidelines for polymer flooding evaluation and development. Paper IPTC 11200 presented at the 2007 International Petroleum Technology Conference, Dubai, UAE, 4-6 December.

Kim, D.H., Lee, S., Ching, H.A., Chun, H., Pope, G., 2010. Development of a viscoelastic property database for EOR polymers. Paper SPE-129971 presented at the 2010 SPE Improved Oil Recovery Symposium in Tulsa, USA, 24-28 April.

Levitt, D.B., Slaughter, W., Pope, G.A., Jouenne, S., 2011. The effect of redox potential and metal solubility on oxidative polymer degradation. *J. SPE Reserv. Eval. Eng.* 14 (3) 287-298.

Macosko, C.W. 1994. *Rheology: principles, measurements, and applications*. Wiley - VCH. P. 568.

Mahdavi, S., James, L.A., Johansen, T.E., 2014. Technical and economic considerations for using CO₂ enhanced oil recovery in an offshore environment. Presented at 64th Canadian Society of Chemical Engineers Conference, Niagara Falls, Canada, 19-22 October.

Maia, A., Borsali, R., Balaban, R., 2009. Residual comparison between a polyacrylamide and a hydrophobically modified polyacrylamide flood in a sandstone core. *Mater. Sci. Eng. C*, 29 (2009) 505-509.

Morel, D., Vert, M., Jouenne, S., Gauchet, R., Bouger, Y., 2012. First polymer injection in deep offshore field Angola: recent advances in the Dalia/Camelina field case. *J. SPE Oil Gas Fac.* 1 (2) 43-52.

Osterloh, W.T. and Law, E. J., 1998. Polymer transport and rheological properties for polymer flooding in the North Sea Captain field. Paper SPE 39694 presented at the 1998 SPE/DOE Improved Oil Recovery Symposium, Tulsa, U.S.A., 19-22 April.

Reid, B.E., Hoyland, L.A., Olsen, S.R., Petterson, O., 1996. The Heidrun field – challenges in reservoir development and production. Paper OTC 8085 presented at the 1996 Offshore Technology Conference, Houston, U.S.A., 6-9 May.

Rothstein, J., 2013. Effect of fluid rheology on enhanced oil recovery in a microfluidic sandstone device. *J. of Non-Newtonian Fluid Mech.*, 202, 112-119.

Saaborian-Jooybary, H., Dejam, M., Chen, Z. 2016. Heavy oil polymer flooding from laboratory core floods to pilot tests and field applications: Half-century studies. *J. Petrol. Sci. Eng.* 142 (2016) 85-100.

Seright, R., Seheult, J.M., Talashek, T. 2009. Injectivity characteristics of EOR polymers. *J. SPE Reserv. Eval. Eng.* 12 (5) 783-792.

Seright, R. and Skejvrak, I. 2015. Effect of dissolved iron and oxygen on stability of hydrolyzed polyacrylamide polymers. *SPE Journal.* 20 (3) 1-9.

Shu, W.R., 1984. A viscosity correlation for mixtures of heavy oil, bitumen, and petroleum fractions. *SPE Journal.* 24 (3) 277-284.

Taber, J.J., Martin, F.D., Seright, R.S. 1997. EOR Screening Criteria Revisited - Part 1: Introduction to Screening Criteria and Enhanced Recovery Field Projects. *J. SPE Reserv. Eng.* 12 (3) 189-198.

Taber, J.J., Martin, F.D., Seright, R.S. 1997. EOR Screening Criteria Revisited - Part 2: Applications and Impact of Oil Prices. *J. SPE Reserv. Eng.* 12 (3) 199-205.

Teletzke, G.F., Wattenbarger, R.C., Wilkinson, J.R., 2010. Enhanced oil recovery pilot testing best practice. *J. SPE Reserv. Eval. Eng.* 13 (1) 143-154.

Vermolen, E.C.M., van Haasterecht, M.J.T., Masalmeh, S.K., 2014. A systematic study of the polymer visco-elastic effect on residual oil saturation by core flooding. Paper SPE-169681-MS presented at the 2014 SPE EOR Conference at Oil and Gas West Asia, Muscat, Oman, 31 March - 2 April.

Wang, D., Cheng, J., Xia, H., Li, Q., Shi, J., 2001. Viscous-elastic fluids can mobilize oil remaining after water-flood by force parallel to the oil-water interface. Paper SPE-72123-MS presented at the 2001 SPE Asia Pacific Improved Oil Recovery Conference, Kuala Lumpur, Malaysia, 6-9 October.

Wang, D., Wang, G., Wu, W., Xia, H., Yin, H. 2007. The influence of viscoelasticity on displacement efficiency from micro to macro scale. Paper SPE-109016-MS presented at the 2007 SPE Annual Technical Conference and Exhibition, Anaheim, California, U.S.A.

Xia, H., Wang, W., Wu, J., Kong, F. 2004. Elasticity of HPAM solutions increases displacement efficiency under mixed wettability conditions. Paper SPE-88456-MS presented at the 2004 SPE Asia Pacific Oil and Gas Conference and Exhibition, Perth, Australia 18-20 October.

CHAPTER 3. IMPLICATIONS OF THE DIAGENETIC HISTORY ON POLYMER FLOODING PERFORMANCE FOR THE BEN NEVIS FORMATION, HEBRON FIELD, OFFSHORE NEWFOUNDLAND, CANADA

To be submitted to *SPE Reservoir Evaluation and Engineering*.

Luis E. Valencia, Lesley A. James*, Karem Azmy

Memorial University of Newfoundland, St. John's, Canada

* Corresponding author e-mail: l james@mun.ca

Keywords: Polymer Flooding, Ben Nevis Formation, Hebron Field, Diagenesis.

3.1. Abstract

The Hebron Project is the fourth major offshore development in Newfoundland and Labrador with an estimated 2620 MBO in place and more than 700 MBO recoverable. This research focuses on the Ben Nevis Formation reservoir (Pool 1) which is anticipated to produce 70% of the Hebron Project's crude oil. In comparison with the density of crude oil from nearby offshore fields, Hebron crude oil is considered heavy with an API gravity of 17 – 24°API. The first oil is expected in 2017, and the current best estimate for recovery factor is 30%. Applying enhanced oil recovery (EOR) methods could increase this recovery factor; however, the effectiveness of these methods will depend on the nature of the reservoir. Considering these premises, the purpose of this research is to experimentally examine potential EOR methods to apply to the Ben Nevis Fm. (Hebron Field) based on its diagenetic history and the recovery mechanism interactions.

Preliminary enhanced oil recovery (EOR) screening, considering the oil and reservoir properties, coupled with difficulties in sourcing potential injection gas, led to the investigation of polymer flooding. The reservoir mineralogy and texture were studied before and after the application of experimental polymer flooding. Pre-flooding investigation showed calcite cement and fine grains (clays) increasing upward the formation (at Pool 1), with the associated diminishment of reservoir properties. This establishes the calcite and clay content as potentially the most critical diagenetic features to influence the EOR performance in

Pool 1. Core flooding experiments showed an additional oil recovery increase in the range of 3-6% after water flooding, with FLOOPAM-5115 being the most effective polymer at the reservoir conditions evaluated. Polymer flooding, as a secondary method, consistently showed a higher increase in oil recovery.

3.2. Introduction

The optimization of oil production from current resources using Enhanced Oil Recovery (EOR) techniques is a leading strategy for many oil producers to add to new oil reserves due to the significant cost associated with finding and developing new discoveries in challenging environments.

Reservoir characterization for EOR requires an understanding of the origin, timing, trend, and magnitude of geologic events that affected the reservoir anatomy. Reservoir heterogeneity controls fluid flow and recovery factors; thus predicting the heterogeneities is important for the prediction of reservoir performance (Weber 1982; Szpakiewicz et al. 1987; Morad et al. 2010).

According to Szpakiewicz et al. (1987) diagenetic effects resulting from geochemical alterations of mineral components (e.g., feldspars) and different types and polymorphs of clays are important but are often neglected in EOR performance evaluation. Having knowledge of the formation anatomy and water chemistry as well as the effects of mineralization during chemical flooding provide the grounds needed to improve reservoir characterization for predicting EOR performance.

This research project focuses on the Ben Nevis Formation (Pool 1) which is considered the main reservoir of the Hebron Field in offshore Newfoundland, Canada. Pool 1 consists of fine-grained sandstones deposited in a marine shoreface depositional environment, with an anticipated production of approximately 70 percent of the Hebron Project's crude oil. However, the much denser crude in this reservoir, with a 20 API, presents some production challenges when compared with the density of crude oil from nearby offshore fields (ExxonMobil, 2011).

Normore (2006) evaluated the origin, distribution and paragenetic sequence of carbonate cements in the Ben Nevis Formation at White Rose Field located in the Jeanne d'Arc Basin, 46 km northwest of the Hebron Field. He found that calcite cemented concretions are the dominant authigenic cement found in the Ben Nevis Formation at the White Rose Field, and suggested that while there is no compartmentalization of the Ben Nevis Formation, the volume of calcite cement will reduce the amount of recoverable oil and gas.

The available information provided in the Hebron Development Plan (ExxonMobil, 2011) was reviewed and compared to EOR screening guidelines published in the literature (Taber et al. 1997a; Taber et al. 1997b, Al Adasani and Bai, 2011; Alvarado and Manrique, 2013). The result of this comparison, coupled with the challenge of sourcing an injection gas, led to considering polymer flooding as a potential EOR candidate for Pool 1 (Valencia et al., 2015; Valencia et al., 2017a).

Polymer flooding consists of adding polymers to increase the viscosity of the injected fluid (water) thus improving the sweep, and reducing oil bypassing and viscous fingering in order to increase oil recovery (Maia et al., 2009; Sheng et al., 2015; Saboorian-Jooybary et al., 2016).

The purpose of this study is to experimentally examine the potential effect of polymer flooding on oil recovery at the Ben Nevis Formation based on its diagenetic history and the recovery mechanism interactions through core flooding experiments designed at Pool 1 temperature and pressure conditions.

3.3. Geological Settings

The Hebron Field is located in the Jeanne d'Arc Basin, approximately 300 km south-east of St. John's, NL in an average water depth of 110 m. The basin structure is a northeast plunging, trough shaped, half graben located on the edge of the Grand Banks. The basin dimensions range from 25 to 80 km wide to 130 km long with a maximum sediment thickness of about 20 km. The main structural components defining the Jeanne d'Arc Basin are the Bonavista platform to the west, the Cumberland Volcanic Belt to the north, the Central Ridge Complex to the east, and the Avalon uplift to the south (Figure 3.1). The western boundary

of the basin is formed by the listric Murre Fault whereas the eastern boundary is defined by the antithetic Voyager fault (Tankard and Welsink, 1987).

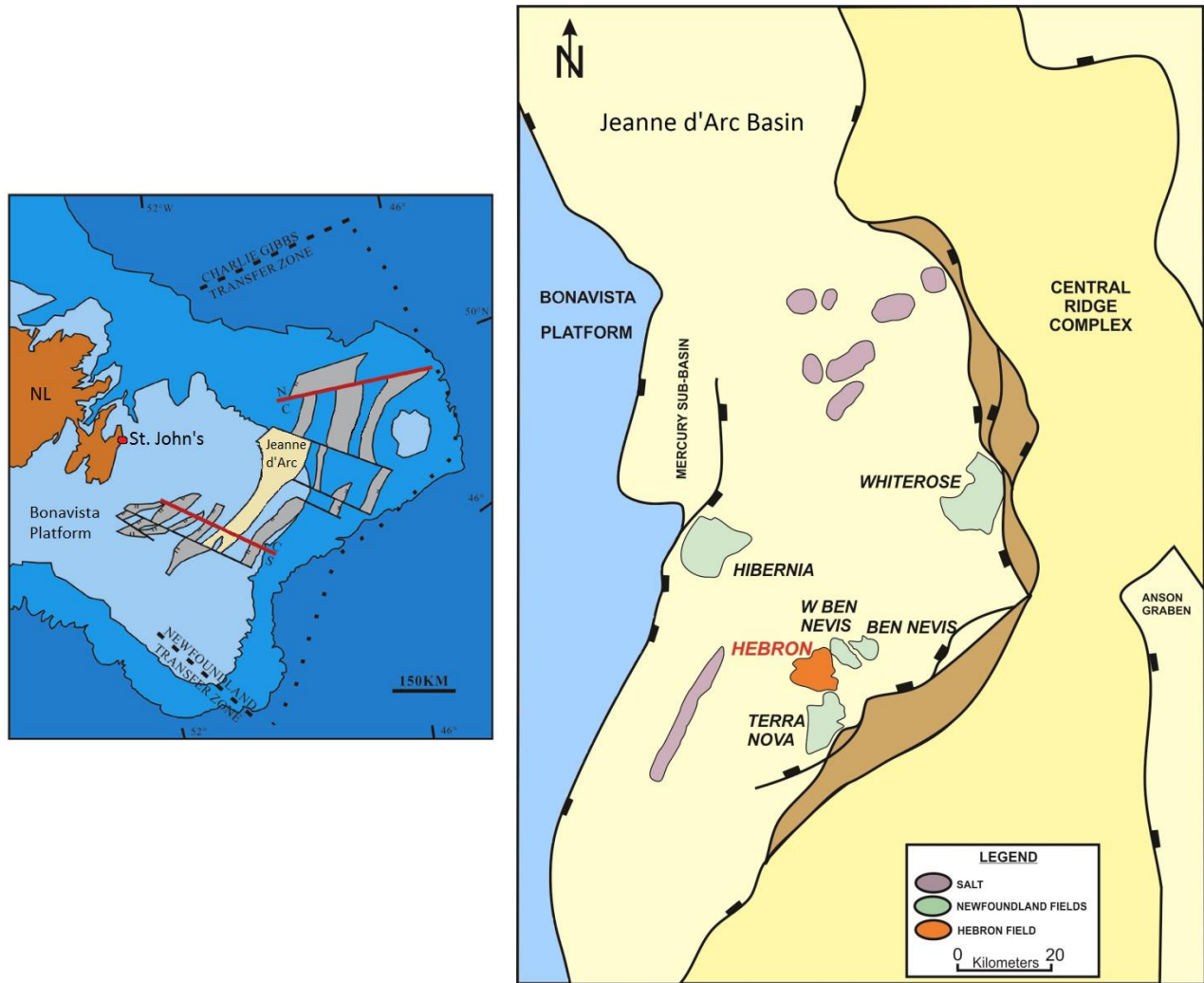


Figure 3.1. Hebron Field location at Jeanne D'Arc Basin (modified after ExxonMobil, 2011, Xiong et al, 2016)

The Hebron Field lies on a horst block with a graben to the southwest and to the northeast (Figure 3.2). The horst block is part of the north-south trending and north-plunging Terra Nova anticline and the fault-bound basin-dividing northwest-southeast “trans-basin” trend. The trapping configuration for the Ben Nevis and

Hibernia reservoirs on the horst block is fault dependent three ways. The Jeanne d'Arc reservoir has a combination of structural and stratigraphic trap configuration (Shannon et al., 1995).

The three main reservoirs for the field are the Ben Nevis, Hibernia, and Jeanne d'Arc Formations. The Ben Nevis Formation (Upper Aptian to Albian), unconformably overlies the Avalon Formation. It consists of 125 m to 500 m thick succession of upward fining fine to very fine grained calcareous sandstone with interbedded thin layers of sandy limestones grading upward into glauconitic siltstone and shale (Shannon et al., 1995).

The depositional environment of the Ben Nevis Formation is primarily lower to upper shoreface environment, with subtle facies changes, highly correlative, and a very high net-to-gross ratio. On a more detailed scale, the depositional environment and stratigraphy are more complicated. The cores show many cycles of wave-dominated marine depositional events that encompass a range of facies (upper shoreface to offshore marine). Individual cycles are thin (tens of centimetres), and are interpreted to be laterally extensive (one to tens of kilometres). The dominant environment of deposition on the horst block of the Hebron Field is proximal lower shoreface. The reservoir package has occasional coquinas, made of shallow marine shell debris, and rare shales (ExxonMobil, 2011).

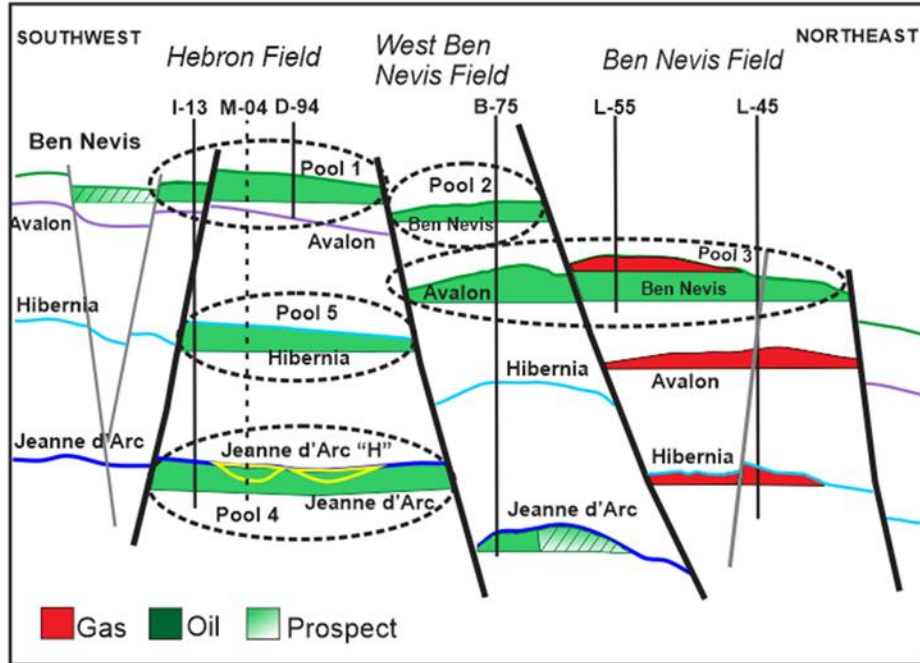


Figure 3.2. Hebron Field structural section (modified after ExxonMobil, 2011).

Normore (2006) in his study in the Ben Nevis Formation at the White Rose Field found that a higher density of concretionary cemented intervals were located at the base of the formation, but that the cementation intensity increased upwards, thus leading to a potential reservoir permeability stratification.

According to ExxonMobil (2011), several scenarios for predictive models have been used to estimate the distribution of calcite cementation in the Ben Nevis reservoir. It is unlikely that the cement zone is laterally continuous across the whole Hebron Field, considering the calcite's multi-point source genesis.

3.4. Methodology

3.4.1. Reservoir Characterization

3.4.1.1. Optical Microscopy

Petrographic analysis was used to determine detailed mineralogical composition, textural characteristics and information on the post-depositional history of Pool 1 sandstone samples. Fifteen polished thin sections from D-94 and M-04 wells core plugs were cut before polymer flooding experiments, and similar eight thin

sections after polymer flooding. Samples were examined by a Nikon Eclipse E600 POL polarizing microscope attached with a Nikon DXM 1200F digital camera.

3.4.1.2. Scanning Electron Microscopy (SEM) - Mineral Liberation Analyzer (MLA)

Polished thin sections, cut before and after flooding, were evaluated using the SEM-MLA technique. The scanning electron microscope used was a FEI MLA 650 FEG, equipped with high throughput energy dispersive x-ray (EDX) and analytical systems from Bruker that included the x-ray aided image analysis MLA.

3.4.2. Core Flooding Experiments

3.4.2.1. Polymers

The polymers used in the experiments were hydrolyzed polyacrylamides (HPAM), provided in the powder-form by SNF Floerger. FLOPAAM 3430S, Lot GH1381 (copolymer of acrylamide and acrylic acid, approximately 25-30% anionicity, stated molecular weight of 11-14 million Daltons) and FLOPAAM 5115, Lot RG2639/4-6 (sulfonated terpolymer, medium in acrylamide tert-butylsulfonic acid, approximately 25% anionicity, stated molecular weight of 8-12 million Daltons). Hereafter, these polymers will be identified as FP-3430S and FP-5115, respectively.

3.4.2.2. Brines

Two brine solutions were used in the experiments, one was simulated to represent the formation water (FW) of Pool 1 with total dissolved solids (TDS) of 60,273 mg/L (ExxonMobil, 2011) and the second brine was seawater from the Grand Banks area in offshore Newfoundland (SW) with 36,155 mg/L TDS, which is the current injection water currently used for water flooding operations in the nearby offshore fields. Prior to

conducting the experiments, each brine solution was filtered under vacuum through 0.22 μm MilliporeTM to eliminate any dust and/or insoluble particles. The detailed compositions are listed in Table 3.1.

Table 3.1. Brine composition (mg/L).

Ions	Grand Banks Seawater (SW)	Synthetic Formation Water (FW)
Na ⁺	10,887	21,058
Ca ²⁺	379	1401
Mg ²⁺	1,323	391
SO ₄ ²⁻	3,248	86
Cl ⁻	20,186	39,440
HCO ₃ ⁻	132	348
TDS	36,155	62,724

3.4.2.3. *Experimental oil*

The simulated oil used in the displacement experiment was compounded by mixing a light crude oil sampled from offshore Newfoundland with Athabasca bitumen in a proportion of 14:1. The simulated oil was degassed and dehydrated, and the measured viscosity was 11 cp at 62 °C, 2775 psi, which represents Pool 1 reservoir conditions. Shu (1984) oil mixing criteria was followed to reach a similar Hebron Field Pool 1 oil viscosity. Detailed information about the simulated oil preparation, chemical composition and its viscosity measurement, could be found in appendix E.

3.4.2.4. *Reducing agents*

Following the procedure outlined by Levitt et al. (2011), and Seright and Skejvrak (2015), a solution of 4% sodium bicarbonate (NaHCO₃), 1% EDTA and 1% sodium isoascorbate (C₆H₇NaO₆) was used to flood the

cores prior to flooding experiments in order to remove any excess iron produced due to oxidation and assure that cores were in a reduced state, similar to subsurface conditions. Additionally, 1000 mg/L of $C_6H_7NaO_6$ solution was added to the polymer solutions and brines before flooding experiments to avoid oxidation effects.

3.4.2.5. Hebron Field Exploration Wells Cores

Core plugs used in this research were selected from Hebron Field exploration wells at Pool 1 reservoir level, cores #1 and #6 of the D-94 well (1999) and core #2 of the M-04 well (2000), as shown in Figure 3.3. These samples were provided by the Canada-Newfoundland and Labrador Offshore Petroleum Board (C-NLOPB), and preliminary selection was based on core availability, permeability ranges obtained from previous SCAL tests, and visual inspection. Composite cores were prepared by stacking individual core plugs from high permeability to low permeability starting at the inlet, in order to minimize experimental errors related to capillary end effect (Langaas et al., 1998; Mosavat et al., 2013). Additionally, the composite core arrangement included thin filter paper between the individual plugs stacked in order to maintain the capillary continuity between composite plugs. Composite core dimensions were 1.5 inches in diameter and 6 inches in length, detailed reservoir properties are shown in table 3.2. The permeability and porosity average and standard deviations are obtained from the individual values that correspond to each core plug included in the composite core arranged. Porosity and permeability measurements were also measured, detailed information at appendix F.

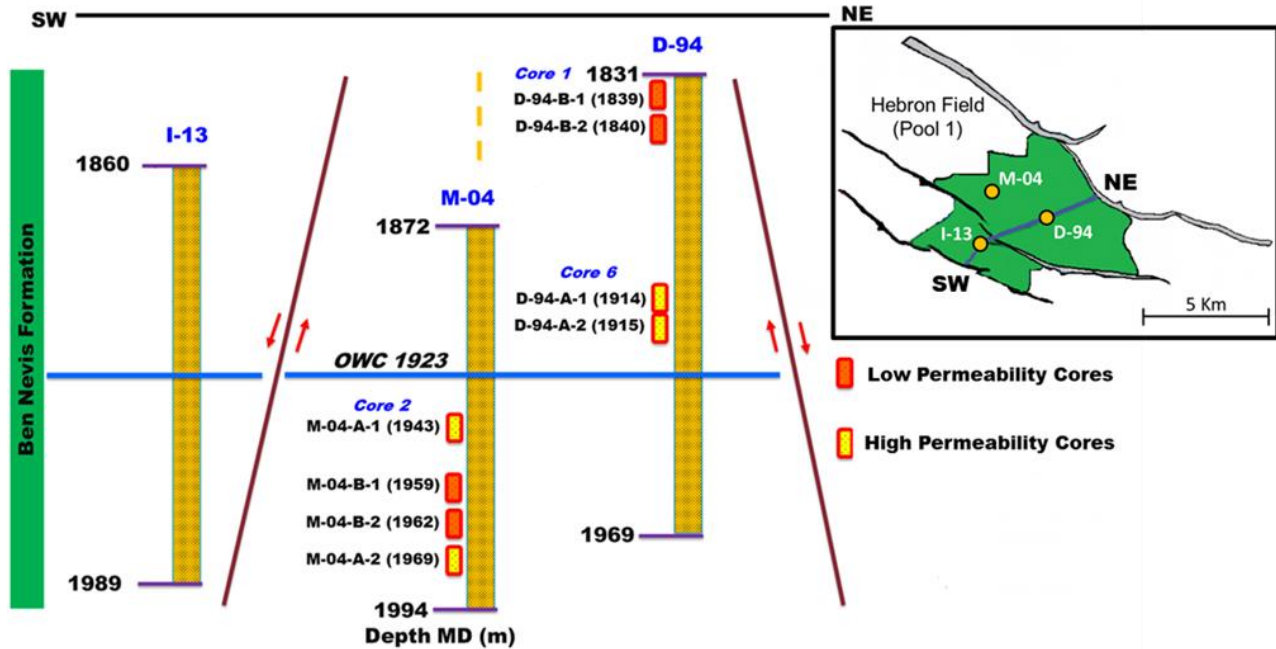


Figure 3.3. Composite cores sample location (map modified after ExxonMobil, 2011).

Table 3.2. Pool 1 composite cores properties.

Experiment #	Composite Core	Average Permeability (mD)	Average Porosity (%)
1	D-94-A-1	1407 ± 49	28.8 ± 0.5
2	M-04-A-2	1370 ± 50	28.8 ± 2.1
3	D-94-A-2	1383 ± 24	29.9 ± 0.7
4	M-04-A-1	1340 ± 20	28.7 ± 2.2
5	D-94-B-2	58 ± 4	22.3 ± 0.6
6	M-04-B-1	122 ± 5	27.3 ± 3.3
7	D-94-B-1	77 ± 22	23.1 ± 1.4
8	M-04-B-2	119 ± 6	24.1 ± 0.6

3.4.2.6. Polymer solutions bulk viscosity measurements

Polymer solutions were prepared following the procedures described in API RP63 (1990) and by using a mechanical stirrer. Initial stock polymer solutions (5000 mg/L) were diluted in SW until they reach the

concentrations previously defined by Valencia et al. (2016a) considering the average live oil viscosity (11 cp), and reservoir temperature (62°C) (ExxonMobil, 2011). All polymer solutions were filtered by gravity through 4-7 μm Whatman™ filters, and degassed in a N₂-purged environment to control oxygen concentration. Polymer solution viscosities were measured using the Anton-Paar Modular Compact Rheometer 300, considering a shear rate interval of 10 s⁻¹, and using a dual gap geometry. Detailed raw data is found at appendix B.

3.4.2.7. Core flooding experimental apparatus

The core flood apparatus was set up to conduct core flood experiments at Pool 1 reservoir conditions, 62 °C, 2775 psi back pressure, and 3500 psi overburden pressure. A schematic diagram of the apparatus is shown in Fig. 3.4. It consists of a high pressure Quizix pump QX-20K (1) that allows injection of distilled water at the desired flow rate or pressure to the bottom part of the custom-made floating piston accumulators. The accumulators (2) are filled with the fluid (brine, polymers, and oil) to be injected into the core held in a Vinci TRC core holder (4). High pressure steel tubing (1/8" OD) carries the fluid to inject it into the core with the assistance of the distributor inlet cap of the core holder. The constant overburden pressure (3500 psi) was maintained by an Enerpac P-392 hand pump (9). The produced fluids were carried through the backpressure regulator into a burette (7), collecting the fluids there. The inlet and outlet pressure were measured using two PARO 9000-10K-101 high pressure transducers (3). The apparatus was set in an oven Despatch model RFD2-35-2E (10) to assure the reservoir temperature. Additional experimental set-up pictures could be found in appendix H.

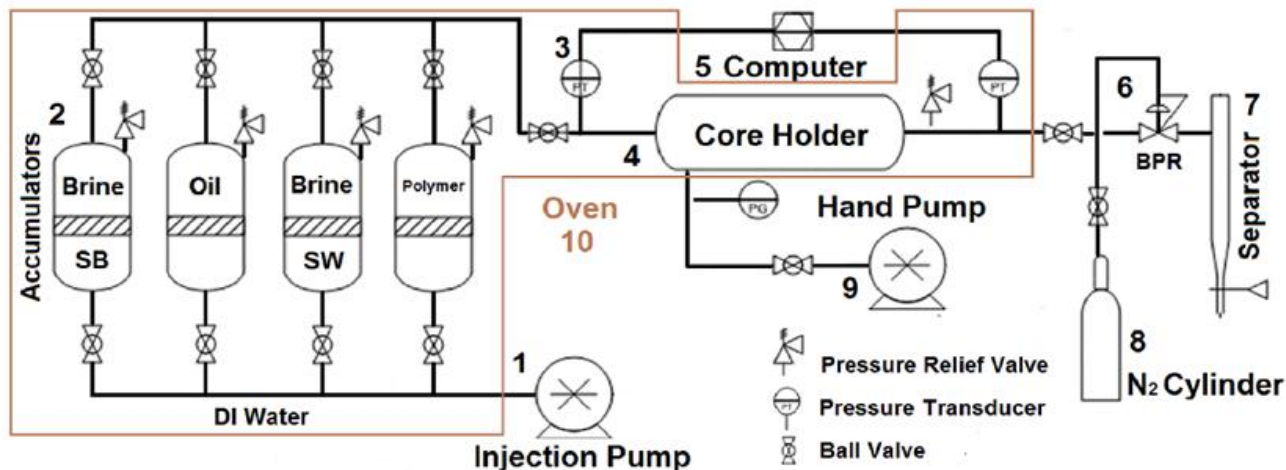


Figure 3.4. Core flooding apparatus scheme.

3.4.2.8. Core flooding procedure

Prior to performing the core flooding oil displacement experiments, the core samples were flooded with a solution of 4% NaHCO_3 , 1% EDTA, and 1% $\text{C}_6\text{H}_7\text{NaO}_6$ at a flow rate of 5 ft./day, previously filtered and degassed, until the iron concentration in the effluent became less than 1 ppm; then the cores were dried in 100 °C oven until constant weight and vacuum-saturated with the synthetic formation water (FW) until constant weight. All brine and polymer solutions were deaerated under vacuum and kept under N_2 bubbling to remove dissolved oxygen and prevents bubble formation during injection. The core flooding procedure can be briefly described as follows: (i) FW saturated core was placed in the setup and flooded with FW to measure the effective permeability at different flow rates; (ii) the core was saturated with oil at 5 ft./day to establish the irreducible water saturation; (iii) the core was aged for one day; (iv) two pore volumes (PV) of SW was injected into the core at 5 ft./day; (v) two PV of polymer solution, at specific concentration according to the polymer type was injected at 1 ft./day; (vi) one PV of SW was injected; and (vii) the core and polymer solutions were changed and the process was repeated from (i) to (vi). This core flooding procedure was previously tested by Valencia et al. (2017a) using standard cores to adjust the experimental conditions.

3.4.2.9. Polymer flooding experiments variables

In order to conduct meaningful experiments considering the quantity of core plugs available; a design of experiments with the variables shown in Table 3.3 was considered following a Plackett-Burman approach (Ledolter and Swersey, 2007). The eight experiments were defined using 4 composite cores with a permeability range of 1340 - 1400 mD (high permeability facies), and 4 composite cores with 50-120 mD permeability range (low permeability facies).

Table 3.3. Polymer flooding experiment variables

Dependent Variable	Independent Variables		
	Permeability Facies (mD)	Polymer	Polymer Flood Timing
Porosity	Low (50 - 120)	FP-5115	Tertiary
	High (1340 - 1400)	FP-3430S	Secondary

3.5. Results

3.5.1. Reservoir characterization

The optical mineralogy and SEM-MLA analysis indicates that Pool 1 sandstones of the current study are mainly composed of quartz, lithic fragments, carbonates, plagioclases and less abundant clays such as illite and kaolinite. As shown in Fig. 3.5, the mineralogical profiles indicate that there is a relative upward increase of carbonate and matrix contents in Pool 1 reservoir, thus causing a decrease in the reservoir quality. Detailed information about samples mineralogy could be found in appendix C.

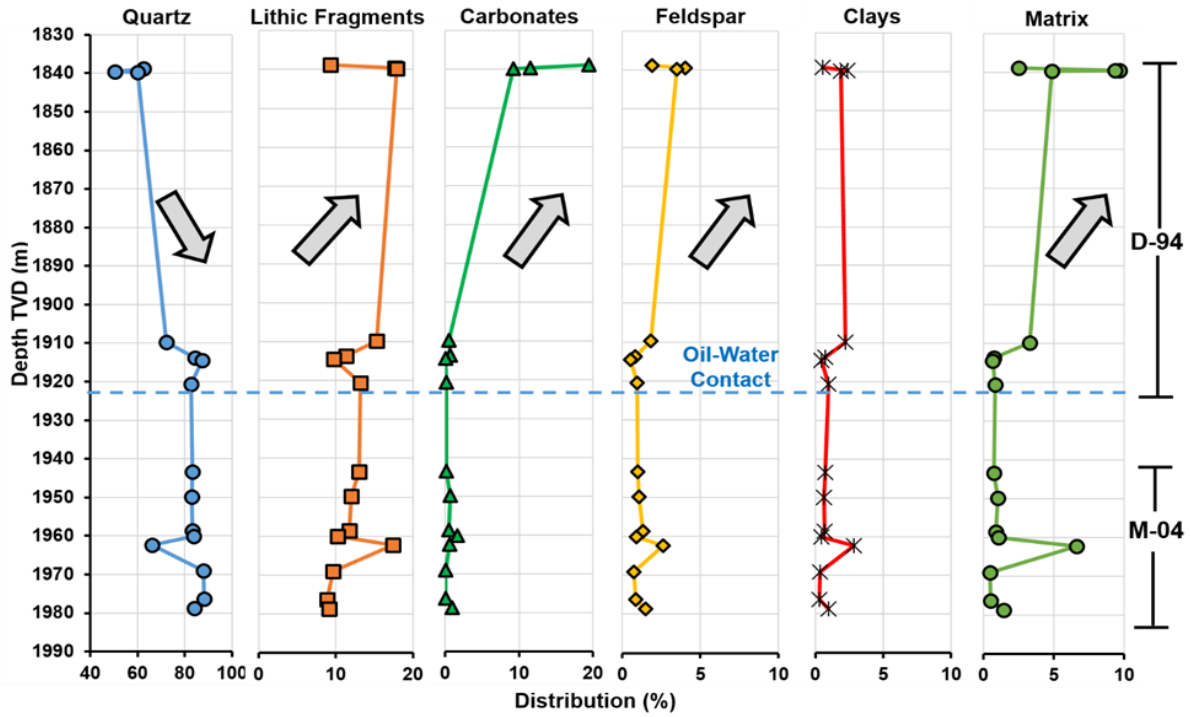


Figure 3.5. Mineralogical profile at Pool 1 reservoir

Sandstones are predominantly composed by quartz, lithic fragments, and contain up to 20% of carbonate content divided in calcareous fossil grains and cements (mainly siderite and calcite) (Figures 3.6 and 3.7). According to Folk (1980) classification, the sandstones are predominantly sublitharenites (Figure 3.8).

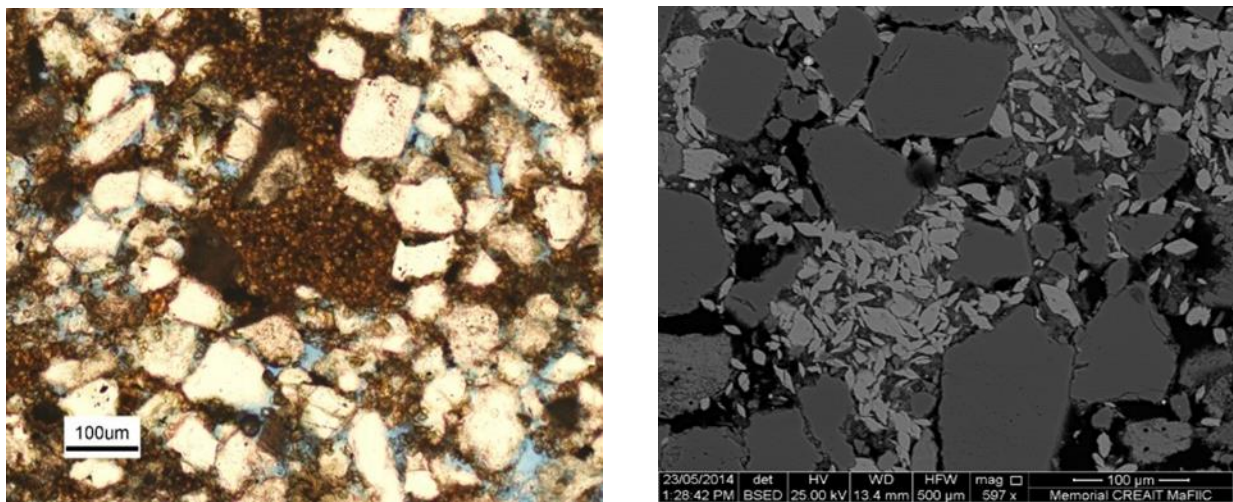


Figure 3.6. Siderite cement. A) Optical petrography (left), B) SEM (right).

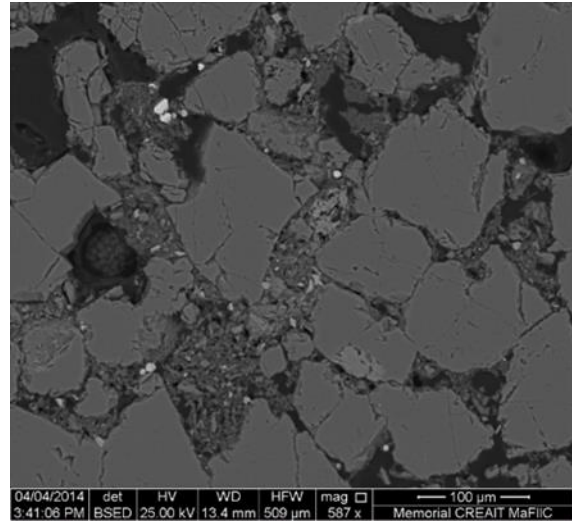
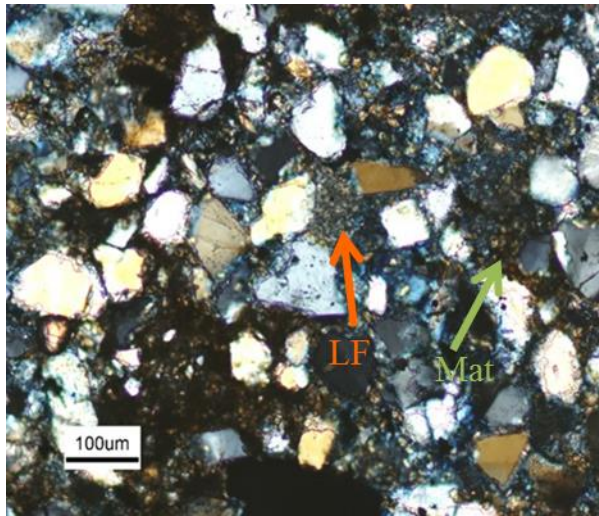


Figure 3.7. Lithic fragments (red arrow) with matrix (green arrow) of fine grains. A) Optical petrography (left), B) SEM (right).

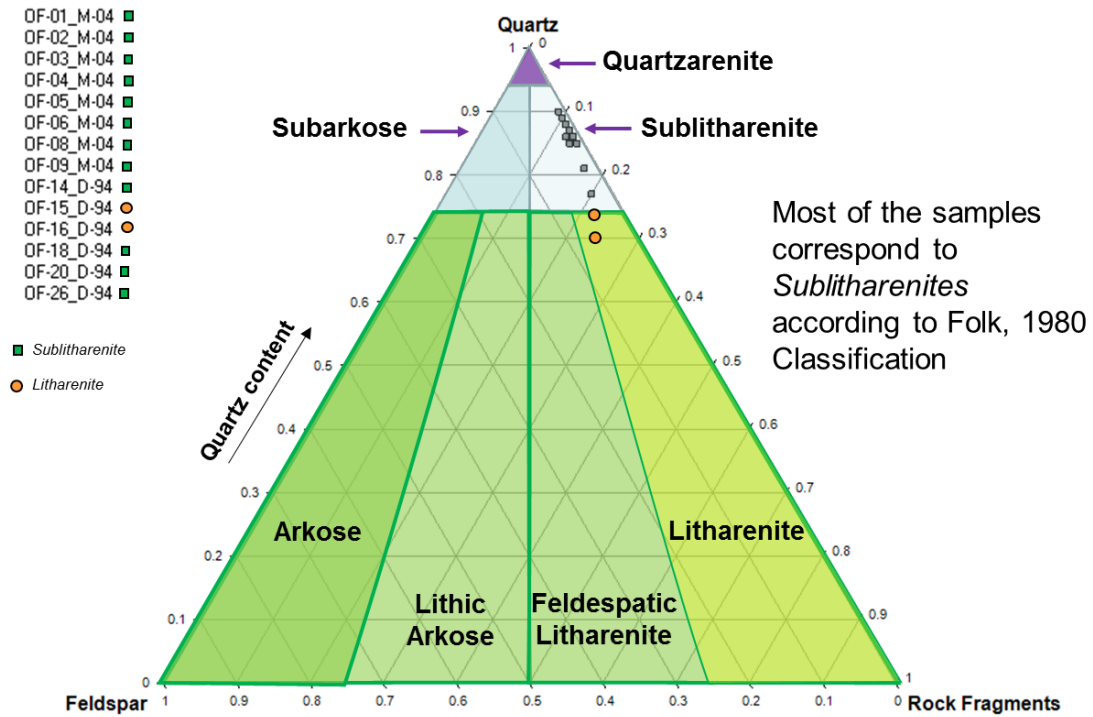


Figure 3.8. Sandstone classification.

The sandstone samples are fine to very fine-grained. Grains are very well to moderately well-sorted, with little evidence of size-sorting trends.

Intergranular porosity is the main type of porosity found in the sandstones (Valencia et al., 2017c). Some evidence of microporosity has been observed in some of the samples but mainly related to partial dissolution of potassium feldspar and other lithics fragments; there is, however, no evidence of carbonate cement dissolution.

The carbonate cements are considered the main control on reservoir quality reduction with respect to diagenetic features. Euhedral crystals of siderite are frequently found encased in calcite cement, the majority of the cement observed shows a poikilotopic and sparry texture. Any additional evidence of chemical diagenesis other than calcite cement is considered as minor in the Ben Nevis sandstones (Normore, 2006).

Normore (2006) found that the distribution and abundance of shells accumulated during the deposition of the Ben Nevis Formation were crucial to the development of authigenic cements. Based on the White Rose Field core description, cemented interval trends are directly related to shell volume and location, while isotopic evidence clearly defines aragonite shells as the source for calcite cements.

The higher content of calcite cements at the top of Pool 1 reservoir could also be explained with the diagenetic model proposed by Normore (2006), considering the transgressive development of the Ben Nevis Formation, along with general basin-wide fluid flow characteristics. According to his model (Figure 3.9), the lower volume of shell debris will result in less nucleation sites for concretions but a constant supply of calcium-rich fluids from the lower Ben Nevis will result in very well to well-cemented horizons above. A second mechanism for fluid flow into the upper Ben Nevis is laterally from the co-eval down-dip offshore transition zone where the aragonite factory is actively providing calcium-rich fluids and the compaction of the overlying Nautilus Shale is directing fluids towards the shoreline. A combination of these two flow regimes is the cause for variable cementation throughout the Ben Nevis Formation.

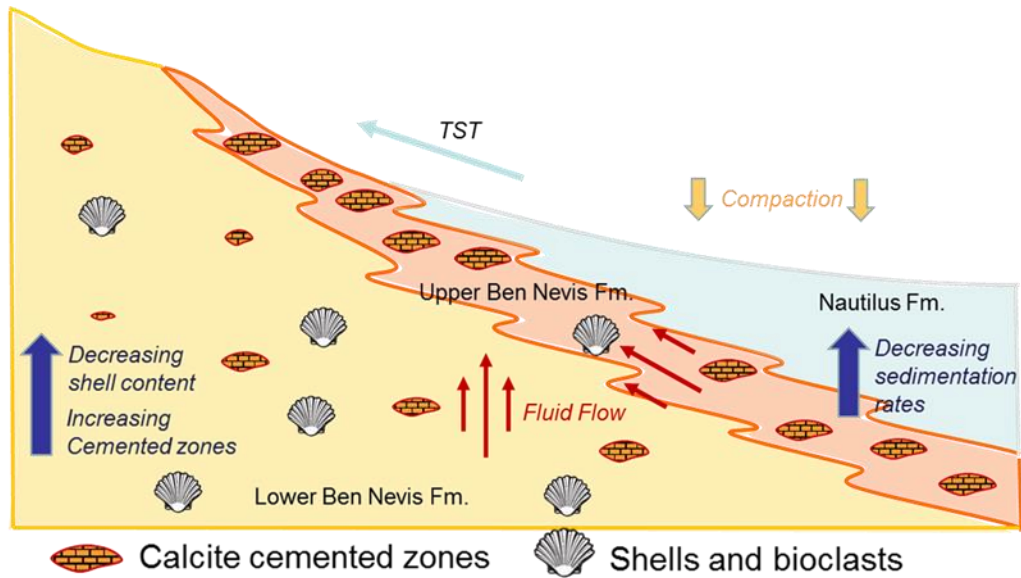


Figure 3.9. Proposed diagenetic model at Ben Nevis Formation (Pool 1). Modified after Normore, 2006.

3.5.2. Polymer Flooding Experiments

3.5.2.1. Experimental methodology error

The use of Hebron well cores for the polymer flooding experiments are representative of the field conditions. However, the heterogeneity of each core influences the results, and this cannot be separated as a single factor since it is difficult to repeat the experiments under the same conditions. Therefore, this study will consider the experimental methodology error reported in previous studies (Valencia et al. 2017a) where the same core flooding setup and experimental methodology were considered using Upper Gray Berea cores for low permeability range ($\pm 0.4\%$ of total oil recovery), and Bentheimer core for high permeability range (± 0.3 of total oil recovery).

3.5.2.2. Oil recovery results

Table 3.4 shows a detailed summary of core flooding runs performed, and figures 3.10 (a,b) and 3.11 (c,d) show the oil recovery incremental for each stage. The flooding sequence followed in this study was designed to evaluate different factors such as reservoir facies performance, polymer type, and polymer flooding timing as EOR technique for Hebron Pool1. Detailed experimental raw data and calculations can be found at appendices A, G, and H.

As discussed in Valencia et al. (2017a) a waterflooding stage after polymer flooding was considered in the flooding sequence of this research as recommended practice in the procedures described in API RP63 (1990), in order to obtain steady state conditions and determine the post-polymer flow permeability in future studies. The pore volume injected was 1 PV (polymer flooding as tertiary method) and 2 PV (polymer flooding as secondary method). Nevertheless, an additional oil recovery was also observed in this phase in both pair of experiments (~ 1%), except when it was injected after polymer flooding as tertiary method in low permeability cores, as can be seen in Fig. 3.11C.

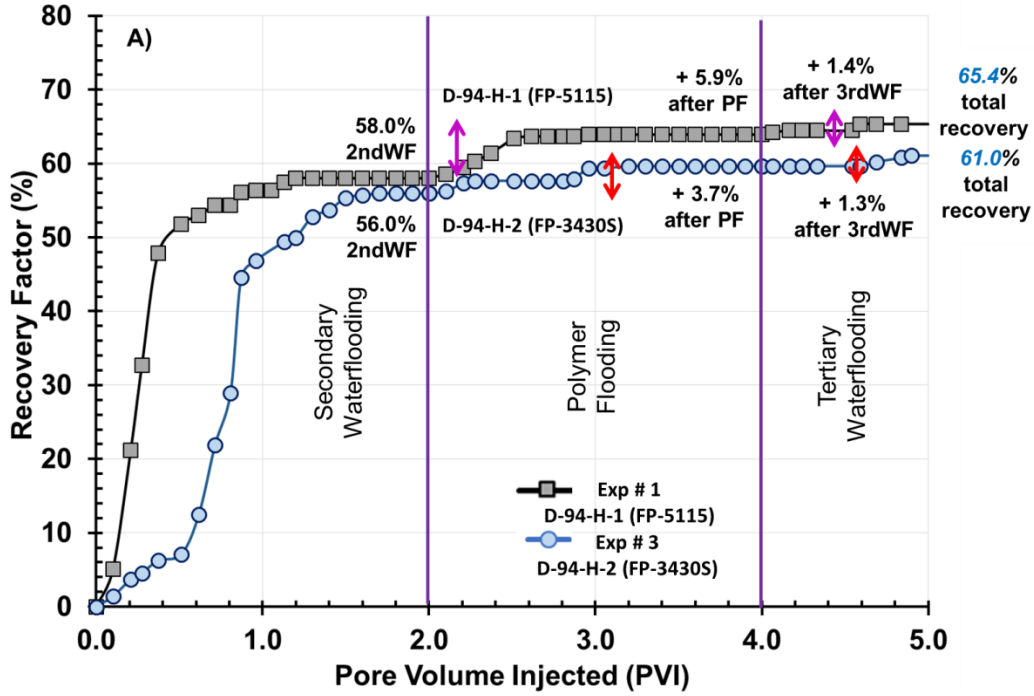
Experimental results indicate three clear trends; first, high permeability cores (labeled “H”) exhibit higher oil recovery (~ 61– 67%), as can be seen in Fig. 3.10 (a and b); this is mainly influenced by the better reservoir properties. Additionally, Figures indicate a faster oil recovery with a lower pore volume of water or polymer injection required compared with the low permeability cores (labeled “L”). According with the experiments, higher permeability seems to be always associated to higher oil recovery.

According to Valencia et al. (2016c), a potential porosity increases in the high permeability sandstones had taken place due to intergranular clay matrix detachment and partial removal from the rock sample (due to polymer flooding input/release drag) (Figure 3.12). However, further studies related to mass balance on solids produced could be helpful to support this assumption.

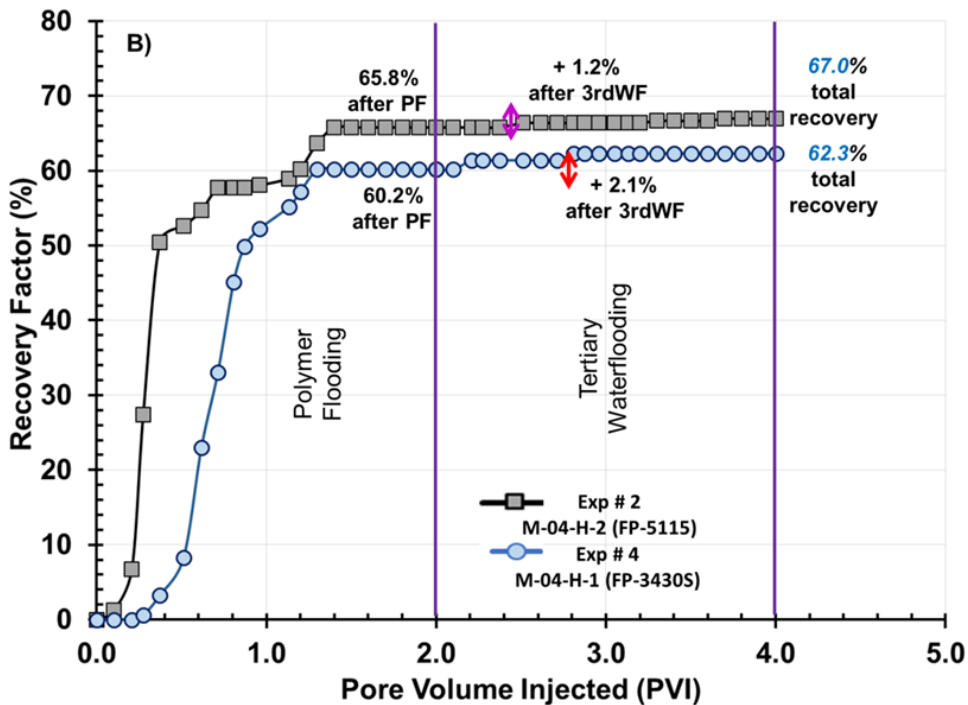
Table 3.4. Core flooding experiments results

Experiment #	Polymer Flooding Sequence	Polymer Type	Composite Core	Swc	Sor 2nd WF	2nd Water flooding Recovery (%OOIP)	Sor PF	Polymer Flooding Recovery (%OOIP)	Sor 3rd WF	3rd Water flooding Recovery (%OOIP)	Total Recovery (%OOIP)
1	Tertiary	FP-5115	D-94-H-1	0.276 ± 0.004	0.304 ± 0.004	58.0 ± 0.4	0.261 ± 0.005	5.9 ± 0.6	0.251 ± 0.005	1.4 ± 0.6	65.4 ± 0.6
2	Secondary	FP-5115	M-04-H-2	0.233 ± 0.004			0.262 ± 0.005	65.8 ± 0.6	0.253 ± 0.005	1.2 ± 0.6	67.0 ± 0.5
3	Tertiary	FP-3430S	D-94-H-2	0.238 ± 0.004	0.336 ± 0.004	56.0 ± 0.4	0.307 ± 0.006	3.7 ± 0.6	0.297 ± 0.005	1.3 ± 0.6	61.0 ± 0.6
4	Secondary	FP-3430S	M-04-H-1	0.235 ± 0.004			0.305 ± 0.007	60.2 ± 0.6	0.288 ± 0.005	2.1 ± 0.6	62.3 ± 0.5
5	Tertiary	FP-5115	D-94-L-2	0.467 ± 0.004	0.273 ± 0.004	48.8 ± 0.4	0.254 ± 0.008	3.5 ± 0.6	0.254 ± 0.005	0.0 ± 0.6	52.4 ± 0.6
6	Secondary	FP-5115	M-04-L-1	0.444 ± 0.004			0.256 ± 0.009	53.9 ± 0.6	0.254 ± 0.005	0.5 ± 0.6	54.3 ± 0.5
7	Tertiary	FP-3430S	D-94-L-1	0.434 ± 0.004	0.314 ± 0.004	44.4 ± 0.4	0.298 ± 0.010	2.9 ± 0.6	0.298 ± 0.005	0.0 ± 0.6	47.3 ± 0.6
8	Secondary	FP-3430S	M-04-L-2	0.428 ± 0.004			0.298 ± 0.010	47.9 ± 0.6	0.289 ± 0.005	1.6 ± 0.6	49.5 ± 0.5

Legend: Swc (connate water saturation), Sor 2nd WF (residual oil saturation after 2nd water flooding), Sor PF (residual oil saturation after polymer flooding), Sor 3rd WF (residual oil saturation after 3rd water flooding).

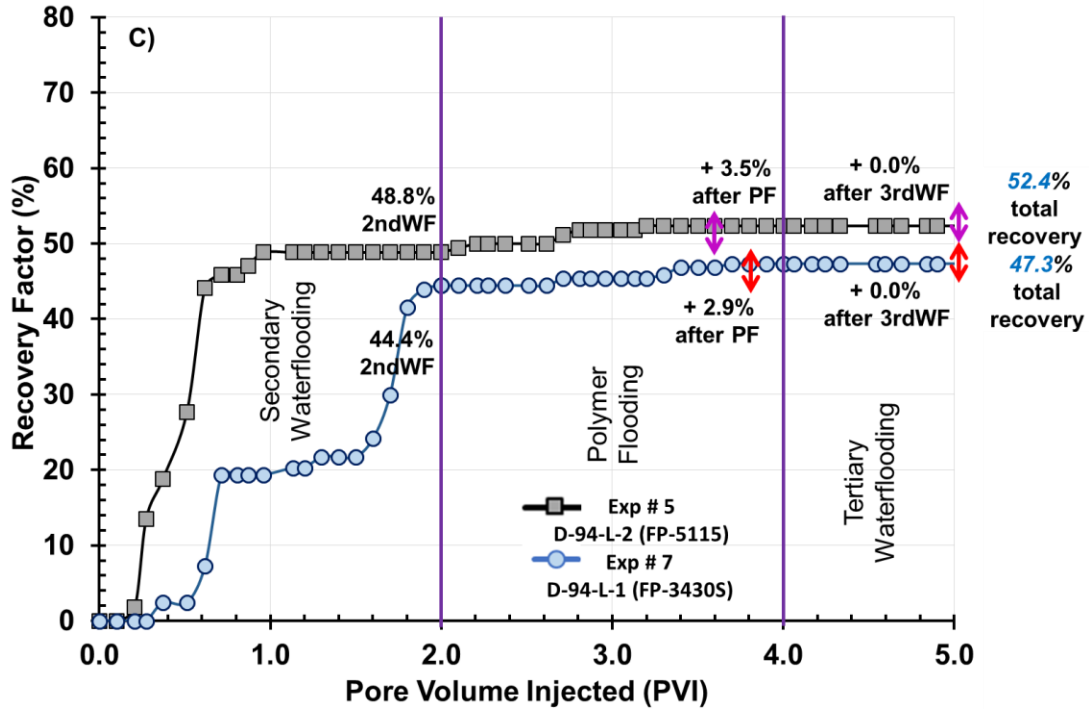


a) Total oil recovery in high permeability cores using polymer flooding as tertiary EOR technique.

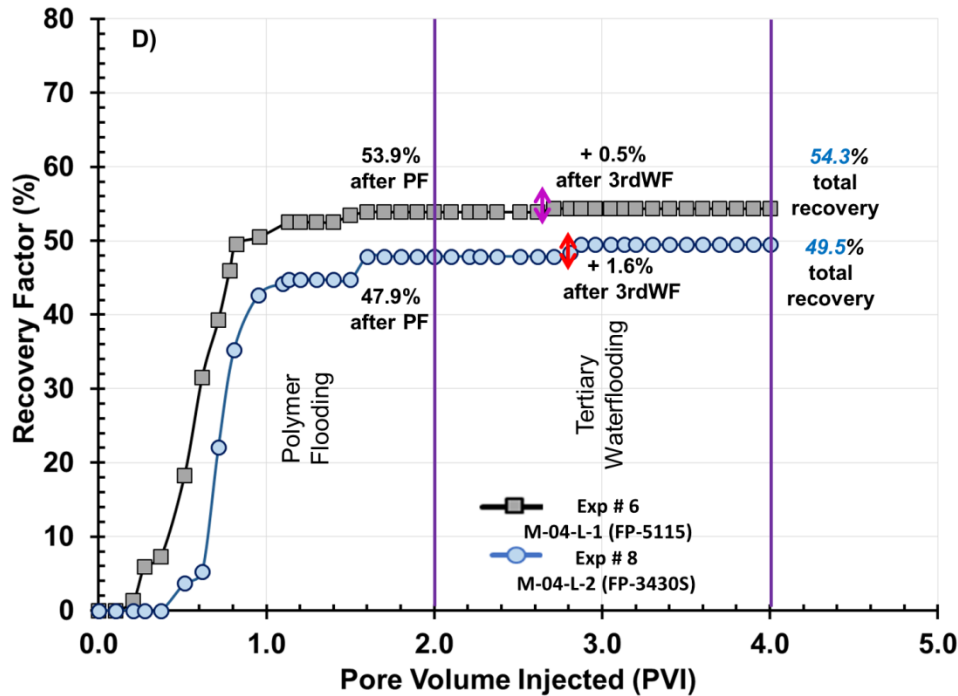


b) Total oil recovery in high permeability cores using polymer flooding as secondary EOR technique.

Figure 3.10. Total oil recovery in high permeability cores.



c) Total oil recovery in low permeability cores using polymer flooding as tertiary EOR technique.



d) Total oil recovery in low permeability cores using polymer flooding as secondary EOR technique.

Figure 3.11. Total oil recovery in low permeability cores.

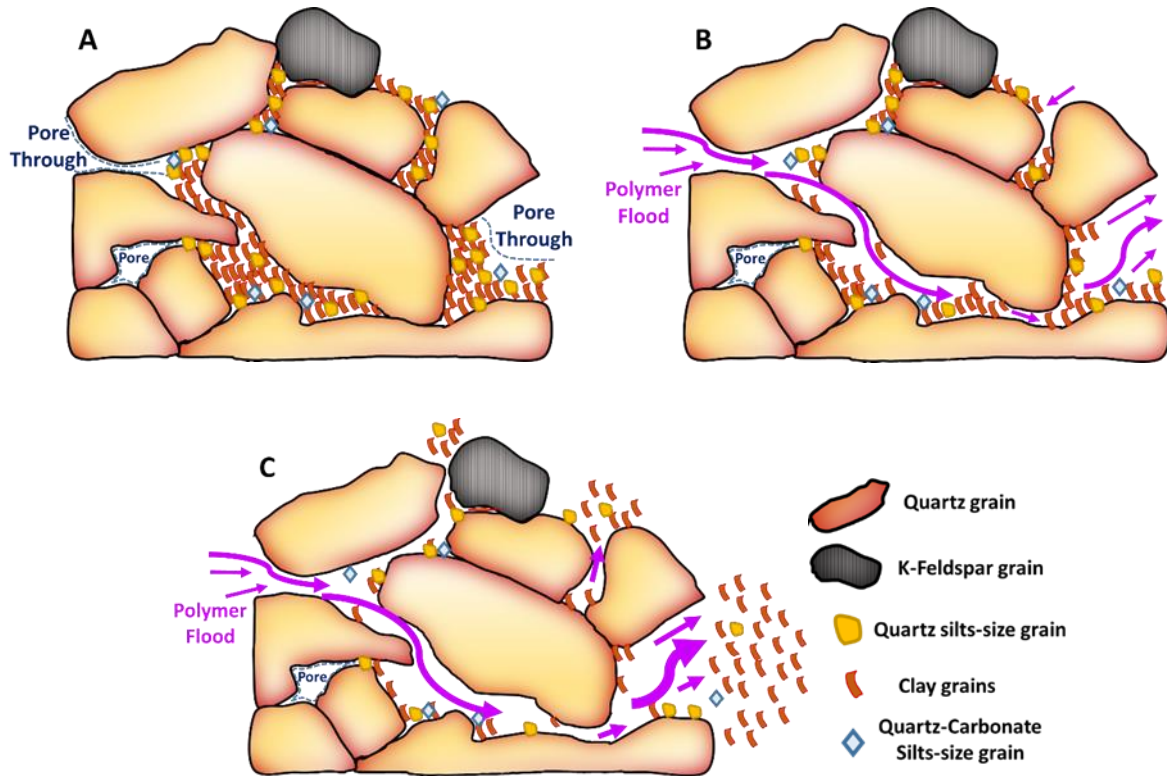


Figure 3.12. Proposed fluid-rock mechanism interaction model (modified after Valencia et al., 2016b).

The second observation from the experimental results is a higher oil recovery from experiments (#1, #2, #5 and #6) using FP-5115 polymer (Figures 3.10a, 3.10b, 3.10c, and 3.10d, respectively) regardless of the permeability facies or flooding sequence order. This could be attributed to the presence of acrylamide tert-butylsulfonic acid (ATBS) in its composition. According to Fink (2015), ATBS molecules are larger in size and provide significant chain rigidity and hence a better shear stability. Further, Gaillard et al. (2014) demonstrated through aging and core flooding experiments that polymers with ATBS in specific amount in their structure improves thermal and salt stability. They also suggested that some such polymers could withstand harsh reservoir conditions with little loss of viscosity for an aging time of at least one year. On the other hand, FP-5115 has a lower molecular weight than FP-3430S allowing it to propagate effectively through smaller pore-throats common in low permeability porous media.

A relatively low but consistent difference is seen in the oil recovery percentage when the evaluating variable is the flooding sequence order. For example, in comparing the second experiment to the first experiment (Fig. 3.10b vs Fig. 3.10a), both have cores with the same polymer (FP-5115) and similar permeability range; however, the second experiment (secondary polymer flooding) showed a higher oil recovery. This trend is repeated in all the experiments where the variable is the flooding sequence order such as experiments: #4 vs. #3 (Fig. 3.10b vs Fig. 3.10a), #6 vs. #5, and #8 vs. #7 (Fig. 3.11d vs. Fig. 3.11c). Based on this, incremental oil recovery is reached much sooner when polymer flooding is applied as secondary method; therefore, applying polymer flooding at early stage in Hebron Pool 1 potentially could generate a higher NPV, in case this EOR technique is considered to be applied anytime during the Hebron Field development cycle.

It is observed that the oil recovery is relatively more continuous in low permeability cores when polymer flooding (experiments #6 and #8, Fig. 3.11d) is applied as secondary method compared to those experiments in which is applied as tertiary method instead (experiments #5 and #7, Fig. 3.11c). All four core types used in these experiments have a similar lithology characterized by 9-12% of carbonates; therefore, more continuous oil recovery could be attributed to the sweep effect of the polymer flood front, even in low permeability cores where carbonate cements could act as barriers.

Thus, establishing polymer flooding operations at an early stage of Pool 1 development could be beneficial for the field to improve the oil recovery factor in a shorter time. Figures 3.10, 3.11, and table 3.4 show that an additional oil recovery of 3 to 6% is obtained when polymer flooding is applied after a water flooding stage; this could be significant depending on the project economics.

The core permeability range is the variable with the highest impact on the oil recovery according to the core flooding results; as can be seen in Fig. 3.13, the highest difference between pair of experiments is related to the core permeability facies. Therefore, a lower sweep efficiency of polymer floods to the top of Pool 1 reservoir is expected, influenced by the calcite cement increase, hence reducing reservoir properties due to the diagenetic history.

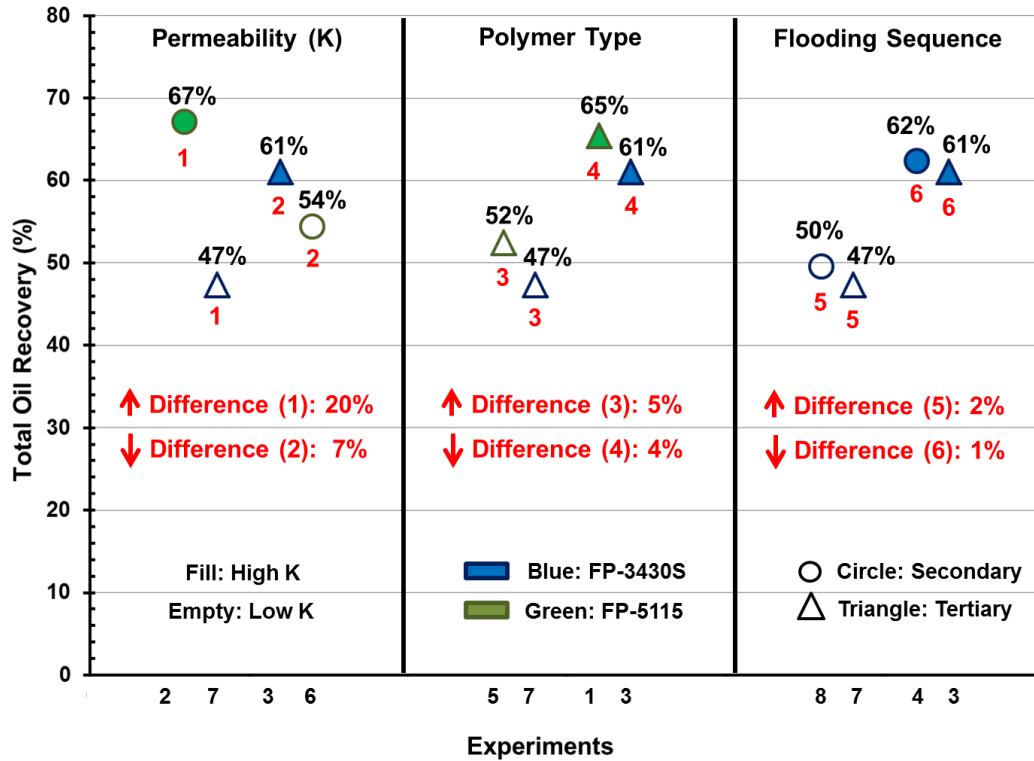


Figure 3.13. Influence of experimental variables on Total oil recovery difference between pair of experiments

Figure 3.14 illustrates the pressure drop along the core sample as a function of the pore volume injected. The pressure differential rate (dP) varies more in the experiments performed in low permeability cores (B) than high permeability cores (A). The injected fluids (injection water and polymers) need to overcome a higher barrier when the pore throats are narrower, generating a higher pressure release once the impediment is passed. In the case of the polymer flooding phase, a mechanical entrapment process also occurs in low permeability cores. Polymer molecules will trap and block the path, and probably cause more trapping upstream of the blockage. Another observation from these experiments is the correlation between the higher pressure drop and higher oil production for all the flooding sequence phases.

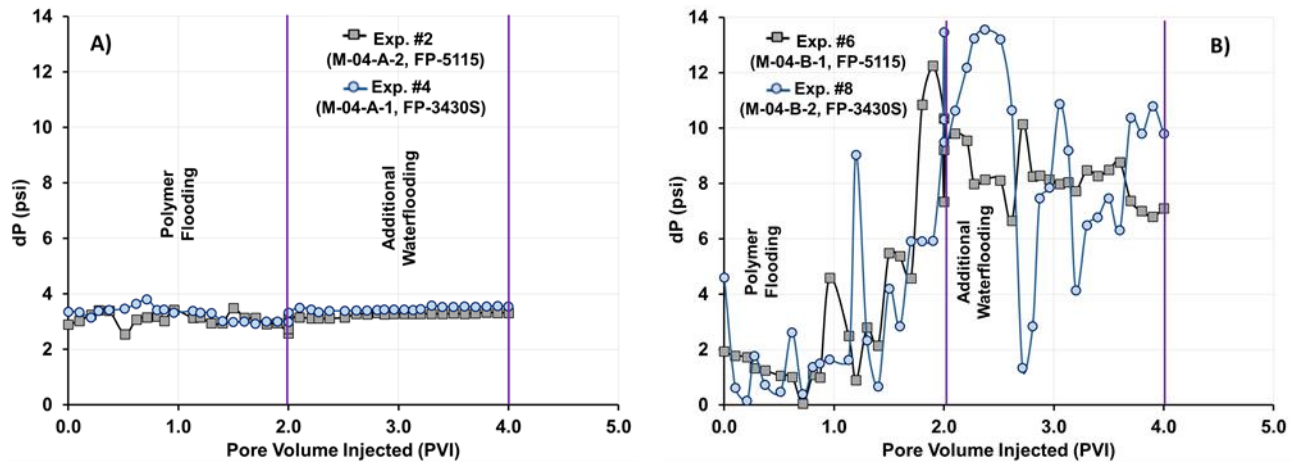


Figure 3.14. Pressure profile during flooding sequence. A) High permeability cores; B) Low permeability cores.

3.6. Conclusions

Coreflooding experiments using Hebron cores at Pool 1 reservoir conditions were used to evaluate potential polymer flooding EOR technique application at Hebron Field. Two polymers were used in the study to investigate how the concentration, salinity and reservoir temperature affected the polymer viscosity. On the other hand, reservoir characterization performed before and after the experiments allowed to identify potential rock fabrics changes due to the polymer flooding.

The effects of the aforementioned parameters on oil recovery at Pool 1 are as follow:

- The Ben Nevis reservoir (Pool 1) mineralogical characterization indicates upward increase in carbonate cementation events and clay content due to the depositional setting, which is correlated with reservoir quality reduction.
- Using polymer flooding as an EOR method in the Ben Nevis Fm. (Pool 1) could potentially increase oil recovery in a range of 3-6%, based on coreflooding experiments conducted using composite Hebron cores at reservoir conditions.

- Permeability facies is the most influential variable on the oil recovery achieved in Ben Nevis Formation (Pool 1). A difference of 20% of total oil recovery could be observed between cores of high and low permeability.
- The FP-5115 polymer consistently proved to be more suitable to increase the oil recovery in Ben Nevis Fm. (Pool 1), potentially due to a higher viscosifying power and stability character.
- Applying polymer flooding as a secondary method showed a consistently higher increase in the incremental oil recovery of 1-2% than applying it as a tertiary method; thus it is highly recommended to apply polymer flooding as soon as possible, preferably before water flooding if this EOR technique is considered in the field development cycle.
- The influence of Pool 1 diagenetic features on enhanced oil recovery may be minimized by using polymer flooding as an initial stage, even in low permeability facies.

3.7. Acknowledgements

Thanks to Hibernia EOR lab and MUN-CREAIT staff for their support during the experimental work. Special thanks to SNF Floerger for generously providing the polymers sample, and Canada Newfoundland Offshore Petroleum Board (C-NLOPB) for the Hebron well core plugs. This work was generously supported by Hibernia Management and Development Company (HMDC), Chevron Canada, the Natural Sciences and Engineering Research Council of Canada (NSERC), the Canada Foundation for Innovation (CFI), Research and Development Corporation of Newfoundland (RDC), and Petroleum Exploration Enhancement Program (PEEP).

4.8. References

Al Adasani, A. and Bai, B., 2011. Analysis of EOR projects and Updated Screening Criteria. *J. Petrol. Sci. Eng.* 79 (2011): 10-24.

Alvarado, V. and Manrique, E. 2013. Engineering Design Challenges and Opportunities beyond Water flooding in Offshore Reservoirs. Presented at the 2013 Offshore Technology Conference, Houston, U.S.A., 6-9 May. OTC 24105.

ExxonMobil 2011. Hebron Project Development Plan. Retrieved from Hebron Project website http://www.hebronproject.com/media/3908/hda_vol_2.pdf (accessed May 2016).

Fink, J. 2015. Petroleum Engineer's Guide to Oil Field Chemicals and Fluids. Elsevier p. 825.

Folk, R.L. 1980. Petrology of Sedimentary Rocks. Hemphill Publishing Co., Austin, Texas, p. 182.

Gaillard, N., Giovannetti, B., Favero, C., Caritey, J.P., Dupuis, G., Zaitoun, A. 2014. New Water Soluble Anionic NVP Acrylamide Terpolymers for Use in Harsh EOR Conditions. Presented at the 2014 SPE Improved Oil Recovery Symposium, Tulsa, U.S.A, 12-16 April. SPE 169108-MA.

Maia, A., Borsali, R. and Balaban, R. 2009. Residual Comparison between a Polyacrylamide and a Hydrophobically Modified Polyacrylamide Flood in a Sandstone Core. Mater. Sci. Eng. C 29 (2009): 505-509.

Mosavat, N., Rasaei, M.R., and Torabi, F. 2013. Experimental Determination of Absolute and Relative Permeability in Composite Cores: Effect of Ordering. Special Topics & Reviews in Porous Media – An International Journal. 4 (1): 33-43.

Morad, S., Al-Ramadan, K., Ketzer, J.M., and De Ros, L.F. 2010. The Impact of Diagenesis on the Heterogeneity of Sandstone Reservoirs: A Review of the Role of Depositional Facies and Sequence Stratigraphy, AAPG Bull. 94 (8): 1267-1309.

Normore, L. 2006. Origin, Distribution and Paragenetic Sequence of Carbonate Cements in the Ben Nevis Formation, White Rose Field, Jeanne d'Arc Basin, Offshore Newfoundland, Canada. Memorial University of Newfoundland, St. John's, Canada.

Langaas, K., Ekram, S., and Ebeltoft, E. 1998. A Criterion for Ordering Individuals in a Composite Core. *J. Petrol. Sci. Eng.* 19 (1998): 21-32.

Ledolter, J., and Swersey, A. 2007. *Testing 1-2-3: experimental design with applications in marketing and service operations.* Stanford University Press. 312 p.

Levitt, D.B., Slaughter, W., Pope, G.A., and Jouenne, S., 2011. The Effect of Redox Potential and Metal Solubility on Oxidative Polymer Degradation. *J. SPE Reserv. Eval. Eng.* 14 (3): 287-298. SPE-129890-PA.

Saboorian-Jooybary, H., Dejam, M., and Chen, Z. 2016. Heavy Oil Polymer Flooding from Laboratory Core Floods to Pilot Tests and Field Applications: Half-Century Studies. *J. Petrol. Sci. Eng.* 142 (2016): 85-100.

Seright, R. and Skejvrak, I. 2015. Effect of Dissolved Iron and Oxygen on Stability of Hydrolyzed Polyacrylamide Polymers. *SPE Journal.* 20 (3): 1-9. SPE-169030-MS.

Shannon, P.M., Croker, P.F. and Sinclair, I.K. 1995. Tectonic Controls on Upper Jurassic to Lower Cretaceous Reservoir Architecture in the Jeanne d'Arc Basin, with some Comparisons from the Porcupine and Moray Firth Basins. *Geological Society, London, Special Publications* 93 (1995): 467-490.

Sheng, J.J., Leonhardt, B., Al-Azri, N. 2015. Status of Polymer Flooding Technology. *J Canadian Petroleum Technology* 54 (02): 116-126. SPE -174541-PA.

Shu, W.R., 1984. A Viscosity Correlation for Mixtures of Heavy Oil, Bitumen, and Petroleum Fractions. *SPE Journal.* 24 (3): 277-284. SPE-11280-PA.

Szpakiewicz, M., McGee, K., and Sharma, B. 1987. Geological Problems Related to Characterization of Clastic Reservoirs for EOR. *SPE Formation Evaluation Journal* 2 (4): 449-460. SPE-14888-PA.

Taber, J.J., Martin, F.D., and Seright, R.S. 1997. EOR Screening Criteria Revisited - Part 1: Introduction to Screening Criteria and Enhanced Recovery Field Projects. *J. SPE Reserv. Eng.* 12 (3): 189-198. SPE-35385-PA.

Taber, J.J., Martin, F.D., and Seright, R.S. 1997. EOR Screening Criteria Revisited - Part 2: Applications and Impact of Oil Prices. *J. SPE Reserv. Eng.* 12 (3): 199-205. SPE-39234-PA.

Tankard, A.J. and Welsink, H. J. 1987. Extensional Tectonics and Stratigraphy of Hibernia Oil Field, Grand Banks, Newfoundland. *AAPG Bulletin* 71 (10): 1210-1232.

Valencia, L.E., James, L.A., Azmy, K. and Walsh, J. 2015. Polymer Screening for the Hebron Field, Offshore Eastern Canada: Facing High Salinity Brines. Presented at 77th EAGE Conference and Exhibition, Madrid, Spain, 1-4 June.

Valencia, L.E., James, L.A., and Azmy, K. 2017a. Laboratory Scale Characterization Methodology for Offshore Polymer Flooding Project: Hebron Field, Eastern Canada (unpublished paper).

Valencia, L.E., James, L.A., and Azmy, K. 2017c. Image Analysis of Pore Network Evolution of Ben Nevis Formation Sandstones under Experimental Polymer Flooding (unpublished paper).

Xiong, D., Azmy, K., Blamey, N. 2016. Diagenesis and origin of calcite cement in the Flemish Pass Basin sandstone reservoir (Upper Jurassic): Implications for porosity development. *Marine and Petroleum Geology* 70 (2016): 93-118.

Weber, K.J. 1982. Influence of Common Sedimentary Structures on Fluid-Flow in Reservoir Models. *J Pet Technol* 34 (3): 665-672. SPE-9247-PA.

CHAPTER 4. IMAGE ANALYSIS OF PORE NETWORK EVOLUTION OF BEN NEVIS FORMATION SANDSTONES UNDER EXPERIMENTAL POLYMER FLOODING

To be submitted to *Bulletin of Canadian Petroleum Geology*.

Luis E. Valencia, Lesley James, Karem Azmy*

Memorial University of Newfoundland, St. John's, Canada

* Corresponding author e-mail: kazmy@mun.ca

Keywords: Image Analysis, Polymer Flooding, Ben Nevis Formation, Hebron Field.

4.1. Abstract

Digital image analysis (DIA), along with microscopic petrographic analysis, can be applied to improve pore system characterization in sedimentary rocks. The current study focuses on the application of these techniques to study the evolution of rock pore networks in Ben Nevis Formation sandstones from the Hebron Field, offshore Newfoundland, which were subjected to experimental polymer flooding injection. DIA protocol can be summarized in the following stages: (i) detailed pre- and post-injection description of mineralogy and texture seen in thin sections using optical and scanning electron microscopy - mineral liberation analysis (SEM-MLA) technique; (ii) adjustment and calibration of DIA tools; (iii) data acquisition protocol; and (iv) study and quantification of porosity by DIA.

The DIA results highlight the petrographic changes observed in the investigated samples. Polymer flooding injection in high permeability sandstones resulted in a relative porosity increase, whereas the low permeability sandstones showed the opposite. Other minor changes, such as variations in the roughness and roundness of pore edges were observed.

4.2 Introduction

The development of quantitative imaging techniques applied to geoscientific approaches provides not only the ability to visualize petrographic changes, but also analyze data (Pirard et al., 2001). Quantitative imaging techniques have been increasingly applied in recent years to geological attributes that are either too large, buried below the ground surface, or too small to be examined.

On the reservoir characterization scale, porosity and mineral textures are essential parameters to better understand the system. The measurement of pore structures can also be valuable in the identification of geologic controls on porosity and permeability distributions.

The digital image analysis represents an important advance over traditional techniques (e.g. point counting) to automate the characterization of objects (Berrezueta et al., 2015) since measurements made from two-dimensional sections record only the porosity as resolvable from an optical image of the sample (total optical porosity).

Identifying minerals in the reservoir is more challenging than establishing the classification of porous systems based on image analysis of thin sections. This research focused on the use of the mineral liberation analyzer (MLA) to identify mineral phases prior to the definition of the pore network quantification.

The MLA is a scanning electron microscope (SEM) combined with energy dispersive X-ray (EDX) spectrometers, and a computer software that automates microscope operations and data acquisition for automated mineralogy evaluation. Samples recommended for this technique are polished surfaces of rocks, sediments or other particulate samples. The technique allows us to quantify data sets such as modal mineralogy, porosity, grain size and shape, mineral associations and digital textural maps. MLA measurements are based on backscattered electron (BSE) image analysis for determining grain boundaries and locations for X-ray spectral acquisition, and classification of the characteristic x-ray spectra of mineral species by comparison to a library of reference spectra (Sylvester, 2012).

According to Sylvester (2012), some of the advantages of the MLA over traditional optical microscopy for mineralogical investigations are: (a) the replacement of tedious manual analysis by systematic, computer-automated analysis, reducing the potential for operator bias and human error; (b) the increased through-put and the number of mineral grain examined, thus providing a more statistically representative analysis of a sample; and (c) the ability to distinguish fine-grained or complex inter-grown minerals at the micrometre scales.

As an interface between the image and the pore network quantification, J MicroVision 1.2.7, image analysis toolbox is used for measuring and quantifying components of SEM high-definition images, specifically porosity values. The software program includes most of the common image processing operations, an efficient visualization system, and tools to quantify either manually or automatically (Roduit, 2015).

Experimental polymer flooding was conducted on Ben Nevis (BN) Formation sandstones from Pool 1, Hebron Field, the first heavy oil field in offshore Eastern Canada (Valencia et al., 2017a). The porosity evolution was investigated as part of an ongoing study aimed at identifying polymers that can be applied to this field. In this study, the application of digital image analysis (DIA) is focused on quantifying changes in the pore system of Ben Nevis Formation sandstones before and after being flooded by polymer solutions at the core scale.

The Ben Nevis Formation at the Hebron Field consists of fine-grained sandstone of a marine shoreface environment. It is anticipated to produce approximately 70% of the Hebron Project's recoverable crude oil, the fourth major offshore development in Newfoundland and Labrador with more than 700 million barrels of recoverable resources. First oil is expected in late 2017. Hebron crude oil is considered heavy with an API gravity of 17 – 24° API (ExxonMobil, 2011).

The project workflow considers segmentation of the porous system by regions, and applying the “thresholding” segmentation method (i.e. based on threshold values to turn a raw image into a binary one, the pixels being partitioned are dependent on their intensity value). Based on this principle, the evolution

of small changes in the configuration of pore network is quantified (Zhou et al. 2004; Berrezueta et al. 2015).

In the following sections, data acquisition methods and porosity quantification are described and explained in detail. The objectives of this study can be summarized as follow:

- Propose an integrated DIA methodology using SEM-MLA images.
- Quantify the porosity changes occurring when the formation rock interacts with polymer floods at Pool 1 temperature and pressure reservoir conditions.
- Evaluate potential textural changes in the rock fabric associated with the polymer injection.

4.3 Geological Settings

4.3.1. Regional Tectonic History

The Hebron Field is located in the Jeanne d’Arc Basin, approximately 300 km south-east of St. John’s, Newfoundland (Fig. 4.1) in an average water depth of 110 m. The basin structure is a northeast plunging, trough shaped, half graben located on the edge of the Grand Banks (Fig. 4.2). The basin dimensions range from 25 to 80 km wide to 130 km long with a maximum sediment thickness of about 20 km. The main structural components defining the Jeanne d’Arc Basin are the Bonavista platform to the west, the Cumberland Volcanic Belt to the north, the Central Ridge Complex to the east, and the Avalon uplift to the south (Figure 4.1). The western boundary of the basin is formed by the listric Murre Fault whereas the eastern boundary is defined by the antithetic Voyager fault (Tankard and Welsink, 1987).

The Jeanne d’Arc rift basin is wider in the north than the south and trends northeast-southwest. The basin formed as a result of prolonged extension from the Triassic to Lower Cretaceous. The Jeanne d’Arc Basin was created from meta-sedimentary and crystalline rocks of Precambrian to Early Paleozoic age Avalon basement (Tankard and Welsink, 1987). The Avalon basement was deformed during the Caledonian and Hercynian orogeny during the development of Pangea.

Multiple Mesozoic rifting episodes on the Grand Banks started in the Late Triassic, preceding the break-up of the Pangaea supercontinent and the ancestral opening of the North Atlantic Ocean, dominated the tectonic and sedimentation style of the Jeanne d'Arc Basin (ExxonMobil, 2011).

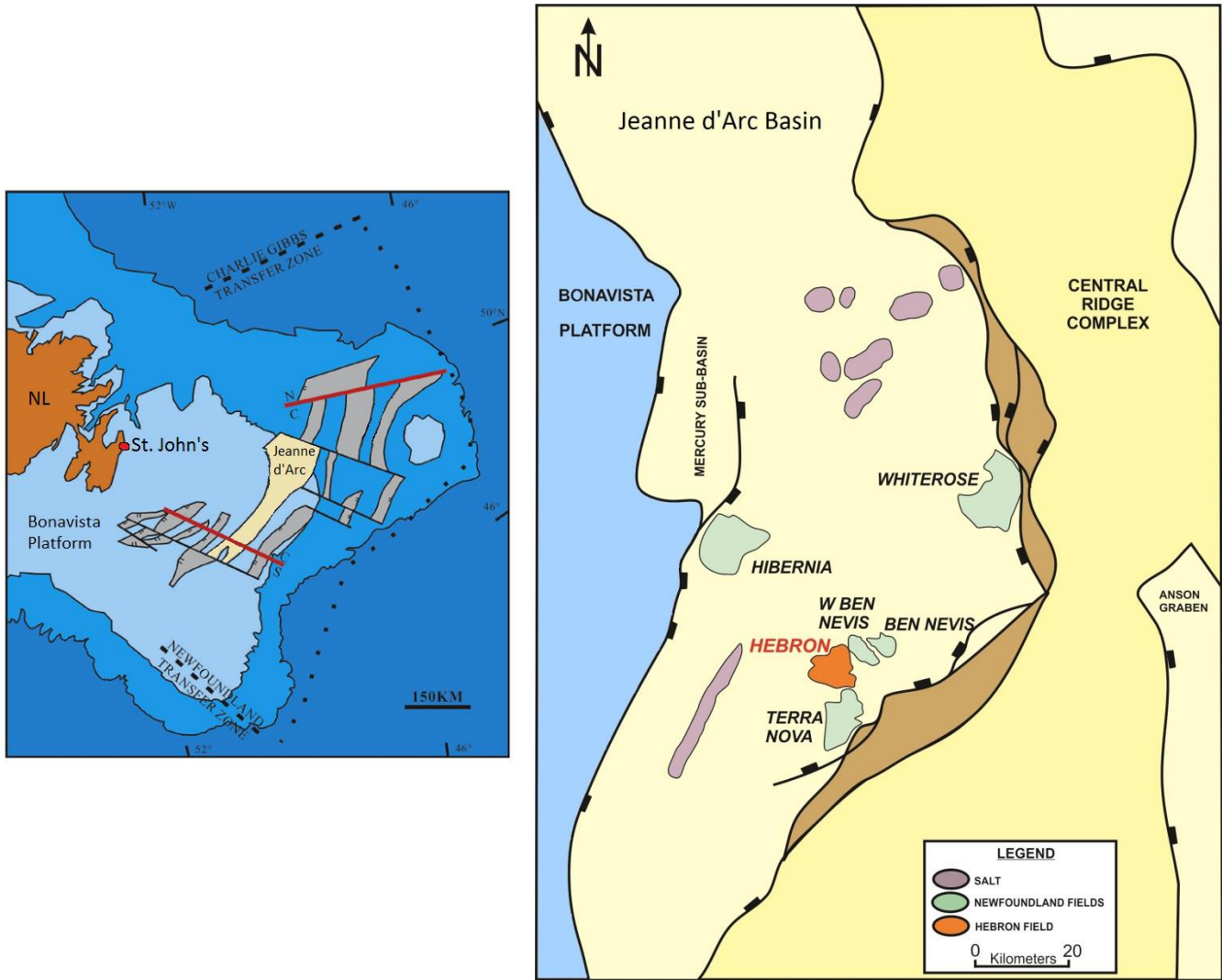


Figure 4.1. Hebron Field location at Jeanne D'Arc Basin (modified after ExxonMobil, 2011, Xiong et al, 2016).

4.3.2. Hebron Field Structural Geology

The Hebron Field lies on a horst block with a graben to the southwest and to the northeast (Fig.4.2). The horst block is part of the north-south trending and north-plunging Terra Nova anticline and the fault-bound basin-dividing northwest-southeast “trans-basin” trend. The trapping configuration of the Ben Nevis and Hibernia Reservoirs on the horst block is fault-dependent three ways. The Jeanne d’Arc Reservoir has a combination of structural and stratigraphic trap configuration (Shannon et al., 1995).

The fault setting is comprised of NW-SE striking faults in the field-range from less than 0.5 km to 4.5 km in length dipping predominantly to the northeast between 55° and 60°. The exception to this is the Hebron Fault, which dips between 55° and 60° to the southwest and creates the Hebron horst fault block. The pools are in structural traps defined by the major faults comprising the fault blocks. The oil-water contacts are determined by spill-points between the fault blocks (ExxonMobil, 2011).

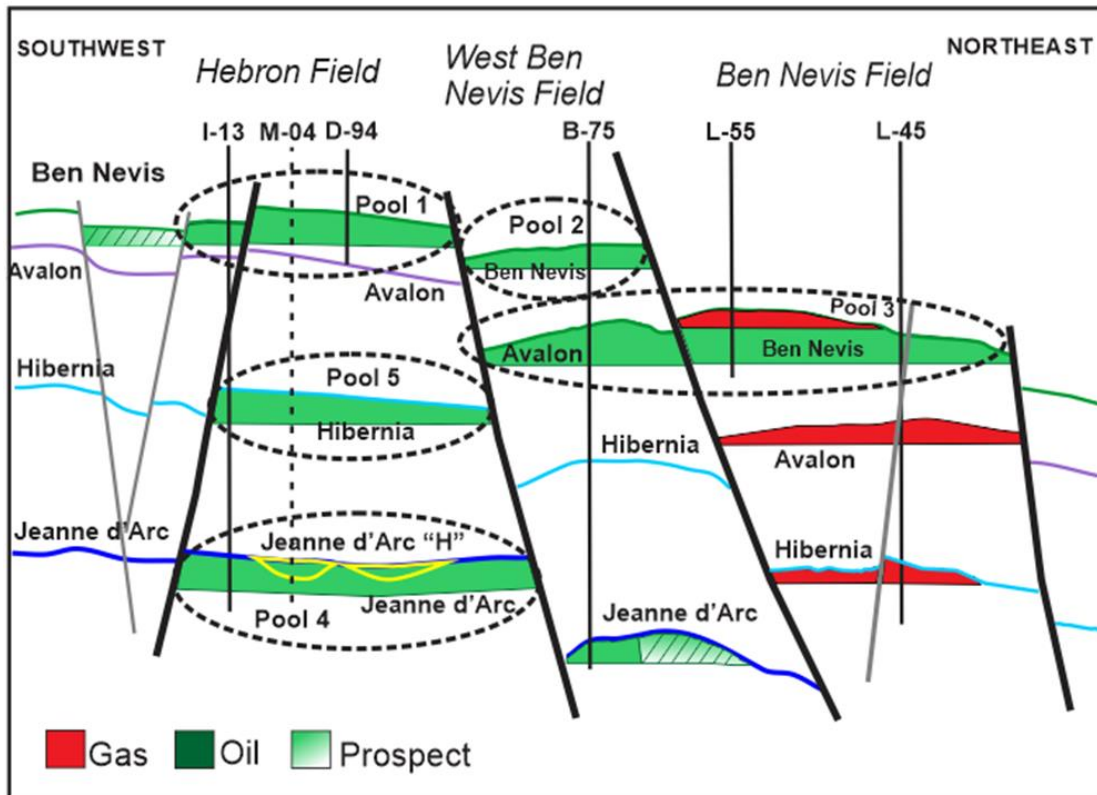


Figure 4.2. Hebron Field structural section (modified after ExxonMobil, 2011).

4.3.3. Hebron Field Stratigraphy

The three main reservoirs for the field are the Ben Nevis, Hibernia, and Jeanne d'Arc Formations. The Ben Nevis Formation (Upper Aptian to Albian), unconformably overlies the Avalon Formation. It consists of 125 m to 500 m thick succession of upward fining of fine- to very fine-grained calcareous sandstone with interbedded thin layers of sandy limestone grading upward into glauconitic siltstone and shale (Shannon et al., 1995).

The depositional environment is primarily lower to upper shoreface, with subtle facies changes, highly correlative, and a very high net-to-gross ratio. On a more detailed scale, the depositional environment and stratigraphy are more complicated and the cores show many cycles of wave-dominated marine depositional events that encompass a range of facies (upper shoreface to offshore marine). Individual cycles are thin (tens of centimetres), and are interpreted to be laterally extensive (one to tens of kilometres). The dominant environment of deposition on the horst block of the Hebron Field is proximal lower shoreface. The reservoir package has occasional coquinas, made of shallow marine shell debris, and rare shales (ExxonMobil, 2011).

4.4. Materials and Methods

4.4.1. Core Plug Samples

The current investigation examines core plugs selected from Hebron Field exploration well cores at Pool 1 reservoir level, cores #1 and #6 of the D-94 well (1999) and core #2 of the M-04 well (2000), as shown in Figure 4.3. These samples were provided by the Canada-Newfoundland and Labrador Offshore Petroleum Board (C-NLOPB), and preliminary selection was based on core availability, permeability ranges obtained from previous SCAL tests, and visual inspection. Composite core dimensions were 1.5 inches in diameter and 6 inches in length (Figure 4.4).

In order to establish meaningful experiments and consider the quantity of core plugs available, eight experiments were defined using four composite cores, with a permeability range of 1340 - 1400 mD

(representing high permeability facies), and four composite cores with a range of 50-120 mD (representing low permeability facies) (Valencia et al., 2017b).

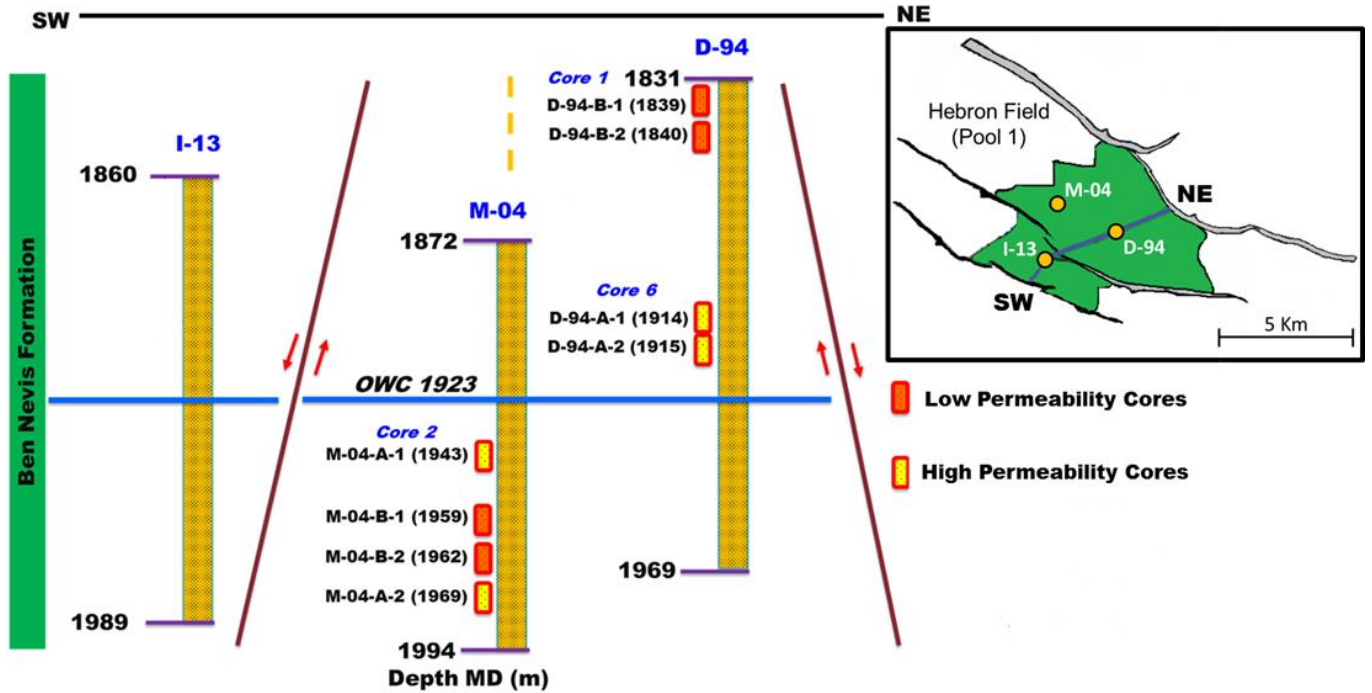


Figure 4.3. Composite cores samples location (map modified after ExxonMobil, 2011).



Figure 4.4. Composite core after polymer flooding.

4.4.2. Rock Mineralogy and Textures

4.4.2.1. Optical Microscopy

Petrographic techniques are used to provide detailed mineralogical composition, textural characteristics and information on post depositional history of sedimentary rocks. Fifteen polished thin sections were cut from D-94 and M-04 wells core plugs before polymer flooding experiments, and eight polished thin sections after polymer flooding; impregnated with blue dyed epoxy to identify porosity and stained with a mixture of alizarin red and potassium ferricyanide distinguish ferroan deep-burial carbonate cements. Prior to flooding, these sections were petrographically examined by a Nikon Eclipse E600 POL polarizing microscope attached to a Nikon DXM 1200F digital camera.

4.4.2.2. Scanning Electron Microscopy (SEM) - Mineral Liberation Analyzer (MLA)

Polished thin sections cut before and after flooding were evaluated using the SEM-MLA technique by a scanning electron microscope (FEI MLA 650 FEG), equipped with high throughput energy dispersive x-ray (EDX) and analytical systems from Bruker that included the x-ray aided image analysis MLA.

4.4.3. Digital Image Analysis (DIA)

4.4.3.1. Image Acquisition

The DIA before and after polymer flooding was performed on eight polished thin sections that were selected based on the preliminary evaluation by optical microscopy, and the number of experiments defined by experimental design. Twelve images or scenes from each thin section were obtained using the SEM technique, following a systematic pattern that had consistent standard image magnification and scale for all the images evaluated. A consistent image selection through a pattern, as shown in Figure 4.5, shows the representativeness of parameters measured in the samples.

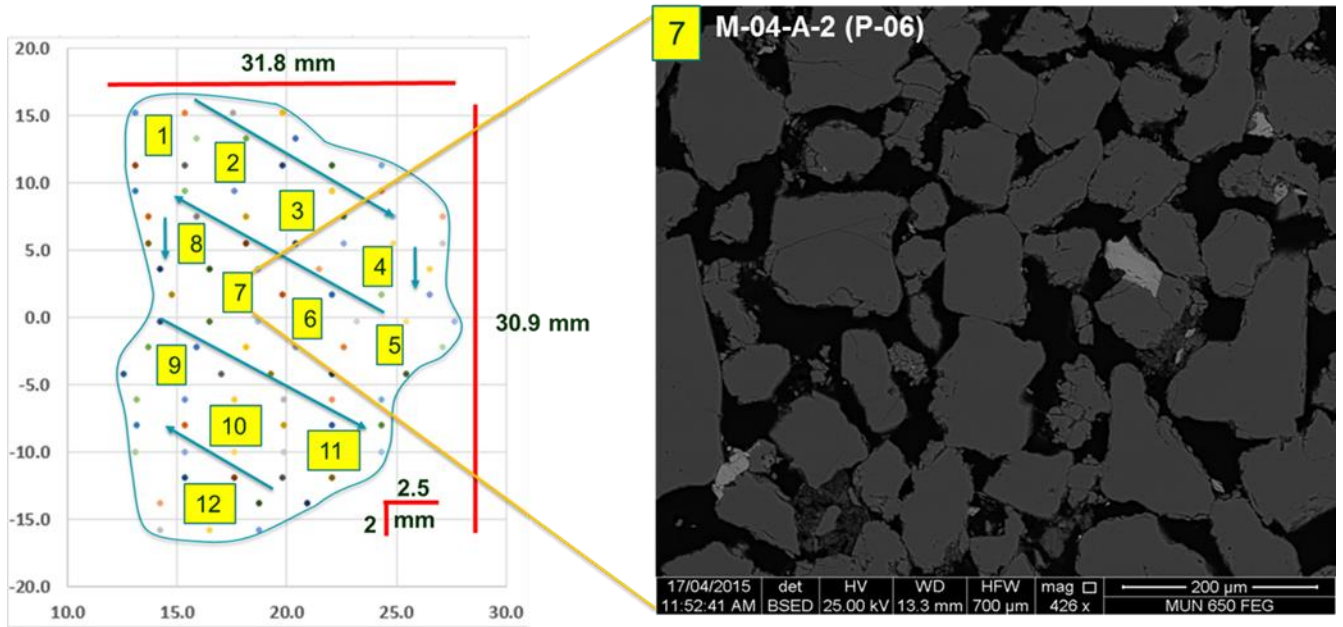


Figure 4.5. Image selection pattern (modified after Valencia, et al. 2015).

4.4.3.2. Processing Software

The DIA was performed using the JMicrovision v.1.2.7 software that has been developed to analyze high definition images of rock thin sections through a simple and intuitive user interface with powerful features (Roduit, 2015).

4.4.3.3. Image Segmentation

The main goal of image segmentation is to find objects of interest from a given image by partitioning it into disjointed compartments or sets of pixels (Shapiro and Stockman, 2001; Li and Feng, 2016). According to Martinez-Martinez et al. (2007) the segmentation involves identification and isolation of pixels that belong to the same category of interest with similar gray level values ranges. Berrezueta et al. (2015) considered the differences in gray level values to separate the pore spaces from the mineral phases of a thin section. In the current study, a similar approach has been applied but based on a simple binarization through the

software JMicrovision v.1.2.7, where the minimum threshold using an automatic histogram thresholding is always equal to zero. The software also uses methods such as iterative bisection, maximum variance, maximum entropy, minimum error or minimum fuzziness to define the maximum threshold (Rouit, 2015).

Prior to performing image segmentation, the image should be calibrated. The calibration process automatically converts the pixel values to any other unit of measurement by multiplying the measured values by a conversion factor. Once the spatial calibration is defined, all the position and measurement values in JMicroVision v.1.2.7 are displayed according to the conversion factor (Rouit, 2015).

4.4.3.4. Data Quantification and Statistics

Berrezueta et al. (2015) postulated that porosity measurements using the DIA-techniques represent an effective, accurate and easy method and that those techniques can be considered statistically robust when compared with point counting. Thus, the investigated porosity values were quantified as the area in the image defined as rock pores, i.e. the sum of pixels having intensity values within the selected ranges, based on segmentation (Figure 4.6).

Additional pore parameters such as shape, elongation, compactness and equivalent circular diameter provided information about the pore throats; MLA map images were used to evaluate potential relationships between mineral groups and pore shape.

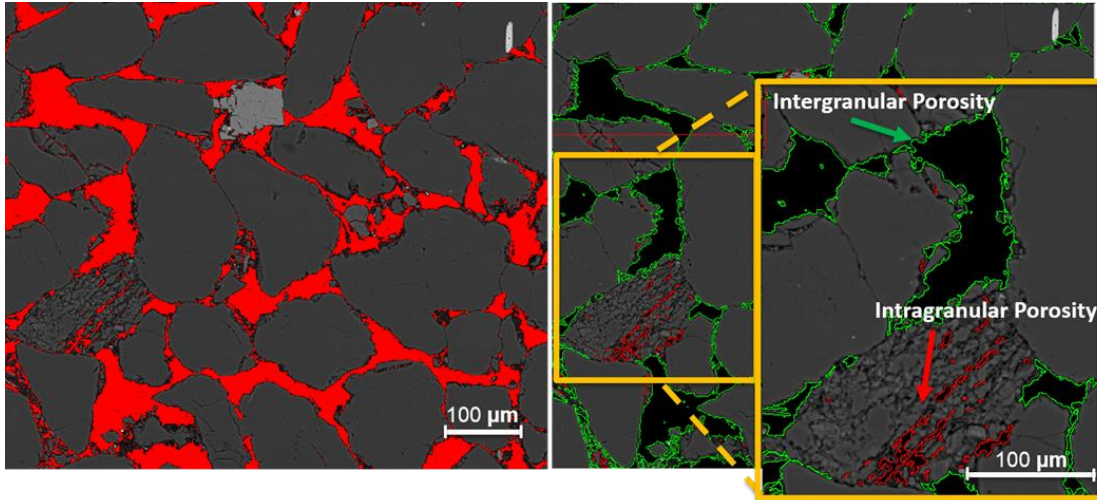


Figure 4.6. Object extraction by gray intensity threshold (modified after Valencia et al., 2015).

4.4.4. Polymer Flooding Experiments

Core flooding experiments were part of an ongoing project related to evaluating the feasibility of polymer flooding as a potential enhanced-oil-recovery (EOR) technique for Pool 1 at the Hebron Field (Valencia et al., 2017b). The core flooding procedure is briefly described as follows: (i) a formation water (synthetic) saturated core was placed in the setup and flooded with formation water to measure the effective permeability at different flow rates; (ii) the core was saturated with oil at 5 ft./day to establish the irreducible water saturation; (iii) the core was aged for one day; (iv) two pore volumes (PV) of seawater (used as injection water for water flooding) were injected into the core at 5 ft./day; (v) two PV of polymer solution, at specific concentration according to the polymer type, were injected at 1 ft./day; (vi) one PV of seawater was injected; and (vii) the core and polymer solutions were changed and the process repeated from i to vi (Valencia et al., 2017a).

The HPAM (hydrolyzed polyacrylamides) polymers utilized in the experiments were provided in the powder-form by SNF Floerger, FLOPAAM 3430S, Lot GH1381 (copolymer of acrylamide and acrylic acid, approximately 25 - 30% anionicity, stated molecular weight 11-14 million Daltons) and FLOPAAM

5115, Lot RG2639/4-6 (sulfonated terpolymer, medium in acrylamide tert-butylsulfonic acid, approximately 25% anionicity, stated molecular weight 8-12 million Daltons).

The polymer flooding experiments were performed at Pool 1 reservoir conditions (62 °C, 2800 psi back pressure) to evaluate the porosity changes.

4.5. Results and Discussion

4.5.1. Standard Mineralogical Study

The investigated Pool 1 reservoir sandstone samples are generally sublitharenite according to Folk, 1980 classification, and have a similar mineralogy (Table 4.1): quartz lithic fragments (mainly feldspars), carbonates, bioclasts, plagioclases and less abundant clays such as illite and kaolinite. Accessory minerals consist of chlorite, ilmenite, rutile, muscovite and zircon. The rock matrix volume in general is low and mainly represented by fine quartz grains and clays, whereas the cement is composed of carbonates such as siderite and calcite. Differences between the rock permeability facies (high and low) used in the current study are influenced by the cement/clay content and the grain sorting (Figures 4.7 and 4.8). The mineralogical compositions determined by MLA before and after polymer flooding are shown in Table 3.1, which are more accurate than modal point counting obtained by optical mineralogy. Detailed information about the mineralogical composition could be found at appendix C.

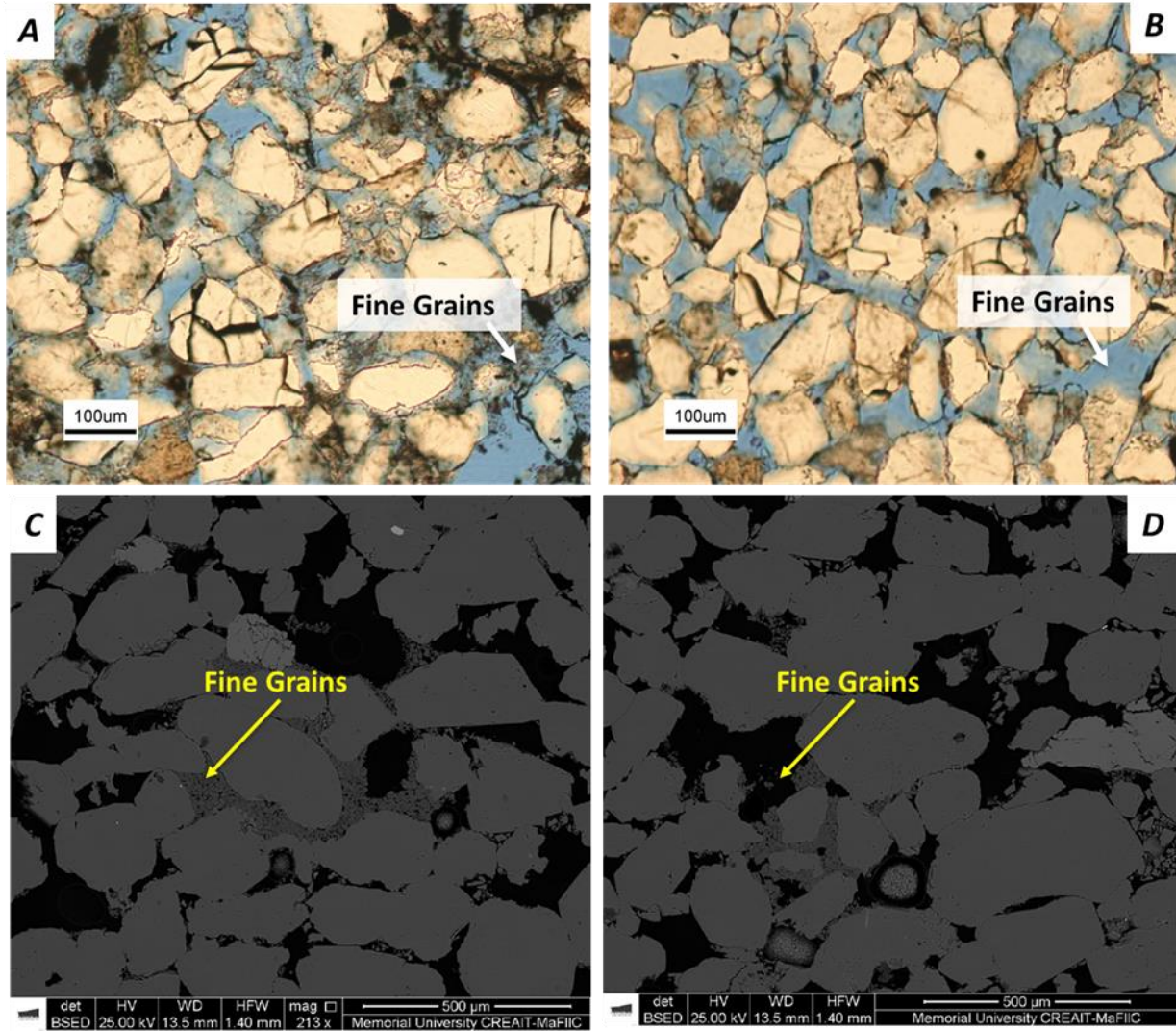


Figure 4.7. Mineral and textural changes observed in the high permeability Pool 1 sandstones. (A) optical microscope image before polymer flooding, (B) optical microscope image after polymer flooding, (C) SEM image before polymer flooding, (D) SEM image after polymer flooding. Blue and black spaces represent porosity in optical microscope and SEM, respectively.

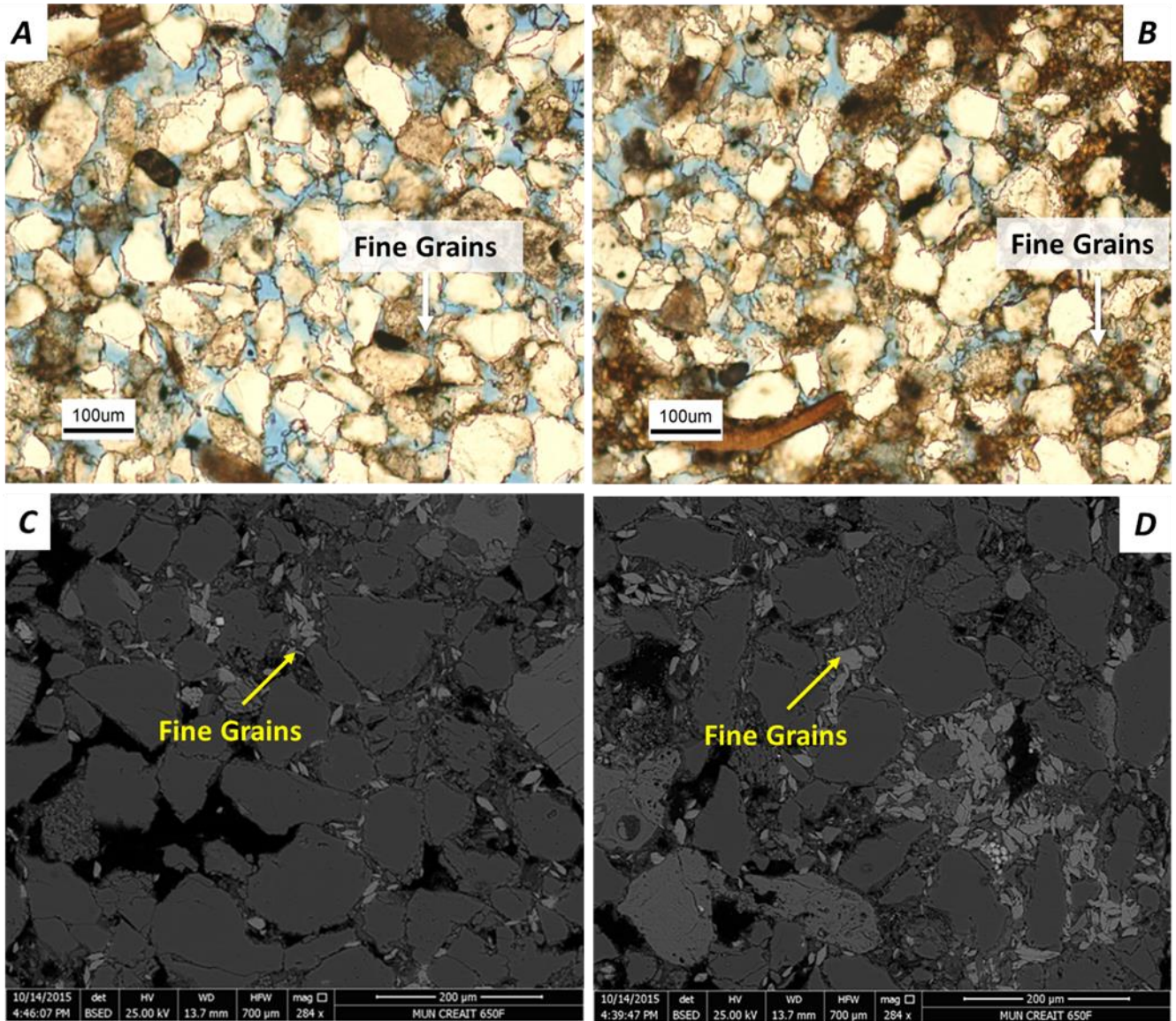


Figure 4.8. Mineral and textural changes observed in the low permeability Pool 1 sandstones. Optical microscope images (A) before and (B) after polymer flooding, and SEM images (C) before and (D) after polymer flooding. Blue and black spaces represent porosity in optical microscope and SEM images, respectively.

Table 4.1 Mineralogical composition difference in polymer flooding experiments.

Mineralogy	Low Perm Facies (50-120 mD)			High Perm Facies (1340-1400 mD)		
	BF (%)	AF (%)	DF (%)	BF (%)	AF (%)	DF (%)
Quartz	67 ± 5	59 ± 2	-7.4	86 ± 2	83 ± 3	-3.1
Lithic Fragments	13 ± 2	20 ± 3	6.9	11 ± 1	14 ± 1	4
Feldspars	2 ± 1	3.3 ± 0.3	0.9	0.8 ± 0.2	1.1 ± 0.2	0.3
Carbonates	8 ± 8	8 ± 8	0.6	0.4 ± 0.3	0.2 ± 0.3	-0.2
Clays	1 ± 1	2 ± 1	1.0	0.5 ± 0.2	0.7 ± 0.2	0.2
Matrix	5 ± 3	4.1 ± 0.4	-0.9	0.7 ± 0.2	0.7 ± 0.2	-0.1
Accessories	1.6 ± 0.5	1.9 ± 0.5	0.3	0.8 ± 0.2	1.0 ± 0.2	0.2

Legend: BF (before flooding), AF (after flooding) and DF (difference)

Table 4.1 shows the difference in mineral composition before and after polymer flooding experiments, considering the evaluation of four (4) composite cores for each permeability phase (high and low) for a total of eight (8) composite cores (Fig. 3.3). Eight (8) thin sections were taken from every composite core to be evaluated using MLA-SEM before polymer flooding, and then in the same core side a thin section was also taken after polymer flooding for other sixteen (8) thin sections. Table 4.1. summarizes the evaluation of sixteen (16) thin sections. Detailed mineralogical composition is found at appendix C.

Quartz and lithic fragments (quartz and feldspars mix) percentages represent the mineralogical phases with the most significant difference in their relative total composition after performing the polymer flooding experiments. In general, the quartz content percentage decreases and the lithic fragments increase, regardless of the established sandstone permeability facies. As expected, this difference is higher in the low permeability facies sandstones where more mineralogical variety exists.

Some studies (e.g., Sorbie, 1991), suggest that polymers may react chemically with other species, such as trivalent metal ions, to cross-link and form gel-like materials in the reservoir; however, there is not enough source of these metals in the sandstones of the current study to generate a high decrease of quartz (Table 4.1). On the other hand, the adsorption density of polyacrylamides on quartz surfaces has been found by Lecourtier et al. (1990) to be generally quite low (< 500 µg/m²), which is attributed to the weak interactions with surface silanols. Based on the rock mineralogy, polymer composition, and experimental conditions

used in this research, chemical reactions are not expected to play an important role in the quartz and lithic fragment changes after polymer flooding.

Several flooding sequences performed during this research project resulted in rock mechanical disintegration. Some quartz grains were disintegrated to smaller size so that the MLA recognized them as lithic fragments (quartz and feldspar mix), which is a more complex structure to identify by the MLA standard mineral library than a single quartz phase, thus generating a relative change in the rock mineral proportions. On the other hand, even thin sections before and after polymer flooding were taken in the same core plug face, the rock heterogeneity could impact the mineralogy distribution obtained after the flooding.

4.5.2. Porosity Network Changes

Intergranular porosity is the main type of porosity observed in both high and low permeability facies sandstones. It is possible to identify in some samples but its relatively low values fall within the DIA technique range of error and the total porosity is therefore reported in the current as intergranular porosity.

Analyzing the percentage of pore area measured by DIA (Table 4.2), using the pattern established in Fig. 4.5 (12 images for each thin section), the porosity of high permeability sandstones prior to polymer floods falls under ranges between 25 % and 30 %, while the total porosity percentage after flooding is between 27 % and 31 %. These values correspond to a potential relative increase of 1% of total porosity after polymer flooding; nevertheless, the difference is close to the data dispersion. The low permeability sandstones showed, in general, a 7% decrease in total porosity after polymer flooding, just one sample showed an increase (M-04-B-2). The total porosity range was between 15 % and 22 % before flooding and 13 % and 19 % after flooding. Detailed raw data is listed at appendix D.

Table 4.2. Total porosity values comparison after applying polymer flooding in Pool 1 composite cores.

Facies	Sample	Porosity (%)		
		Before Core Flooding	After Core Flooding	Difference
High Perm Facies (1340-1400 mD)	D-94-A-1	30 ± 4	31 ± 3	1
	D-94-A-2	27 ± 4	28 ± 1	1
	M-04-A-1	28 ± 1	29 ± 1	1
	M-04-A-2	25 ± 1	27 ± 1	2
Low Perm Facies (50-120 mD)	D-94-B-1	22 ± 1	13 ± 1	-9
	D-94-B-2	21 ± 4	14 ± 3	-7
	M-04-B-1	22 ± 4	17 ± 4	-5
	M-04-B-2	15 ± 2	19 ± 3	4

Increases in total porosity values in the high permeability sandstone could be attributed to an intergranular clay matrix detachment (clay microcoats on clastic grains) and/or partial removal from the rock sample due to polymer flooding input/release drag (Valencia et al., 2015). Total porosity reduction in low permeability facies could be attributed to mechanical rock disintegration caused by the new injected fluid (polymer flood) and then a remobilization of the small mineral grains until their mechanical entrapment due to the narrower flow channels in this type of cores, thus blocking some of the previously empty pores.

On the other hand, the porosity in low permeability sandstones was observed to be more heterogeneous. Figure 4.9 shows the range of the porosity probability S-curves performed using the total porosity percentages obtained by DIA technique. As expected, the high permeability sandstones show porosity values range in a narrower spectrum. Detailed distribution percentiles are summarized in Table 4.3.

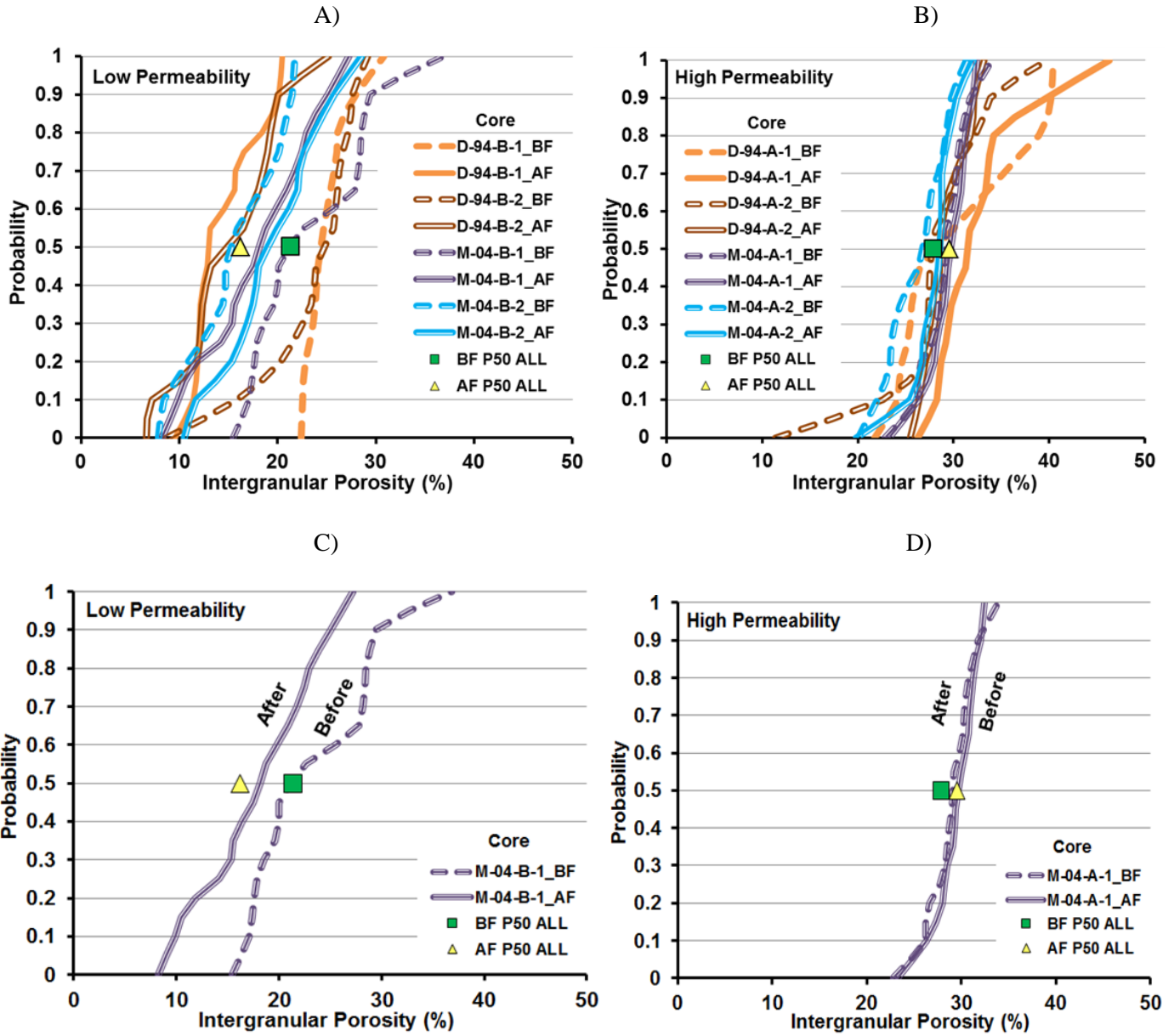


Figure 4.9. Porosity probability S-curves, A) Low permeability sandstones cores, B) High permeability sandstones cores, C) M-04-B-1 low permeability sandstone core, D) M-04-A-1 high permeability sandstone core.

Table 4.3. Total porosity percentile distribution obtained from S-curves.

Permeability	Sample	Before Flooding			After Flooding		
		P10	P50	P90	P10	P50	P90
High Perm Facies (1340-1400 mD)	D-94-A-1	24	28	40	25	31	36
	D-94-A-2	22	27	31	26	28	31
	M-04-A-1	26	28	31	26	29	32
	M-04-A-2	21	26	29	25	27	30
Low Perm Facies (50-120 mD)	D-94-B-1	19	23	24	9	11	18
	D-94-B-2	14	23	26	7	14	20
	M-04-B-1	15	21	29	9	18	25
	M-04-B-2	8	15	21	11	18	25

4.5.3. Pores Shape Characterization

Pore characterization using the JMicrovision v.1.2.7 software includes the measurement of multiple pore features such as elongation, compactness, and orientation. The use of combinations of these parameters allows the definition of geometric forms related to the pore shape so that it provides an understanding of the pore network heterogeneity, and its potential influence on enhanced oil recovery (EOR) during polymer flooding.

Table 4.4. Pore geometric equivalent forms (modified after Palacios, 2013)





Elongation (Width / Height)	Compactness or Roundness $(4\pi * \text{Area}) / (\text{Perimeter}^2)$	Geometric Equivalent Form
Low (0.51 - 1.00)	Rounded (> 0.90)	Circle 
Low (0.51 - 1.00)	No Rounded (≤ 0.90)	Square 
High (0.01 - 0.50)	Rounded (> 0.90)	Elipse 
Low (0.01 - 0.50)	No Rounded (≤ 0.90)	Rectangle 

Table 4.4 shows circles, squares, ellipses and rectangles as examples of geometric forms that can be defined. Pore features of sandstones with high permeability and low permeability facies were plotted before and after polymer flooding.

The pore shape analysis included the same pattern established in Fig. 4.5 (12 images for each thin section) and considered in section 4.5.2. The total area analyzed followed the same pattern regarding magnification (426x) and scale (200 μm), in order to be able to compare different samples. It is not expected a change in the pore shape distribution if the area to be evaluated increase; nevertheless, specific localized diagenetic features, such as secondary porosity in a fossil shell could affect the distribution.

The results show a consistent trend of rectangle pore type decrease after flooding experiments in Pool 1 (Figures 4.10 and 4.11). On the other hand, specifically the low permeability facies sandstones showed an increase in the relative proportion of circle and ellipse forms. A more rounded pore type in the majority of the samples after flooding reflects the potential effect of the polymer flood to release/drag the small grains that generate a more “clean” pore structure; this effect is more pronounced in low permeability facies sandstones due to the higher pressure that the polymer flood needs to develop in order to flow through the narrower channels in the rock. Detailed raw data analysis could be found at appendix D.

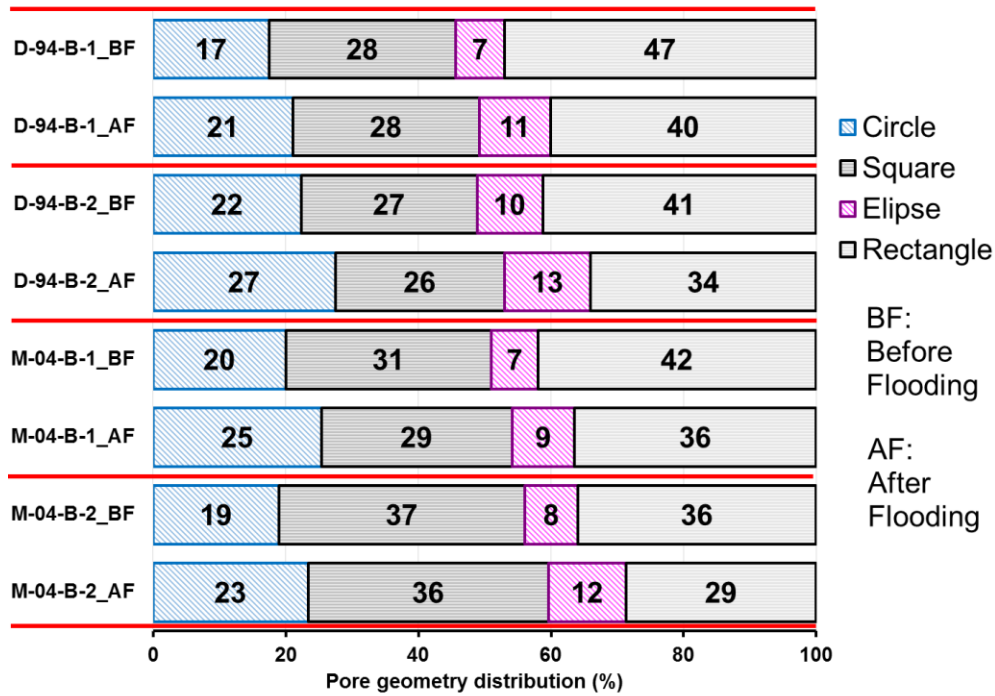


Figure 4.10. Pore shape proportions before and after polymer flooding injection in low permeability sandstones.

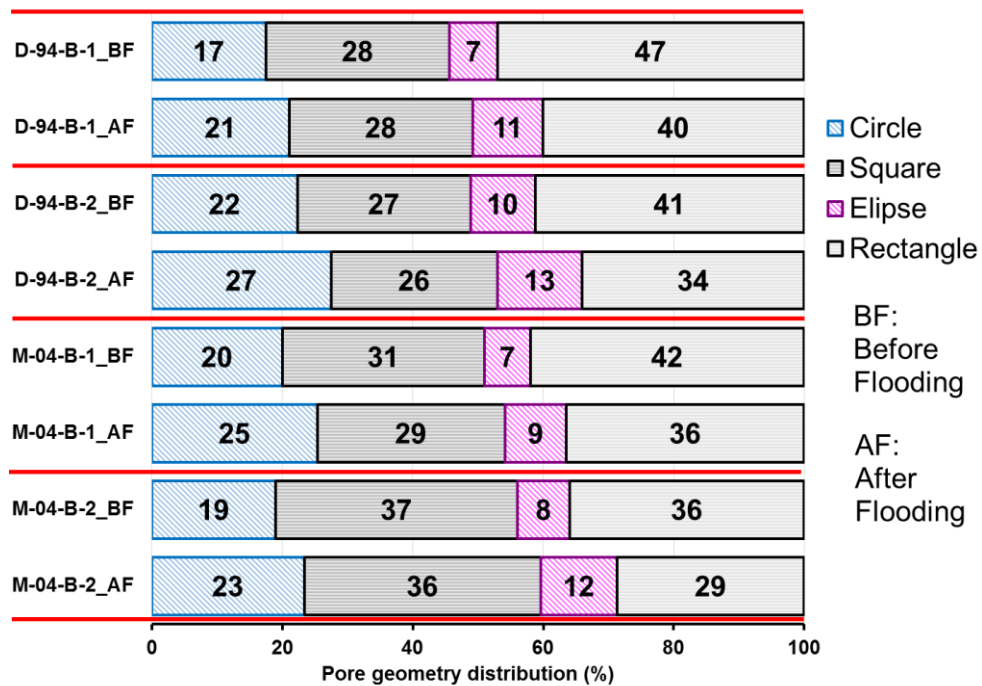


Figure 4.11. Pore shape proportions before and after polymer flooding injection in high permeability sandstones.

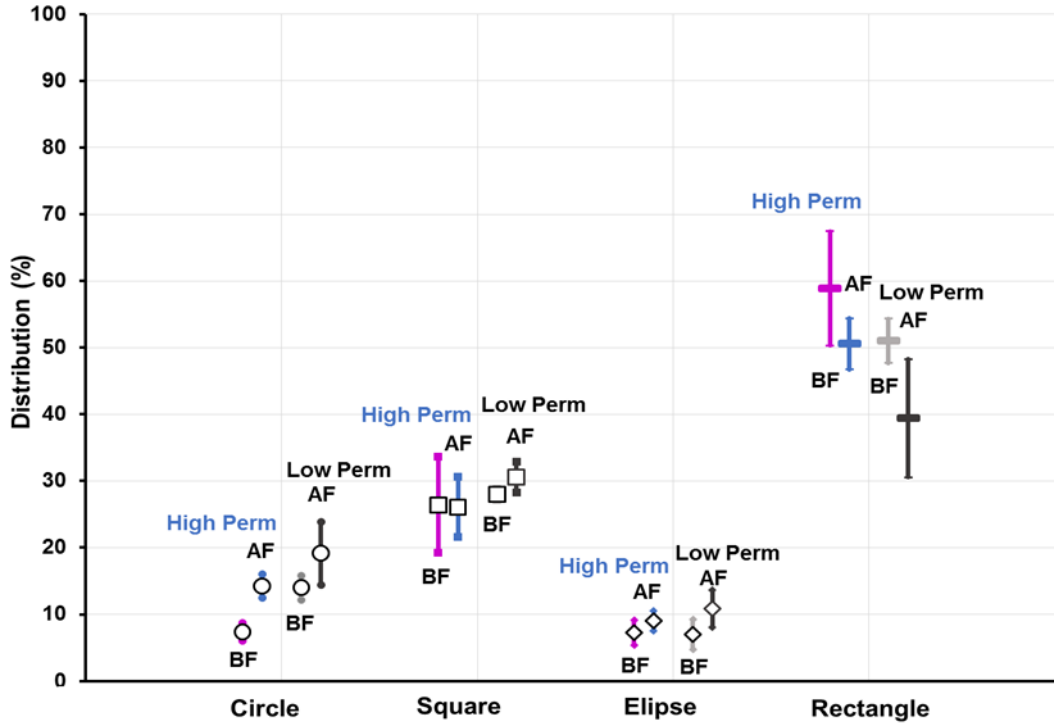


Figure 4.12. Pore shapes proportions dispersion before and after polymer flooding injection in Pool 1 cores samples. Legend: (BF) before flooding, (AF) after flooding.

Figure 4.12 shows that the less rounded forms (square and rectangular) have more variance in their proportion, regardless of the permeability facies.

In order to understand pore shape type and mineral relationship, MLA maps with the mineralogical characterization were compared with the SEM images previously evaluated with the DIA technique (Figure 4.13). In general, pores related to quartz grains showed rectangular and square forms, which is expected considering the hardness, non-cleavability, and high stability of the mineral phase. However, other minerals with cleavability and lower hardness were also evaluated but no specific trend was recognized. Pore shape distribution could be useful for future studies where pore network need to be included in simulation studies to evaluate EOR technique performance at pore scale.

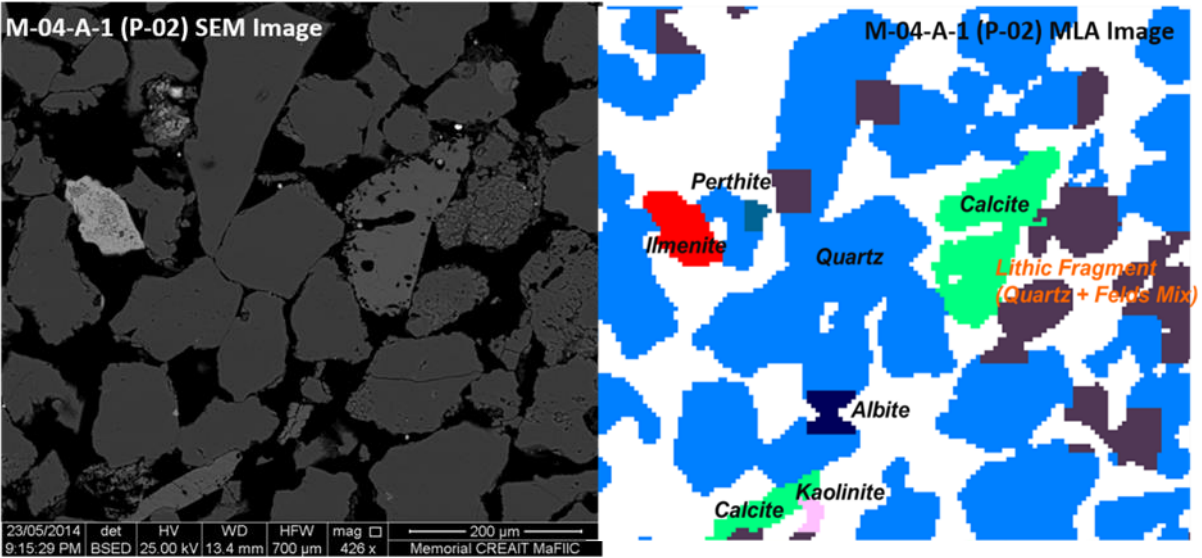


Figure 4.13. SEM-MLA images comparison used to define pore shape and mineral relationship.

4.6. Conclusions

By combining the standard mineralogical analysis and DIA technique, some conclusions can be made regarding the pore network evolution of sandstones from the Ben Nevis Formation (Pool 1) at Hebron Field after experimental polymer flooding:

- High permeability facies sandstones showed a relative total porosity increase after polymer flooding; however, the low permeability facies experienced a relative total porosity loss.
- The porosity increase in the high permeability sandstones is suggested to be due to intergranular clay matrix detachment and partial removal from the rock sample (due to polymer flooding input/release drag).
- The total porosity reduction in the low permeability facies may be attributed to mechanical rock disintegration caused by the injected polymer flood at reservoir conditions.

- Minor textural changes observed after polymer flooding showed variations in the roughness of grain-pore contacts and pore shape, leading to a general enhancement in pore roundness in the majority of the high permeability facies samples, and hence a better fluid flow.
- The primary texture of the rock subjected to polymer flooding injection could be a factor that affects the oil recovery; thus, understanding the pore network shape distribution is key to understand the porosity changes after polymer flooding.

4.7. Acknowledgements

Thanks to MUN-CREAIT staff, especially to Elizabeth Baird for all her support during the DIA study. This work was supported generously by Hibernia Management and Development Company (HMDC), Chevron Canada, the Natural Sciences and Engineering Research Council of Canada (NSERC), the Canada Foundation for Innovation (CFI), Research and Development Corporation of Newfoundland (RDC), and Petroleum Exploration Enhancement Program (PEEP).

4.8. References

Berrezueta, E., Gonzalez-Menendez, L., Ordoñez-Casado, B. and Olaya, P. 2015. Pore network quantification of sandstones under experimental CO₂ injection using image analysis. *Computer & Geoscience*, v. 77, p. 97-110.

ExxonMobil 2011. Hebron Project Development Plan.
http://www.hebronproject.com/media/3908/hda_vol_2.pdf

Folk, R.L. 1980. *Petrology of Sedimentary Rocks*. Hemphill Publishing Co., Austin, Texas, p. 182.

- Martinez-Martinez, J., Benavente, D., Garcia del Cura, M.A. 2007. Petrographic quantification of brecciated rocks by image analysis. Application to the interpretation of elastic wave velocities. *J. Eng. Geol.*, v. 90, p. 41-54.
- Lecourtier, J., Lee, L.T. and Chauveteau, G. 1990. Adsorption of polyacrylamides on siliceous minerals. *Colloids and Surfaces*, v. 47, p. 219-231.
- Li, Y. and Feng, X. 2016. A multiscale image segmentation method. *Pattern Recognition*, v. 52, p. 332-345.
- Palacios, Y. 2013. Pore system characterization in carbonate rocks through digital image analysis using thin sections from Gulf of Venezuela. Bachelor thesis. Central University of Venezuela, p. 127.
- Pirard, E., Jongmans, D. and Marsh, S. 2001. Geological application of digital imaging. *Computer & Geoscience*, v. 27, p. 1015-1017.
- Roduit, N. 2015. JMicroVision: Image analysis toolbox for measuring and quantifying components of high-definition images. Version 1.2.7. <http://www.jmicrovision.com> (accessed on August, 10 2015).
- Shannon, P.M., Croker, P.F. and Sinclair, I.K. 1995. Tectonic controls on Upper Jurassic to Lower Cretaceous reservoir architecture in the Jeanne d'Arc Basin, with some comparisons from the Porcupine and Moray Firth Basins. Geological Society, London, Special Publications, v. 93, p 467-490.
- Shapiro, L. and Stockman, G. 2001. Computer vision. Prentice-Hall, New Jersey, p. 279-325.
- Sorbie, K.S. 1991. Polymer-improved oil recovery. Blackie and Son Ltd, Glasgow, p. 358.
- Sylvester, P. 2012. Use of the mineral liberation analyzer (MLA) for mineralogical studies of sediments and sedimentary rocks. Mineralogical Association of Canada, short course 42, p. 1-16.
- Tankard, A.J. and Welsink, H. J. 1987. Extensional tectonics and stratigraphy of Hibernia oil field, Grand Banks, Newfoundland. *AAPG Bulletin*, v. 71 (10), p. 1210-1232.

Valencia, L.E., James, L.A., Azmy, K. 2015. Pore system changes during experimental polymer flooding in Ben Nevis Formation sandstones, Hebron Field, Offshore Eastern Canada. Search and Discovery article #20349 presented at 2015 AAPG/SEG/PESA International Conference & Exhibition, Melbourne, 13-16 September.

Valencia, L.E., James, L.A., Azmy, K. 2017a. Laboratory scale characterization methodology for offshore polymer flooding project: Hebron Field, Eastern Canada (unpublished paper).

Valencia, L.E., James, L.A., Azmy, K. 2017b. Implications of the diagenetic history on enhanced oil recovery performance for the Ben Nevis Formation, Hebron Field, Offshore Newfoundland, Canada (unpublished paper).

Xiong, D., Azmy, K., Blamey, N. 2016. Diagenesis and origin of calcite cement in the Flemish Pass Basin sandstone reservoir (Upper Jurassic): Implications for porosity development. *Marine and Petroleum Geology*, v. 70, p. 93-118.

Zhou, Y., Starkey, J. and Mansinha, L. 2004. Segmentation of petrographic images by integrating edge detection and region growing. *Computer & Geoscience*, v. 30, p. 817-831.

CHAPTER 5. SUMMARY

5.1. Conclusions

A systematic laboratory characterization methodology was carried out in this study, starting with a comprehensive literature review about EOR methods screening criteria that pointed out polymer flooding as a potential feasible EOR methodology for Hebron Pool 1. A comparison between Hebron pool 1 reservoir properties with offshore analog fields where polymer flooding has been applied, highlighted that low permeability facies (5 - 220 mD) and high salinity formation water (> 60,000 ppm TDS) are the main Pool 1 reservoir properties that slightly differ from the analog fields reservoir properties general trend. Based on this, HPAMs (FP-3430S and FP-5115) polymers and the biopolymer (Guar Gum) were evaluated in order to understand their viscosity stability at Pool 1 reservoir conditions, in general the HPAMs showed similar viscosity responses to salinity and temperature changes compared with the biopolymer Guar Gum that was screened out of additional evaluation, due to its poor resistance to high temperature and high salinity environments over the time. Additional, polymer viscoelastic evaluation suggests that the elasticity of the polymers does not play an important role on this experimental design.

On the other hand, combining the standard mineralogical analysis and DIA technique allow to observe an increase in carbonate cementation events and clay content moving upward at Ben Nevis reservoir (Pool 1), which is correlated with reservoir quality reduction due to the depositional setting.

This allowed better understanding of how carbonate cementation events at Ben Nevis Formation (Pool 1) are probably the most critical diagenetic event that causes permeability reduction at the reservoir hence reducing the polymer flood sweep efficiency. Additionally, a porosity increase in the high permeability sandstones is suggested to be due to intergranular clay matrix detachment and partial removal from the rock sample (due to polymer flooding input/release drag).

Core flooding experiments indicate using polymer flooding as an EOR method in the Ben Nevis Fm. (Pool 1) could potentially increase oil recovery in a range of 3-6%; also, applying polymer flooding in an early stage of the field development would be beneficial.

This research study is a contribution to evaluate a potential application of polymer flooding in Hebron Field; nevertheless, considering the limited information available from a field without production history with first oil expected late 2017; further studies are required to have a more comprehensive idea about the project feasibility.

5.2. Directions for future research

While this study shows that polymer flooding is an EOR technique that could be applied in Pool 1 at Hebron field, further reservoir simulations and economics evaluations are required to fully understand the timing of this phase in the Hebron Field development plan. A reservoir simulation study would be useful for designing and interpreting pilot performance and translating that performance to field-scale predictions.

Additional EOR techniques are required to be evaluated in order to get a better understanding of rock-fluids influence in oil recovery at Pool 1, then laboratory tests and simulations studies could indicate which EOR technique is likely to yield the highest recovery and best overall economic value among recovery processes considered.

REFERENCES

- Abid, I. 1988. Mineral Diagenesis and Porosity Evolution in the Hibernia Oil Field, Jurassic-Cretaceous Jeanne d'Arc Rift Graben, Eastern Grand Banks of Newfoundland, Canada. Master's Thesis, McGill University, Montreal, Quebec, 280 p.
- Abidin, A.Z., Puspasari, T., Nugroho, W.A., 2012. Polymers for enhanced oil recovery technology. *Procedia Chemistry* 4 (2012) 11-16.
- Al Adasani, A. and Bai, B., 2011. Analysis of EOR projects and updated screening criteria. *J. Petrol. Sci. Eng.* 79 (2011) 10-24.
- Al Mjeni, R., Arora, S., Cherukupalli, P., van Wunnik, J., Edwards, J., Felber, B.J., Gurpinar, O., Hirasaki, G., Miller, C., Jackson, C., Kristensen, M., Lim, F., Ramamoorthy, R., 2011. Has the time come for EOR? *Schlumberger Oilfield Review*. 22 (4) 16-35.
- Alvarado, V. and Manrique, E. 2013. Engineering design challenges and opportunities beyond water flooding in offshore reservoirs. Paper OTC 24105 presented at the 2013 Offshore Technology Conference, Houston, U.S.A., 6-9 May.
- API, 1990. API Recommended practice 63 (RP63). Recommended practices for evaluation of polymers used in enhanced oil recovery operations.
- Berg, E.A., Silcock, S., Ostbo-Bjastad, B, 2013. Next step in offshore heavy oil - Mariner reservoir development. Paper SPE 166575 presented at the 2013 SPE Offshore Europe Oil and Gas Conference and Exhibition, Aberdeen, U.K., 3-6 September.
- Berrezueta, E., Gonzalez-Menendez, L., Ordoñez-Casado, B. and Olaya, P. 2015. Pore network quantification of sandstones under experimental CO₂ injection using image analysis. *Computer & Geoscience*, v. 77, p. 97-110.
- Cox, W. P. and Merz, E.H. 1958. Correlation of dynamic steady flow viscosities. *J. Polymer Sci.* (28) 619-622.

- de Melo, M.A, Da Silva, I.P.G, de Godoy, G.M.R., Sanmartim, A.N., 2002. Polymer injection projects in Brazil: dimensioning, field application and evaluation. Paper SPE 75194 presented at the 2002 SPE/DOE Improved Oil Recovery Symposium, Tulsa, U.S.A., 13-17 April.
- Delshad, M., Kim, D.H., Magbagbeola, O.A., Huh, C., Pope, G.A., Tarahhom, F., 2008. Mechanistic interpretation and utilization of viscoelastic behaviour of polymer solutions for improved polymer-flood efficiency. Paper SPE-113620-MS presented at the 2008 SPE/DOE Symposium on Improved Oil Recovery, Tulsa, USA, 20-23 April.
- Dickey, P.A., 1979. Petroleum development geology. PennWell Publishing Co. p. 350.
- ExxonMobil, 2011. Hebron Project Development Plan.
<http://www.cnlopb.ca/pdfs/conhebdevplan.pdf>
- Ewoldt, R.H., Johnston, M.T., Caretta, L.M. 2015. Experimental challenges of shear rheology: how to avoid bad data, in complex fluids in biological systems: experiment, theory, and computation, E.S. Spagnolie, Editor. Springer New York: New York, NY. p. 207-241
- Fink, J. 2015. Petroleum engineer's guide to oil field chemicals and fluids. Elsevier p. 825.
- Folk, R.L. 1980. Petrology of Sedimentary Rocks. Hemphill Publishing Co., Austin, Texas, p. 182.
- Gaillard, N., Giovannetti, B., Favero, C., Caritey, J.P., Dupuis, G., Zaitoun, A. 2014. New water soluble anionic NVP acrylamide terpolymers for use in harsh EOR conditions. Paper SPE 169108 presented at the 2014 SPE Improved Oil Recovery Symposium, Tulsa, U.S.A, 12-16 April.
- Galindo-Rosales, F.J., Campo-Deaño, L., Pinho, F. T., Bokhorst, E., Hamersma, P. J., Oliveira, M. S. N., Alves, M. A. 2011. Microfluidic systems for the analysis of viscoelastic fluid flow phenomena in porous media. *Microfluidics and Nanofluidics*. 12(1) 485-498.

- Gogarty, W.B., Levy, G. L., Fox, V. G. 1972. Viscoelastic effects in polymer flow through porous media. Paper SPE 4025-MS, San Antonio, Texas.
- Han, M., Xiang, W., Zhang, J., Jiang, W., Sun, F., 2006. Application of EOR technology by means of polymer flooding in Bohai oil fields. Paper SPE 104432 presented at the 2006 SPE International Oil & Gas Conference and Exhibition, Beijing, China, 5-7 December.
- Hincapie, R.E., Duffy, J., O'Grady, C., Ganzer, L., 2015. An approach to determine polymer viscoelasticity under flow through porous media by combining complimentary rheological techniques. Paper SPE-174689-MS presented at the 2015 SPE Enhanced Oil Recovery Conference, Kuala Lumpur, Malaysia, 11-13 August.
- Hincapie, R., Ganzer, L. 2015. Assessment of polymer injectivity with regards to viscoelasticity: lab evaluations towards better field operations. Paper SPE-174346-MS presented at the EUROPEC 2015. Madrid, Spain, 1-4 June.
- Jones, D.M., Walters, K. 1989. The behaviour of polymer solutions in extension-dominated flows, with applications to enhanced oil recovery. *Rheologica Acta*, 28(6) 482-498.
- Kaminsky, R.D., Wattenbarger, R.C, Szafranski, R.C., Coutee, A.S., 2007. Guidelines for polymer flooding evaluation and development. Paper IPTC 11200 presented at the 2007 International Petroleum Technology Conference, Dubai, UAE, 4-6 December.
- Kim, D.H., Lee, S., Ching, H.A., Chun, H., Pope, G., 2010. Development of a viscoelastic property database for EOR polymers. Paper SPE-129971 presented at the 2010 SPE Improved Oil Recovery Symposium in Tulsa, USA, 24-28 April.
- Ledolter, J., and Swersey, A. 2007. Testing 1-2-3: experimental design with applications in marketing and service operations. Stanford University Press. 312 p.
- Levitt, D.B., Slaughter, W., Pope, G.A., Jouenne, S., 2011. The effect of redox potential and metal solubility on oxidative polymer degradation. *J. SPE Reserv. Eval. Eng.* 14 (3) 287-298.

- Macosko, C.W. 1994. Rheology: principles, measurements, and applications. Wiley - VCH. p. 568.
- Mahdavi, S., James, L.A., Johansen, T.E., 2014. Technical and economic considerations for using CO2 enhanced oil recovery in an offshore environment. Presented at 64th Canadian Society of Chemical Engineers Conference, Niagara Falls, Canada, 19-22 October.
- Maia, A., Borsali, R., Balaban, R., 2009. Residual comparison between a polyacrylamide and a hydrophobically modified polyacrylamide flood in a sandstone core. Mater. Sci. Eng. C, 29 (2009) 505-509.
- Manrique, E., Thomas, C., Ravikiran, R., Izadi, M., Lantz, M., Romero, J., Alvarado, V. 2010. EOR: Current Status and Opportunities. Presented at the 2010 SPE Improved Oil Recovery Symposium, Tulsa, U.S.A, 24-28 April. SPE 130113-MA.
- Martinez-Martinez, J., Benavente, D., Garcia del Cura, M.A. 2007. Petrographic quantification of brecciated rocks by image analysis. Application to the interpretation of elastic wave velocities. J. Eng. Geol., v. 90, p. 41-54.
- Moayedi, M. 2015. An experimental study on surfactant-alternating-gas process. Memorial University of Newfoundland, St. John's, Canada.
- Morel, D., Vert, M., Jouenne, S., Gauchet, R., Bouger, Y., 2012. First polymer injection in deep offshore field Angola: recent advances in the Dalia/Camelia field case. J. SPE Oil Gas Fac. 1 (2) 43-52.
- Mosavat, N., Rasaei, M.R., and Torabi, F. 2013. Experimental Determination of Absolute and Relative Permeability in Composite Cores: Effect of Ordering. Special Topics & Reviews in Porous Media – An International Journal. 4 (1): 33-43.
- Morad, S., Al-Ramadan, K., Ketzer, J.M., and De Ros, L.F. 2010. The Impact of Diagenesis on the Heterogeneity of Sandstone Reservoirs: A Review of the Role of Depositional Facies and Sequence Stratigraphy, AAPG Bull. 94 (8): 1267-1309.

- Normore, L. 2006. Origin, Distribution and Paragenetic Sequence of Carbonate Cements in the Ben Nevis Formation, White Rose Field, Jeanne d'Arc Basin, Offshore Newfoundland, Canada. Memorial University of Newfoundland, St. John's, Canada.
- Langaas, K., Ekrann, S., and Ebeltoft, E. 1998. A Criterion for Ordering Individuals in a Composite Core. *J. Petrol. Sci. Eng.* 19 (1998): 21-32.
- Lake, L., Walsh, M. 2008. Enhanced Oil Recovery (EOR) Field Data Literature Search. Technical Report, UT at Austin, U.S.A., 112 p.
- Lecourtier, J., Lee, L.T. and Chauveteau, G. 1990. Adsorption of polyacrylamides on siliceous minerals. *Colloids and Surfaces*, v. 47, p. 219-231.
- Levitt, D.B., Slaughter, W., Pope, G.A., and Jouenne, S., 2011. The Effect of Redox Potential and Metal Solubility on Oxidative Polymer Degradation. *J. SPE Reserv. Eval. Eng.* 14 (3): 287-298. SPE-129890-PA.
- Li, Y. and Feng, X. 2016. A multiscale image segmentation method. *Pattern Recognition*, v. 52, p. 332-345.
- Osterloh, W.T. and Law, E. J., 1998. Polymer transport and rheological properties for polymer flooding in the North Sea Captain field. Paper SPE 39694 presented at the 1998 SPE/DOE Improved Oil Recovery Symposium, Tulsa, U.S.A., 19-22 April.
- Palacios, Y. 2013. Pore system characterization in carbonate rocks through digital image analysis using thin sections from Gulf of Venezuela. Bachelor thesis. Central University of Venezuela, p. 127.
- Pirard, E., Jongmans, D. and Marsh, S. 2001. Geological application of digital imaging. *Computer & Geoscience*, v. 27, p. 1015-1017.

- Reid, B.E., Hoyland, L.A., Olsen, S.R., Petterson, O., 1996. The Heidrun field – challenges in reservoir development and production. Paper OTC 8085 presented at the 1996 Offshore Technology Conference, Houston, U.S.A., 6-9 May.
- Roduit, N. 2015. JMicroVision: Image analysis toolbox for measuring and quantifying components of high-definition images. Version 1.2.7. <http://www.jmicrovision.com> (accessed on August, 10 2015).
- Rothstein, J., 2013. Effect of fluid rheology on enhanced oil recovery in a microfluidic sandstone device. *J. of Non-Newtonian Fluid Mech.*, 202, 112-119.
- Saaborian-Jooybary, H., Dejam, M., Chen, Z. 2016. Heavy oil polymer flooding from laboratory core floods to pilot tests and field applications: Half-century studies. *J. Petrol. Sci. Eng.* 142 (2016) 85-100.
- Selle, O., Fischer, H., Standnes, D., Auflem, I., Lambersten, A., Svela, P., Mebratu, A., Gundersen, E., Melien, I. 2013. Offshore Polymer/LPS injectivity test with Focus on Operational Feasibility and Near Wellbore Response in a Heidrun Injector. Presented at the 2013 SPE Annual Technical Conference and Exhibition, New Orleans, Louisiana, U.S.A, September, 30 – October, 2. SPE-166343-MA.
- Seright, R., Seheult, J.M., Talashek, T. 2009. Injectivity characteristics of EOR polymers. *J. SPE Reserv. Eval. Eng.* 12 (5) 783-792.
- Seright, R. and Skejvrak, I. 2015. Effect of dissolved iron and oxygen on stability of hydrolyzed polyacrylamide polymers. *SPE Journal.* 20 (3) 1-9.
- Shannon, P.M., Croker, P.F. and Sinclair, I.K. 1995. Tectonic controls on Upper Jurassic to Lower Cretaceous reservoir architecture in the Jeanne d'Arc Basin, with some comparisons from the Porcupine and Moray Firth Basins. Geological Society, London, Special Publications, v. 93, p 467-490.

- Shapiro, L. and Stockman, G. 2001. Computer vision. Prentice-Hall, New Jersey, p. 279-325.
- Sheng, J.J., Leonhardt, B., Al-Azri, N. 2015. Status of Polymer Flooding Technology. J Canadian Petroleum Technology 54 (02): 116-126. SPE -174541-PA.
- Shu, W.R., 1984. A viscosity correlation for mixtures of heavy oil, bitumen, and petroleum fractions. SPE Journal. 24 (3) 277-284.
- Sorbie, K.S. 1991. Polymer-improved oil recovery. Blackie and Son Ltd, Glasgow, p. 358.
- Sylvester, P. 2012. Use of the mineral liberation analyzer (MLA) for mineralogical studies of sediments and sedimentary rocks. Mineralogical Association of Canada, short course 42, p. 1-16.
- Szpakiewicz, M., McGee, K., and Sharma, B. 1987. Geological Problems Related to Characterization of Clastic Reservoirs for EOR. SPE Formation Evaluation Journal 2 (4): 449-460. SPE-14888-PA.
- Taber, J.J., Martin, F.D., Seright, R.S. 1997. EOR Screening Criteria Revisited - Part 1: Introduction to Screening Criteria and Enhanced Recovery Field Projects. J. SPE Reserv. Eng. 12 (3) 189-198.
- Taber, J.J., Martin, F.D., Seright, R.S. 1997. EOR Screening Criteria Revisited - Part 2: Applications and Impact of Oil Prices. J. SPE Reserv. Eng. 12 (3) 199-205.
- Tankard, A.J. and Welsink, H. J. 1987. Extensional tectonics and stratigraphy of Hibernia oil field, Grand Banks, Newfoundland. AAPG Bulletin, v. 71 (10), p. 1210-1232.
- Teletzke, G.F., Wattenbarger, R.C., Wilkinson, J.R., 2010. Enhanced oil recovery pilot testing best practice. J. SPE Reserv. Eval. Eng. 13 (1) 143-154.

- Valencia, L.E., James, L.A., Azmy, K. and Walsh, J. 2015. Polymer Screening for the Hebron Field, Offshore Eastern Canada: Facing High Salinity Brines. Presented at 77th EAGE Conference and Exhibition, Madrid, Spain, 1-4 June.
- Valencia, L.E., James, L.A., Azmy, K. 2015. Pore system changes during experimental polymer flooding in Ben Nevis Formation sandstones, Hebron Field, Offshore Eastern Canada. Search and Discovery article #20349 presented at 2015 AAPG/SEG/PESA International Conference & Exhibition, Melbourne, 13-16 September.
- Valencia, L.E., James, L.A., Azmy, K. 2017. Laboratory scale characterization methodology for offshore polymer flooding project: Hebron Field, Eastern Canada (unpublished paper).
- Valencia, L.E., James, L.A., Azmy, K. 2017. Implications of the diagenetic history on enhanced oil recovery performance for the Ben Nevis Formation, Hebron Field, Offshore Newfoundland, Canada (unpublished paper).
- Valencia, L.E., James, L.A., Azmy, K. 2017. Image Analysis of Pore Network Evolution of Ben Nevis Formation Sandstones under Experimental Polymer Flooding (unpublished paper).
- Vermolen, E.C.M., van Haasterecht, M.J.T., Masalmeh, S.K., 2014. A systematic study of the polymer visco-elastic effect on residual oil saturation by core flooding. Paper SPE-169681-MS presented at the 2014 SPE EOR Conference at Oil and Gas West Asia, Muscat, Oman, 31 March - 2 April.
- Wang, D., Cheng, J., Xia, H., Li, Q., Shi, J., 2001. Viscous-elastic fluids can mobilize oil remaining after water-flood by force parallel to the oil-water interface. Paper SPE-72123-MS presented at the 2001 SPE Asia Pacific Improved Oil Recovery Conference, Kuala Lumpur, Malaysia, 6-9 October.

- Wang, Z.; Le, X.; Feng, Y.; Zhang, C. 2013. The role of matching relationship between polymer injection parameters and reservoir in enhanced oil recovery. *Journal of Petroleum Science and Engineering*, 111, 139-143.
- Wang, D., Wang, G., Wu, W., Xia, H., Yin, H. 2007. The influence of viscoelasticity on displacement efficiency from micro to macro scale. Paper SPE-109016-MS presented at the 2007 SPE Annual Technical Conference and Exhibition, Anaheim, California, U.S.A.
- Weber, K.J. 1982. Influence of Common Sedimentary Structures on Fluid-Flow in Reservoir Models. *J Pet Technol* 34 (3): 665-672. SPE-9247-PA.
- Xia, H., Wang, W., Wu, J., Kong, F. 2004. Elasticity of HPAM solutions increases displacement efficiency under mixed wettability conditions. Paper SPE-88456-MS presented at the 2004 SPE Asia Pacific Oil and Gas Conference and Exhibition, Perth, Australia 18-20 October.
- Xiong, D., Azmy, K., Blamey, N. 2016. Diagenesis and origin of calcite cement in the Flemish Pass Basin sandstone reservoir (Upper Jurassic): Implications for porosity development. *Marine and Petroleum Geology* 70 (2016): 93-118.
- Zhou, Y., Starkey, J. and Mansinha, L. 2004. Segmentation of petrographic images by integrating edge detection and region growing. *Computer & Geoscience*, v. 30, p. 817-831.

APPENDICES

APPENDIX A: Error Analysis

A.1. Reading Errors:

A rule of thumb for evaluating the reading error on measuring devices, such as ruler is $\pm 1/2$ of the smallest division, and for many digital instruments, it is assumed that the reading error is $\pm 1/2$ of the last digit displayed; e.g. in our case that the mass of one of the core plug was measured 139.5842 (g) using a mass balance, the error can be assumed to be ± 0.00005 (g).

In the coreflooding experiments, a 50 mL burette with the 0.1 mL graduation level was used for measuring produced fluids volume. The level of water and oil is read to the nearest 0.1 mL; therefore, a reasonable estimate of the uncertainty in this case would be ± 0.05 ml; e.g. a water or oil measurement could be read as 12.3 ± 0.05 mL.

A.2. Mean Value and Standard Deviation:

The best estimate of a quantity x measured n times (oil recovery in our case), is assumed to be the average or mean value of x (Taylor, 1982):

$$X = \frac{1}{n} \sum_1^n X_i \quad \text{Eq. A.1}$$

The standard deviation of x is given by:

$$\sigma = \sqrt{\frac{\sum_1^n (X_i - X)^2}{n-1}} \quad \text{Eq. A.2}$$

A.3. Propagation of Errors:

For any value of X_1 and X_2 with uncertainty Δx_1 and Δx_2 , respectively. If:

$$y = f(x_1, x_2) \quad \text{Eq. A.3}$$

The simple error calculation is:

$$\Delta y \sim \frac{df}{dx_1} \Delta x_1 + \frac{df}{dx_2} \Delta x_2 \quad \text{Eq. A.4}$$

A.3.1. Calculation of Δy According to the Standard Deviation:

Rule 1: If two mutually independent quantities are being added or subtracted:

$$y = x_1 + x_2 \quad \text{or} \quad y = x_1 - x_2 \quad \text{Eq. A.5}$$

then,

$$\Delta y = \sqrt{(\Delta x_1)^2 + (\Delta x_2)^2} \quad \text{Eq. A.6}$$

Rule 2: If two mutually independent quantities are being multiplied or divided:

$$y = x_1 x_2 \quad \text{or} \quad y = \frac{x_1}{x_2} \quad \text{Eq. A.7}$$

Rule 3: If a quantity is raised to a power:

$$y = x^n \quad \text{Eq. A.8}$$

then,

$$\frac{\Delta y}{y} = n \frac{\Delta x}{x} \quad \text{Eq. A.9}$$

APPENDIX B: Rheology Experiments Raw Data

B.1. Evaluation of viscosity variation of FP-3430S polymer solution at different concentrations, shear rates, and reservoir temperature 62°C.

B.1.1 Deionized water (DW) as solvent for polymer solution preparation

Table B.1.1.1. Rheology results in polymer solution @ 400 mg/L concentrations in DW.

Meas. Pts.	Shear Rate [1/s]	Shear Stress [Pa]	Viscosity [mPa·s]	Speed [1/min]	Torque [μNm]
1	0.10	0.04	357.0	0.03	3.3
2	0.13	0.10	727.0	0.04	8.9
3	0.18	0.14	805.0	0.06	13.1
4	0.24	0.18	753.0	0.08	16.3
5	0.32	0.20	631.0	0.10	18.2
6	0.42	0.21	508.0	0.14	19.6
7	0.56	0.23	404.0	0.18	20.8
8	0.75	0.24	319.0	0.25	21.9
9	1.00	0.26	263.0	0.33	24.0
10	1.33	0.28	209.0	0.44	25.5
11	1.78	0.30	169.0	0.58	27.5
12	2.37	0.34	144.0	0.78	31.2
13	3.16	0.36	115.0	1.03	33.1
14	4.22	0.39	91.9	1.38	35.4
15	5.62	0.42	74.3	1.84	38.2
16	7.50	0.44	59.2	2.45	40.6
17	10.00	0.50	49.7	3.27	45.4
18	13.30	0.53	39.8	4.36	48.5
19	17.80	0.60	33.6	5.82	54.6
20	23.70	0.66	27.7	7.75	60.1
21	31.60	0.73	23.1	10.30	66.8
22	42.20	0.81	19.2	13.80	74.1
23	56.20	0.91	16.2	18.40	83.1
24	75.00	1.02	13.6	24.50	93.4
25	100.00	1.15	11.5	32.70	105.0
26	133.00	1.30	9.8	43.60	119.0
27	178.00	1.47	8.3	58.20	135.0
28	237.00	1.67	7.1	77.50	153.0
29	316.00	1.90	6.0	103.00	174.0
30	422.00	2.20	5.2	138.00	201.0
31	562.00	2.54	4.5	184.00	232.0
32	750.00	2.96	4.0	245.00	270.0
33	1000.00	3.48	3.5	327.00	318.0

Table B.1.1.2. Rheology results in polymer solution @ 1200 mg/L concentrations in DW.

Meas. Pts.	Shear Rate [1/s]	Shear Stress [Pa]	Viscosity [mPa·s]	Speed [1/min]	Torque [μ Nm]
1	0.10	0.15	1450.0	0.03	13.2
2	0.13	0.25	1890.0	0.04	23.0
3	0.18	0.32	1820.0	0.06	29.5
4	0.24	0.37	1570.0	0.08	34.1
5	0.32	0.41	1280.0	0.10	37.0
6	0.42	0.42	1000.0	0.14	38.7
7	0.56	0.44	783.0	0.18	40.2
8	0.75	0.46	609.0	0.25	41.7
9	1.00	0.48	484.0	0.33	44.2
10	1.33	0.51	379.0	0.44	46.2
11	1.78	0.54	303.0	0.58	49.3
12	2.37	0.60	252.0	0.78	54.5
13	3.16	0.63	200.0	1.03	57.9
14	4.22	0.68	161.0	1.38	62.0
15	5.62	0.72	128.0	1.84	65.9
16	7.50	0.78	104.0	2.45	70.9
17	10.00	0.85	85.0	3.27	77.7
18	13.30	0.91	68.0	4.36	82.8
19	17.80	1.00	56.0	5.82	91.1
20	23.70	1.08	45.6	7.75	98.8
21	31.60	1.18	37.3	10.30	108.0
22	42.20	1.29	30.5	13.80	118.0
23	56.20	1.41	25.1	18.40	129.0
24	75.00	1.56	20.9	24.50	143.0
25	100.00	1.74	17.4	32.70	159.0
26	133.00	1.94	14.6	43.60	178.0
27	178.00	2.18	12.3	58.20	199.0
28	237.00	2.46	10.4	77.50	225.0
29	316.00	2.76	8.7	103.00	252.0
30	422.00	3.15	7.5	138.00	288.0
31	562.00	3.54	6.3	184.00	323.0
32	750.00	4.11	5.5	245.00	375.0
33	1000.00	4.73	4.7	327.00	433.0

Table B.1.1.3. Rheology results in polymer solution @ 2000 mg/L concentrations in DW.

Meas. Pts.	Shear Rate [1/s]	Shear Stress [Pa]	Viscosity [mPa·s]	Speed [1/min]	Torque [μ Nm]
1	0.10	0.26	2620.0	0.03	23.8
2	0.13	0.47	3520.0	0.04	42.8
3	0.18	0.61	3440.0	0.06	55.9
4	0.24	0.72	3020.0	0.08	65.4
5	0.32	0.79	2480.0	0.10	71.8
6	0.42	0.83	1960.0	0.14	75.5
7	0.56	0.86	1520.0	0.18	78.2
8	0.75	0.89	1180.0	0.25	80.9
9	1.00	0.93	934.0	0.33	85.4
10	1.33	0.98	738.0	0.44	89.9
11	1.78	1.05	592.0	0.58	96.2
12	2.37	1.14	480.0	0.78	104.0
13	3.16	1.21	383.0	1.03	111.0
14	4.22	1.29	306.0	1.38	118.0
15	5.62	1.37	244.0	1.84	125.0
16	7.50	1.47	196.0	2.45	134.0
17	10.00	1.59	159.0	3.27	146.0
18	13.30	1.69	127.0	4.36	155.0
19	17.80	1.83	103.0	5.82	168.0
20	23.70	1.97	83.1	7.75	180.0
21	31.60	2.12	67.2	10.30	194.0
22	42.20	2.29	54.4	13.80	209.0
23	56.20	2.49	44.3	18.40	228.0
24	75.00	2.72	36.3	24.50	249.0
25	100.00	2.98	29.8	32.70	272.0
26	133.00	3.29	24.6	43.60	300.0
27	178.00	3.63	20.4	58.20	332.0
28	237.00	4.03	17.0	77.50	368.0
29	316.00	4.48	14.2	103.00	410.0
30	422.00	5.07	12.0	138.00	463.0
31	562.00	5.67	10.1	184.00	518.0
32	750.00	6.47	8.6	245.00	591.0
33	1000.00	7.36	7.4	327.00	672.0

Table B.1.1.4. Rheology results in polymer solution @ 2500 mg/L concentrations in DW.

Meas. Pts.	Shear Rate [1/s]	Shear Stress [Pa]	Viscosity [mPa·s]	Speed [1/min]	Torque [μ Nm]
1	0.10	0.33	3330.0	0.03	30.4
2	0.13	0.60	4460.0	0.04	54.3
3	0.18	0.78	4390.0	0.06	71.3
4	0.24	0.91	3850.0	0.08	83.4
5	0.32	1.00	3170.0	0.10	91.5
6	0.42	1.06	2500.0	0.14	96.4
7	0.56	1.10	1950.0	0.18	100.0
8	0.75	1.14	1520.0	0.25	104.0
9	1.00	1.20	1200.0	0.33	110.0
10	1.33	1.26	947.0	0.44	115.0
11	1.78	1.35	757.0	0.58	123.0
12	2.37	1.45	612.0	0.78	133.0
13	3.16	1.55	489.0	1.03	141.0
14	4.22	1.64	390.0	1.38	150.0
15	5.62	1.74	310.0	1.84	159.0
16	7.50	1.86	248.0	2.45	170.0
17	10.00	2.01	201.0	3.27	183.0
18	13.30	2.13	160.0	4.36	195.0
19	17.80	2.30	129.0	5.82	210.0
20	23.70	2.46	104.0	7.75	225.0
21	31.60	2.64	83.6	10.30	242.0
22	42.20	2.85	67.6	13.80	260.0
23	56.20	3.09	54.9	18.40	282.0
24	75.00	3.36	44.8	24.50	307.0
25	100.00	3.67	36.7	32.70	335.0
26	133.00	4.01	30.0	43.60	366.0
27	178.00	4.41	24.8	58.20	403.0
28	237.00	4.88	20.6	77.50	446.0
29	316.00	5.35	16.9	103.00	489.0
30	422.00	6.06	14.4	138.00	554.0
31	562.00	6.79	12.1	184.00	621.0
32	750.00	7.64	10.2	245.00	699.0
33	1000.00	8.66	8.7	327.00	792.0

Table B.1.1.5. Rheology results in polymer solution @ 3000 mg/L concentrations in DW.

Meas. Pts.	Shear Rate [1/s]	Shear Stress [Pa]	Viscosity [mPa·s]	Speed [1/min]	Torque [μNm]
1	0.10	0.41	4100.0	0.03	37.4
2	0.13	0.72	5420.0	0.04	66.0
3	0.18	0.94	5300.0	0.06	86.1
4	0.24	1.10	4650.0	0.08	101.0
5	0.32	1.21	3820.0	0.10	110.0
6	0.42	1.28	3030.0	0.14	117.0
7	0.56	1.34	2380.0	0.18	122.0
8	0.75	1.40	1860.0	0.25	128.0
9	1.00	1.48	1480.0	0.33	135.0
10	1.33	1.57	1170.0	0.44	143.0
11	1.78	1.67	940.0	0.58	153.0
12	2.37	1.80	760.0	0.78	165.0
13	3.16	1.92	608.0	1.03	176.0
14	4.22	2.05	487.0	1.38	188.0
15	5.62	2.19	389.0	1.84	200.0
16	7.50	2.35	313.0	2.45	215.0
17	10.00	2.54	254.0	3.27	232.0
18	13.30	2.72	204.0	4.36	249.0
19	17.80	2.95	166.0	5.82	269.0
20	23.70	3.17	134.0	7.75	290.0
21	31.60	3.41	108.0	10.30	311.0
22	42.20	3.66	86.9	13.80	335.0
23	56.20	3.96	70.5	18.40	362.0
24	75.00	4.29	57.3	24.50	393.0
25	100.00	4.67	46.7	32.70	427.0
26	133.00	5.10	38.3	43.60	466.0
27	178.00	5.59	31.4	58.20	511.0
28	237.00	6.12	25.8	77.50	559.0
29	316.00	6.74	21.3	103.00	616.0
30	422.00	7.51	17.8	138.00	687.0
31	562.00	8.31	14.8	184.00	760.0
32	750.00	9.41	12.5	245.00	860.0
33	1000.00	10.60	10.6	327.00	966.0

Table B.1.1.6. Rheology results in polymer solution @ 3500 mg/L concentrations in DW

Meas. Pts.	Shear Rate [1/s]	Shear Stress [Pa]	Viscosity [mPa·s]	Speed [1/min]	Torque [μ Nm]
1	0.10	1.08	10800.0	0.03	98.5
2	0.13	1.74	13100.0	0.04	159.0
3	0.18	2.17	12200.0	0.06	198.0
4	0.24	2.47	10400.0	0.08	226.0
5	0.32	2.69	8510.0	0.10	246.0
6	0.42	2.84	6730.0	0.14	260.0
7	0.56	2.93	5210.0	0.18	268.0
8	0.75	3.01	4010.0	0.25	275.0
9	1.00	3.10	3100.0	0.33	283.0
10	1.33	3.24	2430.0	0.44	296.0
11	1.78	3.44	1930.0	0.58	314.0
12	2.37	3.65	1540.0	0.78	333.0
13	3.16	3.86	1220.0	1.03	353.0
14	4.22	4.11	974.0	1.38	375.0
15	5.62	4.37	777.0	1.84	399.0
16	7.50	4.66	621.0	2.45	426.0
17	10.00	4.97	497.0	3.27	455.0
18	13.30	5.30	397.0	4.36	484.0
19	17.80	5.62	316.0	5.82	514.0
20	23.70	5.95	251.0	7.75	543.0
21	31.60	6.30	199.0	10.30	576.0
22	42.20	6.69	159.0	13.80	611.0
23	56.20	7.11	126.0	18.40	650.0
24	75.00	7.58	101.0	24.50	693.0
25	100.00	8.10	81.0	32.70	741.0
26	133.00	8.69	65.1	43.60	794.0
27	178.00	9.35	52.6	58.20	855.0
28	237.00	10.10	42.5	77.50	920.0
29	316.00	10.90	34.3	103.00	992.0
30	422.00	11.80	28.0	138.00	1080.0
31	562.00	12.90	23.0	184.00	1180.0
32	750.00	14.40	19.2	245.00	1320.0
33	1000.00	15.90	15.9	327.00	1460.0

Table B.1.1.7. Rheology results in polymer solution @ 4000 mg/L concentrations in DW

Meas. Pts.	Shear Rate [1/s]	Shear Stress [Pa]	Viscosity [mPa·s]	Speed [1/min]	Torque [μ Nm]
1	0.10	1.52	15200.0	0.03	139.0
2	0.13	2.41	18100.0	0.04	220.0
3	0.18	2.99	16800.0	0.06	273.0
4	0.24	3.45	14600.0	0.08	316.0
5	0.32	3.82	12100.0	0.10	349.0
6	0.42	4.08	9680.0	0.14	373.0
7	0.56	4.24	7540.0	0.18	388.0
8	0.75	4.34	5790.0	0.25	397.0
9	1.00	4.46	4460.0	0.33	408.0
10	1.33	4.65	3490.0	0.44	425.0
11	1.78	4.92	2770.0	0.58	450.0
12	2.37	5.23	2210.0	0.78	478.0
13	3.16	5.56	1760.0	1.03	508.0
14	4.22	5.91	1400.0	1.38	540.0
15	5.62	6.29	1120.0	1.84	575.0
16	7.50	6.68	891.0	2.45	611.0
17	10.00	7.09	709.0	3.27	648.0
18	13.30	7.53	564.0	4.36	688.0
19	17.80	7.95	447.0	5.82	726.0
20	23.70	8.39	354.0	7.75	767.0
21	31.60	8.87	281.0	10.30	811.0
22	42.20	9.39	223.0	13.80	858.0
23	56.20	9.95	177.0	18.40	909.0
24	75.00	10.60	141.0	24.50	965.0
25	100.00	11.20	112.0	32.70	1030.0
26	133.00	11.90	89.5	43.60	1090.0
27	178.00	12.70	71.7	58.20	1170.0
28	237.00	13.60	57.5	77.50	1250.0
29	316.00	14.60	46.2	103.00	1340.0
30	422.00	15.80	37.4	138.00	1440.0
31	562.00	17.10	30.4	184.00	1560.0
32	750.00	18.90	25.2	245.00	1730.0
33	1000.00	20.70	20.7	327.00	1890.0

Table B.1.1.8. Rheology results in polymer solution @ 4500 mg/L concentrations in DW

Meas. Pts.	Shear Rate [1/s]	Shear Stress [Pa]	Viscosity [mPa·s]	Speed [1/min]	Torque [μ Nm]
1	0.10	1.82	18200.0	0.03	166.0
2	0.13	2.87	21500.0	0.04	262.0
3	0.18	3.54	19900.0	0.06	323.0
4	0.24	4.05	17100.0	0.08	370.0
5	0.32	4.46	14100.0	0.10	408.0
6	0.42	4.76	11300.0	0.14	435.0
7	0.56	4.94	8790.0	0.18	452.0
8	0.75	5.05	6740.0	0.25	462.0
9	1.00	5.18	5180.0	0.33	474.0
10	1.33	5.40	4050.0	0.44	493.0
11	1.78	5.72	3210.0	0.58	522.0
12	2.37	6.09	2570.0	0.78	556.0
13	3.16	6.47	2050.0	1.03	591.0
14	4.22	6.88	1630.0	1.38	629.0
15	5.62	7.33	1300.0	1.84	670.0
16	7.50	7.79	1040.0	2.45	712.0
17	10.00	8.25	825.0	3.27	754.0
18	13.30	8.73	655.0	4.36	798.0
19	17.80	9.20	518.0	5.82	841.0
20	23.70	9.70	409.0	7.75	887.0
21	31.60	10.20	323.0	10.30	935.0
22	42.20	10.80	256.0	13.80	986.0
23	56.20	11.40	203.0	18.40	1040.0
24	75.00	12.10	161.0	24.50	1100.0
25	100.00	12.80	128.0	32.70	1170.0
26	133.00	13.60	102.0	43.60	1240.0
27	178.00	14.50	81.5	58.20	1320.0
28	237.00	15.50	65.4	77.50	1420.0
29	316.00	16.60	52.4	103.00	1510.0
30	422.00	17.80	42.3	138.00	1630.0
31	562.00	19.40	34.4	184.00	1770.0
32	750.00	21.10	28.1	245.00	1930.0
33	1000.00	23.30	23.3	327.00	2130.0

B.1.2 Seawater (SW) as solution for polymer solution preparation

Table B.1.2.1. Rheology results in polymer solution @ 400 mg/L concentrations in SW

Meas. Pts.	Shear Rate [1/s]	Shear Stress [Pa]	Viscosity [mPa·s]	Speed [1/min]	Torque [μ Nm]
1	0.10	0.003	35.0	0.03	0.3
2	0.13	0.004	29.2	0.04	0.4
3	0.18	0.003	23.0	0.06	0.3
4	0.24	0.004	17.7	0.08	0.4
5	0.32	0.005	16.0	0.10	0.5
6	0.42	0.004	11.0	0.14	0.4
7	0.56	0.006	9.9	0.18	0.5
8	0.75	0.007	9.1	0.25	0.6
9	1.00	0.007	7.1	0.33	0.7
10	1.33	0.009	6.5	0.44	0.8
11	1.78	0.012	6.7	0.58	1.1
12	2.37	0.014	5.9	0.78	1.3
13	3.16	0.018	5.6	1.03	1.6
14	4.22	0.028	6.5	1.38	2.5
15	5.62	0.037	6.3	1.84	3.4
16	7.50	0.039	5.3	2.45	3.6
17	10.00	0.037	3.7	3.27	3.4
18	13.30	0.037	2.8	4.36	3.4
19	17.80	0.031	1.7	5.82	2.8
20	23.70	0.030	1.3	7.75	2.7
21	31.60	0.033	1.0	10.30	3.0
22	42.20	0.042	1.0	13.80	3.8
23	56.20	0.054	1.0	18.40	4.9
24	75.00	0.072	1.0	24.50	6.5
25	100.00	0.094	0.9	32.70	8.6
26	133.00	0.126	0.9	43.60	11.5
27	178.00	0.166	0.9	58.20	15.1
28	237.00	0.216	0.9	77.50	19.7
29	316.00	0.294	0.9	103.00	26.9
30	422.00	0.395	0.9	138.00	36.1
31	562.00	0.515	0.9	184.00	47.1
32	750.00	0.677	0.9	245.00	61.8
33	1000.00	1.020	1.0	327.00	93.6

Table B.1.2.2. Rheology results in polymer solution @ 1000 mg/L concentrations in SW

Meas. Pts.	Shear Rate [1/s]	Shear Stress [Pa]	Viscosity [mPa·s]	Speed [1/min]	Torque [μNm]
1	0.10	0.013	66.0	0.03	1.2
2	0.13	0.012	57.0	0.04	1.1
3	0.18	0.012	42.1	0.06	1.1
4	0.24	0.012	34.2	0.08	1.1
5	0.32	0.013	29.9	0.10	1.2
6	0.42	0.014	25.0	0.14	1.3
7	0.56	0.016	20.4	0.18	1.4
8	0.75	0.016	18.9	0.25	1.4
9	1.00	0.017	17.4	0.33	1.6
10	1.33	0.018	13.7	0.44	1.7
11	1.78	0.022	12.1	0.58	2.0
12	2.37	0.027	11.2	0.78	2.4
13	3.16	0.031	9.7	1.03	2.8
14	4.22	0.037	8.9	1.38	3.4
15	5.62	0.046	8.1	1.84	4.2
16	7.50	0.058	7.7	2.45	5.3
17	10.00	0.059	5.9	3.27	5.4
18	13.30	0.071	5.3	4.36	6.5
19	17.80	0.084	4.7	5.82	7.7
20	23.70	0.108	4.6	7.75	9.9
21	31.60	0.134	4.3	10.30	12.3
22	42.20	0.171	4.0	13.80	15.6
23	56.20	0.211	3.8	18.40	19.3
24	75.00	0.258	3.4	24.50	23.6
25	100.00	0.303	3.0	32.70	27.7
26	133.00	0.363	2.7	43.60	33.2
27	178.00	0.431	2.4	58.20	39.4
28	237.00	0.518	2.2	77.50	47.3
29	316.00	0.654	2.1	103.00	59.8
30	422.00	0.834	2.0	138.00	76.2
31	562.00	1.080	1.9	184.00	98.4
32	750.00	1.400	1.9	245.00	128.0
33	1000.00	1.870	1.9	327.00	171.0

Table B.1.2.2. Rheology results in polymer solution @ 1800 mg/L concentrations in SW

Meas. Pts.	Shear Rate [1/s]	Shear Stress [Pa]	Viscosity [mPa·s]	Speed [1/min]	Torque [μ Nm]
1	0.10	0.003	144.0	0.03	0.3
2	0.13	0.004	123.0	0.04	0.4
3	0.18	0.003	93.0	0.06	0.3
4	0.24	0.005	67.0	0.08	0.4
5	0.32	0.006	49.0	0.10	0.6
6	0.42	0.008	38.3	0.14	0.7
7	0.56	0.010	31.5	0.18	0.9
8	0.75	0.011	27.4	0.25	1.0
9	1.00	0.014	23.2	0.33	1.2
10	1.33	0.017	20.1	0.44	1.5
11	1.78	0.021	18.5	0.58	1.9
12	2.37	0.026	16.5	0.78	2.4
13	3.16	0.034	14.3	1.03	3.1
14	4.22	0.046	12.9	1.38	4.2
15	5.62	0.060	11.8	1.84	5.5
16	7.50	0.073	10.3	2.45	6.7
17	10.00	0.091	9.1	3.27	8.3
18	13.30	0.119	8.9	4.36	10.8
19	17.80	0.148	8.3	5.82	13.5
20	23.70	0.188	7.9	7.75	17.2
21	31.60	0.237	7.5	10.30	21.7
22	42.20	0.299	7.1	13.80	27.3
23	56.20	0.372	6.6	18.40	34.0
24	75.00	0.465	6.2	24.50	42.5
25	100.00	0.578	5.8	32.70	52.8
26	133.00	0.720	5.4	43.60	65.8
27	178.00	0.892	5.0	58.20	81.5
28	237.00	1.100	4.6	77.50	100.0
29	316.00	1.360	4.3	103.00	124.0
30	422.00	1.700	4.0	138.00	155.0
31	562.00	2.150	3.8	184.00	196.0
32	750.00	2.670	3.6	245.00	244.0
33	1000.00	3.410	3.4	327.00	312.0

Table B.1.2.3. Rheology results in polymer solution @ 2000 mg/L concentrations in SW

Meas. Pts.	Shear Rate [1/s]	Shear Stress [Pa]	Viscosity [mPa·s]	Speed [1/min]	Torque [μ Nm]
1	0.10	0.007	212.0	0.03	0.7
2	0.13	0.009	185.0	0.04	0.9
3	0.18	0.012	140.0	0.06	1.1
4	0.24	0.012	120.0	0.08	1.1
5	0.32	0.013	95.0	0.10	1.2
6	0.42	0.011	76.0	0.14	1.0
7	0.56	0.015	63.0	0.18	1.4
8	0.75	0.019	55.0	0.25	1.8
9	1.00	0.024	50.0	0.33	2.2
10	1.33	0.030	42.0	0.44	2.8
11	1.78	0.039	35.0	0.58	3.6
12	2.37	0.051	31.0	0.78	4.6
13	3.16	0.066	29.0	1.03	6.0
14	4.22	0.086	26.0	1.38	7.9
15	5.62	0.111	23.0	1.84	10.2
16	7.50	0.139	20.0	2.45	12.7
17	10.00	0.171	17.1	3.27	15.6
18	13.30	0.218	16.3	4.36	19.9
19	17.80	0.266	14.9	5.82	24.3
20	23.70	0.330	13.9	7.75	30.2
21	31.60	0.406	12.8	10.30	37.1
22	42.20	0.499	11.8	13.80	45.6
23	56.20	0.607	10.8	18.40	55.5
24	75.00	0.738	9.9	24.50	67.5
25	100.00	0.890	8.9	32.70	81.3
26	133.00	1.070	8.0	43.60	97.9
27	178.00	1.290	7.2	58.20	117.0
28	237.00	1.540	6.5	77.50	141.0
29	316.00	1.880	5.9	103.00	171.0
30	422.00	2.280	5.4	138.00	208.0
31	562.00	2.830	5.0	184.00	259.0
32	750.00	3.500	4.7	245.00	320.0
33	1000.00	4.380	4.4	327.00	400.0

Table B.1.2.4. Rheology results in polymer solution @ 2500 mg/L concentrations in SW

Meas. Pts.	Shear Rate [1/s]	Shear Stress [Pa]	Viscosity [mPa·s]	Speed [1/min]	Torque [μ Nm]
1	0.10	0.007	212.0	0.03	0.7
2	0.13	0.009	185.0	0.04	0.9
3	0.18	0.012	140.0	0.06	1.1
4	0.24	0.012	120.0	0.08	1.1
5	0.32	0.013	95.0	0.10	1.2
6	0.42	0.011	76.0	0.14	1.0
7	0.56	0.015	63.0	0.18	1.4
8	0.75	0.019	55.0	0.25	1.8
9	1.00	0.024	50.0	0.33	2.2
10	1.33	0.030	42.0	0.44	2.8
11	1.78	0.039	35.0	0.58	3.6
12	2.37	0.051	31.0	0.78	4.6
13	3.16	0.066	29.0	1.03	6.0
14	4.22	0.086	26.0	1.38	7.9
15	5.62	0.111	23.0	1.84	10.2
16	7.50	0.139	20.0	2.45	12.7
17	10.00	0.171	17.1	3.27	15.6
18	13.30	0.218	16.3	4.36	19.9
19	17.80	0.266	14.9	5.82	24.3
20	23.70	0.330	13.9	7.75	30.2
21	31.60	0.406	12.8	10.30	37.1
22	42.20	0.499	11.8	13.80	45.6
23	56.20	0.607	10.8	18.40	55.5
24	75.00	0.738	9.9	24.50	67.5
25	100.00	0.890	8.9	32.70	81.3
26	133.00	1.070	8.0	43.60	97.9
27	178.00	1.290	7.2	58.20	117.0
28	237.00	1.540	6.5	77.50	141.0
29	316.00	1.880	5.9	103.00	171.0
30	422.00	2.280	5.4	138.00	208.0
31	562.00	2.830	5.0	184.00	259.0
32	750.00	3.500	4.7	245.00	320.0
33	1000.00	4.380	4.4	327.00	400.0

Table B.1.2.5. Rheology results in polymer solution @ 3000 mg/L concentrations in SW

Meas. Pts.	Shear Rate [1/s]	Shear Stress [Pa]	Viscosity [mPa·s]	Speed [1/min]	Torque [μ Nm]
1	0.10	0.045	265.0	0.03	4.2
2	0.13	0.045	230.0	0.04	4.1
3	0.18	0.046	199.0	0.06	4.2
4	0.24	0.047	174.0	0.08	4.3
5	0.32	0.052	150.0	0.10	4.8
6	0.42	0.058	128.0	0.14	5.3
7	0.56	0.064	113.0	0.18	5.8
8	0.75	0.076	101.0	0.25	7.0
9	1.00	0.090	90.1	0.33	8.2
10	1.33	0.108	80.9	0.44	9.9
11	1.78	0.127	71.5	0.58	11.6
12	2.37	0.149	63.0	0.78	13.6
13	3.16	0.169	53.5	1.03	15.5
14	4.22	0.200	47.5	1.38	18.3
15	5.62	0.240	42.6	1.84	21.9
16	7.50	0.295	39.3	2.45	27.0
17	10.00	0.361	36.1	3.27	33.0
18	13.30	0.429	32.2	4.36	39.3
19	17.80	0.523	29.4	5.82	47.8
20	23.70	0.628	26.5	7.75	57.4
21	31.60	0.745	23.6	10.30	68.1
22	42.20	0.881	20.9	13.80	80.5
23	56.20	1.030	18.3	18.40	94.1
24	75.00	1.210	16.1	24.50	110.0
25	100.00	1.410	14.1	32.70	129.0
26	133.00	1.660	12.4	43.60	151.0
27	178.00	1.950	11.0	58.20	178.0
28	237.00	2.300	9.7	77.50	210.0
29	316.00	2.760	8.7	103.00	252.0
30	422.00	3.350	7.9	138.00	306.0
31	562.00	4.060	7.2	184.00	371.0
32	750.00	4.940	6.6	245.00	451.0
33	1000.00	6.030	6.0	327.00	551.0

Table B.1.2.6. Rheology results in polymer solution @ 3500 mg/L concentrations in SW

Meas. Pts.	Shear Rate [1/s]	Shear Stress [Pa]	Viscosity [mPa·s]	Speed [1/min]	Torque [μ Nm]
1	0.10	0.020	320.0	0.03	1.9
2	0.13	0.025	305.0	0.04	2.3
3	0.18	0.028	262.0	0.06	2.5
4	0.24	0.032	221.0	0.08	3.0
5	0.32	0.040	179.0	0.10	3.6
6	0.42	0.050	158.0	0.14	4.6
7	0.56	0.063	138.0	0.18	5.7
8	0.75	0.078	124.0	0.25	7.2
9	1.00	0.098	118.0	0.33	9.0
10	1.33	0.123	102.0	0.44	11.3
11	1.78	0.156	90.6	0.58	14.2
12	2.37	0.192	81.2	0.78	17.6
13	3.16	0.236	74.6	1.03	21.5
14	4.22	0.284	67.4	1.38	26.0
15	5.62	0.339	60.4	1.84	31.0
16	7.50	0.407	54.3	2.45	37.2
17	10.00	0.489	48.9	3.27	44.7
18	13.30	0.584	43.8	4.36	53.4
19	17.80	0.694	39.0	5.82	63.4
20	23.70	0.820	34.6	7.75	75.0
21	31.60	0.965	30.5	10.30	88.2
22	42.20	1.130	26.9	13.80	104.0
23	56.20	1.330	23.6	18.40	121.0
24	75.00	1.550	20.7	24.50	142.0
25	100.00	1.800	18.0	32.70	165.0
26	133.00	2.110	15.8	43.60	192.0
27	178.00	2.470	13.9	58.20	226.0
28	237.00	2.920	12.3	77.50	267.0
29	316.00	3.480	11.0	103.00	318.0
30	422.00	4.150	9.9	138.00	380.0
31	562.00	4.960	8.8	184.00	453.0
32	750.00	5.950	7.9	245.00	544.0
33	1000.00	7.210	7.2	327.00	659.0

Table B.1.2.7. Rheology results in polymer solution @ 4000 mg/L concentrations in SW

Meas. Pts.	Shear Rate [1/s]	Shear Stress [Pa]	Viscosity [mPa·s]	Speed [1/min]	Torque [μ Nm]
1	0.10	0.043	385.0	0.03	3.9
2	0.13	0.050	376.0	0.04	4.6
3	0.18	0.059	331.0	0.06	5.4
4	0.24	0.064	271.0	0.08	5.9
5	0.32	0.077	244.0	0.10	7.1
6	0.42	0.090	212.0	0.14	8.2
7	0.56	0.107	191.0	0.18	9.8
8	0.75	0.131	175.0	0.25	12.0
9	1.00	0.155	155.0	0.33	14.2
10	1.33	0.188	141.0	0.44	17.2
11	1.78	0.230	129.0	0.58	21.0
12	2.37	0.276	116.0	0.78	25.2
13	3.16	0.329	104.0	1.03	30.1
14	4.22	0.394	93.3	1.38	36.0
15	5.62	0.468	83.3	1.84	42.8
16	7.50	0.547	73.0	2.45	50.0
17	10.00	0.647	64.7	3.27	59.1
18	13.30	0.760	57.0	4.36	69.5
19	17.80	0.887	49.9	5.82	81.1
20	23.70	1.030	43.5	7.75	94.4
21	31.60	1.200	37.8	10.30	109.0
22	42.20	1.380	32.8	13.80	126.0
23	56.20	1.590	28.3	18.40	145.0
24	75.00	1.840	24.5	24.50	168.0
25	100.00	2.120	21.2	32.70	194.0
26	133.00	2.470	18.5	43.60	226.0
27	178.00	2.890	16.3	58.20	264.0
28	237.00	3.400	14.3	77.50	311.0
29	316.00	4.010	12.7	103.00	367.0
30	422.00	4.750	11.3	138.00	434.0
31	562.00	5.640	10.0	184.00	515.0
32	750.00	6.710	8.9	245.00	613.0
33	1000.00	8.050	8.1	327.00	736.0

Table B.1.2.7. Rheology results in polymer solution @ 4500 mg/L concentrations in SW

Meas. Pts.	Shear Rate [1/s]	Shear Stress [Pa]	Viscosity [mPa·s]	Speed [1/min]	Torque [μ Nm]
1	0.10	0.043	434.0	0.03	4.0
2	0.13	0.061	455.0	0.04	5.5
3	0.18	0.078	439.0	0.06	7.1
4	0.24	0.099	417.0	0.08	9.0
5	0.32	0.123	388.0	0.10	11.2
6	0.42	0.150	355.0	0.14	13.7
7	0.56	0.180	321.0	0.18	16.5
8	0.75	0.213	285.0	0.25	19.5
9	1.00	0.251	251.0	0.33	22.9
10	1.33	0.294	220.0	0.44	26.9
11	1.78	0.341	192.0	0.58	31.2
12	2.37	0.402	170.0	0.78	36.8
13	3.16	0.476	150.0	1.03	43.5
14	4.22	0.562	133.0	1.38	51.4
15	5.62	0.664	118.0	1.84	60.6
16	7.50	0.762	102.0	2.45	69.6
17	10.00	0.888	88.8	3.27	81.2
18	13.30	1.060	79.3	4.36	96.7
19	17.80	1.220	68.9	5.82	112.0
20	23.70	1.430	60.4	7.75	131.0
21	31.60	1.670	52.8	10.30	153.0
22	42.20	1.940	46.0	13.80	177.0
23	56.20	2.240	39.8	18.40	205.0
24	75.00	2.590	34.5	24.50	237.0
25	100.00	2.990	29.9	32.70	273.0
26	133.00	3.460	25.9	43.60	316.0
27	178.00	4.020	22.6	58.20	367.0
28	237.00	4.690	19.8	77.50	429.0
29	316.00	5.490	17.4	103.00	502.0
30	422.00	6.410	15.2	138.00	586.0
31	562.00	7.580	13.5	184.00	692.0
32	750.00	8.950	11.9	245.00	818.0
33	1000.00	10.600	10.6	327.00	970.0

B.1.3 Synthetic formation water (FW) as solution for polymer solution preparation

Table B.1.3.1. Rheology results in polymer solution @ 400 mg/L concentrations in FW

Meas. Pts.	Shear Rate [1/s]	Shear Stress [Pa]	Viscosity [mPa·s]	Speed [1/min]	Torque [μNm]
1	0.10	0.003	15.50	0.03	0.26
2	0.13	0.003	14.70	0.04	0.31
3	0.18	0.004	15.00	0.06	0.40
4	0.24	0.005	13.50	0.08	0.46
5	0.32	0.006	12.00	0.10	0.51
6	0.42	0.004	8.44	0.14	0.33
7	0.56	0.004	7.64	0.18	0.39
8	0.75	0.005	6.48	0.25	0.44
9	1.00	0.005	4.58	0.33	0.42
10	1.33	0.004	3.11	0.44	0.38
11	1.78	0.004	2.12	0.58	0.34
12	2.37	0.004	1.58	0.78	0.34
13	3.16	0.004	1.37	1.03	0.40
14	4.22	0.007	1.45	1.38	0.60
15	5.62	0.008	1.41	1.84	0.73
16	7.50	0.010	1.31	2.45	0.90
17	10.00	0.013	1.25	3.27	1.14
18	13.30	0.016	1.20	4.36	1.47
19	17.80	0.021	1.19	5.82	1.93
20	23.70	0.029	1.22	7.75	2.64
21	31.60	0.037	1.18	10.30	3.42
22	42.20	0.049	1.16	13.80	4.47
23	56.20	0.064	1.13	18.40	5.82
24	75.00	0.085	1.13	24.50	7.72
25	100.00	0.110	1.10	32.70	10.00
26	133.00	0.147	1.10	43.60	13.40
27	178.00	0.191	1.07	58.20	17.40
28	237.00	0.249	1.05	77.50	22.80
29	316.00	0.330	1.04	103.00	30.10
30	422.00	0.438	1.04	138.00	40.00
31	562.00	0.586	1.04	184.00	53.50
32	750.00	0.772	1.03	245.00	70.50
33	1000.00	1.090	1.09	327.00	99.80

Table B.1.3.2. Rheology results in polymer solution @ 1200 mg/L concentrations in FW

Meas. Pts.	Shear Rate [1/s]	Shear Stress [Pa]	Viscosity [mPa·s]	Speed [1/min]	Torque [μ Nm]
1	0.10	0.002	22.10	0.03	0.21
2	0.13	0.004	20.80	0.04	0.35
3	0.18	0.005	22.00	0.06	0.48
4	0.24	0.006	20.00	0.08	0.51
5	0.32	0.005	16.20	0.10	0.47
6	0.42	0.006	14.30	0.14	0.55
7	0.56	0.006	10.70	0.18	0.55
8	0.75	0.007	9.03	0.25	0.62
9	1.00	0.007	6.58	0.33	0.60
10	1.33	0.007	5.21	0.44	0.64
11	1.78	0.008	4.43	0.58	0.72
12	2.37	0.010	4.27	0.78	0.93
13	3.16	0.013	4.25	1.03	1.23
14	4.22	0.019	4.46	1.38	1.72
15	5.62	0.025	4.42	1.84	2.27
16	7.50	0.031	4.16	2.45	2.85
17	10.00	0.040	3.97	3.27	3.62
18	13.30	0.051	3.79	4.36	4.62
19	17.80	0.063	3.54	5.82	5.76
20	23.70	0.080	3.35	7.75	7.26
21	31.60	0.102	3.22	10.30	9.31
22	42.20	0.133	3.15	13.80	12.20
23	56.20	0.170	3.03	18.40	15.60
24	75.00	0.220	2.93	24.50	20.10
25	100.00	0.280	2.80	32.70	25.60
26	133.00	0.360	2.70	43.60	32.90
27	178.00	0.457	2.57	58.20	41.80
28	237.00	0.581	2.45	77.50	53.10
29	316.00	0.744	2.35	103.00	68.00
30	422.00	0.956	2.27	138.00	87.40
31	562.00	1.240	2.20	184.00	113.00
32	750.00	1.590	2.12	245.00	145.00
33	1000.00	2.060	2.06	327.00	188.00

Table B.1.3.3. Rheology results in polymer solution @ 1800 mg/L concentrations in FW

Meas. Pts.	Shear Rate [1/s]	Shear Stress [Pa]	Viscosity [mPa·s]	Speed [1/min]	Torque [μ Nm]
1	0.10	0.003	27.40	0.03	0.25
2	0.13	0.004	26.50	0.04	0.32
3	0.18	0.005	27.10	0.06	0.44
4	0.24	0.006	25.40	0.08	0.55
5	0.32	0.007	20.50	0.10	0.59
6	0.42	0.007	17.70	0.14	0.68
7	0.56	0.009	15.60	0.18	0.80
8	0.75	0.010	13.70	0.25	0.94
9	1.00	0.012	12.10	0.33	1.10
10	1.33	0.014	10.60	0.44	1.30
11	1.78	0.018	9.92	0.58	1.61
12	2.37	0.023	9.52	0.78	2.06
13	3.16	0.028	8.96	1.03	2.59
14	4.22	0.036	8.58	1.38	3.31
15	5.62	0.045	8.04	1.84	4.13
16	7.50	0.060	7.93	2.45	5.44
17	10.00	0.075	7.53	3.27	6.88
18	13.30	0.097	7.28	4.36	8.88
19	17.80	0.125	7.00	5.82	11.40
20	23.70	0.160	6.73	7.75	14.60
21	31.60	0.202	6.39	10.30	18.50
22	42.20	0.256	6.07	13.80	23.40
23	56.20	0.321	5.71	18.40	29.30
24	75.00	0.403	5.38	24.50	36.90
25	100.00	0.503	5.03	32.70	45.90
26	133.00	0.630	4.72	43.60	57.50
27	178.00	0.782	4.40	58.20	71.40
28	237.00	0.971	4.09	77.50	88.70
29	316.00	1.210	3.83	103.00	111.00
30	422.00	1.520	3.60	138.00	139.00
31	562.00	1.920	3.41	184.00	175.00
32	750.00	2.410	3.22	245.00	221.00
33	1000.00	3.100	3.10	327.00	284.00

Table B.1.3.4. Rheology results in polymer solution @ 2000 mg/L concentrations in FW

Meas. Pts.	Shear Rate [1/s]	Shear Stress [Pa]	Viscosity [mPa·s]	Speed [1/min]	Torque [μ Nm]
1	0.10	0.003	33.40	0.03	0.31
2	0.13	0.004	31.80	0.04	0.39
3	0.18	0.006	33.20	0.06	0.54
4	0.24	0.008	31.70	0.08	0.69
5	0.32	0.009	28.40	0.10	0.82
6	0.42	0.010	24.10	0.14	0.93
7	0.56	0.012	21.70	0.18	1.11
8	0.75	0.014	19.20	0.25	1.31
9	1.00	0.018	18.00	0.33	1.65
10	1.33	0.022	16.80	0.44	2.04
11	1.78	0.028	15.50	0.58	2.52
12	2.37	0.036	15.10	0.78	3.27
13	3.16	0.044	13.90	1.03	4.01
14	4.22	0.056	13.40	1.38	5.16
15	5.62	0.072	12.70	1.84	6.54
16	7.50	0.090	12.00	2.45	8.24
17	10.00	0.114	11.40	3.27	10.40
18	13.30	0.145	10.90	4.36	13.30
19	17.80	0.184	10.30	5.82	16.80
20	23.70	0.232	9.78	7.75	21.20
21	31.60	0.290	9.16	10.30	26.50
22	42.20	0.361	8.56	13.80	33.00
23	56.20	0.447	7.95	18.40	40.90
24	75.00	0.554	7.38	24.50	50.60
25	100.00	0.681	6.81	32.70	62.30
26	133.00	0.840	6.30	43.60	76.80
27	178.00	1.030	5.79	58.20	94.10
28	237.00	1.260	5.32	77.50	115.00
29	316.00	1.550	4.91	103.00	142.00
30	422.00	1.920	4.54	138.00	175.00
31	562.00	2.400	4.27	184.00	220.00
32	750.00	3.020	4.02	245.00	276.00
33	1000.00	3.830	3.83	327.00	350.00

Table B.1.3.5. Rheology results in polymer solution @ 2500 mg/L concentrations in FW

Meas. Pts.	Shear Rate [1/s]	Shear Stress [Pa]	Viscosity [mPa·s]	Speed [1/min]	Torque [μ Nm]
1	0.10	0.003	41.80	0.03	0.30
2	0.13	0.003	41.30	0.04	0.30
3	0.18	0.005	42.00	0.06	0.49
4	0.24	0.007	39.00	0.08	0.63
5	0.32	0.008	36.50	0.10	0.77
6	0.42	0.010	32.00	0.14	0.94
7	0.56	0.013	29.00	0.18	1.19
8	0.75	0.016	26.20	0.25	1.47
9	1.00	0.021	23.50	0.33	1.88
10	1.33	0.028	21.10	0.44	2.58
11	1.78	0.038	21.20	0.58	3.44
12	2.37	0.049	20.60	0.78	4.47
13	3.16	0.063	19.90	1.03	5.74
14	4.22	0.082	19.40	1.38	7.48
15	5.62	0.105	18.80	1.84	9.64
16	7.50	0.132	17.70	2.45	12.10
17	10.00	0.167	16.70	3.27	15.20
18	13.30	0.212	15.90	4.36	19.30
19	17.80	0.263	14.80	5.82	24.00
20	23.70	0.327	13.80	7.75	29.90
21	31.60	0.402	12.70	10.30	36.70
22	42.20	0.494	11.70	13.80	45.20
23	56.20	0.603	10.70	18.40	55.10
24	75.00	0.736	9.81	24.50	67.20
25	100.00	0.894	8.94	32.70	81.70
26	133.00	1.090	8.15	43.60	99.30
27	178.00	1.310	7.39	58.20	120.00
28	237.00	1.590	6.72	77.50	146.00
29	316.00	1.940	6.15	103.00	178.00
30	422.00	2.400	5.68	138.00	219.00
31	562.00	3.000	5.33	184.00	274.00
32	750.00	3.750	5.00	245.00	343.00
33	1000.00	4.720	4.72	327.00	432.00

Table B.1.3.6. Rheology results in polymer solution @ 3000 mg/L concentrations in FW

Meas. Pts.	Shear Rate [1/s]	Shear Stress [Pa]	Viscosity [mPa·s]	Speed [1/min]	Torque [μ Nm]
1	0.10	0.006	58.80	0.03	0.54
2	0.13	0.007	54.70	0.04	0.67
3	0.18	0.010	55.10	0.06	0.90
4	0.24	0.013	52.90	0.08	1.15
5	0.32	0.015	48.30	0.10	1.40
6	0.42	0.019	44.40	0.14	1.71
7	0.56	0.024	43.20	0.18	2.22
8	0.75	0.031	41.50	0.25	2.84
9	1.00	0.040	40.10	0.33	3.67
10	1.33	0.052	39.10	0.44	4.76
11	1.78	0.068	38.00	0.58	6.17
12	2.37	0.087	36.80	0.78	7.98
13	3.16	0.111	35.20	1.03	10.20
14	4.22	0.142	33.80	1.38	13.00
15	5.62	0.180	32.10	1.84	16.50
16	7.50	0.226	30.20	2.45	20.70
17	10.00	0.280	28.00	3.27	25.60
18	13.30	0.345	25.90	4.36	31.60
19	17.80	0.422	23.80	5.82	38.60
20	23.70	0.514	21.70	7.75	47.00
21	31.60	0.623	19.70	10.30	56.90
22	42.20	0.751	17.80	13.80	68.60
23	56.20	0.901	16.00	18.40	82.30
24	75.00	1.080	14.40	24.50	98.50
25	100.00	1.290	12.90	32.70	118.00
26	133.00	1.540	11.50	43.60	140.00
27	178.00	1.830	10.30	58.20	167.00
28	237.00	2.190	9.24	77.50	200.00
29	316.00	2.640	8.36	103.00	242.00
30	422.00	3.230	7.66	138.00	295.00
31	562.00	3.980	7.08	184.00	364.00
32	750.00	4.890	6.52	245.00	447.00
33	1000.00	6.060	6.06	327.00	554.00

Table B.1.3.7. Rheology results in polymer solution @ 3500 mg/L concentrations in FW

Meas. Pts.	Shear Rate [1/s]	Shear Stress [Pa]	Viscosity [mPa·s]	Speed [1/min]	Torque [μ Nm]
1	0.10	0.007	69.70	0.03	0.64
2	0.13	0.009	65.40	0.04	0.80
3	0.18	0.012	65.70	0.06	1.07
4	0.24	0.016	65.40	0.08	1.42
5	0.32	0.020	62.10	0.10	1.79
6	0.42	0.025	59.00	0.14	2.27
7	0.56	0.032	56.90	0.18	2.93
8	0.75	0.042	55.70	0.25	3.81
9	1.00	0.054	54.00	0.33	4.93
10	1.33	0.070	52.40	0.44	6.39
11	1.78	0.090	50.80	0.58	8.26
12	2.37	0.117	49.20	0.78	10.70
13	3.16	0.150	47.40	1.03	13.70
14	4.22	0.190	45.10	1.38	17.40
15	5.62	0.240	42.60	1.84	21.90
16	7.50	0.298	39.80	2.45	27.30
17	10.00	0.368	36.80	3.27	33.60
18	13.30	0.450	33.80	4.36	41.10
19	17.80	0.547	30.80	5.82	50.00
20	23.70	0.661	27.90	7.75	60.40
21	31.60	0.791	25.00	10.30	72.30
22	42.20	0.944	22.40	13.80	86.30
23	56.20	1.120	19.90	18.40	102.00
24	75.00	1.330	17.70	24.50	121.00
25	100.00	1.570	15.70	32.70	143.00
26	133.00	1.850	13.90	43.60	169.00
27	178.00	2.190	12.30	58.20	200.00
28	237.00	2.590	10.90	77.50	237.00
29	316.00	3.090	9.78	103.00	283.00
30	422.00	3.730	8.84	138.00	341.00
31	562.00	4.540	8.07	184.00	415.00
32	750.00	5.500	7.34	245.00	503.00
33	1000.00	6.780	6.78	327.00	619.00

Table B.1.3.8. Rheology results in polymer solution @ 4000 mg/L concentrations in FW

Meas. Pts.	Shear Rate [1/s]	Shear Stress [Pa]	Viscosity [mPa·s]	Speed [1/min]	Torque [μ Nm]
1	0.10	0.009	88.10	0.03	0.81
2	0.13	0.012	87.40	0.04	1.07
3	0.18	0.016	90.20	0.06	1.46
4	0.24	0.021	87.40	0.08	1.89
5	0.32	0.026	82.10	0.10	2.37
6	0.42	0.034	81.20	0.14	3.13
7	0.56	0.044	78.40	0.18	4.03
8	0.75	0.057	76.20	0.25	5.23
9	1.00	0.075	74.50	0.33	6.80
10	1.33	0.096	72.00	0.44	8.77
11	1.78	0.123	69.10	0.58	11.20
12	2.37	0.156	66.00	0.78	14.30
13	3.16	0.197	62.20	1.03	18.00
14	4.22	0.245	58.10	1.38	22.40
15	5.62	0.302	53.80	1.84	27.60
16	7.50	0.370	49.30	2.45	33.80
17	10.00	0.451	45.10	3.27	41.20
18	13.30	0.542	40.70	4.36	49.60
19	17.80	0.652	36.60	5.82	59.60
20	23.70	0.777	32.80	7.75	71.00
21	31.60	0.922	29.20	10.30	84.30
22	42.20	1.090	25.80	13.80	99.60
23	56.20	1.280	22.80	18.40	117.00
24	75.00	1.510	20.20	24.50	138.00
25	100.00	1.780	17.80	32.70	163.00
26	133.00	2.090	15.70	43.60	191.00
27	178.00	2.470	13.90	58.20	226.00
28	237.00	2.950	12.40	77.50	269.00
29	316.00	3.530	11.20	103.00	323.00
30	422.00	4.270	10.10	138.00	390.00
31	562.00	5.180	9.21	184.00	474.00
32	750.00	6.270	8.36	245.00	573.00
33	1000.00	7.650	7.65	327.00	699.00

Table B.1.3.9. Rheology results in polymer solution @ 4500 mg/L concentrations in FW

Meas. Pts.	Shear Rate [1/s]	Shear Stress [Pa]	Viscosity [mPa·s]	Speed [1/min]	Torque [μ Nm]
1	0.10	0.016	156.00	0.03	1.43
2	0.13	0.021	154.00	0.04	1.88
3	0.18	0.027	149.00	0.06	2.42
4	0.24	0.035	149.00	0.08	3.22
5	0.32	0.046	145.00	0.10	4.18
6	0.42	0.060	142.00	0.14	5.46
7	0.56	0.078	138.00	0.18	7.12
8	0.75	0.101	134.00	0.25	9.20
9	1.00	0.129	129.00	0.33	11.80
10	1.33	0.163	122.00	0.44	14.90
11	1.78	0.206	116.00	0.58	18.80
12	2.37	0.258	109.00	0.78	23.50
13	3.16	0.319	101.00	1.03	29.20
14	4.22	0.392	93.00	1.38	35.90
15	5.62	0.475	84.50	1.84	43.40
16	7.50	0.572	76.30	2.45	52.30
17	10.00	0.682	68.20	3.27	62.30
18	13.30	0.810	60.70	4.36	74.00
19	17.80	0.954	53.70	5.82	87.20
20	23.70	1.120	47.20	7.75	102.00
21	31.60	1.310	41.30	10.30	119.00
22	42.20	1.520	36.10	13.80	139.00
23	56.20	1.760	31.30	18.40	161.00
24	75.00	2.040	27.20	24.50	186.00
25	100.00	2.360	23.60	32.70	216.00
26	133.00	2.740	20.60	43.60	251.00
27	178.00	3.210	18.00	58.20	293.00
28	237.00	3.790	16.00	77.50	346.00
29	316.00	4.490	14.20	103.00	410.00
30	422.00	5.350	12.70	138.00	489.00
31	562.00	6.410	11.40	184.00	586.00
32	750.00	7.690	10.20	245.00	702.00
33	1000.00	9.310	9.31	327.00	851.00

B.2. Polymer solutions viscosity in seawater (injection water) at different polymer concentrations, at 10 s⁻¹ shear rate and reservoir temperature 62°C

Table B.2.1. FP-3430S polymer viscosity

Polymer Concentration (mg/L)	Viscosity (mPa.S) at SW
400	3.7
1000	5.92
1800	9.07
1955	10.0
2000	12.2
2500	17.1
3000	36.1
3500	48.9
4000	64.7
4500	88.8

Table B.2.2. FP-5115 polymer viscosity

Polymer Concentration (ppm)	Viscosity (mPa.S) at SW
400	4.28
1200	6.33
1800	8.25
2000	10.3
2500	17.9
3000	27.0
3500	46.0
4500	111

Table B.2.3. Guar Gum polymer viscosity

Polymer Concentration (ppm)	Viscosity (mPa.S) at SW
400	1.25
1200	2.85
1400	7.14
2000	9.5
2100	12.0
2500	18.0
3000	31.7
3500	45.4
4000	63.1

B.3. Polymer solutions viscosity in synthetic formation water at different polymer concentrations, at 10 s⁻¹ shear rate and reservoir temperature 62°C

Table B.3.1. FP-3430S polymer viscosity

Polymer Concentration (mg/L)	Viscosity (mPa.S) at SW
400	1.25
1200	3.97
1800	7.53
2000	11.4
2500	16.7
3000	28
3500	36.8
4000	45.1
4500	68.2

Table B.3.2. FP-5115 polymer viscosity

Polymer Concentration (ppm)	Viscosity (mPa.S) at SW
400	1.25
1200	3.82
1800	7.57
2000	9.12
2500	14.5
3000	21.7
3500	36.8
4000	56.5
4500	126

Table B.3.3. Guar Gum polymer viscosity

Polymer Concentration (ppm)	Viscosity (mPa.S) at SW
400	1.15
1200	3.82
1800	5.80
2000	7.58
2164	8.40
2500	13.7
3000	21.7
3500	36.8
4000	69.9
4500	92.0

B.4. Salinity effect in the polymers solution viscosity in different brines at 2000 mg/L, 10 s⁻¹ shear rate, and reservoir temperature 62°C

B.4.1. FP-3430S polymer

Table B.4.1.1. Rheology results in FP-3430S polymer solution @ 2000 mg/L concentrations in DW

Meas. Pts.	Shear Rate [1/s]	Shear Stress [Pa]	Viscosity [mPa·s]	Speed [1/min]	Torque [μNm]
1	0.10	0.41	4100.0	0.03	37.4
2	0.13	0.72	5420.0	0.04	66.0
3	0.18	0.94	5300.0	0.06	86.1
4	0.24	1.10	4650.0	0.08	101.0
5	0.32	1.21	3820.0	0.10	110.0
6	0.42	1.28	3030.0	0.14	117.0
7	0.56	1.34	2380.0	0.18	122.0
8	0.75	1.40	1860.0	0.25	128.0
9	1.00	1.48	1480.0	0.33	135.0
10	1.33	1.57	1170.0	0.44	143.0
11	1.78	1.67	940.0	0.58	153.0
12	2.37	1.80	760.0	0.78	165.0
13	3.16	1.92	608.0	1.03	176.0
14	4.22	2.05	487.0	1.38	188.0
15	5.62	2.19	389.0	1.84	200.0
16	7.50	2.35	313.0	2.45	215.0
17	10.00	2.54	254.0	3.27	232.0
18	13.30	2.72	204.0	4.36	249.0
19	17.80	2.95	166.0	5.82	269.0
20	23.70	3.17	134.0	7.75	290.0
21	31.60	3.41	108.0	10.30	311.0
22	42.20	3.66	86.9	13.80	335.0
23	56.20	3.96	70.5	18.40	362.0
24	75.00	4.29	57.3	24.50	393.0
25	100.00	4.67	46.7	32.70	427.0
26	133.00	5.10	38.3	43.60	466.0
27	178.00	5.59	31.4	58.20	511.0
28	237.00	6.12	25.8	77.50	559.0
29	316.00	6.74	21.3	103.00	616.0
30	422.00	7.51	17.8	138.00	687.0
31	562.00	8.31	14.8	184.00	760.0
32	750.00	9.41	12.5	245.00	860.0
33	1000.00	10.60	10.6	327.00	966.0

Table B.4.1.2. Rheology results in FP-3430S polymer solution @ 2000 mg/L concentrations in SW

Meas. Pts.	Shear Rate [1/s]	Shear Stress [Pa]	Viscosity [mPa·s]	Speed [1/min]	Torque [μ Nm]
1	0.10	0.02	203.0	0.03	1.9
2	0.13	0.02	162.0	0.04	2.0
3	0.18	0.02	129.0	0.06	2.1
4	0.24	0.02	96.7	0.08	2.1
5	0.32	0.03	79.3	0.10	2.3
6	0.42	0.03	63.0	0.14	2.4
7	0.56	0.03	50.9	0.18	2.6
8	0.75	0.03	42.2	0.25	2.9
9	1.00	0.03	34.0	0.33	3.1
10	1.33	0.04	28.8	0.44	3.5
11	1.78	0.05	25.4	0.58	4.1
12	2.37	0.05	21.5	0.78	4.7
13	3.16	0.06	19.3	1.03	5.6
14	4.22	0.07	16.5	1.38	6.4
15	5.62	0.08	14.5	1.84	7.5
16	7.50	0.10	13.3	2.45	9.1
17	10.00	0.12	12.2	3.27	11.2
18	13.30	0.15	11.5	4.36	14.0
19	17.80	0.19	10.8	5.82	17.5
20	23.70	0.24	10.0	7.75	21.7
21	31.60	0.29	9.3	10.30	26.8
22	42.20	0.36	8.6	13.80	33.0
23	56.20	0.44	7.9	18.40	40.6
24	75.00	0.54	7.3	24.50	49.7
25	100.00	0.66	6.6	32.70	60.6
26	133.00	0.81	6.1	43.60	73.8
27	178.00	0.99	5.5	58.20	90.0
28	237.00	1.20	5.1	77.50	110.0
29	316.00	1.47	4.7	103.00	135.0
30	422.00	1.81	4.3	138.00	166.0
31	562.00	2.27	4.0	184.00	208.0
32	750.00	2.84	3.8	245.00	260.0
33	1000.00	3.61	3.6	327.00	330.0

Table B.4.1.3. Rheology results in FP-3430S polymer solution @ 2000 mg/L concentrations in FW

Meas. Pts.	Shear Rate [1/s]	Shear Stress [Pa]	Viscosity [mPa·s]	Speed [1/min]	Torque [μ Nm]
1	0.10	0.003	33.4	0.03	0.3
2	0.13	0.004	31.8	0.04	0.4
3	0.18	0.006	33.2	0.06	0.5
4	0.24	0.008	31.7	0.08	0.7
5	0.32	0.009	28.4	0.10	0.8
6	0.42	0.010	24.1	0.14	0.9
7	0.56	0.012	21.7	0.18	1.1
8	0.75	0.014	19.2	0.25	1.3
9	1.00	0.018	18.0	0.33	1.7
10	1.33	0.022	16.8	0.44	2.0
11	1.78	0.028	15.5	0.58	2.5
12	2.37	0.036	15.1	0.78	3.3
13	3.16	0.044	13.9	1.03	4.0
14	4.22	0.056	13.4	1.38	5.2
15	5.62	0.072	12.7	1.84	6.5
16	7.50	0.090	12.0	2.45	8.2
17	10.00	0.114	11.4	3.27	10.4
18	13.30	0.145	10.9	4.36	13.3
19	17.80	0.184	10.3	5.82	16.8
20	23.70	0.232	9.8	7.75	21.2
21	31.60	0.290	9.2	10.30	26.5
22	42.20	0.361	8.6	13.80	33.0
23	56.20	0.447	8.0	18.40	40.9
24	75.00	0.554	7.4	24.50	50.6
25	100.00	0.681	6.8	32.70	62.3
26	133.00	0.840	6.3	43.60	76.8
27	178.00	1.030	5.8	58.20	94.1
28	237.00	1.260	5.3	77.50	115.0
29	316.00	1.550	4.9	103.00	142.0
30	422.00	1.920	4.5	138.00	175.0
31	562.00	2.400	4.3	184.00	220.0
32	750.00	3.020	4.0	245.00	276.0
33	1000.00	3.830	3.8	327.00	350.0

B.4.2. FP-5115 polymer

Table B.4.2.1. Rheology results in FP-5115 polymer solution @ 2000 mg/L concentrations in DW

Meas. Pts.	Shear Rate [1/s]	Shear Stress [Pa]	Viscosity [mPa·s]	Speed [1/min]	Torque [μNm]
1	0.10	0.37	3660.0	0.03	33.3
2	0.13	0.63	4730.0	0.04	57.6
3	0.18	0.82	4630.0	0.06	75.3
4	0.24	0.97	4100.0	0.08	88.9
5	0.32	1.09	3430.0	0.10	99.2
6	0.42	1.17	2780.0	0.14	107.0
7	0.56	1.25	2220.0	0.18	114.0
8	0.75	1.33	1770.0	0.25	121.0
9	1.00	1.42	1420.0	0.33	129.0
10	1.33	1.52	1140.0	0.44	139.0
11	1.78	1.64	920.0	0.58	150.0
12	2.37	1.77	748.0	0.78	162.0
13	3.16	1.91	604.0	1.03	175.0
14	4.22	2.05	487.0	1.38	188.0
15	5.62	2.21	393.0	1.84	202.0
16	7.50	2.39	319.0	2.45	219.0
17	10.00	2.60	260.0	3.27	238.0
18	13.30	2.79	209.0	4.36	255.0
19	17.80	3.02	170.0	5.82	276.0
20	23.70	3.24	137.0	7.75	296.0
21	31.60	3.48	110.0	10.30	318.0
22	42.20	3.74	88.7	13.80	342.0
23	56.20	4.04	71.8	18.40	369.0
24	75.00	4.38	58.5	24.50	401.0
25	100.00	4.76	47.6	32.70	435.0
26	133.00	5.19	39.0	43.60	475.0
27	178.00	5.67	31.9	58.20	518.0
28	237.00	6.24	26.3	77.50	570.0
29	316.00	6.86	21.7	103.00	627.0
30	422.00	7.57	17.9	138.00	691.0
31	562.00	8.44	15.0	184.00	771.0
32	750.00	9.37	12.5	245.00	856.0
33	1000.00	10.50	10.5	327.00	956.0

Table B.4.2.2. Rheology results in FP-5115 polymer solution @ 2000 mg/L concentrations in SW

Meas. Pts.	Shear Rate [1/s]	Shear Stress [Pa]	Viscosity [mPa·s]	Speed [1/min]	Torque [μ Nm]
1	0.10	0.003	34.7	0.03	0.3
2	0.13	0.004	29.8	0.04	0.4
3	0.18	0.005	26.5	0.06	0.4
4	0.24	0.006	23.7	0.08	0.5
5	0.32	0.006	20.5	0.10	0.6
6	0.42	0.008	18.2	0.14	0.7
7	0.56	0.010	18.3	0.18	0.9
8	0.75	0.012	16.5	0.25	1.1
9	1.00	0.015	15.3	0.33	1.4
10	1.33	0.018	13.7	0.44	1.7
11	1.78	0.024	13.2	0.58	2.2
12	2.37	0.030	12.7	0.78	2.8
13	3.16	0.040	12.5	1.03	3.6
14	4.22	0.048	11.4	1.38	4.4
15	5.62	0.060	10.7	1.84	5.5
16	7.50	0.078	10.4	2.45	7.1
17	10.00	0.099	9.9	3.27	9.1
18	13.30	0.126	9.4	4.36	11.5
19	17.80	0.160	9.0	5.82	14.6
20	23.70	0.203	8.5	7.75	18.5
21	31.60	0.253	8.0	10.30	23.2
22	42.20	0.319	7.6	13.80	29.1
23	56.20	0.396	7.0	18.40	36.2
24	75.00	0.493	6.6	24.50	45.1
25	100.00	0.608	6.1	32.70	55.6
26	133.00	0.752	5.6	43.60	68.7
27	178.00	0.928	5.2	58.20	84.8
28	237.00	1.130	4.8	77.50	103.0
29	316.00	1.400	4.4	103.00	128.0
30	422.00	1.740	4.1	138.00	159.0
31	562.00	2.200	3.9	184.00	201.0
32	750.00	2.760	3.7	245.00	252.0
33	1000.00	3.550	3.6	327.00	325.0

Table B.4.2.3. Rheology results in FP-5115 polymer solution @ 2000 mg/L concentrations in FW

Meas. Pts.	Shear Rate [1/s]	Shear Stress [Pa]	Viscosity [mPa·s]	Speed [1/min]	Torque [μ Nm]
1	0.10	0.008	84.9	0.03	0.8
2	0.13	0.009	67.4	0.04	0.8
3	0.18	0.009	48.3	0.06	0.8
4	0.24	0.010	41.7	0.08	0.9
5	0.32	0.010	30.6	0.10	0.9
6	0.42	0.010	24.1	0.14	0.9
7	0.56	0.012	20.7	0.18	1.1
8	0.75	0.013	16.9	0.25	1.2
9	1.00	0.015	15.2	0.33	1.4
10	1.33	0.018	13.4	0.44	1.6
11	1.78	0.022	12.2	0.58	2.0
12	2.37	0.026	11.2	0.78	2.4
13	3.16	0.033	10.3	1.03	3.0
14	4.22	0.041	9.8	1.38	3.8
15	5.62	0.054	9.6	1.84	5.0
16	7.50	0.070	9.4	2.45	6.4
17	10.00	0.091	9.1	3.27	8.3
18	13.30	0.117	8.8	4.36	10.7
19	17.80	0.149	8.4	5.82	13.6
20	23.70	0.189	8.0	7.75	17.3
21	31.60	0.237	7.5	10.30	21.7
22	42.20	0.298	7.1	13.80	27.2
23	56.20	0.373	6.6	18.40	34.1
24	75.00	0.465	6.2	24.50	42.5
25	100.00	0.576	5.8	32.70	52.6
26	133.00	0.715	5.4	43.60	65.4
27	178.00	0.886	5.0	58.20	81.0
28	237.00	1.100	4.6	77.50	100.0
29	316.00	1.370	4.3	103.00	125.0
30	422.00	1.710	4.1	138.00	157.0
31	562.00	2.170	3.9	184.00	199.0
32	750.00	2.720	3.6	245.00	249.0
33	1000.00	3.450	3.5	327.00	316.0

B.4.3. Guar Gum polymer

Table B.4.3.1. Rheology results in Guar Gum polymer solution @ 2000 mg/L concentrations in DW

Meas. Pts.	Shear Rate [1/s]	Shear Stress [Pa]	Viscosity [mPa·s]	Speed [1/min]	Torque [μNm]
1	0.10	0.009	86.5	0.03	0.79
2	0.13	0.009	68.6	0.04	0.84
3	0.18	0.010	56.7	0.06	0.92
4	0.24	0.010	41.7	0.08	0.90
5	0.32	0.011	33.8	0.10	0.98
6	0.42	0.013	31.7	0.14	1.22
7	0.56	0.015	27.5	0.18	1.41
8	0.75	0.019	24.9	0.25	1.70
9	1.00	0.022	21.7	0.33	1.98
10	1.33	0.027	20.4	0.44	2.48
11	1.78	0.033	18.8	0.58	3.05
12	2.37	0.042	17.6	0.78	3.81
13	3.16	0.052	16.4	1.03	4.73
14	4.22	0.067	15.8	1.38	6.09
15	5.62	0.084	15.0	1.84	7.70
16	7.50	0.107	14.3	2.45	9.80
17	10.00	0.140	14.0	3.27	12.80
18	13.30	0.182	13.7	4.36	16.60
19	17.80	0.238	13.4	5.82	21.80
20	23.70	0.307	12.9	7.75	28.10
21	31.60	0.398	12.6	10.30	36.40
22	42.20	0.511	12.1	13.80	46.70
23	56.20	0.650	11.6	18.40	59.40
24	75.00	0.820	10.9	24.50	74.90
25	100.00	1.020	10.2	32.70	93.70
26	133.00	1.280	9.6	43.60	117.00
27	178.00	1.580	8.9	58.20	145.00
28	237.00	1.950	8.2	77.50	179.00
29	316.00	2.410	7.6	103.00	220.00
30	422.00	2.970	7.0	138.00	271.00
31	562.00	3.650	6.5	184.00	333.00
32	750.00	4.460	5.9	245.00	407.00
33	1000.00	5.470	5.5	327.00	500.00

Table B.4.3.2. Rheology results in Guar Gum polymer solution @ 2000 mg/L concentrations in SW

Meas. Pts.	Shear Rate [1/s]	Shear Stress [Pa]	Viscosity [mPa·s]	Speed [1/min]	Torque [μ Nm]
1	0.10	0.004	43.1	0.03	0.4
2	0.13	0.008	58.9	0.04	0.7
3	0.18	0.011	60.4	0.06	1.0
4	0.24	0.019	81.4	0.08	1.8
5	0.32	0.020	64.5	0.10	1.9
6	0.42	0.013	31.8	0.14	1.2
7	0.56	0.015	26.4	0.18	1.4
8	0.75	0.014	18.2	0.25	1.3
9	1.00	0.027	26.9	0.33	2.5
10	1.33	0.021	15.7	0.44	1.9
11	1.78	0.017	9.4	0.58	1.5
12	2.37	0.037	15.4	0.78	3.3
13	3.16	0.031	9.8	1.03	2.8
14	4.22	0.031	7.2	1.38	2.8
15	5.62	0.049	8.7	1.84	4.5
16	7.50	0.063	8.4	2.45	5.8
17	10.00	0.084	8.4	3.27	7.7
18	13.30	0.101	7.5	4.36	9.2
19	17.80	0.143	8.1	5.82	13.1
20	23.70	0.187	7.9	7.75	17.1
21	31.60	0.249	7.9	10.30	22.8
22	42.20	0.325	7.7	13.80	29.7
23	56.20	0.428	7.6	18.40	39.2
24	75.00	0.558	7.4	24.50	51.0
25	100.00	0.704	7.0	32.70	64.3
26	133.00	0.892	6.7	43.60	81.5
27	178.00	1.120	6.3	58.20	102.0
28	237.00	1.390	5.9	77.50	127.0
29	316.00	1.700	5.4	103.00	155.0
30	422.00	2.080	4.9	138.00	191.0
31	562.00	2.580	4.6	184.00	236.0
32	750.00	3.180	4.2	245.00	290.0
33	1000.00	3.960	4.0	327.00	362.0

Table B.4.3.3. Rheology results in Guar Gum polymer solution @ 2000 mg/L concentrations in FW

Meas. Pts.	Shear Rate [1/s]	Shear Stress [Pa]	Viscosity [mPa·s]	Speed [1/min]	Torque [μ Nm]
1	0.10	0.012	121.0	0.03	1.1
2	0.13	0.015	110.0	0.04	1.4
3	0.18	0.012	67.2	0.06	1.1
4	0.24	0.012	48.9	0.08	1.1
5	0.32	0.011	36.1	0.10	1.0
6	0.42	0.011	25.1	0.14	1.0
7	0.56	0.010	18.4	0.18	0.9
8	0.75	0.013	17.1	0.25	1.2
9	1.00	0.014	13.7	0.33	1.3
10	1.33	0.014	10.8	0.44	1.3
11	1.78	0.017	9.5	0.58	1.5
12	2.37	0.020	8.5	0.78	1.8
13	3.16	0.026	8.1	1.03	2.4
14	4.22	0.033	7.8	1.38	3.0
15	5.62	0.045	7.9	1.84	4.1
16	7.50	0.058	7.7	2.45	5.3
17	10.00	0.076	7.6	3.27	6.9
18	13.30	0.101	7.6	4.36	9.3
19	17.80	0.132	7.4	5.82	12.0
20	23.70	0.173	7.3	7.75	15.8
21	31.60	0.226	7.1	10.30	20.6
22	42.20	0.290	6.9	13.80	26.5
23	56.20	0.372	6.6	18.40	34.0
24	75.00	0.476	6.4	24.50	43.5
25	100.00	0.606	6.1	32.70	55.3
26	133.00	0.770	5.8	43.60	70.4
27	178.00	0.974	5.5	58.20	89.0
28	237.00	1.230	5.2	77.50	112.0
29	316.00	1.550	4.9	103.00	142.0
30	422.00	1.950	4.6	138.00	178.0
31	562.00	2.450	4.4	184.00	224.0
32	750.00	3.050	4.1	245.00	279.0
33	1000.00	3.830	3.8	327.00	350.0

B.5. Polymer performance vs. temperature for defined concentrations at 10 s^{-1}

Table. B.5.1. Polymer viscosity vs. temperature

Temp (°C)	FP-3430S		FP-5115		Guar Gum	
	SW (mPa.S)	FW (mPa.S)	SW (mPa.S)	FW (mPa.S)	SW (mPa.S)	FW (mPa.S)
15	25.3	24.2	22.9	23.3	55.6	41.9
30	18.9	17.7	17.4	17.5	35.6	24.9
40	15.9	14.4	15.0	14.6	25.4	18.6
50	13.0	12.0	12.3	12.4	17.9	13.9
62	11.6	10.7	10.8	10.5	12.3	10.8
70	9.7	8.5	9.9	9.3	11.3	9.5
80	11.0	7.0	9.6	9.2	11.2	9.1

Polymer solutions concentrations:

FP-3430S @ SW: 1997 mg/L / @ FW: 2000 mg/L

FP-5115 @ SW: 2069 mg/L / @ FW: 2204 mg/L

Guar Gum @ SW: 2100 mg/L / @ FW: 2349 mg/L

B.6. Thermal stability at 62°C and 10 s^{-1} shear rate of polymers in SW and FW brines

Table. B.6.1. Polymer thermal stability

Time (days)	FP-3430S		FP-5115		Guar Gum	
	SW (mPa.S)	FW (mPa.S)	SW (mPa.S)	FW (mPa.S)	SW (mPa.S)	FW (mPa.S)
0	11.6	10.7	10.8	10.5	12.3	10.8
3					6.2	4.4
14					1.3	2.3
28			11.0	11.2	1.3	2.4
53	10.8	10.2			1.5	1.8
91	10.0	10.4	9.4	11.0	0.7	0.9
120	7.2	10.1	9.8	11.1	1.4	0.8
150	6.6	9.6	8.7	10.5	2.0	0.8

Polymer solutions concentrations:

FP-3430S @ SW: 1997 mg/L / @ FW: 2000 mg/L

FP-5115 @ SW: 2069 mg/L / @ FW: 2204 mg/L

Guar Gum @ SW: 2100 mg/L / @ FW: 2349 mg/L

B.7. Polymers viscoelasticity evaluation

Table B.7.1.Viscoelasticity evaluation of FP-3430S in deionized water @ 62°C

Textp (s)	t (s)	T (°C)	f (Hz)	ω (rad/s)	Shear Strain γ^* (%)	σ^* (Pa)	Complex Modulus G^* (Pa)	Elastic (Storage) Modulus G' (Pa)	Viscous (Loss) Modulus G'' (Pa)	Complex Viscosity η^* (Pa s)	Phase Angle (Shift) δ (°)	F (N)	T (N m)	Angular Absolut Velocity θ abs (rad)	HD (%)
27.65	10.67	62	15.000	94.257	1.29E-03	4.37E-05	3.386	4.587	2.849	35.93	57.26	0.788	4.59E-09	5.781	6.464
38.61	21.63	62	11.250	70.693	2.69E-03	1.05E-04	3.896	4.356	1.994	55.12	30.79	0.787	1.10E-08	5.781	6.552
49.9	32.91	62	8.435	53.004	5.35E-03	2.36E-04	4.414	4.125	1.572	83.29	20.87	0.788	2.48E-08	5.781	1.205
61.63	44.64	62	6.325	39.745	0.011	4.37E-04	3.998	3.738	1.420	100.6	20.8	0.789	4.58E-08	5.781	0.690
73.87	56.89	62	4.743	29.804	0.025	9.15E-04	3.651	3.415	1.293	122.5	20.74	0.789	9.59E-08	5.781	0.231
86.82	69.84	62	3.557	22.351	0.068	2.33E-03	3.404	3.190	1.186	152.3	20.39	0.789	2.44E-07	5.781	0.106
100.7	83.72	62	2.667	16.759	0.077	2.43E-03	3.156	2.957	1.102	188.3	20.44	0.789	2.55E-07	5.781	0.085
116.2	99.25	62	2.000	12.568	0.056	1.64E-03	2.924	2.737	1.029	232.6	20.61	0.789	1.72E-07	5.781	0.195
133.6	116.6	62	1.500	9.426	0.049	1.32E-03	2.692	2.513	0.964	285.6	20.98	0.791	1.39E-07	5.781	0.303
153.1	136.2	62	1.125	7.069	0.045	1.17E-03	2.597	2.414	0.957	367.5	21.62	0.791	1.22E-07	5.781	0.383
175.7	158.7	62	0.844	5.300	0.046	1.10E-03	2.389	2.213	0.900	450.7	22.13	0.790	1.15E-07	5.781	1.195
202.6	185.6	62	0.633	3.974	0.047	1.06E-03	2.225	2.051	0.861	559.7	22.77	0.791	1.11E-07	5.781	0.284
234.2	217.2	62	0.474	2.980	0.049	1.03E-03	2.116	1.937	0.853	710	23.77	0.792	1.08E-07	5.781	0.319
273.6	256.6	62	0.356	2.235	0.049	1.02E-03	2.061	1.869	0.870	922.2	24.95	0.791	1.07E-07	5.78	0.382
322.4	305.4	62	0.267	1.676	0.052	1.01E-03	1.946	1.737	0.877	1.16E+03	26.79	0.793	1.06E-07	5.78	0.514
387.4	370.4	62	0.200	1.257	0.059	1.01E-03	1.706	1.517	0.780	1.36E+03	27.19	0.794	1.06E-07	5.78	0.916
460.7	443.7	62	0.150	0.943	0.067	1.00E-03	1.508	1.321	0.728	1.60E+03	28.86	0.795	1.05E-07	5.78	0.996
538.5	521.5	62	0.113	0.707	0.069	1.00E-03	1.448	1.259	0.716	2.05E+03	29.64	0.796	1.05E-07	5.78	0.663
610.4	593.4	62	0.084	0.530	0.075	1.00E-03	1.334	1.131	0.708	2.52E+03	32.04	0.798	1.05E-07	5.78	0.514
686.2	669.2	62	0.063	0.397	0.088	1.00E-03	1.132	0.942	0.627	2.85E+03	33.65	0.800	1.05E-07	5.779	0.810
767.3	750.3	62	0.047	0.298	0.103	1.00E-03	0.968	0.796	0.551	3.25E+03	34.67	0.801	1.05E-07	5.779	1.475
855.4	838.5	62	0.036	0.224	0.111	1.00E-03	0.899	0.732	0.523	4.02E+03	35.59	0.802	1.05E-07	5.779	2.000
952.9	936	62	0.027	0.168	0.111	1.00E-03	0.899	0.693	0.572	5.36E+03	39.54	0.804	1.05E-07	5.779	1.520
1.06E+03	1.05E+03	62	0.020	0.126	0.136	1.00E-03	0.736	0.555	0.482	5.85E+03	40.97	0.806	1.05E-07	5.778	1.878
1.19E+03	1.17E+03	62	0.015	0.094	0.159	1.00E-03	0.630	0.462	0.429	6.69E+03	42.92	0.808	1.05E-07	5.778	1.816
1.34E+03	1.32E+03	62	0.011	0.071	0.169	1.00E-03	0.592	0.419	0.418	8.38E+03	44.96	0.811	1.05E-07	5.778	1.466
1.52E+03	1.50E+03	62	8.44E-03	0.053	0.208	1.00E-03	0.480	0.317	0.361	9.06E+03	48.71	0.815	1.05E-07	5.777	1.378
1.74E+03	1.72E+03	62	6.33E-03	0.040	0.254	1.00E-03	0.394	0.257	0.299	9.92E+03	49.26	0.819	1.05E-07	5.777	2.160
2.01E+03	1.99E+03	62	4.74E-03	0.030	0.285	1.00E-03	0.351	0.204	0.285	1.18E+04	54.39	0.823	1.05E-07	5.777	1.348
2.35E+03	2.33E+03	62	3.56E-03	0.022	0.362	1.00E-03	0.276	0.178	0.211	1.24E+04	49.99	0.828	1.05E-07	5.776	2.953
2.78E+03	2.77E+03	62	2.67E-03	0.017	0.434	1.00E-03	0.231	0.127	0.192	1.38E+04	56.47	0.833	1.05E-07	5.775	1.030
3.34E+03	3.33E+03	62	2.00E-03	0.013	0.496	1.00E-03	0.202	0.106	0.172	1.60E+04	58.36	0.841	1.05E-07	5.773	3.065
4.07E+03	4.05E+03	62	1.50E-03	0.009	0.610	1.00E-03	0.164	0.089	0.138	1.74E+04	57.06	0.856	1.05E-07	5.771	1.663
5.02E+03	5.00E+03	62	1.13E-03	0.007	0.785	1.00E-03	0.127	0.060	0.113	1.80E+04	62.14	0.870	1.05E-07	5.77	3.422
6.08E+03	6.06E+03	62	8.44E-04	0.005	1.031	1.00E-03	0.097	0.038	0.089	1.83E+04	66.83	0.888	1.05E-07	5.768	1.143
				0.000											
1.34E+03	1.32E+03	62	0.01121	0.070				0.418	0.418		44.98				
32.14	15.16	62	13.39	84.14				2.482	2.482		44.97				

Table B.7.2. Viscoelasticity evaluation of FP-3430S in seawater brine @ 62°C

Text _p (s)	t (s)	T (°C)	f (Hz)	ω (rad/s)	Shear Strain γ^* (%)	σ^* (Pa)	Complex Modulus G*(Pa)	Elastic (Storage) Modulus G'(Pa)	Viscous (Loss) Modulus G''(Pa)	Complex Viscosity η^* (Pa s)	Phase Angle (Shift) δ (°)	F (N)	T (N m)	Angular Absolut Velocity θ_{abs} (rad)	HD (%)
327.2	10.67	62	15.000	94.257	9.06E-04	5.95E-05	6.569	5.948	2.79	69.7	25.12	0.48	6.24E-09	4.72	7.71
338.2	21.64	62	11.250	70.693	1.70E-03	3.47E-05	2.045	2.592	1.28	28.93	38.89	0.49	3.64E-09	4.67	7.26
349.4	32.92	62	8.435	53.004	2.99E-03	2.18E-05	0.729	1.454	0.78	13.75	29.16	0.49	2.28E-09	4.62	4.86
361.1	44.63	62	6.325	39.745	5.66E-03	9.04E-05	1.597	1.182	0.49	40.17	42.26	0.49	9.48E-09	4.58	2.29
373.4	56.87	62	4.743	29.804	9.07E-03	8.29E-06	0.091	0.750	0.35	3.066	-160.31	0.49	8.69E-10	4.54	0.90
386.3	69.83	62	3.557	22.351	0.02	8.00E-05	0.472	0.373	0.24	21.13	68.58	0.49	8.39E-09	4.51	0.74
400.2	83.71	62	2.667	16.759	0.03	5.29E-05	0.185	0.256	0.18	11.01	90	0.49	5.54E-09	4.47	0.94
415.7	99.23	62	2.000	12.568	0.05	6.19E-05	0.116	0.142	0.11	9.257	68.68	0.49	6.49E-09	4.43	0.94
433.1	116.6	62	1.500	9.426	0.10	8.13E-05	0.085	0.096	0.08	8.998	65.65	0.49	8.52E-09	4.39	0.53
452.7	136.2	62	1.125	7.069	0.17	1.44E-04	0.083	0.034	0.08	11.68	65.62	0.49	1.51E-08	4.35	0.77
475.2	158.7	62	0.844	5.300	0.30	1.65E-04	0.055	0.015	0.05	10.35	74.48	0.49	1.73E-08	4.30	0.82
502.1	185.6	62	0.633	3.974	0.53	2.21E-04	0.042	9.66E-03	0.04	10.55	76.68	0.49	2.32E-08	4.25	0.54
533.7	217.2	62	0.474	2.980	0.91	2.95E-04	0.032	6.82E-03	0.03	10.87	77.86	0.49	3.10E-08	4.19	0.49
573.1	256.6	62	0.356	2.235	1.52	3.77E-04	0.025	4.45E-03	0.02	11.11	79.69	0.49	3.95E-08	4.12	0.15
621.9	305.4	62	0.267	1.676	2.44	4.61E-04	0.019	3.14E-03	0.02	11.26	80.42	0.49	4.83E-08	4.05	0.27
686.9	370.4	62	0.200	1.257	3.77	5.39E-04	0.014	2.40E-03	0.01	11.37	80.33	0.49	5.65E-08	3.95	0.22
760.2	443.7	62	0.150	0.943	5.55	6.00E-04	0.011	1.88E-03	0.01	11.47	80	0.50	6.29E-08	3.87	0.36
838	521.5	62	0.113	0.707	7.80	6.45E-04	8.27E-03	1.63E-03	8.10E-03	11.69	78.66	0.50	6.76E-08	3.78	0.06
909.9	593.4	62	0.084	0.530	10.51	6.76E-04	6.43E-03	1.56E-03	6.24E-03	12.13	75.94	0.50	7.09E-08	3.73	0.19
985.7	669.2	62	0.063	0.397	13.71	6.86E-04	5.01E-03	1.38E-03	4.81E-03	12.59	73.98	0.50	7.20E-08	3.69	0.17
1.07E+03	750.3	62	0.047	0.298	17.47	6.89E-04	3.95E-03	1.26E-03	3.74E-03	13.24	71.33	0.50	7.23E-08	3.66	0.24
1.16E+03	838.4	62	0.036	0.224	21.96	6.85E-04	3.12E-03	1.07E-03	2.93E-03	13.96	69.88	0.51	7.18E-08	3.62	0.21
1.25E+03	935.9	62	0.027	0.168	27.40	6.80E-04	2.48E-03	9.11E-04	2.31E-03	14.81	68.46	0.51	7.13E-08	3.62	0.22
1.36E+03	1.05E+03	62	0.020	0.126	32.40	6.72E-04	2.07E-03	6.72E-04	1.96E-03	16.51	71.1	0.51	7.05E-08	3.60	1.12
1.49E+03	1.17E+03	62	0.015	0.094	40.66	6.69E-04	1.65E-03	5.50E-04	1.55E-03	17.46	70.47	0.51	7.01E-08	3.64	0.72
1.64E+03	1.32E+03	62	0.011	0.071	47.17	6.66E-04	1.41E-03	4.80E-04	1.33E-03	19.98	70.13	0.52	6.98E-08	3.68	0.87
1.82E+03	1.50E+03	62	8.44E-03	0.053	60.71	6.65E-04	1.10E-03	3.91E-04	1.02E-03	20.66	69.07	0.52	6.97E-08	3.65	0.80
2.04E+03	1.72E+03	62	6.33E-03	0.040	76.87	6.63E-04	8.62E-04	2.69E-04	8.19E-04	21.7	71.83	0.53	6.95E-08	3.67	1.37
2.31E+03	1.99E+03	62	4.74E-03	0.030	97.82	6.63E-04	6.77E-04	2.62E-04	6.25E-04	22.73	67.29	0.53	6.95E-08	3.71	2.78
2.65E+03	2.33E+03	62	3.56E-03	0.022	124.13	6.62E-04	5.33E-04	1.72E-04	5.04E-04	23.85	71.15	0.54	6.94E-08	3.68	3.10
3.08E+03	2.77E+03	62	2.67E-03	0.017	151.33	6.61E-04	4.37E-04	1.09E-04	4.23E-04	26.05	75.51	0.55	6.93E-08	3.65	2.13
3.64E+03	3.33E+03	62	2.00E-03	0.013	174.41	6.61E-04	3.79E-04	1.12E-04	3.62E-04	30.13	72.81	0.56	6.93E-08	3.64	3.97
4.37E+03	4.05E+03	62	1.50E-03	0.009	220.77	6.60E-04	2.99E-04	8.31E-05	2.87E-04	31.74	73.88	0.57	6.92E-08	3.65	2.05
				0.000											
375.3	58.77	62	4.54	28.528				0.1008	0.1008		-139.17				

Table B.7.3. Viscoelasticity evaluation of FP-5115 in seawater brine @ 22°C

Text _p (s)	t (s)	T (°C)	f (Hz)	ω (rad/s)	Shear Strain γ^* (%)	σ^* (Pa)	Complex Modulus G^* (Pa)	Elastic (Storage) Modulus G' (Pa)	Viscous (Loss) Modulus G'' (Pa)	Complex Viscosity η^* (Pa s)	Phase Angle (Shift) δ (°)	F (N)	T (N m)	Angular Absolut Velocity Θ_{abs} (rad)	HD (%)
349.6	10.67	22	15.000	94.257	1.17E-03	3.84E-04	32.780	21.260	12.96	347.8	49.58	0.11	4.03E-08	6.28	9.64
360.5	21.62	22	11.250	70.693	2.11E-03	1.53E-04	7.232	6.053	3.96	102.3	33.18	0.11	1.60E-08	6.28	8.20
371.8	32.9	22	8.435	53.004	3.28E-03	3.20E-05	0.975	2.026	0.82	18.39	57.35	0.11	3.36E-09	6.28	10.87
383.5	44.61	22	6.325	39.745	5.61E-03	1.27E-05	0.226	0.923	0.62	5.695	90	0.11	1.33E-09	6.28	1.89
395.8	56.85	22	4.743	29.804	1.04E-02	6.12E-05	0.587	0.711	0.45	19.68	68.92	0.11	6.41E-09	6.27	2.50
408.7	69.81	22	3.557	22.351	0.02	8.04E-05	0.412	0.317	0.26	18.42	39.67	0.11	8.43E-09	6.27	1.99
422.6	83.69	22	2.667	16.759	0.03	4.51E-05	0.139	0.211	0.24	8.276	77.04	0.11	4.73E-09	6.27	1.96
438.1	99.21	22	2.000	12.568	0.06	1.30E-04	0.225	0.098	0.20	17.88	80.39	0.11	1.36E-08	6.27	2.64
455.5	116.6	22	1.500	9.426	0.11	2.07E-04	0.188	0.079	0.17	19.91	65.05	0.11	2.17E-08	6.26	1.97
475.1	136.1	22	1.125	7.069	0.20	2.92E-04	0.147	0.060	0.13	20.86	65.79	0.11	3.06E-08	6.26	0.77
497.6	158.7	22	0.844	5.300	0.34	4.02E-04	0.119	0.042	0.11	22.53	69.58	0.11	4.22E-08	6.26	1.07
524.5	185.6	22	0.633	3.974	0.55	5.30E-04	0.096	3.18E-02	0.09	24.1	70.59	0.11	5.56E-08	6.25	0.27
556.1	217.2	22	0.474	2.980	0.83	6.35E-04	0.077	2.29E-02	0.07	25.67	72.61	0.11	6.66E-08	6.25	0.98
595.5	256.6	22	0.356	2.235	1.15	6.96E-04	0.060	1.57E-02	0.06	27	74.97	0.11	7.29E-08	6.24	0.12
644.2	305.3	22	0.267	1.676	1.54	7.24E-04	0.047	1.06E-02	0.05	28.08	76.95	0.12	7.59E-08	6.24	0.40
709.3	370.3	22	0.200	1.257	2.01	7.35E-04	0.037	7.09E-03	0.04	29.16	78.85	0.12	7.70E-08	6.23	0.23
782.6	443.7	22	0.150	0.943	2.60	7.35E-04	0.028	4.31E-03	0.03	29.95	81.22	0.12	7.70E-08	6.22	0.82
860.4	521.5	22	0.113	0.707	3.41	7.35E-04	2.15E-02	2.78E-03	2.14E-02	30.48	82.59	0.12	7.70E-08	6.21	0.51
932.3	593.3	22	0.084	0.530	4.47	7.34E-04	1.64E-02	1.76E-03	1.63E-02	30.99	83.84	0.12	7.69E-08	6.21	0.63
1008	669.2	22	0.063	0.397	5.93	7.33E-04	1.24E-02	1.07E-03	1.23E-02	31.07	85.02	0.12	7.68E-08	6.20	0.50
1.09E+03	750.3	22	0.047	0.298	7.82	7.32E-04	9.35E-03	6.59E-04	9.33E-03	31.38	85.96	0.12	7.67E-08	6.20	0.32
1.18E+03	838.4	22	0.036	0.224	10.42	7.31E-04	7.01E-03	3.76E-04	7.00E-03	31.39	86.93	0.13	7.66E-08	6.19	0.28
1.28E+03	935.9	22	0.027	0.168	13.85	7.31E-04	5.28E-03	2.69E-04	5.27E-03	31.5	87.08	0.13	7.66E-08	6.18	0.24
1.39E+03	1.05E+03	22	0.020	0.126	18.40	7.31E-04	3.97E-03	2.05E-04	3.97E-03	31.6	87.04	0.13	7.66E-08	6.18	0.15
1.51E+03	1.17E+03	22	0.015	0.094	24.51	7.30E-04	2.98E-03	1.21E-04	2.98E-03	31.62	87.67	0.13	7.66E-08	6.17	0.21
1.66E+03	1.32E+03	22	0.011	0.071	32.58	7.30E-04	2.24E-03	7.84E-05	2.24E-03	31.72	88	0.13	7.66E-08	6.14	0.81
1.84E+03	1.50E+03	22	8.44E-03	0.053	43.55	7.30E-04	1.68E-03	7.23E-05	1.68E-03	31.64	87.53	0.13	7.66E-08	6.17	0.22
2.06E+03	1.72E+03	22	6.33E-03	0.040	57.86	7.30E-04	1.26E-03	5.31E-05	1.26E-03	31.75	87.59	0.14	7.65E-08	6.11	0.14
				0.000											
4.13E+02	7.42E+01	22	3.25E+00	20.441				2.19E-01	2.19E-01		50.69				
4.07E+02	6.78E+01	22	3.72E+00	23.382				3.02E-01	3.02E-01		42.09				
3.88E+02	4.86E+01	22	5.77E+00	36.270				2.18E-01	2.18E-01		85.22				
3.79E+02	3.99E+01	22	7.13E+00	44.785				3.38E-01	3.38E-01		77.99				
370.3	31.37	22	8.782	55.184				1.208	1.208		53.48				
356.5	17.62	22	12.6	79.176				11.55	11.55		38.89				

Table B.7.4. Viscoelasticity evaluation of FP-5115 in seawater brine @ 62°C.

Text _p (s)	t (s)	T (°C)	f (Hz)	ω (rad/s)	Shear Strain γ^* (%)	σ^* (Pa)	Complex Modulus G^* (Pa)	Elastic (Storage) Modulus G' (Pa)	Viscous (Loss) Modulus G'' (Pa)	Complex Viscosity η^* (Pa s)	Phase Angle (Shift) δ (°)	F (N)	T (N m)	Angular Absolut Velocity θ_{abs} (rad)	HD (%)
362.5	10.67	62	15.000	94.257	3.50E-03	7.79E-05	2.225	1.252	0.87	23.61	55.75	0.24	8.16E-09	3.96	2.10
373.4	21.63	62	11.250	70.693	6.84E-03	8.62E-05	1.260	0.517	0.49	17.83	65.78	0.24	9.03E-09	3.95	1.97
384.7	32.91	62	8.435	53.004	1.21E-02	7.79E-05	0.642	0.255	0.32	12.11	66.61	0.24	8.17E-09	3.94	1.09
396.4	44.63	62	6.325	39.745	2.16E-02	7.79E-05	0.361	0.126	0.28	9.085	69.5	0.24	8.16E-09	3.93	0.80
408.7	56.88	62	4.743	29.804	3.83E-02	9.26E-05	0.242	0.086	0.23	8.112	74.17	0.24	9.71E-09	3.92	0.59
421.7	69.84	62	3.557	22.351	0.07	1.39E-04	0.203	0.061	0.20	9.079	76.62	0.24	1.45E-08	3.91	0.54
435.5	83.72	62	2.667	16.759	0.12	2.02E-04	0.164	0.057	0.15	9.794	69.76	0.24	2.12E-08	3.90	0.43
451.1	99.26	62	2.000	12.568	0.22	2.73E-04	0.125	0.036	0.12	9.945	73.26	0.25	2.87E-08	3.88	0.21
468.4	116.6	62	1.500	9.426	0.39	3.81E-04	0.097	0.028	0.09	10.31	73.28	0.25	3.99E-08	3.87	0.20
488	136.2	62	1.125	7.069	0.70	5.32E-04	0.076	0.022	0.07	10.72	72.97	0.25	5.58E-08	3.86	0.30
510.5	158.7	62	0.844	5.300	1.24	7.30E-04	0.059	0.014	0.06	11.13	76.07	0.25	7.65E-08	3.84	0.25
537.4	185.6	62	0.633	3.974	2.16	1.00E-03	0.046	9.59E-03	0.05	11.69	78.09	0.25	1.05E-07	3.83	0.23
569.1	217.2	62	0.474	2.980	3.67	1.30E-03	0.035	6.21E-03	0.03	11.91	79.93	0.25	1.37E-07	3.83	0.15
608.4	256.6	62	0.356	2.235	6.05	1.64E-03	0.027	4.14E-03	0.03	12.12	81.21	0.25	1.72E-07	3.83	0.21
657.2	305.4	62	0.267	1.676	9.58	2.00E-03	0.021	3.06E-03	0.02	12.45	81.56	0.25	2.10E-07	3.86	0.04
722.2	370.4	62	0.200	1.257	14.47	2.29E-03	0.016	2.22E-03	0.02	12.57	81.91	0.25	2.40E-07	3.90	0.03
795.5	443.7	62	0.150	0.943	20.88	2.52E-03	0.012	1.81E-03	0.01	12.79	81.38	0.25	2.64E-07	3.92	0.06
873.3	521.5	62	0.113	0.707	29.03	2.66E-03	9.17E-03	1.47E-03	9.05E-03	12.97	80.79	0.25	2.79E-07	3.92	0.07
945.2	593.4	62	0.084	0.530	39.62	2.77E-03	6.99E-03	1.45E-03	6.84E-03	13.19	78.05	0.26	2.91E-07	3.92	0.04
1021	669.2	62	0.063	0.397	51.77	2.82E-03	5.45E-03	1.39E-03	5.27E-03	13.72	75.27	0.26	2.96E-07	3.89	0.11
1.10E+03	750.3	62	0.047	0.298	64.62	2.83E-03	4.39E-03	1.32E-03	4.18E-03	14.72	72.47	0.26	2.97E-07	3.88	0.25
1.19E+03	838.4	62	0.036	0.224	79.63	2.84E-03	3.57E-03	1.42E-03	3.27E-03	15.97	66.51	0.26	2.98E-07	3.85	0.38
1.29E+03	935.9	62	0.027	0.168	93.80	2.83E-03	3.01E-03	1.44E-03	2.65E-03	17.98	61.45	0.26	2.96E-07	3.92	0.19
1.40E+03	1.05E+03	62	0.020	0.126	101.86	2.80E-03	2.75E-03	1.53E-03	2.28E-03	21.88	56.12	0.27	2.94E-07	3.84	0.70
1.52E+03	1.17E+03	62	0.015	0.094	115.49	2.77E-03	2.40E-03	1.24E-03	2.06E-03	25.47	58.92	0.27	2.91E-07	3.84	1.34
1.67E+03	1.32E+03	62	0.011	0.071	134.58	2.76E-03	2.05E-03	1.17E-03	1.68E-03	29.03	55.11	0.27	2.90E-07	3.89	1.36
1.85E+03	1.50E+03	62	8.44E-03	0.053	150.31	2.75E-03	1.83E-03	1.07E-03	1.49E-03	34.53	54.38	0.28	2.88E-07	3.75	1.04
2.07E+03	1.72E+03	62	6.33E-03	0.040	171.94	2.74E-03	1.60E-03	8.86E-04	1.33E-03	40.14	56.25	0.28	2.88E-07	3.84	2.25
2.34E+03	1.99E+03	62	4.74E-03	0.030	237.14	2.74E-03	1.16E-03	6.29E-04	9.69E-04	38.77	57	0.29	2.87E-07	3.90	3.74
2.68E+03	2.33E+03	62	3.56E-03	0.022	308.74	2.74E-03	8.87E-04	4.60E-04	7.58E-04	39.67	58.72	0.30	2.87E-07	3.66	4.63
3.12E+03	2.77E+03	62	2.67E-03	0.017	384.94	2.73E-03	7.10E-04	3.07E-04	6.41E-04	42.38	64.42	0.30	2.87E-07	3.45	4.20
3.68E+03	3.33E+03	62	2.00E-03	0.013	534.95	2.73E-03	5.11E-04	2.35E-04	4.54E-04	40.66	62.64	0.31	2.87E-07	3.38	4.94
4.40E+03	4.05E+03	62	1.50E-03	0.009	689.43	2.73E-03	3.96E-04	1.78E-04	3.54E-04	42.06	63.38	0.32	2.87E-07	3.47	5.22

Table B.7.5. Viscoelasticity evaluation of FP-5115 in deionized water @ 62°C.

Text ₀ (s)	t (s)	T (°C)	f (Hz)	ω (rad/s)	Shear Strain γ^* (%)	σ^* (Pa)	Complex Modulus G^* (Pa)	Elastic (Storage) Modulus G' (Pa)	Viscous (Loss) Modulus G'' (Pa)	Complex Viscosity η^* (Pa s)	Phase Angle (Shift) δ (°)	F (N)	T (N m)	Angular Absolut Velocity θ_{abs} (rad)	HD (%)
329	10.67	62	15.000	94.257	6.57E-04	2.51E-05	3.824	2.996	2.38	0.041	38.41	1.03	2.63E-09	5.57	6.54
340	21.65	62	11.250	70.693	1.37E-03	5.59E-05	4.077	3.961	0.97	0.058	13.72	1.03	5.86E-09	5.57	8.09
351.3	32.93	62	8.435	53.004	2.55E-03	8.65E-05	3.395	3.149	1.27	0.064	21.95	1.03	9.07E-09	5.57	3.03
363	44.64	62	6.325	39.745	4.53E-03	9.73E-05	2.147	1.813	1.15	0.054	32.36	1.03	1.02E-08	5.57	1.41
375.3	56.88	62	4.743	29.804	8.84E-03	1.77E-04	1.996	1.649	1.12	0.067	34.29	1.03	1.85E-08	5.57	2.39
388.2	69.84	62	3.557	22.351	0.02	4.25E-04	2.057	1.819	0.96	0.092	27.81	1.03	4.45E-08	5.57	0.69
402.1	83.72	62	2.667	16.759	0.05	9.24E-04	1.897	1.697	0.85	0.113	26.6	1.03	9.68E-08	5.57	0.22
417.6	99.23	62	2.000	12.568	0.06	1.04E-03	1.709	1.520	0.78	0.136	27.22	1.03	1.10E-07	5.57	0.16
435	116.6	62	1.500	9.426	0.05	7.88E-04	1.567	1.379	0.74	0.166	28.32	1.03	8.26E-08	5.57	0.28
454.5	136.2	62	1.125	7.069	0.04	6.38E-04	1.541	1.333	0.77	0.218	30.11	1.03	6.68E-08	5.57	0.36
477.1	158.7	62	0.844	5.300	0.04	5.81E-04	1.361	1.173	0.69	0.257	30.48	1.03	6.09E-08	5.57	0.39
504	185.6	62	0.633	3.974	0.05	5.51E-04	1.162	9.94E-01	0.60	0.292	31.16	1.03	5.77E-08	5.57	0.32
535.6	217.3	62	0.474	2.980	0.05	5.28E-04	1.144	9.62E-01	0.62	0.384	32.77	1.03	5.53E-08	5.57	0.67
575	256.6	62	0.356	2.235	0.05	5.18E-04	0.967	8.06E-01	0.53	0.433	33.52	1.03	5.43E-08	5.57	1.02
623.8	305.4	62	0.267	1.676	0.06	5.11E-04	0.862	7.07E-01	0.49	0.515	34.96	1.03	5.36E-08	5.57	0.77
688.8	370.4	62	0.200	1.257	0.06	5.06E-04	0.798	6.42E-01	0.47	0.635	36.38	1.03	5.31E-08	5.57	0.78
762.1	443.7	62	0.150	0.943	0.07	5.04E-04	0.760	6.11E-01	0.45	0.806	36.43	1.03	5.28E-08	5.57	1.61
839.9	521.5	62	0.113	0.707	0.08	5.03E-04	5.95E-01	4.69E-01	3.67E-01	0.842	38.06	1.03	5.27E-08	5.57	0.58
911.8	593.4	62	0.084	0.530	0.08	5.01E-04	5.93E-01	4.50E-01	3.87E-01	1.119	40.68	1.03	5.26E-08	5.57	1.28
987.6	669.2	62	0.063	0.397	0.10	5.01E-04	4.91E-01	3.78E-01	3.13E-01	1.235	39.57	1.03	5.25E-08	5.57	1.43
1.07E+03	750.3	62	0.047	0.298	0.12	5.01E-04	4.16E-01	2.91E-01	2.98E-01	1.397	45.73	1.04	5.25E-08	5.57	1.27
1.16E+03	838.5	62	0.036	0.224	0.13	5.00E-04	3.80E-01	2.61E-01	2.76E-01	1.700	46.54	1.03	5.25E-08	5.57	1.77
1.25E+03	936	62	0.027	0.168	0.17	5.00E-04	3.01E-01	1.98E-01	2.26E-01	1.794	48.76	1.04	5.24E-08	5.57	2.52
1.36E+03	1.05E+03	62	0.020	0.126	0.20	5.00E-04	2.53E-01	1.58E-01	1.98E-01	2.014	51.54	1.04	5.24E-08	5.56	1.84
1.49E+03	1.17E+03	62	0.015	0.094	0.21	5.00E-04	2.38E-01	1.43E-01	1.90E-01	2.525	53.01	1.04	5.24E-08	5.56	2.50
1.64E+03	1.32E+03	62	0.011	0.071	0.26	5.00E-04	1.94E-01	1.20E-01	1.52E-01	2.738	51.81	1.04	5.24E-08	5.56	2.35
1.82E+03	1.50E+03	62	8.44E-03	0.053	0.30	5.00E-04	1.66E-01	9.42E-02	1.37E-01	3.134	55.45	1.04	5.24E-08	5.56	3.43
2.04E+03	1.72E+03	62	6.33E-03	0.040	0.37	5.00E-04	1.34E-01	7.32E-02	1.12E-01	3.371	56.87	1.04	5.24E-08	5.56	1.93
2.31E+03	1.99E+03	62	4.74E-03	0.030	0.45	5.00E-04	1.11E-01	5.49E-02	9.69E-02	3.735	60.47	1.04	5.24E-08	5.56	1.75
2.65E+03	2.33E+03	62	3.56E-03	0.022	0.54	5.00E-04	9.25E-02	4.20E-02	8.24E-02	4.136	63.01	1.05	5.24E-08	5.56	1.77
3.08E+03	2.77E+03	62	2.67E-03	0.017	0.64	5.00E-04	7.80E-02	3.64E-02	6.90E-02	4.656	62.21	1.05	5.24E-08	5.56	1.94
3.64E+03	3.33E+03	62	2.00E-03	0.013	0.77	5.00E-04	6.46E-02	3.11E-02	5.65E-02	5.136	61.15	1.05	5.24E-08	5.56	2.20
4.37E+03	4.05E+03	62	1.50E-03	0.009	0.94	5.00E-04	5.33E-02	2.36E-02	4.78E-02	5.659	63.73	1.06	5.24E-08	5.55	2.71
5319	5001	62	0.001	0.007	1.20161	0.0005	0.042	0.016	0.04	5.887	67.73	1.059	5.24E-08	5.549	1.647
6379	6061	62	0.001	0.005	1.40637	0.0005	0.036	0.004	0.04	6.708	82.93	1.065	5.24E-08	5.544	1.338
				0.000											
1059	741	62	0.049	0.308				0.300	0.30		45.34				

Table B.7.6. Extensional data - FP-3430S in Deionized water @ 22°C

Segment	Temp, C	dPc, Pa	Flow Rate, ul/min	N1 Stress Diff, Pa	% Full Scale	Apparent Extensional Rate, 1/s	Apparent Extensional Visc, Pa-s	Apparent Extensional Visc, mPa-s	P Coeff	Extensional Rate, 1/s	Measurement Time, s	Waiting Time, s
1	22.03	666	44.1	314.9	1.1	21.5	14.7	14667	0.625	21.5	479.5	3
2	22.03	694	51.5	327.9	1.6	25.1	13.1	13078	0.654	25.1	410.7	3
3	22.03	757	60.2	357.9	2.2	29.3	12.2	12211	0.687	29.3	351.9	3
4	22.03	848	70.2	400.9	2.7	34.2	11.7	11729	0.719	34.2	301.4	3
5	22.03	971	81.9	459.1	3.3	39.9	11.5	11513	0.753	39.9	258.4	3
6	22.03	1118	95.7	528.4	4	46.6	11.3	11341	0.784	46.6	221.2	3
7	22.02	1252	111.7	591.9	4.7	54.4	10.9	10883	0.804	54.4	189.5	3
8	22.03	1386	13.5	655.5	5.5	66.5	10.3	10325	0.814	63.5	162.4	3
9	22.04	1605	152	78.7	6.4	74.1	10.2	10245	0.839	74.1	139.1	3
10	22.04	1831	177.5	865.9	7.5	86.5	10.0	10014	0.861	86.5	119.2	3
11	22.06	2161	207.3	1022	9	101.0	10.1	10121	0.879	101	102.1	3
12	22.11	2569	242	1214.8	10.6	117.9	10.3	10306	0.894	117.9	87.4	3
13	22.13	2994	282.4	1415.8	12.4	137.5	10.3	10294	0.967	137.6	74.9	3
14	22.13	3559	329.6	1682.8	14.7	160.5	10.5	10483	0.919	160.6	64.2	3
15	22.15	4230	384.7	2000.2	17.3	187.4	10.7	10673	0.930	187.5	55	3
16	22.14	5202	449.2	2459.6	21	218.8	11.2	11241	0.942	218.9	47.1	3
17	22.14	6307	524.4	2981.9	25.1	255.4	11.7	11675	0.947	255.5	40.3	3
18	22.15	7661	611.9	3622.4	30.3	298.1	12.2	12153	0.952	298.2	34.6	3
19	22.15	9628	714.4	4552.5	37.7	348.0	13.1	13083	0.960	348.1	29.6	3
20	22.16	10907	834.1	5156.9	44.1	406.3	12.7	12694	0.964	406.4	25.4	3
21	22.16	14856	973.6	7024.2	56.5	474.2	14.8	14812	0.973	474.3	21.7	3
22	22.15	2506	1136.5	1184.7	9.6	553.6	14.9	14900	0.874	553.7	18.6	3
23	22.16	21683	1326.5	10252.2	81.4	646.1	15.9	15868	0.974	646.3	16	3
24	22.16	32455	1548.4	11090.3	88.5	754.2	14.7	14705	0.977	754.5	13.7	3
25	22.16	423	1807.3	200.2	0.6	880.3	14.5	14500	0.639	880.7	11.7	3

Table B.7.7. Extensional data - FP-3430S in Seawater @ 22°C

Segment	Temp, C	dPc, Pa	Flow Rate, ul/min	N1 Stress Diff, Pa	% Full Scale	Apparent Extensional Rate, 1/s	Apparent Extensional Visc, Pa-s	Apparent Extensional Visc, mPa-s	P Coeff	Extensional Rate, 1/s	Measurement Time, s	Waiting Time, s
1	22	106	44.1	49.9	-0.9	21.5	2.3	2325	0.48	21.5	479.5	3
2	21.98	99	51.5	46.6	-0.9	25.1	1.9	1859	0.54	25.1	410.7	3
3	21.99	98	60.2	46.4	-0.7	29.3	1.6	1582	0.58	29.3	351.9	3
4	21.98	105	70.2	49.5	-0.5	34.2	1.4	1449	0.60	34.2	301.4	3
5	21.99	142	81.9	67.1	-0.3	39.9	1.7	1683	0.65	39.9	258.4	3
6	21.98	180	95.7	84.9	-0.1	46.6	1.8	1823	0.68	46.6	221.2	3
7	21.98	229	111.7	108.3	0.2	54.4	2.0	1991	0.70	54.4	189.5	3
8	22	197	130.3	93	0.3	63.5	1.5	1465	0.67	63.5	162.4	3
9	22.01	244	152	115.6	0.6	74.1	1.6	1561	0.69	74.1	139.1	3
10	22	316	177.5	149.4	1	86.5	1.7	1728	0.72	86.5	119.2	3
11	22	408	207.3	193.1	1.5	101.0	1.9	1912	0.75	101	102.1	3
12	21.99	545	242	257.8	2.2	117.9	2.2	2187	0.78	117.9	87.4	3
13	21.98	706	282.4	333.9	3	137.5	2.4	2427	0.80	137.6	74.9	3
14	21.99	966	329.6	456.8	4.1	160.5	2.8	2846	0.83	160.6	64.2	3
15	21.98	1156	384.7	546.4	4.9	187.4	2.9	2916	0.85	187.5	55	3
16	21.99	1481	449.2	700.1	6.1	218.8	3.2	3200	0.88	218.9	47.1	3
17	21.98	1857	524.4	878.1	7.6	255.4	3.4	3438	0.91	255.5	40.3	3
18	21.98	2390	611.9	1130	9.8	298.1	3.8	3791	0.94	298.2	34.6	3
19	21.99	2990	714.4	1413.6	12.2	348.0	4.1	4062	0.96	348.1	29.6	3
20	21.99	4003	834.1	1892.8	16	406.3	4.7	4659	0.96	406.4	25.4	3
21	21.99	6145	973.6	2905.5	23.6	474.2	6.1	6127	0.97	474.3	21.7	3
22	21.99	9127	1136.5	4315.6	33.8	553.6	7.8	7796	0.97	553.7	18.6	3
23	22.01	12443	1326.5	5883.4	44.6	646.1	9.1	9106	0.98	646.3	16	3
24	22.01	17866	1548.4	8447.6	62.6	754.2	11.2	11201	0.98	754.5	13.7	3
25	22	24436	1807.3	11554.1	83.6	880.3	13.1	13126	0.99	880.7	11.7	3
26	21.99	190	2110.1	89.8	-0.3					1028	10	3
27	21.99	38	2463	17.9	-1.2					1200	8.6	3

Table B.7.8. Extensional data - FP-3430S in Seawater @ 62°C

Segment	Temp, C	dPc, Pa	Flow Rate, ul/min	N1 Stress Diff, Pa	% Full Scale	Apparent Extensional Rate, 1/s	Apparent Extensional Visc, Pa-s	Apparent Extensional Visc, mPa-s	P Coeff	Extensional Rate, 1/s	Measurement Time, s	Waiting Time, s
1	62.01	368	44.1	174	-0.1	21.5	0.9	900	-0.03	21.5	479.5	3
2	62	39	51.5	18.6	0	25.1	0.7	743	0.30	25.1	410.7	3
3	62	-124	60.2	-58.6	0.6	29.3	0.8	800	0.80	29.3	351.9	3
4	62	-77	70.2	-36.2	-0.2	34.2	0.4	400	0.49	34.2	301.4	3
5	61.99	-115	81.9	-54.4	-0.2	39.9	0.4	380	0.51	39.9	258.4	3
6	62	5	95.7	2.2	-0.3	46.6	0.3	250	0.37	46.6	221.2	3
7	62	-227	111.7	-107.2	0.3	54.4	0.3	300	0.64	54.4	189.5	3
8	62	-245	130.3	-115.9	0.5	63.5	0.4	350	0.67	63.5	162.4	3
9	61.99	-1	152	-0.3	0	74.1	0.4	400	0.38	74.1	139.1	3
10	61.98	-46	177.5	-21.6	0	86.5	0.5	450	0.41	86.5	119.2	3
11	61.99	125	207.3	59.1	0.5	101.0	0.6	585	0.26	101	102.1	3
12	62	49	242	23	0.6	117.9	0.4	395	0.33	117.9	87.4	3
13	61.98	133	282.4	62.9	1.1	137.5	0.5	457	0.24	137.6	74.9	3
14	61.98	77	329.6	36.4	1.1	160.5	0.4	427	0.30	160.6	64.2	3
15	61.99	188	384.7	88.9	1.7	187.4	0.5	475	0.14	187.5	55	3
16	62	-164	449.2	-77.4	1.4	218.8	0.5	480	0.57	218.9	47.1	3
17	61.99	-167	524.4	-79.1	1.8	255.4	0.5	500	0.61	255.5	40.3	3
18	62	-23	611.9	-11.1	2.4	298.1	0.6	550	0.42	298.2	34.6	3
19	62	324	714.4	153	3.6	348.0	0.4	440	4.81	348.1	29.6	3
20	61.99	547	834.1	258.5	4.5	406.3	0.6	636	1.63	406.4	25.4	3
21	61.98	999	973.6	472.5	6.2	474.2	1.0	996	1.30	474.3	21.7	3
22	61.97	1771	1136.5	837.2	8.3	553.6	1.5	1512	1.30	553.7	18.6	3
23	61.97	2510	1326.5	1186.9	10.9	646.1	1.8	1837	1.24	646.3	16	3
24	61.97	3690	1548.4	1744.5	15.1	754.2	2.3	2313	1.14	754.5	13.7	3
25	61.96	3956	1807.3	1870.6	16.8	880.3	2.1	2125	1.12	880.7	11.7	3
26	61.98	4175	2110.1	1974.2	18.6					1028	10	3
27	61.99	5139	2463	2429.7	22.3					1200	8.6	3

Table B.7.9. Extensional data - FP-5115 in Deionized water @ 22°C

Segment	Temp, C	dPc, Pa	Flow Rate, ul/min	N1 Stress Diff, Pa	% Full Scale	Apparent Extensional Rate, 1/s	Apparent Extensional Visc, Pa-s	Apparent Extensional Visc, mPa-s	P Coeff	Extensional Rate, 1/s	Measurement Time, s	Waiting Time, s
1	22	250	44.1	118.4	7	21.5	2.7	2740	0.10	21.5	479.5	3
2	21.99	146	51.5	69	11	25.1	2.8	2750	0.34	25.1	410.7	3
3	21.99	183	60.2	86.7	12.1	29.3	3.0	2958	0.34	29.3	351.9	3
4	21.99	206	70.2	97.2	12.9	34.2	2.8	2843	0.33	34.2	301.4	3
5	21.99	66	81.9	31.2	13.8	39.9	2.8	2830	0.36	39.9	258.4	3
6	22.01	41	95.7	19.5	15.1	46.6	2.8	2836	0.37	46.6	221.2	3
7	22.01	91	111.7	42.9	15.5	54.4	2.8	2840	0.36	54.4	189.5	3
8	22.02	228	130.3	107.9	16	63.5	2.8	2841	0.33	63.5	162.4	3
9	22.02	369	152	174.6	16.7	74.1	2.8	2843	0.31	74.1	139.1	3
10	22.02	521	177.5	246.2	17.6	86.5	2.8	2847	0.28	86.5	119.2	3
11	22.02	731	207.3	345.5	18.5	101.0	3.4	3421	0.22	101	102.1	3
12	22.01	938	242	443.7	19.5	117.9	3.8	3764	0.16	117.9	87.4	3
13	22.02	1179	282.4	557.5	20.7	137.5	4.1	4053	0.09	137.6	74.9	3
14	22	1467	329.6	693.8	22.3	160.5	4.3	4322	-0.02	160.6	64.2	3
15	22.01	1773	384.7	838.3	23.7	187.4	4.5	4473	-0.20	187.5	55	3
16	22.02	2300	449.2	1087.4	26.1	218.8	5.0	4970	-0.70	218.9	47.1	3
17	22.02	2851	524.4	1348.2	28.8	255.4	5.3	5279	-2.06	255.5	40.3	3
18	22.02	3493	611.9	1651.4	31.7	298.1	5.5	5540	40.63	298.2	34.6	3
19	22.02	4346	714.4	2055.1	35.4	348.0	5.9	5906	3.00	348.1	29.6	3
20	22.02	5571	834.1	2633.9	40.7	406.3	6.5	6483	1.81	406.4	25.4	3
21	22.02	6984	973.6	3302.3	46.4	474.2	7.0	6964	1.47	474.3	21.7	3
22	22.02	8397	1136.5	3970.2	52.3	553.6	7.2	7172	1.31	553.7	18.6	3
23	22.03	10288	1326.5	4864.3	59.8	646.1	7.5	7529	1.21	646.3	16	3
24	22.02	12429	1548.4	5876.6	68.4	754.2	7.8	7792	1.15	754.5	13.7	3
25	22.02	15729	1807.3	7437	82.1	880.3	8.4	8449	1.09	880.7	11.7	3
26	22.02	18898	2110.1	8935.3	94.7					1028	10	3
27	22.02	223	2463	105.2	14.6					1200	8.6	3

Table B.7.10. Extensional data - FP-5115 in Seawater @ 22°C

Segment	Temp, C	dPc, Pa	Flow Rate, ul/min	N1 Stress Diff, Pa	% Full Scale	Apparent Extensional Rate, 1/s	Apparent Extensional Visc, Pa-s	Apparent Extensional Visc, mPa-s	P Coeff	Extensional Rate, 1/s	Measurement Time, s	Waiting Time, s
1	22.02	35	44.1	16.4	0.9	21.5	0.8	765	0.31	21.5	479.5	3
2	22.03	62	51.5	29.5	1.3	25.1	1.2	1175	0.25	25.1	410.7	3
3	22.03	84	60.2	39.5	1.6	29.3	1.3	1347	0.18	29.3	351.9	3
4	22.04	114	70.2	53.9	1.8	34.2	1.6	1576	0.07	34.2	301.4	3
5	22.04	141	81.9	66.5	2	39.9	1.7	1667	-0.07	39.9	258.4	3
6	22.04	173	95.7	82	2.2	46.6	1.8	1759	-0.32	46.6	221.2	3
7	22.04	219	111.7	103.7	2.4	54.4	1.9	1907	-0.92	54.4	189.5	3
8	22.04	263	130.3	124.2	2.6	63.5	2.0	1956	-3.82	63.5	162.4	3
9	22.03	316	152	149.5	2.9	74.1	2.0	2019	6.70	74.1	139.1	3
10	22.04	385	177.5	182.1	3.3	86.5	2.1	2106	2.63	86.5	119.2	3
11	22.04	478	207.3	226.2	3.8	101.0	2.2	2240	1.72	101	102.1	3
12	22.04	585	242	276.7	4.3	117.9	2.3	2347	1.41	117.9	87.4	3
13	22.04	799	282.4	377.7	5.2	137.5	2.7	2746	1.22	137.6	74.9	3
14	22.05	1045	329.6	494.2	6.3	160.5	3.1	3079	1.12	160.6	64.2	3
15	22.04	1367	384.7	646.4	7.6	187.4	3.4	3449	1.08	187.5	55	3
16	22.05	1660	449.2	785	7.9	218.8	3.6	3588	1.19	218.9	47.1	3
17	22.04	1794	524.4	848.4	8.5	255.4	3.3	3322	1.19	255.5	40.3	3
18	22.05	2120	611.9	1002.5	10	298.1	3.4	3363	1.16	298.2	34.6	3
19	22.06	2776	714.4	1312.7	12.8	348.0	3.8	3772	1.12	348.1	29.6	3
20	22.06	3417	834.1	1615.7	15.5	406.3	4.0	3977	1.09	406.4	25.4	3
21	22.04	4482	973.6	2119.2	19.7	474.2	4.5	4469	1.06	474.3	21.7	3
22	22.05	5939	1136.5	2808.3	25.3	553.6	5.1	5073	1.04	553.7	18.6	3
23	22.06	8162	1326.5	3859	33.7	646.1	6.0	5973	1.03	646.3	16	3
24	22.06	10621	1548.4	5021.9	42.2	754.2	6.7	6659	1.01	754.5	13.7	3
25	22.05	14070	1807.3	6652.6	54.7	880.3	7.6	7557	1.01	880.7	11.7	3
26	22.05	18311	2110.1	8657.7	71					1028	10	3
27	22.05	24017	2463	11355.8	92.5					1200	8.6	3

Table B.7.11. Extensional data - FP-5115 in Seawater @ 62°C

Segment	Temp, C	dPc, Pa	Flow Rate, ul/min	N1 Stress Diff, Pa	% Full Scale	Apparent Extensional Rate, 1/s	Apparent Extensional Visc, Pa-s	Apparent Extensional Visc, mPa-s	P Coeff	Extensional Rate, 1/s	Measurement Time, s	Waiting Time, s
1	62	1635	44.1	773.2	0.2	21.5	36.0	36010	-0.71	21.5	479.5	3
2	61.98	2022	51.5	956.2	0.4	25.1	38.1	38134	-0.67	25.1	410.7	3
3	62	2102	60.2	994	-0.2	29.3	33.9	33914	-0.50	29.3	351.9	3
4	62	2058	70.2	973.1	-0.4	34.2	28.5	28470	-0.46	34.2	301.4	3
5	61.99	1883	81.9	890.4	0.4	39.9	22.3	22330	-0.47	39.9	258.4	3
6	62	2088	95.7	987	-0.9	46.6	21.2	21183	-0.34	46.6	221.2	3
7	62.01	2097	111.7	991.7	-1	54.4	18.2	18235	-0.30	54.4	189.5	3
8	62.01	2055	130.3	971.5	-0.7	63.5	15.3	15301	-0.29	63.5	162.4	3
9	62.01	2083	152	985.1	-0.3	74.1	13.3	13303	-0.31	74.1	139.1	3
10	62	2112	177.5	998.6	-0.2	86.5	11.5	11549	-0.30	86.5	119.2	3
11	62.02	2196	207.3	1038.1	0	101.0	10.3	10281	-0.36	101	102.1	3
12	62.01	2011	242	950.8	-0.1	117.9	8.1	8066	-0.31	117.9	87.4	3
13	62.01	1732	282.4	819	-0.2	137.5	6.0	5955	-0.20	137.6	74.9	3
14	62.01	1839	329.6	869.6	0.3	160.5	5.4	5417	-0.27	160.6	64.2	3
15	62	2397	384.7	1133.3	1.4	187.4	6.0	6047	-0.66	187.5	55	3
16	62	2424	449.2	1146	1.7	218.8	5.2	5238	-0.72	218.9	47.1	3
17	61.99	2120	524.4	1002.3	2.4	255.4	3.9	3924	-0.70	255.5	40.3	3
18	61.99	1968	611.9	930.3	2.4	298.1	3.1	3121	-0.56	298.2	34.6	3
19	62	2267	714.4	1072	3.2	348.0	3.1	3081	-0.93	348.1	29.6	3
20	61.99	2445	834.1	1156.1	4.1	406.3	2.8	2846	-1.32	406.4	25.4	3
21	62	2662	973.6	1258.8	5.3	474.2	2.7	2655	-2.03	474.3	21.7	3
22	61.98	3003	1136.5	1419.9	6.9	553.6	2.6	2565	-4.57	553.7	18.6	3
23	61.98	3335	1326.5	1576.8	8.6	646.1	2.4	2440	-25.82	646.3	16	3
24	62	3803	1548.4	1798	10.9	754.2	2.4	2384	6.99	754.5	13.7	3
25	61.99	4807	1807.3	2272.9	14.2	880.3	2.6	2582	3.19	880.7	11.7	3
26	61.97	5448	2110.1	2575.7	17.2					1028	10	3
27	61.97	5661	2463	2676.8	18.3					1200	8.6	3

APPENDIX C: Reservoir Characterization

C.1. Detailed mineralogical composition using MLA

Table C.1.1. MLA-SEM results in low permeability facies core plugs

Mineralogy	Core Plugs by Well - Low Perm Facies											
	D-94 (%)						M-04 (%)					
	OF-14 BF	OF-14 AF	DIF	OF-15 BF	OF-15 AF	DIF	OF-04 BF	OF-04 AF	DIF	OF-05 BF	OF-05 AF	DIF
Quartz (SiO ₂)	62.5	54.5	7.9	54.6	56.6	-2.0	83.9	64.6	19.3	66.1	61.9	4.2
TOTAL	62.5	54.5	7.9	54.6	56.6	-2.0	83.9	64.6	19.3	66.1	61.9	4.2
Lithic Fragments												
Quartz-feldspar-mix	8.9	16.5	-7.6	15.3	16.7	-1.4	10.2	21.5	-11.3	17.2	25.2	-8.0
Calcite-feldspar-mix	0.2	0.2	0.1	0.5	0.3	0.2			0.0	0.1		0.1
Calcite-pyrite-mix	0.1	0.1	0.0	0.1	0.1	0.0			0.0			0.0
Feldspar-pyrite-mix	0.1		0.1			0.0			0.0	0.1		0.1
TOTAL	9.3	16.8	-7.5	15.9	17.0	-1.2	10.2	21.5	-11.3	17.4	25.2	-7.8
Feldspars												
Albite (NaAlSi ₃ O ₈)	1.3	2.0	-0.7	2.2	1.9	0.2	0.4	1.3	-1.0	1.2	1.6	-0.4
Orthoclase (KAlSi ₃ O ₈)	0.4	0.9	-0.4	1.1	1.0	0.2	0.4	0.6	-0.2	1.0	0.8	0.2
Perthite (KAlSi ₃ O ₈ - NaAlSi ₃ O ₈)	0.2	0.5	-0.3	0.6	0.5	0.1	0.2	0.7	-0.6	0.5	1.0	-0.5
Plagioclase (An10-30)		0.1	-0.1	0.1	0.1	0.0		0.1	-0.1		0.1	-0.1
Plagioclase (NaAlSi ₃ O ₈ to CaAl ₂ Si ₂ O ₈)			0.0	0.1		0.1			0.0			0.0
TOTAL	1.9	3.4	-1.5	4.1	3.5	0.6	0.9	2.7	-1.9	2.6	3.4	-0.8
Carbonates												
Calcite (CaCO ₃)	15.5	13.9	1.6	9.3	15.2	-5.9	0.6	0.5	0.2	0.5	0.6	-0.1
Siderite (FeCO ₃)	3.8	2.5	1.3	0.1	0.2	-0.1	1.1	0.8	0.3	0.1	0.1	0.1
Ankerite (Ca(Fe,Mg,Mn)(CO ₃) ₂)	0.1	0.1	0.0	0.1		0.1			0.0			0.0
Dolomite (CaMg(CO ₃) ₂)			0.0	0.1		0.1			0.0			0.0
TOTAL	19.5	16.6	2.9	9.5	15.4	-5.9	1.7	1.2	0.4	0.6	0.6	0.0
Clays												
Illite ((K,H ₃ O)(Al,Mg,Fe) ₂ (Si,Al) ₄ O ₁₀ (OH) ₂ (H ₂ O))	0.4	0.9	-0.5	1.3	0.9	0.4	0.3	1.6	-1.3	1.8	1.6	0.1
Kaolinite (Al ₂ Si ₂ O ₅ (OH) ₄)	0.2	0.6	-0.4	0.4	0.4	0.0	0.2	1.7	-1.5	1.1	2.1	-1.0
TOTAL	0.6	1.5	-0.9	1.7	1.3	0.4	0.4	3.3	-2.8	2.8	3.7	-0.9
Matrix												
Finegrain-quartz-clay	1.8	3.2	-1.3	7.5	3.2	4.3	1.0	3.8	-2.7	6.3	3.3	3.0
Finegrain-silicates-carbonates	0.7	1.1	-0.4	2.2	1.4	0.8	0.1	0.2	-0.2	0.4	0.2	0.2
TOTAL	2.5	4.2	-1.7	9.7	4.6	5.1	1.1	4.0	-2.9	6.6	3.4	3.2
Accessories												
Chlorit-Fe ((Fe ₅ Al)(AlSi ₃)O ₁₀ (OH) ₈)	2.1	1.9	0.2	0.9	0.8	0.1	0.8	1.6	-0.8	1.0	1.0	0.0
Ilmenite (FeTiO ₃)	0.2	0.3	-0.1	0.2	0.3	-0.1	0.1	0.3	-0.1	0.1	0.2	-0.1
Rutile (TiO ₂)	0.2	0.2	0.0	0.1	0.2	-0.1	0.2	0.2	0.0	0.1	0.2	0.0
Zircon (ZrSiO ₄)	0.1	0.1	0.0		0.1	-0.1	0.1	0.1	0.0		0.1	-0.1
Muscovite (KAl ₂ (AlSi ₃ O ₁₀)(F,OH) ₂)	0.1		0.1	0.1	0.1	0.0	0.1	0.1	0.0	0.2	0.1	0.0
TOTAL	2.6	2.5	0.1	1.3	1.3	0.0	1.3	2.2	-0.9	1.4	1.5	-0.1
Organic												
Organic	0.3	0.5	-0.2	1.7	0.2	1.6	0.1	0.3	-0.2	1.4	0.1	1.3
TOTAL	0.3	0.5	-0.2	1.7	0.2	1.6	0.1	0.3	-0.2	1.4	0.1	1.3

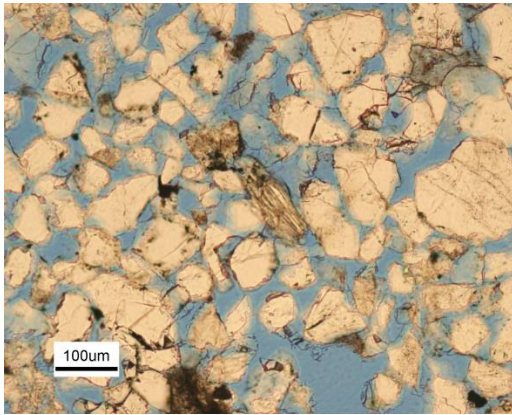
BF: Before flooding, **AF:** After flooding, **DIF:** Difference before and after flooding.

Table C.1.2. MLA-SEM results in low permeability facies core plugs

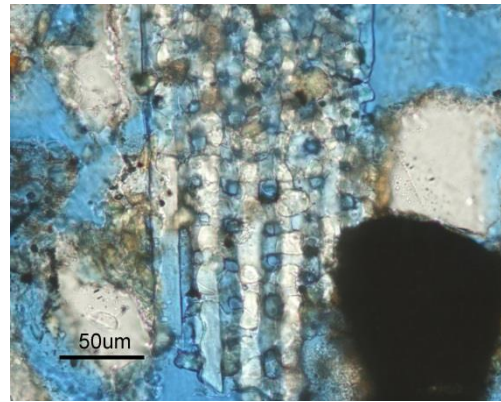
Mineralogy	Core Plugs by Well - Low Perm Facies											
	D-94 (%)						M-04 (%)					
	OF-20 BF	OF-20 AF	DIF	OF-21 BF	OF-21 AF	DIF	OF-02 BF	OF-02 AF	DIF	OF-06 BF	OF-06 AF	DIF
Quartz (SiO ₂)	84.4	83.4	1.0	87.3	86.0	1.3	82.9	78.0	4.9	87.9	82.7	5.2
TOTAL	84.4	83.4	1.0	87.3	86.0	1.3	82.9	78.0	4.9	87.9	82.7	5.2
Lithic Fragments												
Quartz-feldspar-mix	11.4	14.0	-2.6	9.7	12.0	-2.3	12.0	15.0	-3.0	9.7	16.0	-6.3
Calcite-feldspar-mix												
Calcite-pyrite-mix												
Feldspar-pyrite-mix												
TOTAL	11.4	14.0	-2.6	9.7	12.0	-2.3	12.0	15.0	-3.0	9.7	16.0	-6.3
Feldspars												
Albite (NaAlSi ₃ O ₈)	0.2	0.4	-0.2	0.1	0.3	-0.2	0.5	0.6	-0.1	0.3	0.4	-0.1
Orthoclase (KAlSi ₃ O ₈)	0.4	0.5	-0.1	0.3	0.3	0.0	0.4	0.4	0.0	0.4	0.3	0.1
Perthite (KAlSi ₃ O ₈ - NaAlSi ₃ O ₈)	0.2	0.3	-0.1	0.1	0.2	-0.1	0.2	0.3	-0.1	0.1	0.2	-0.1
Plagioclase(An10-30)												
Plagioclase (NaAlSi ₃ O ₈ to CaAl ₂ Si ₂ O ₈)												
TOTAL	0.8	1.2	-0.4	0.5	0.8	-0.3	1.1	1.3	-0.2	0.7	0.9	-0.2
Carbonates												
Calcite (CaCO ₃)	0.7		0.7	0.1		0.1	0.6	0.6	0.0			
Siderite (FeCO ₃)	0.1		0.1				0.1	0.1	0.0	0.1	0.1	0.0
Ankerite (Ca(Fe,Mg,Mn)(CO ₃) ₂)									0.0			
Dolomite (CaMg(CO ₃) ₂)									0.0			
TOTAL	0.7	0.0	0.7	0.1	0.0	0.1	0.7	0.7	0.0	0.1	0.1	0.0
Clays												
Illite ((K,H ₃ O)(Al,Mg,Fe) ₂ (Si,Al) ₄ O ₁₀ (OH) ₂ (H ₂ O))	0.5	0.4	0.1	0.3	0.2	0.1	0.4	0.2	0.2	0.2	0.1	0.1
Kaolinite (Al ₂ Si ₂ O ₅ (OH) ₄)	0.3	0.6	-0.3	0.2	0.3	-0.1	0.3	0.7	-0.4	0.2	0.5	-0.3
TOTAL	0.7	1.0	-0.3	0.4	0.5	-0.1	0.6	0.9	-0.3	0.4	0.6	-0.2
Matrix												
Finegrain-quartz-clay	0.8	0.7	0.1	0.6	0.5	0.1	1.0	1.0	0.0	0.5	0.4	0.1
Finegrain-silicates-carbonates												
TOTAL	0.8	0.7	0.1	0.6	0.5	0.1	1.0	1.0	0.0	0.5	0.4	0.1
Accessories												
Chlorit-Fe ((Fe ₅ Al)(AlSi ₃ O ₁₀ (OH) ₈)	0.3	0.4	-0.2	0.2	0.4	-0.2	0.4	0.5	-0.1	0.2	0.3	-0.1
Ilmenite (FeTiO ₃)	0.1	0.2	-0.1	0.2	0.4	-0.2	0.2	0.3	-0.1	0.1	0.2	-0.1
Rutile (TiO ₂)	0.1	0.1	0.0	0.2	0.3	-0.1	0.2	0.2	0.0	0.1	0.1	0.0
Zircon (ZrSiO ₄)			0.0	0.1	0.2	0.0	0.2	0.1	0.1	0.1	0.1	0.0
Muscovite (KAl ₂ (AlSi ₃ O ₁₀)(F,OH) ₂)	0.2	0.2	0.0				0.1	0.1	0.0	0.1	0.2	-0.1
TOTAL	0.6	0.9	-0.2	0.8	1.2	-0.4	1.1	1.2	-0.1	0.6	0.8	-0.3
Organic												
Organic	0.1		0.1	0.1	0.0	0.1	0.2	0.0	0.1		0.0	0.0
TOTAL	0.1	0.0	0.1	0.1	0.0	0.1	0.2	0.0	0.1			0.0

BF: Before flooding, **AF:** After flooding, **DIF:** Difference before and after flooding.

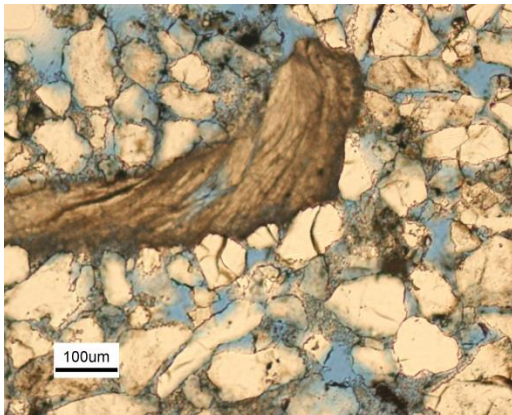
C.2. General thin sections



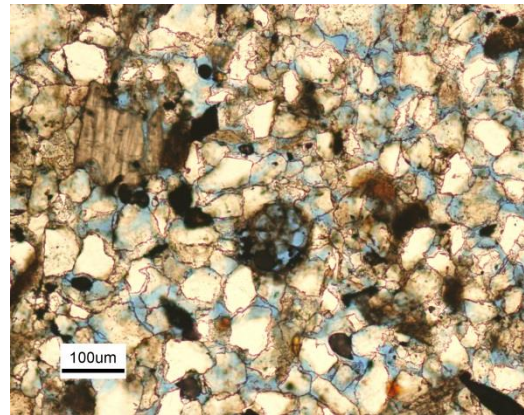
A) Chlorite



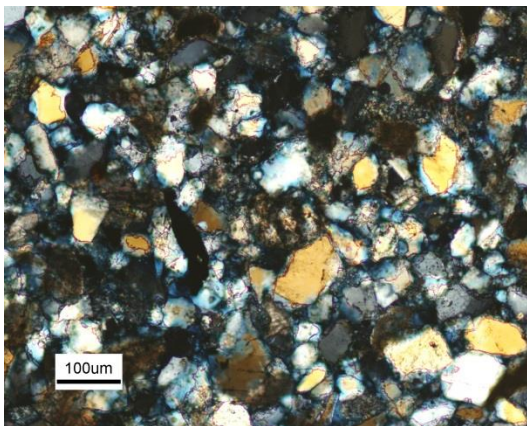
B) Feldspar grain dissolution



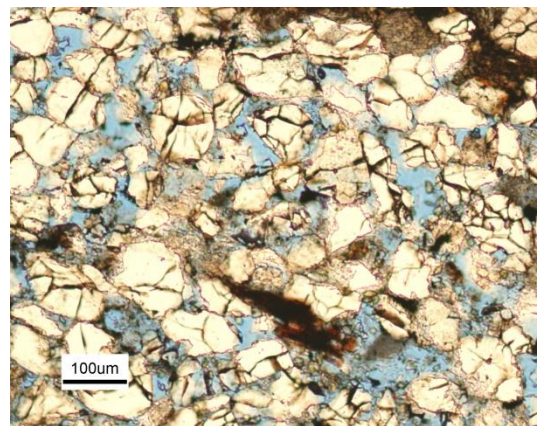
C) Fossil grain



D) Foraminifera fossil grain



E) Lithic fragments – cross-polarized light



F) Quartz grains fractures

C.3. Core plugs selections from Hebron exploration cores (core slabs)



A) Core slabs at CNLOPB



B) Core slabs after core plug sampling



C) Composite core

APPENDIX D: Digital Image Analysis (DIA)

Table D.1. Porosity distribution by DIA – D-94 well

Image	Intergranular Porosity (%)	Intragranular Porosity (%)	Total Porosity (%)
D-94-A-1_OF-20_DIA_02	29.0	0.7	29.6
D-94-A-1_OF-20_DIA_04	26.1	0.4	26.5
D-94-A-1_OF-20_DIA_06	21.4	0.3	21.8
D-94-A-1_OF-20_DIA_08	23.7	0.4	24.1
D-94-A-1_OF-20_DIA_10	25.3	0.3	25.6
D-94-A-1_OF-20_DIA_12	23.8	0.7	24.4
D-94-A-1_OF-20_DIA_18	36.0	0.1	36.1
D-94-A-1_OF-20_DIA_19	40.2	0.2	40.4
D-94-A-1_OF-20_DIA_21	39.8	0.5	40.3
D-94-A-1_OF-20_DIA_22	25.1	0.4	25.5
D-94-A-1_OF-20_DIA_27	39.2	0.4	39.6
D-94-A-1_OF-20_DIA_28	32.7	0.2	33.0
D-94-A-2_OF-21_DIA_01	39.1	0.7	39.7
D-94-A-2_OF-21_DIA_02	27.4	0.6	28.0
D-94-A-2_OF-21_DIA_03	25.9	1.0	26.9
D-94-A-2_OF-21_DIA_04	29.4	1.0	30.4
D-94-A-2_OF-21_DIA_11	9.4	1.9	11.4
D-94-A-2_OF-21_DIA_13	26.9	0.5	27.4
D-94-A-2_OF-21_DIA_14	26.4	1.1	27.5
D-94-A-2_OF-21_DIA_16	26.9	2.9	29.7
D-94-A-2_OF-21_DIA_24	21.2	0.9	22.1
D-94-A-2_OF-21_DIA_25	31.5	2.5	34.0
D-94-A-2_OF-21_DIA_27	31.1	1.6	32.7
D-94-A-2_OF-21_DIA_28	24.4	2.9	27.3
D-94-B-1_OF-16_DIA_003	23.7	7.1	30.8
D-94-B-1_OF-16_DIA_010	18.8	3.6	22.4
D-94-B-1_OF-16_DIA_019	22.8	1.8	24.6
D-94-B-1_OF-16_DIA_027	25.7	2.5	28.1
D-94-B-1_OF-16_DIA_101	19.5	3.1	22.5
D-94-B-1_OF-16_DIA_111	23.4	2.6	26.0
D-94-B-1_OF-16_DIA_119	20.8	2.6	23.5
D-94-B-1_OF-16_DIA_128	23.5	1.8	25.3
D-94-B-1_OF-16_DIA_170	24.5	1.6	26.1
D-94-B-1_OF-16_DIA_180	15.4	7.2	22.7
D-94-B-1_OF-16_DIA_189	22.6	1.3	23.9
D-94-B-1_OF-16_DIA_196	22.5	1.6	24.1
D-94-B-2_OF-14_DIA_03	24.7	1.0	25.6
D-94-B-2_OF-14_DIA_04	17.1	2.8	19.9
D-94-B-2_OF-14_DIA_05	17.1	5.0	22.1
D-94-B-2_OF-14_DIA_06	23.8	2.6	26.3
D-94-B-2_OF-14_DIA_08	19.4	4.5	23.9
D-94-B-2_OF-14_DIA_10	13.6	1.9	15.4
D-94-B-2_OF-14_DIA_14	26.3	1.0	27.4
D-94-B-2_OF-14_DIA_17	4.1	4.7	8.7
D-94-B-2_OF-14_DIA_19	26.9	2.2	29.2
D-94-B-2_OF-14_DIA_20	24.5	1.5	26.0
D-94-B-2_OF-14_DIA_26	22.1	1.5	23.7
D-94-B-2_OF-14_DIA_27	26.4	1.3	27.6

Table D.2. Porosity distribution by DIA – M-04 well

Image	Intergranular Porosity (%)	Intragranular Porosity (%)	Total Porosity (%)
M-04-A-1_OF-02_DIA_01	28.4	0.7	29.1
M-04-A-1_OF-02_DIA_03	25.5	0.7	26.2
M-04-A-1_OF-02_DIA_04	29.8	0.6	30.4
M-04-A-1_OF-02_DIA_06	29.7	0.4	30.1
M-04-A-1_OF-02_DIA_08	31.6	0.3	31.9
M-04-A-1_OF-02_DIA_09	28.2	0.3	28.5
M-04-A-1_OF-02_DIA_11	33.5	0.5	34.0
M-04-A-1_OF-02_DIA_12	30.5	0.4	30.9
M-04-A-1_OF-02_DIA_21	28.4	0.8	29.2
M-04-A-1_OF-02_DIA_22	27.7	0.5	28.2
M-04-A-1_OF-02_DIA_26	22.5	0.3	22.8
M-04-A-1_OF-02_DIA_27	25.5	0.7	26.2
M-04-A-2_OF-06_DIA-8	24.2	0.3	24.5
M-04-A-2_OF-06_DIA-11	28.9	0.4	29.3
M-04-A-2_OF-06_DIA-24	23.0	0.4	23.4
M-04-A-2_OF-06_DIA-29	29.3	0.5	29.8
M-04-A-2_OF-06_DIA-33	21.0	1.0	21.9
M-04-A-2_OF-06_DIA-45	30.8	0.5	31.3
M-04-A-2_OF-06_DIA-50	26.8	0.8	27.5
M-04-A-2_OF-06_DIA-55	28.1	0.6	28.7
M-04-A-2_OF-06_DIA-62	22.8	0.7	23.5
M-04-A-2_OF-06_DIA-75	25.7	0.7	26.4
M-04-A-2_OF-06_DIA-80	25.5	1.7	27.2
M-04-A-2_OF-06_DIA-90	18.7	1.3	20.0
M-04-B-2-OF-08_2	8.1	0.1	8.2
M-04-B-2-OF-08_5	15.4	0.4	15.8
M-04-B-2-OF-08_7	14.3	0.4	14.7
M-04-B-2-OF-08_11	12.6	0.2	12.9
M-04-B-2-OF-08_12	20.8	0.7	21.5
M-04-B-2-OF-08_14	20.4	0.3	20.7
M-04-B-2-OF-08_17	19.3	0.6	19.9
M-04-B-2-OF-08_20	7.5	0.4	7.9
M-04-B-2-OF-08_22	21.2	0.5	21.7
M-04-B-2-OF-08_24	14.4	0.3	14.7
M-04-B-2-OF-08_27	17.8	0.2	18.0
M-04-B-2-OF-08_29	10.2	0.2	10.4
M-04-B-1-OF-03_2	26.4	2.2	28.5
M-04-B-1-OF-03_4	26.1	1.6	27.7
M-04-B-1-OF-03_5	36.3	0.5	36.8
M-04-B-1-OF-03_7	15.0	0.5	15.5
M-04-B-1-OF-03_8	12.7	4.9	17.5
M-04-B-1-OF-03_10	19.4	0.6	20.0
M-04-B-1-OF-03_15	15.6	1.4	17.0
M-04-B-1-OF-03_18	29.5	0.0	29.5
M-04-B-1-OF-03_20	17.5	0.5	18.0
M-04-B-1-OF-03_23	27.0	1.4	28.4
M-04-B-1-OF-03_26	21.9	0.5	22.4
M-04-B-1-OF-03_28	19.6	0.5	20.1

Table D.3. Pore shapes distribution by permeability facies using D-94 and M-04 wells core plugs

STATISTICS	Pore Shapes															
	Circle				Square				Ellipse				Rectangle			
	High Permeability		Low Permeability		High Permeability		Low Permeability		High Permeability		Low Permeability		High Permeability		Low Permeability	
	BF (%)	AF (%)	BF (%)	AF (%)	BF (%)	AF (%)	BF (%)	AF (%)	BF (%)	AF (%)	BF (%)	AF (%)	BF (%)	AF (%)	BF (%)	AF (%)
MIN	6	12	16	14	19	22	27	28	5	7	10	7	48	47	47	30
MAX	9	17	12	25	36	33	29	34	10	11	4	14	69	57	55	52
AVG	7	14	14	19	26	26	28	31	7	9	7	11	59	51	51	39
STDEV	1	2	2	5	7	5	1	2	2	2	2	3	9	4	3	9

BF: Before flooding

AF: After flooding

MIN: Minimum value

MAX: Maximum value

AVG: Average value

STDEV: Standard Deviation

Table E.3. shows the difference in pore shapes before and after polymer flooding experiments, considering the evaluation of four (4) composites cores for each permeability phase (high and low) for a total of eight (8) composite cores . Eight (8) thin sections were taken from every composite core to be evaluated using MLA-SEM before polymer flooding, and then in the same core side a thin section was also taken after polymer flooding for other sixteen (8) thin sections. Table E.3. summarizes the evaluation of sixteen (16) thin sections.

APPENDIX E: Synthetic Oil Viscosity Measurement

E.1. Oil mix calculation following Shu's correlation

Oil properties (viscosity and density) were measured at the lab using a VISCOLab PVT apparatus (viscosity), and a densitometer Anton Paar DMA HPM, the properties are listed below:

Table E.1.1. Oil mix properties

Properties	Newfoundland Oil (NL)	Athabasca Bitumen (Ab)
Viscosity (cps)	6.7	2500
Density (g/L)	0.8782	1.0356
Oil weight in the mix (g)	28	2

E.1.1. Shu correlation (1984)

- Density difference

$$\Delta\rho = \rho_{Ab} - \rho_{NL} = 1.0356 - 0.8782 = 0.1574 \text{ g/L} \quad \text{Eq. E.1}$$

- Einsteinian constant Υ

$$\Upsilon = ((17.04 * ((\Delta\rho)^{0.5237}) * (\rho_{Ab})^{3.2745}) * (\rho_{NL})^{1.6316})) = 5.870 \quad \text{Eq. E.2}$$

- Empirical constant α

$$\alpha = \Upsilon / (\ln ((\mu_{Ab})/(\mu_{NL}))) = 1.031 \quad \text{Eq. E.3}$$

- Volume fraction from the mass fraction

$$Ab_{\text{ mass fraction}} = Ab_{\text{ Weight (g)}} / (Ab_{\text{ Weight (g)}} + NL_{\text{ Weight (g)}}) = 0.0333$$

$$NL_{\text{ mass fraction}} = 1 - Ab_{\text{ mass fraction}} = 0.967$$

$$NL_{\text{ volume fraction}} = (NL_{\text{ mass fraction}} / \rho_{NL}) / ((1 - NL_{\text{ mass fraction}}) / \rho_{Ab}) + (NL_{\text{ mass fraction}} / \rho_{NL}) = 0.972$$

$$Ab_{\text{ volume fraction}} = 1 - NL_{\text{ volume fraction}} = 0.0284 \quad \text{Eq. E.4 to Eq. E.7}$$

- Compositional parameters (X) for the Shu correlation

$$Ab_X = (\alpha * Ab_{\text{volume fraction}}) / ((\alpha * Ab_{\text{volume fraction}}) + NL_{\text{volume fraction}}) = 0.0293 \quad \text{Eq. E.8}$$

$$NL_X = 1 - Ab_X = 0.971 \quad \text{Eq. E.9}$$

- Oil mixture viscosity based on the Shu correlation

$$\text{Oil Mixture viscosity} = ((Ab\mu)^{Ab_X}) \times ((NL\mu)^{NL_X}) = 9.9 \quad \text{Eq. E.10}$$

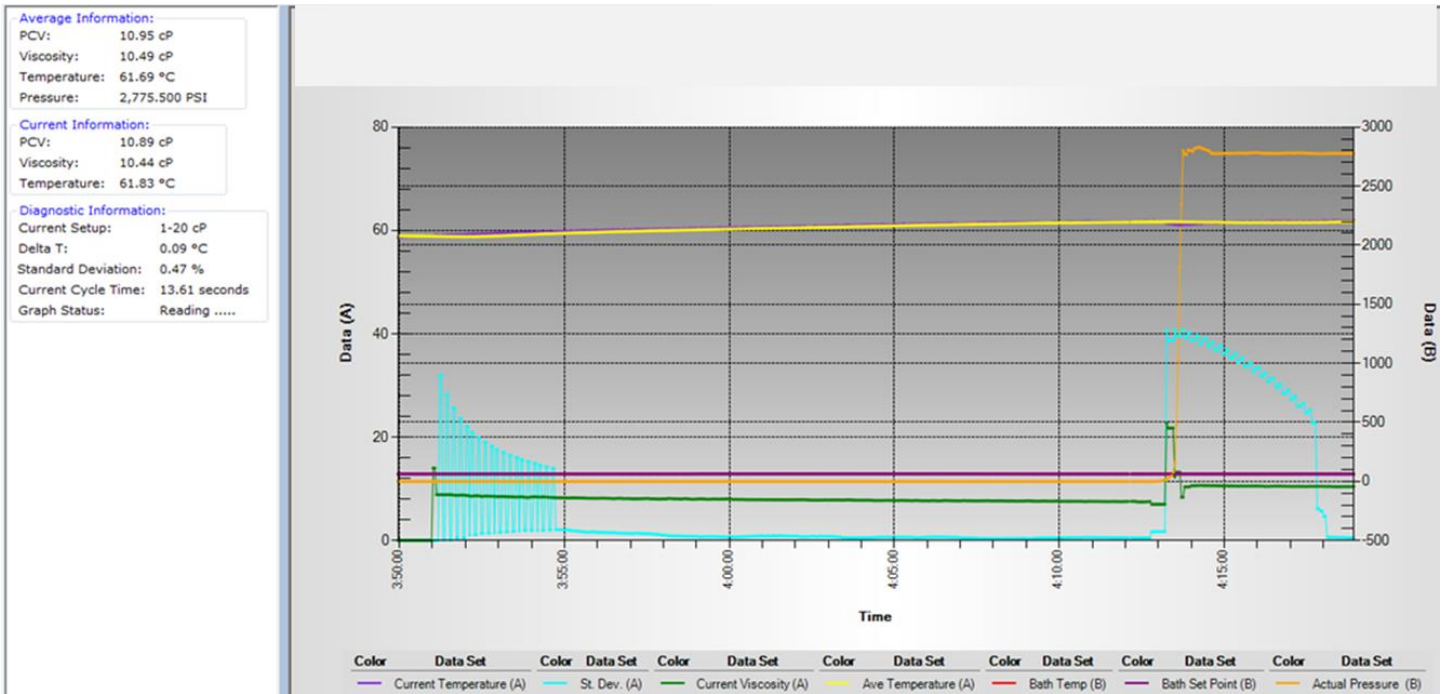
This proportion 14:1 $NL:Ab$ oils was the most similar combination to reach 11 mPa.s at Pool 1 reservoir conditions (2800 psi, 62°C). Shu correlation provides a lower value. Nevertheless, oil mix viscosity data obtained using the viscometer provides a closer value to actual Hebron oil viscosity, as shown in the following tables.

E.1.2. Oil mix viscosity data by viscometer

Table E.1.2. Oil mix viscosity raw data using the viscometer

Date/Time	Average PCV (mPa.s)	Average Viscosity (mPa.S)	Average Temperature (°C)	Current PCV (mPa.S)	Current Temperature (°C)	Current Setup	Delta T	Standard Deviation	Current Cycle Time	Current Viscosity (mPa.S)	Bath Setpoint (°C)	Bath Temperature (°C)	Pressure Gauge Reading (PSI)	Viscometer Pressure (PSI)	Pressure Gauge Reading (converted)	Pressure (converted) PSI
7/16/2015 15:49	0.00	0.00	58.96	0.00	58.68	1-20cP	0.35	0.00	0.00	0.00	62	62	-0.7	-0.6	-0.7	-0.6
7/16/2015 15:50	0.00	0.00	58.89	0.00	58.96	1-20cP	0.30	0.00	0.00	0.00	62	62.04	-0.6	-0.7	-0.6	-0.7
7/16/2015 15:51	8.90	8.81	58.81	8.86	59.22	1-20cP	0.22	0.51	11.57	8.77	62	62.06	-0.7	-0.5	-0.7	-0.5
7/16/2015 15:52	9.26	9.16	58.94	8.59	59.50	1-20cP	0.27	17.61	11.23	8.50	62	62.08	-0.6	0.7	-0.6	0.7
7/16/2015 15:53	8.68	8.60	59.24	8.50	59.66	1-20cP	0.24	1.96	11.13	8.41	62	62.03	-0.9	-0.8	-0.9	-0.8
7/16/2015 15:54	8.59	8.51	59.48	8.33	59.77	1-20cP	0.17	2.03	10.92	8.24	62	62.06	-0.8	-0.6	-0.8	-0.6
7/16/2015 15:55	8.44	8.36	59.67	8.25	60.03	1-20cP	0.20	1.58	10.82	8.16	62	62.09	0.1	-0.5	0.1	-0.5
7/16/2015 15:56	8.34	8.25	59.83	8.19	60.13	1-20cP	0.16	1.37	10.75	8.11	62	61.99	-0.8	-0.6	-0.8	-0.6
7/16/2015 15:57	8.24	8.16	59.99	8.13	60.22	1-20cP	0.15	1.01	10.68	8.05	62	62.07	-0.6	-0.4	-0.6	-0.4
7/16/2015 15:58	8.19	8.10	60.13	8.06	60.39	1-20cP	0.15	0.78	10.62	8.00	62	62.12	-0.7	-1.3	-0.7	-1.3
7/16/2015 15:59	8.14	8.05	60.26	8.13	60.46	1-20cP	0.14	0.65	10.67	8.04	63	62.48	-0.4	0	-0.4	0
7/16/2015 16:00	8.08	8.00	60.39	7.98	60.59	1-20cP	0.13	0.84	10.50	7.90	63	62.63	-0.3	-0.7	-0.3	-0.7
7/16/2015 16:01	8.03	7.95	60.50	7.96	60.73	1-20cP	0.13	0.82	10.47	7.88	63	62.89	-0.6	-0.9	-0.6	-0.9
7/16/2015 16:02	7.98	7.89	60.64	7.89	60.84	1-20cP	0.14	0.75	10.39	7.81	63	62.84	0.1	0	0.1	0
7/16/2015 16:03	7.94	7.85	60.76	7.86	60.96	1-20cP	0.13	0.53	10.36	7.78	63	62.89	-1.1	0.9	-1.1	0.9
7/16/2015 16:04	7.89	7.81	60.89	7.82	61.07	1-20cP	0.15	0.63	10.31	7.74	63	62.91	-0.2	-0.5	-0.2	-0.5
7/16/2015 16:05	7.85	7.77	61.03	7.76	61.24	1-20cP	0.13	0.64	10.23	7.68	63	62.96	-1.6	-1.8	-1.6	-1.8
7/16/2015 16:06	7.82	7.73	61.15	7.76	61.26	1-20cP	0.11	0.59	10.22	7.67	63	63.06	-0.5	-1.3	-0.5	-1.3
7/16/2015 16:07	7.79	7.70	61.27	7.74	61.48	1-20cP	0.12	0.40	10.21	7.66	62	62.98	-0.8	-0.4	-0.8	-0.4
7/16/2015 16:08	7.76	7.67	61.38	7.74	61.48	1-20cP	0.12	0.37	10.21	7.66	62	62.35	-1.3	-1.2	-1.3	-1.2
7/16/2015 16:09	7.73	7.65	61.47	7.69	61.51	1-20cP	0.10	0.47	10.15	7.61	62	62.22	-1.3	-0.7	-1.3	-0.7
7/16/2015 16:10	7.69	7.61	61.55	7.64	61.64	1-20cP	0.09	0.58	10.08	7.56	62	62.18	-0.5	-0.2	-0.5	-0.2
7/16/2015 16:11	7.66	7.57	61.61	7.63	61.74	1-20cP	0.08	0.52	10.07	7.54	62	62.09	-1.7	-0.3	-1.7	-0.3
7/16/2015 16:12	7.60	7.52	61.66	7.07	61.65	1-20cP	0.09	1.70	9.36	6.99	62	62.07	3.5	2.8	3.5	2.8
7/16/2015 16:13	9.10	8.72	61.59	10.84	61.18	1-20cP	0.19	40.25	13.55	10.39	62	62.02	2802.7	2800.8	2,802.70	2,800.80
7/16/2015 16:14	9.82	9.41	61.56	11.00	61.53	1-20cP	0.16	36.12	13.75	10.55	62	61.94	2775.1	2775.9	2,775.10	2,775.90
7/16/2015 16:15	10.51	10.07	61.54	10.98	61.74	1-20cP	0.16	33.43	13.72	10.52	62	62.01	2783.3	2783.4	2,783.30	2,783.40
7/16/2015 16:16	11.13	10.66	61.54	10.93	61.75	1-20cP	0.15	29.14	13.67	10.48	62	61.84	2781.6	2779.7	2,781.60	2,779.70
7/16/2015 16:17	11.11	10.65	61.58	10.94	61.80	1-20cP	0.14	5.69	13.68	10.49	62	62.04	2773.7	2772.8	2,773.70	2,772.80
7/16/2015 16:18	10.95	10.49	61.69	10.89	61.87	1-20cP	0.09	0.47	13.61	10.44	62	62	2775.5	2774.9	2,775.50	2,774.90
7/16/2015 16:19	10.92	10.47	61.76	10.88	61.83	1-20cP	0.05	0.32	13.60	10.43	62	61.97	2771.9	2772.8	2,771.90	2,772.80

E.1.3 Viscosity plot obtained during viscosity measurement at reservoir conditions using a VISCOLab PVT apparatus



E.1.4. Oil mix composition by gas chromatography (GC)

Table E.1.3. Oil mix gas chromatography

Carbon Number	Test 1	Test 2	Test 3	Test 4	Test 5	Average	Standard Deviation
C6	0.47%	0.50%	0.40%	0.40%	0.50%	0.45%	50.9
C7	2.54%	2.50%	2.50%	2.50%	2.50%	2.51%	19.2
C8	4.30%	4.30%	4.30%	4.30%	4.30%	4.30%	0
C9	4.01%	4.00%	4.10%	4.10%	4.00%	4.04%	52.5
C10	4.49%	4.50%	4.50%	4.50%	4.50%	4.50%	6.39
C11	4.04%	4.00%	4.10%	4.10%	4.00%	4.04%	50.1
C12	4.27%	4.20%	4.30%	4.30%	4.30%	4.27%	43.3
C13	4.73%	4.70%	4.70%	4.70%	4.80%	4.72%	43.3
C14	4.39%	4.30%	4.40%	4.40%	4.40%	4.38%	43.6
C15	4.77%	4.70%	4.80%	4.80%	4.80%	4.77%	43.3
C16	4.70%	4.70%	4.70%	4.70%	4.70%	4.70%	0
C17	4.07%	4.00%	4.10%	4.10%	4.10%	4.07%	43.3
C18	4.00%	4.00%	4.00%	4.00%	4.00%	4.00%	0
C19	3.50%	3.50%	3.50%	3.50%	3.50%	3.50%	0
C20	3.89%	3.80%	3.90%	3.90%	3.90%	3.90%	43.6
C21	3.50%	3.50%	3.50%	3.50%	3.50%	3.50%	0
C22	3.30%	3.30%	3.30%	3.30%	3.30%	3.30%	0
C23	2.80%	2.80%	2.80%	2.80%	2.80%	2.80%	0
C24	2.90%	2.90%	2.90%	2.90%	2.90%	2.90%	0
C25	2.80%	2.80%	2.80%	2.80%	2.80%	2.80%	0
C26	2.80%	2.80%	2.80%	2.80%	2.80%	2.80%	0
C27	2.70%	2.70%	2.70%	2.70%	2.70%	2.70%	0
C28	2.61%	2.60%	2.70%	2.60%	2.60%	2.62%	43.6
C29	2.80%	2.80%	2.80%	2.80%	2.80%	2.80%	0
C30	15.61%	16.10%	15.40%	15.50%	15.50%	15.62%	277

APPENDIX F: Porosity and Absolute Permeability Measurement

F.1. Porosity Measurement and Pore Volume Calculation

1. Mass of dry core = $M_{\text{dry}} = 139.5842 \pm 0.00005$ (g)
2. Mass of wet core after 1 hour saturating = $M_{\text{wet, 1 hr}} = 162.1284 \pm 0.00005$ (g)
3. Mass of wet core after 2 hours saturating = $M_{\text{wet, 2 hrs}} = 162.3365 \pm 0.00005$ (g)
4. Mass of wet core after 3 hours saturating = $M_{\text{wet, 3 hrs}} = 162.4826 \pm 0.00005$ (g)
5. Total volume of core = $V_{\text{total}} = 75 \pm 0.5$ cm³
6. $\Delta M = M_{\text{wet, 3 hrs}} - M_{\text{dry}} = (162.4826 \pm 0.00005) - (139.5842 \pm 0.00005) = 22.8984 \pm 0.00007$ (g) Eq. F.1
7. Water density = $\rho = 0.9982$ (g/cm³)

8. Porosity =

$$\Phi = \frac{\Delta M \text{ (g)} / \rho \text{ (g/cm}^3\text{)}}{V_{\text{total}} \text{ (cm}^3\text{)}} = \frac{(22.8984 \pm 0.00007 \text{ (g)}) / 0.9982 \text{ (g/cm}^3\text{)}}{75 \pm 0.5 \text{ cm}^3} = 0.2932 \pm 0.0001 \quad \text{Eq. F.2}$$

$$9. \text{ Pore Volume (PV)} = V_{\text{total}} \times \Phi = (75 \pm 0.5 \text{ (cm}^3\text{)}) \times (0.2932 \pm 0.0001) = 22.0 \pm 0.1 \text{ (cm}^3\text{)} \quad \text{Eq. F.3}$$

The porosity and pore volume calculations described in this section corresponds to one single core plug (D-94-P-20); however, composite cores were used in the core flooding experiments therefore the final composite porosity corresponds to the average porosity obtained from both core plugs, and the final pore volume is the summation of the singles pore volumes. These steps are described below using D-94-A-1 composite core, which include D-94-P-20 and D-94-P-25.

$$10. \text{ Composite core porosity} = \text{Avg. Porosity} \pm \text{StDev} = \frac{(0.2932+0.2830)}{2} = 0.2881 \pm 0.005 = 28.8 \pm 0.5 \%$$

$$11. \text{ Composite pore volume} = 22.0 \pm 0.1 \text{ (cm}^3\text{)} + 22.6 \pm 0.1 \text{ (cm}^3\text{)} = 44.6 \text{ (cm}^3\text{)} \quad \text{Eq. F.4 to Eq. F.5}$$

F.2. Absolute Permeability Calculation

Core plugs absolute permeability values were measured for each single core plug during primary water flooding, using the core flooding set-up.

Table F.2.1. Core flooding results for absolute permeability calculations.

Flow Rate (ml/min)	Time	Pressure In (psi)	Pressure Out (psi)	dP (psi)
0.110	1	2861.04	2860.98	0.06
	2	2860.60	2860.55	0.05
	3	2860.36	2860.33	0.03
	4	2859.80	2859.77	0.03
	5	2858.87	2858.84	0.03

Using Darcy’s law:

$$K = \frac{Q \cdot \mu \cdot L}{A \cdot \Delta P} \tag{Eq. F.6}$$

$$Q = 0.110 \text{ (cm}^3\text{/min)} = 0.0018 \text{ (cm}^3\text{/s)}$$

$$\mu = 1.08 \text{ (cp)}$$

$$L = 6 \text{ inches} = 15.24 \text{ cm}$$

$$A = 11.39 \text{ cm}^2$$

$$\Delta P = 0.03 \text{ psi} = 0.002 \text{ atm}$$

$$1. K = \frac{0.0018 \times 1.08 \times 15.24}{11.39 \times 0.002} = 1.320 \text{ (Darcy)} = 1320 \text{ mD} \tag{Eq. F.7}$$

Like the total composite core porosity, the absolute permeability was calculated following the procedure described in the previous section where composite porosity corresponds to the average porosity obtained from both core plugs. These steps are described below using M-04-A-2 composite core.

$$2. \text{ Composite core permeability} = \text{Avg. } K \pm \text{StDev} = \frac{(1320+1420)}{2} = 1370 \pm 50 \text{ mD} \tag{Eq. F.8}$$

APPENDIX G: Core flooding experiments raw data

G.1 Standard Cores

Table G.1.1. Bentheimer cores – High permeability - Secondary water flooding

BEN-A-1						
By Fluid		Total		Pressure Inlet	Pressure Outlet	Pressure Dif
Total Produced Oil (mL)	PV (unit)	Total Produced Oil (mL)	PV (unit)	PSI	PSI	PSI
1.80	0.06	1.80	0.06	2825.04	2821.23	3.80
3.80	0.08	3.80	0.08	2801.61	2797.87	3.74
4.80	0.11	4.80	0.11	2830.12	2825.62	4.50
6.80	0.12	6.80	0.12	2793.38	2789.64	3.74
9.80	0.14	9.80	0.14	2825.44	2821.14	4.30
11.80	0.14	11.80	0.14	2828.44	2823.64	4.80
12.05	0.15	12.05	0.15	2797.14	2792.64	4.50
12.80	0.16	12.80	0.16	2737.09	2733.65	3.45
13.90	0.16	13.90	0.16	2709.92	2706.28	3.64
16.90	0.25	16.90	0.25	2737.18	2733.59	3.59
17.30	0.40	17.30	0.40	2728.06	2723.06	5.00
17.32	0.60	17.32	0.60	2748.02	2743.82	4.20
17.35	0.80	17.35	0.80	2751.39	2747.83	3.57
17.42	0.89	17.42	0.89	2735.92	2732.56	3.36
17.50	1.00	17.50	1.00	2724.85	2721.39	3.46
17.55	1.15	17.55	1.15	2819.22	2815.67	3.55
17.60	1.40	17.60	1.40	2821.15	2817.59	3.56
17.65	1.45	17.65	1.45	2801.42	2797.84	3.57
17.88	1.67	17.88	1.67	2790.19	2786.74	3.44
18.08	1.75	18.08	1.75	2863.67	2860.17	3.50
18.26	1.90	18.26	1.90	2845.37	2842.03	3.34
18.41	2.01	18.41	2.01	2866.15	2862.83	3.32
18.53	2.15	18.53	2.15	2857.18	2853.87	3.31
18.60	2.23	18.60	2.23	2875.29	2871.89	3.40
18.62	2.31	18.62	2.31	2876.54	2872.84	3.70
18.65	2.41	18.65	2.41	2859.09	2855.89	3.20
18.67	2.56	18.67	2.56	2889.37	2885.91	3.45
18.68	2.63	18.68	2.63	2891.52	2888.09	3.43
18.69	2.72	18.69	2.72	2833.87	2829.65	4.22
18.69	2.80	18.69	2.80	2877.92	2874.50	3.43
18.69	2.88	18.69	2.88	2871.98	2868.53	3.45
18.69	2.95	18.69	2.95	2888.45	2884.88	3.57
18.69	3.00	18.69	3.00	2865.12	2861.60	3.52

Flow Rate: 0.28 cm³/min (5 ft/day)

Table G.1.2. Bentheimer cores – High permeability – Polymer flooding

BEN-A-1						
By Fluid		Total		Pressure Inlet	Pressure Outlet	Pressure Dif
Total Produced Oil (mL)	PV (unit)	Total Produced Oil (mL)	PV (unit)	PSI	PSI	PSI
0.02	0.00	18.71	3.00	2824.61	2820.90	3.71
0.08	0.08	18.77	3.08	2825.08	2821.38	3.70
0.23	0.16	18.92	3.16	2826.46	2822.28	4.18
0.43	0.24	19.12	3.24	2824.99	2820.19	4.80
0.61	0.32	19.30	3.32	2824.57	2820.06	4.51
0.73	0.40	19.42	3.40	2827.27	2822.86	4.40
1.04	0.48	19.73	3.48	2833.69	2829.39	4.30
1.14	0.57	19.83	3.57	2833.10	2828.88	4.21
1.22	0.65	19.91	3.65	2832.45	2828.32	4.13
1.30	0.73	19.99	3.73	2832.51	2828.47	4.05
1.33	0.81	20.02	3.81	2831.04	2827.09	3.95
1.35	0.89	20.04	3.89	2830.96	2827.04	3.92
1.40	0.97	20.09	3.97	2832.57	2828.73	3.83
1.47	1.05	20.16	4.05	2829.44	2825.58	3.86
1.50	1.13	20.19	4.13	2829.42	2825.60	3.82
1.57	1.21	20.26	4.21	2829.95	2826.19	3.76
1.62	1.29	20.31	4.29	2830.51	2826.78	3.73
1.66	1.37	20.35	4.37	2831.91	2828.19	3.72
1.68	1.45	20.37	4.45	2832.75	2829.00	3.75
1.69	1.53	20.38	4.53	2832.92	2829.14	3.78
1.70	1.61	20.39	4.61	2832.43	2828.69	3.74
1.70	1.69	20.39	4.69	2832.67	2828.88	3.79
1.70	1.77	20.39	4.77	2832.53	2828.78	3.75
1.70	1.85	20.39	4.85	2832.74	2829.00	3.74
1.70	1.93	20.39	4.93	2833.01	2829.29	3.72
1.70	2.01	20.39	5.01	2833.01	2829.28	3.73

Flow Rate: 0.06 cm³/min (1 ft/day)

Table G.1.3. Bentheimer cores – High permeability – Tertiary water flooding

BEN-A-1						
By Fluid		Total		Pressure Inlet	Pressure Outlet	Pressure Dif
Total Produced Oil (mL)	PV (unit)	Total Produced Oil (mL)	PV (unit)	PSI	PSI	PSI
0.02	0.00	20.41	5.01	2833.17	2829.43	3.74
0.02	0.08	20.41	5.09	2832.71	2828.87	3.84
0.02	0.16	20.41	5.17	2832.48	2828.68	3.80
0.02	0.24	20.41	5.25	2833.08	2829.03	4.05
0.02	0.32	20.41	5.33	2833.09	2828.89	4.20
0.02	0.40	20.41	5.41	2832.79	2828.49	4.30
0.02	0.48	20.41	5.49	2832.70	2828.40	4.30
0.02	0.57	20.41	5.57	2832.50	2828.10	4.40
0.12	0.65	20.51	5.66	2832.29	2828.01	4.29
0.22	0.73	20.61	5.74	2832.04	2827.14	4.90
0.22	0.81	20.61	5.82	2832.10	2827.10	5.00
0.31	0.89	20.70	5.90	2831.97	2827.60	4.37
0.31	0.97	20.70	5.98	2764.72	2760.02	4.70

Flow Rate: 0.28 cm³/min (5 ft/day)

Table G.1.4. Bentheimer cores – High permeability - Secondary water flooding

BEN-A-2						
By Fluid		Total		Pressure Inlet	Pressure Outlet	Pressure Dif
Total Produced Oil (mL)	PV (unit)	Total Produced Oil (mL)	PV (unit)	PSI	PSI	PSI
0.00	0.00	0.00	0.00	2747.08	2743.77	3.32
5.10	0.10	5.10	0.10	2765.81	2761.51	4.30
12.10	0.20	12.10	0.20	2771.75	2767.25	4.50
16.10	0.30	16.10	0.30	2789.13	2784.33	4.80
17.10	0.40	17.10	0.40	2794.99	2790.69	4.30
17.40	0.50	17.40	0.50	2795.22	2792.09	3.13
17.42	0.60	17.42	0.60	2799.69	2796.26	3.43
17.72	0.70	17.72	0.70	2811.73	2807.63	4.10
17.74	0.80	17.74	0.80	2810.85	2807.54	3.30
17.75	0.90	17.75	0.90	2795.01	2791.87	3.14
17.77	1.00	17.77	1.00	2787.62	2784.46	3.16
17.79	1.10	17.79	1.10	2789.89	2786.65	3.24
17.83	1.20	17.83	1.20	2794.60	2791.35	3.25
17.84	1.30	17.84	1.30	2813.09	2809.88	3.21
18.04	1.40	18.04	1.40	2813.87	2810.58	3.28
18.06	1.50	18.06	1.50	2815.27	2811.93	3.34
18.14	1.60	18.14	1.60	2818.72	2815.34	3.37
18.34	1.70	18.34	1.70	2802.75	2799.43	3.32
18.36	1.80	18.36	1.80	2811.37	2808.57	2.80
18.38	1.90	18.38	1.90	2828.03	2823.93	4.10
18.40	2.00	18.40	2.00	2879.06	2875.67	3.40
18.42	2.10	18.42	2.10	2706.40	2702.93	3.46
18.45	2.20	18.45	2.20	2713.05	2709.54	3.51
18.48	2.30	18.48	2.30	2740.37	2736.88	3.48
18.50	2.40	18.50	2.40	2769.32	2765.86	3.46
18.55	2.50	18.55	2.50	2894.35	2890.92	3.43
18.56	2.60	18.56	2.60	2888.45	2884.86	3.59
18.57	2.70	18.57	2.70	2892.04	2888.29	3.75
18.58	2.80	18.58	2.80	2872.83	2869.43	3.40
18.59	2.90	18.59	2.90	2887.72	2884.26	3.46
18.59	3.00	18.59	3.00	2890.56	2887.12	3.45

Flow Rate: 0.28 cm³/min (5 ft/day)

Table G.1.5. Bentheimer cores – High permeability – Polymer flooding

BEN-A-2						
By Fluid		Total		Pressure Inlet	Pressure Outlet	Pressure Dif
Total Produced Oil (mL)	PV (unit)	Total Produced Oil (mL)	PV (unit)	PSI	PSI	PSI
0.00	0.00	0.00	0.00	2858.98	2854.98	4.00
0.02	0.05	0.02	0.05	2844.00	2840.07	3.93
0.08	0.08	0.08	0.08	2837.81	2833.95	3.86
0.16	0.19	0.16	0.19	2833.53	2829.70	3.84
0.31	0.25	0.31	0.25	2831.65	2827.45	4.20
0.41	0.45	0.41	0.45	2834.22	2830.46	3.76
0.56	0.55	0.56	0.55	2838.08	2833.88	4.20
0.66	0.65	0.66	0.65	2842.60	2838.87	3.73
0.81	0.75	0.81	0.75	2847.44	2843.24	4.20
1.01	0.85	1.01	0.85	2853.10	2848.40	4.70
1.16	0.95	1.16	0.95	2866.02	2861.82	4.20
1.23	1.05	1.23	1.05	2878.67	2874.85	3.83
1.31	1.15	1.31	1.15	2885.26	2881.26	4.00
1.41	1.25	1.41	1.25	2899.71	2895.98	3.74
1.46	1.35	1.46	1.35	2872.64	2868.89	3.76
1.48	1.45	1.48	1.45	2861.50	2857.69	3.81
1.49	1.55	1.49	1.55	2857.73	2853.92	3.81
1.50	1.65	1.50	1.65	2858.54	2854.71	3.83
1.50	1.75	1.50	1.75	2866.03	2862.20	3.83
1.51	1.85	1.51	1.85	2875.11	2871.26	3.85
1.51	1.95	1.51	1.95	2891.98	2888.15	3.83
1.51	2.01	1.51	2.01	2898.96	2895.12	3.84
1.51	2.01	20.10	5.01	2897.96	2894.12	3.84

Flow Rate: 0.06 cm³/min (1 ft/day)

Table G.1.6. Bentheimer cores – High permeability – Tertiary water flooding

BEN-A-2						
By Fluid		Total		Pressure Inlet	Pressure Outlet	Pressure Dif
Total Produced Oil (mL)	PV (unit)	Total Produced Oil (mL)	PV (unit)	PSI	PSI	PSI
0.00	0.00	20.10	5.01	2738.54	2734.54	4.00
0.00	0.05	20.10	5.07	2753.47	2749.55	3.93
0.00	0.15	20.10	5.17	2768.75	2764.90	3.86
0.00	0.25	20.10	5.26	2788.20	2784.36	3.84
0.00	0.35	20.10	5.36	2809.14	2805.34	3.80
0.10	0.45	20.20	5.46	2829.44	2824.74	4.70
0.10	0.55	20.20	5.56	2852.35	2848.61	3.74
0.10	0.65	20.20	5.66	2876.94	2873.21	3.73
0.10	0.75	20.20	5.76	2896.08	2892.35	3.73
0.20	0.85	20.30	5.86	2893.45	2888.75	4.70
0.30	0.99	20.40	6.00	2894.82	2890.12	4.70

Flow Rate: 0.28 cm³/min (5 ft/day)

Table. G.1.7. Upper Gray Berea cores – Low permeability - Secondary water flooding

UGB-A-1						
By Fluid		Total		Pressure Inlet	Pressure Outlet	Pressure Dif
Total Produced Oil (mL)	PV (unit)	Total Produced Oil (mL)	PV (unit)	PSI	PSI	PSI
0	0.00	0	0.00	2849.42	2846.38	3.04
0.05	0.10	0.05	0.10	2854.91	2850.91	4.00
0.1	0.20	0.1	0.20	2854.94	2848.94	6.00
0.15	0.30	0.15	0.30	2854.08	2851.08	3.00
0.2	0.40	0.2	0.40	2863.55	2857.40	6.15
0.28	0.50	0.28	0.50	2864.99	2858.81	6.18
0.38	0.60	0.38	0.60	2861.03	2854.03	7.00
0.78	0.70	0.78	0.70	2859.61	2854.61	5.00
3.08	0.79	3.08	0.79	2864.28	2856.78	7.50
4.58	0.89	4.58	0.89	2864.53	2853.53	11.00
10.78	0.92	10.78	0.92	2864.91	2853.61	11.30
11.58	1.02	11.58	1.02	2860.55	2852.15	8.40
12.58	1.08	12.58	1.08	2863.71	2853.71	10.00
12.66	1.18	12.66	1.18	2866.65	2860.88	5.77
12.68	1.28	12.68	1.28	2869.06	2865.15	3.91
12.69	1.38	12.69	1.38	2869.18	2864.67	4.51
12.69	1.48	12.69	1.48	2872.15	2868.50	3.65
12.7	1.58	12.7	1.58	2873.99	2871.11	2.88
12.74	1.68	12.74	1.68	2871.17	2867.69	3.47
12.79	1.78	12.79	1.78	2868.78	2865.78	3.00
12.8	1.88	12.8	1.88	2869.45	2863.15	6.30
12.8	1.98	12.8	1.98	2879.00	2877.21	1.79
12.8	2.08	12.8	2.08	2869.21	2865.91	3.30
12.8	2.18	12.8	2.18	2870.36	2863.86	6.50
12.8	2.28	12.8	2.28	2863.99	2858.89	5.10
12.8	2.38	12.8	2.38	2864.73	2860.93	3.80
12.8	2.48	12.8	2.48	2863.70	2860.61	3.09
12.8	2.58	12.8	2.58	2863.18	2857.18	6.00
12.8	2.68	12.8	2.68	2861.05	2856.05	5.00
12.8	2.78	12.8	2.78	2863.48	2856.48	7.00
12.8	3.00	12.8	3.00	2861.55	2857.75	3.80
12.8	3.00	12.8	3.00	2853.07	2849.27	3.80

Flow Rate: 0.28 cm³/min (5 ft/day)

Table G.1.8. Upper Gray Berea cores – Low permeability - Polymer flooding

UGB-A-1						
By Fluid		Total		Pressure Inlet	Pressure Outlet	Pressure Dif
Total Produced Oil (mL)	PV (unit)	Total Produced Oil (mL)	PV (unit)	PSI	PSI	PSI
0.00	0.00	12.80	3.00	2656.90	2653.56	3.34
0.00	0.05	12.80	3.05	2638.84	2635.83	3.01
0.02	0.21	12.82	3.21	2631.95	2628.75	3.20
0.05	0.39	12.85	3.39	2625.63	2622.63	3.00
0.10	0.47	12.90	3.47	2617.42	2613.32	4.10
0.30	0.64	13.10	3.64	2626.55	2624.05	2.50
0.52	0.76	13.32	3.76	2630.12	2626.32	3.80
0.57	0.80	13.37	3.80	2745.76	2742.86	2.90
0.60	0.80	13.40	3.80	2792.61	2790.11	2.50
0.66	0.82	13.46	3.82	2817.02	2814.72	2.30
0.72	0.86	13.52	3.86	2815.95	2814.14	1.81
0.77	0.90	13.57	3.90	2801.28	2799.50	1.78
0.82	0.93	13.62	3.93	2797.70	2795.37	2.33
0.92	0.97	13.72	3.97	2798.21	2793.41	4.80
1.22	1.01	14.02	4.01	2803.65	2798.65	5.00
1.28	1.17	14.08	4.17	2805.63	2803.07	2.55
1.31	1.31	14.11	4.31	2805.97	2802.47	3.50
1.36	1.37	14.16	4.37	2802.84	2800.92	1.92
1.40	1.41	14.20	4.41	2806.97	2805.45	1.52
1.45	1.44	14.25	4.44	2806.99	2805.59	1.40
1.48	1.47	14.28	4.47	2805.73	2803.93	1.80
1.48	1.45	14.28	4.45	2804.20	2802.20	2.00
1.48	1.51	14.28	4.51	2810.39	2808.84	1.55
1.48	1.77	14.28	4.77	2803.26	2801.76	1.50
1.49	1.86	14.29	4.86	2816.20	2815.20	1.00
1.49	1.95	14.29	4.95	2813.83	2813.03	0.80

Flow Rate: 0.06 cm³/min (1 ft/day)

Table G.1.9. Upper Gray Berea cores – Low permeability – Tertiary water flooding

UGB-A-1						
By Fluid		Total		Pressure Inlet	Pressure Outlet	Pressure Dif
Total Produced Oil (mL)	PV (unit)	Total Produced Oil (mL)	PV (unit)	PSI	PSI	PSI
0	0.00	14.29	4.95	2807.32	2804.82	2.50
0	0.05	14.34	5.00	2824.58	2821.58	3.00
0.1	0.15	14.44	5.10	2832.80	2828.82	3.98
0.1	0.25	14.54	5.20	2836.56	2833.36	3.20
0.2	0.35	14.64	5.30	2842.06	2838.45	3.62
0.2	0.45	14.74	5.40	2842.26	2839.96	2.30
0.2	0.55	14.84	5.50	2841.31	2839.21	2.10
0.2	0.65	14.94	5.60	2839.97	2838.17	1.80
0.2	0.75	15.04	5.70	2839.24	2838.04	1.20
0.2	0.85	15.14	5.80	2838.80	2837.70	1.10
0.2	0.99	15.28	5.94	2838.66	2838.06	0.60

Flow Rate: 0.28 cm³/min (5 ft/day)

Table G.1.10. *Upper Gray Berea cores – Low permeability - Secondary water flooding*

UGB-A-2						
By Fluid		Total		Pressure Inlet	Pressure Outlet	Pressure Dif
Total Produced Oil (mL)	PV (unit)	Total Produced Oil (mL)	PV (unit)	PSI	PSI	PSI
0	0.00	0.00	0.00	2776.69	2774.19	2.50
0.06	0.10	0.06	0.10	2773.79	2768.99	4.80
0.11	0.19	0.11	0.19	2719.44	2713.44	6.00
0.19	0.29	0.19	0.29	2694.58	2691.08	3.50
0.29	0.39	0.29	0.39	2679.73	2671.03	8.70
0.42	0.49	0.42	0.49	2670.06	2662.56	7.50
0.52	0.58	0.52	0.58	2691.49	2688.49	3.00
1.22	0.68	1.22	0.68	2739.38	2728.60	10.78
3.52	0.78	3.52	0.78	2730.17	2722.17	8.00
5.02	0.87	5.02	0.87	2643.10	2634.10	9.00
11.02	0.97	11.02	0.97	2566.86	2550.55	16.31
12.02	1.07	12.02	1.07	2806.83	2798.83	8.00
13.02	1.17	13.02	1.17	2833.15	2825.15	8.00
13.1	1.26	13.10	1.26	2876.09	2871.09	5.00
13.19	1.36	13.19	1.36	2894.37	2891.57	2.80
13.24	1.46	13.24	1.46	2275.35	2269.84	5.51
13.29	1.56	13.29	1.56	2806.83	2801.53	5.30
13.34	1.65	13.34	1.65	2833.15	2829.75	3.40
13.38	1.75	13.38	1.75	2856.64	2854.14	2.50
13.42	1.85	13.42	1.85	2876.09	2867.66	8.43
13.46	1.94	13.46	1.94	2894.37	2888.07	6.30
13.49	2.04	13.49	2.04	2914.42	2911.42	3.00
13.5	2.14	13.50	2.14	2935.32	2931.32	4.00
13.5	2.24	13.50	2.24	2958.19	2952.19	6.00
13.5	2.33	13.50	2.33	2731.36	2724.36	7.00
13.5	2.43	13.50	2.43	2732.90	2727.49	5.40
13.5	2.53	13.50	2.53	2734.40	2730.80	3.60
13.5	2.62	13.50	2.62	2735.70	2731.70	4.00
13.5	2.72	13.50	2.72	2736.79	2731.19	5.60
13.5	2.82	13.50	2.82	2737.99	2735.99	2.00
13.5	3.01	13.50	3.01	2738.95	2734.55	4.40
13.5	3.01	13.50	3.01	2739.38	2734.98	4.40

Flow Rate: 0.28 cm³/min (5 ft/day)

Table G.1.11. Upper Gray Berea cores – Low permeability - Polymer flooding

UGB-A-2						
By Fluid		Total		Pressure Inlet	Pressure Outlet	Pressure Dif
Total Produced Oil (mL)	PV (unit)	Total Produced Oil (mL)	PV (unit)	PSI	PSI	PSI
0.00	0.00	13.50	3.01	2632.54	2629.74	2.80
0.00	0.08	13.50	3.09	2630.14	2627.14	3.00
0.02	0.16	13.52	3.17	2743.73	2740.73	3.00
0.05	0.24	13.55	3.25	2792.06	2788.56	3.50
0.10	0.32	13.60	3.33	2753.42	2750.22	3.20
0.13	0.40	13.63	3.41	2768.54	2765.74	2.80
0.16	0.48	13.66	3.49	2788.97	2786.07	2.90
0.20	0.56	13.70	3.57	2800.73	2797.59	3.14
0.24	0.64	13.74	3.65	2802.40	2800.36	2.04
0.30	0.72	13.80	3.73	2806.66	2803.76	2.90
0.50	0.80	14.00	3.81	2806.86	2802.76	4.10
0.60	0.88	14.10	3.89	2805.35	2803.85	1.50
0.75	0.96	14.25	3.97	2804.99	2801.19	3.80
1.15	1.04	14.65	4.05	2789.45	2785.25	4.20
1.45	1.12	14.95	4.13	2803.56	2798.66	4.90
1.55	1.20	15.05	4.21	2746.11	2741.91	4.20
1.63	1.28	15.13	4.29	2730.43	2728.05	2.38
1.69	1.36	15.19	4.37	2832.93	2831.01	1.92
1.74	1.44	15.24	4.45	2804.56	2802.76	1.80
1.78	1.52	15.28	4.53	2811.34	2810.04	1.30
1.81	1.60	15.31	4.61	2849.22	2847.72	1.50
1.81	1.68	15.31	4.69	2789.23	2787.42	1.81
1.81	1.76	15.31	4.77	2630.14	2628.24	1.90
1.81	1.84	15.31	4.85	2743.73	2742.84	0.89
1.81	1.92	15.31	4.93	2792.06	2791.26	0.80
1.81	2.00	15.31	5.01	2789.45	2788.95	0.50

Flow Rate: 0.06 cm³/min (1 ft/day)

Table G.1.12. *Upper Gray Berea cores – Low permeability – Tertiary water flooding*

UGB-A-2						
By Fluid		Total		Pressure Inlet	Pressure Outlet	Pressure Dif
Total Produced Oil (mL)	PV (unit)	Total Produced Oil (mL)	PV (unit)	PSI	PSI	PSI
0.00	0.00	15.31	5.01	2729.46	2727.16	2.30
0.00	0.05	15.31	5.06	2754.86	2752.06	2.80
0.00	0.15	15.31	5.16	2794.61	2792.11	2.50
0.00	0.25	15.31	5.26	2813.93	2811.33	2.60
0.00	0.35	15.31	5.36	2822.70	2819.70	3.00
0.10	0.45	15.41	5.46	2832.69	2829.19	3.50
0.20	0.55	15.51	5.56	2832.51	2828.41	4.10
0.20	0.65	15.51	5.66	2832.02	2830.22	1.80
0.20	0.75	15.51	5.76	2836.58	2834.88	1.70
0.20	0.85	15.51	5.86	2833.59	2832.09	1.50
0.20	0.99	15.51	6.00	2832.65	2831.85	0.80

Flow Rate: 0.28 cm³/min (5 ft/day)

G.2. Hebron Well Cores

Table G.2.1. D-94-H-1 – High permeability – Secondary water flooding

D-94-H-1						
By Fluid		Total		Pressure Inlet	Pressure Outlet	Pressure Dif
% Oil Recovered	PV (unit)	% Oil Recovered	PV (unit)	PSI	PSI	PSI
0.00	0.00	0.00	0.00	2749.36	2746.36	3.00
5.07	0.10	5.07	0.10	2758.25	2755.48	2.77
21.13	0.21	21.13	0.21	2770.13	2767.95	2.18
32.68	0.27	32.68	0.27	2783.72	2781.12	2.60
47.89	0.37	47.89	0.37	2799.81	2796.99	2.82
51.83	0.51	51.83	0.51	2816.51	2813.49	3.02
52.96	0.62	52.96	0.62	2833.99	2830.74	3.25
54.37	0.71	54.37	0.71	2843.42	2840.06	3.36
54.37	0.81	54.37	0.81	2851.04	2847.66	3.38
56.06	0.87	56.06	0.87	2858.58	2855.23	3.35
56.34	0.96	56.34	0.96	2858.32	2854.86	3.46
56.34	1.05	56.34	1.05	2856.33	2852.89	3.44
57.46	1.13	57.46	1.13	2855.74	2852.32	3.42
58.03	1.20	58.03	1.20	2856.54	2853.09	3.45
58.03	1.30	58.03	1.30	2859.77	2856.21	3.56
58.03	1.40	58.03	1.40	2858.04	2854.49	3.55
58.03	1.50	58.03	1.50	2857.04	2853.50	3.54
58.03	1.60	58.03	1.60	2857.61	2854.07	3.54
58.03	1.70	58.03	1.70	2859.79	2856.22	3.57
58.03	1.80	58.03	1.80	2860.52	2856.92	3.60
58.03	1.90	58.03	1.90	2861.73	2858.16	3.57
58.03	2.00	58.03	2.00	2864.71	2861.16	3.55

Flow Rate: 0.28 cm³/min (5 ft/day)

Table G.2.2. D-94-H-1 – High permeability – Polymer flooding

D-94-H-1						
By Fluid		Total		Pressure Inlet	Pressure Outlet	Pressure Dif
% Oil Recovered	PV (unit)	% Oil Recovered	PV (unit)	PSI	PSI	PSI
0.00	0.00	0.00	0.00	2652.84	2649.16	3.68
0.56	0.10	0.56	0.10	2645.45	2641.72	3.73
1.41	0.21	1.41	0.21	2641.07	2637.31	3.76
2.25	0.27	2.25	0.27	2638.12	2634.36	3.76
3.38	0.37	3.38	0.37	2636.60	2632.88	3.72
5.35	0.51	5.35	0.51	2636.68	2633.00	3.68
5.63	0.62	5.63	0.62	2638.02	2634.33	3.69
5.63	0.71	5.63	0.71	2639.63	2635.97	3.66
5.63	0.81	5.63	0.81	2643.01	2639.36	3.65
5.63	0.87	5.63	0.87	2647.12	2643.46	3.66
5.92	0.96	5.92	0.96	2651.04	2647.36	3.68
5.92	1.05	5.92	1.05	2655.92	2652.27	3.65
5.92	1.13	5.92	1.13	2661.08	2657.44	3.64
5.92	1.20	5.92	1.20	2666.57	2662.95	3.62
5.92	1.30	5.92	1.30	2672.89	2669.27	3.62
5.92	1.40	5.92	1.40	2678.59	2674.96	3.63
5.92	1.50	5.92	1.50	2684.04	2680.58	3.46
5.92	1.60	5.92	1.60	2689.21	2685.77	3.44
5.92	1.70	5.92	1.70	2694.62	2691.20	3.42
5.92	1.80	5.92	1.80	2700.35	2697.15	3.20
5.92	1.90	5.92	1.90	2697.51	2694.31	3.20
5.92	2.00	5.92	2.00	2694.08	2690.78	3.30

Flow Rate: 0.06 cm³/min (1 ft/day)

Table G.2.3. D-94-H-1 – High permeability – Tertiary water flooding

D-94-H-1						
By Fluid		Total		Pressure Inlet	Pressure Outlet	Pressure Dif
% Oil Recovered	PV (unit)	% Oil Recovered	PV (unit)	PSI	PSI	PSI
0.00	0.00	63.94	4.00	2810.55	2807.25	3.30
0.28	0.06	64.23	4.06	2822.00	2818.70	3.30
0.56	0.17	64.51	4.17	2833.60	2830.42	3.18
0.56	0.24	64.51	4.24	2839.41	2836.18	3.23
0.56	0.33	64.51	4.33	2838.07	2834.75	3.32
0.56	0.54	64.51	4.54	2828.52	2825.09	3.43
1.41	0.59	65.35	4.59	2829.49	2826.00	3.49
1.41	0.69	65.35	4.69	2836.86	2833.38	3.48
1.41	0.84	65.35	4.84	2833.31	2829.83	3.48
1.41	1.00	65.35	5.00	2830.36	2826.77	3.59

Flow Rate: 0.28 cm³/min (5 ft/day)

Table G.2.4. D-94-H-2 – High permeability – Secondary water flooding

D-94-H-2						
By Fluid		Total		Pressure Inlet	Pressure Outlet	Pressure Dif
% Oil Recovered	PV (unit)	% Oil Recovered	PV (unit)	PSI	PSI	PSI
0.00	0.00	0.00	0.00	2719.60	2716.70	2.9
1.42	0.10	1.42	0.10	2753.25	2750.85	2.4
3.69	0.21	3.69	0.21	2750.34	2747.54	2.8
4.55	0.27	4.55	0.27	2793.77	2790.97	2.8
6.25	0.37	6.25	0.37	2789.81	2787.31	2.5
7.10	0.51	7.10	0.51	2826.11	2823.48	2.63
12.50	0.62	12.50	0.62	2846.33	2843.83	2.5
21.88	0.71	21.88	0.71	2845.74	2842.94	2.8
28.98	0.81	28.98	0.81	2866.54	2863.71	2.83
44.60	0.87	44.60	0.87	2879.79	2876.89	2.9
46.88	0.96	46.88	0.96	2848.10	2845.01	3.09
49.43	1.13	49.43	1.13	2847.03	2843.98	3.05
50.00	1.20	50.00	1.20	2799.81	2796.73	3.08
52.84	1.30	52.84	1.30	2811.11	2807.99	3.12
53.69	1.40	53.69	1.40	2838.90	2835.77	3.13
55.40	1.50	55.40	1.50	2833.17	2829.86	3.31
55.68	1.60	55.68	1.60	2850.03	2846.88	3.15
55.97	1.70	55.97	1.70	2860.57	2857.38	3.19
55.97	1.80	55.97	1.80	2857.24	2854.10	3.14
55.97	1.90	55.97	1.90	2847.84	2844.55	3.29
55.97	2.00	55.97	2.00	2827.98	2824.71	3.27
55.97	2.00	55.97	2.00	2863.20	2859.85	3.35

Flow Rate: 0.28 cm³/min (5 ft/day)

Table G.2.5. D-94-H-2 – High permeability – Polymer flooding

D-94-H-2						
By Fluid		Total		Pressure Inlet	Pressure Outlet	Pressure Dif
% Oil Recovered	PV (unit)	% Oil Recovered	PV (unit)	PSI	PSI	PSI
0.00	0.00	55.97	2.00	2646.80	2643.48	3.32
0.28	0.10	56.25	2.10	2631.00	2627.68	3.32
1.42	0.21	57.39	2.21	2649.35	2646.05	3.30
1.70	0.27	57.67	2.27	2640.07	2636.78	3.29
1.70	0.37	57.67	2.37	2642.16	2638.89	3.27
1.70	0.51	57.67	2.51	2655.40	2652.23	3.17
1.70	0.62	57.67	2.62	2652.21	2649.00	3.21
1.70	0.71	57.67	2.71	2663.76	2660.58	3.18
1.70	0.81	57.67	2.81	2686.54	2683.31	3.23
1.99	0.87	57.95	2.87	2652.40	2648.97	3.43
3.41	0.96	59.38	2.96	2652.21	2649.01	3.20
3.41	1.05	59.38	3.05	2660.06	2656.84	3.22
3.69	1.20	59.66	3.20	2628.20	2625.02	3.18
3.69	1.30	59.66	3.30	2640.35	2637.15	3.20
3.69	1.40	59.66	3.40	2642.07	2638.89	3.18
3.69	1.50	59.66	3.50	2645.12	2642.25	2.87
3.69	1.60	59.66	3.60	2650.00	2647.10	2.90
3.69	1.70	59.66	3.70	2625.92	2623.03	2.89
3.69	1.80	59.66	3.80	2671.08	2668.18	2.90
3.69	1.90	59.66	3.90	2665.54	2662.62	2.92
3.69	2.00	59.66	4.00	2635.21	2633.14	2.07

Flow Rate: 0.06 cm³/min (1 ft/day)

Table G.2.6. D-94-H-2 – High permeability – Tertiary water flooding

D-94-H-2						
By Fluid		Total		Pressure Inlet	Pressure Outlet	Pressure Dif
% Oil Recovered	PV (unit)	% Oil Recovered	PV (unit)	PSI	PSI	PSI
0.00	0.00	59.66	4.00	2815.49	2813.19	2.30
0.00	0.06	59.66	4.06	2823.99	2821.59	2.40
0.00	0.17	59.66	4.17	2835.59	2833.24	2.35
0.00	0.24	59.66	4.24	2839.41	2836.94	2.47
0.00	0.33	59.66	4.33	2838.07	2835.47	2.60
0.00	0.54	59.66	4.54	2828.52	2825.81	2.71
0.00	0.59	59.66	4.59	2829.49	2826.69	2.80
0.57	0.69	60.23	4.69	2836.86	2834.19	2.67
1.14	0.84	60.80	4.84	2833.31	2830.72	2.59
1.42	0.90	61.08	4.90	2830.36	2827.71	2.65
1.42	1.00	61.08	5.00	2838.07	2835.39	2.68

Flow Rate: 0.28 cm³/min (5 ft/day)

Table G.2.7. M-04-H-1 – High permeability – Polymer flooding

M-04-H-1						
By Fluid		Total		Pressure Inlet	Pressure Outlet	Pressure Dif
% Oil Recovered	PV (unit)	% Oil Recovered	PV (unit)	PSI	PSI	PSI
0.00	0.00	0.00	0.00	2559.97	2556.61	3.36
0.00	0.10	0.00	0.10	2572.75	2569.41	3.34
0.00	0.21	0.00	0.21	2585.53	2582.39	3.14
0.59	0.27	0.59	0.27	2598.60	2595.21	3.39
3.24	0.37	3.24	0.37	2611.85	2608.44	3.41
8.26	0.51	8.26	0.51	2625.98	2622.51	3.47
23.01	0.62	23.01	0.62	2639.42	2635.78	3.64
33.04	0.71	33.04	0.71	2652.96	2649.16	3.80
45.13	0.81	45.13	0.81	2666.49	2663.07	3.42
49.85	0.87	49.85	0.87	2676.27	2672.85	3.42
52.21	0.96	52.21	0.96	2685.26	2681.94	3.32
55.16	1.13	55.16	1.13	2694.01	2690.62	3.38
57.23	1.20	57.23	1.20	2702.82	2699.50	3.32
60.18	1.30	60.18	1.30	2712.10	2708.79	3.31
60.18	1.40	60.18	1.40	2721.14	2718.13	3.01
60.18	1.50	60.18	1.50	2730.97	2727.99	2.98
60.18	1.60	60.18	1.60	2740.04	2737.04	2.99
60.18	1.70	60.18	1.70	2748.73	2745.81	2.92
60.18	1.80	60.18	1.80	2756.63	2753.63	3.00
60.18	1.90	60.18	1.90	2762.90	2759.90	3.00
60.18	2.00	60.18	2.00	2767.59	2764.58	3.01

Flow Rate: 0.06 cm³/min (1 ft/day)

Table G.2.8. M-04-H-1 – High permeability – Tertiary water flooding

M-04-H-1						
By Fluid		Total		Pressure Inlet	Pressure Outlet	Pressure Dif
% Oil Recovered	PV (unit)	% Oil Recovered	PV (unit)	PSI	PSI	PSI
0.00	0.00	0.00	0.00	2670.69	2667.37	3.32
0.00	0.10	0.00	0.10	2684.77	2681.27	3.50
1.22	0.21	1.22	0.21	2699.67	2696.23	3.44
1.22	0.27	1.22	0.27	2715.99	2712.65	3.34
1.22	0.37	1.22	0.37	2732.83	2729.45	3.38
1.22	0.51	1.22	0.51	2749.17	2745.78	3.39
1.22	0.62	1.22	0.62	2759.20	2755.80	3.40
1.22	0.71	1.22	0.71	2750.09	2746.69	3.40
2.13	0.81	2.13	0.81	2750.91	2747.50	3.41
2.13	0.87	2.13	0.87	2750.29	2746.86	3.44
2.13	0.96	2.13	0.96	2751.33	2747.90	3.43
2.13	1.05	2.13	1.05	2753.62	2750.19	3.44
2.13	1.13	2.13	1.13	2754.23	2750.81	3.42
2.13	1.20	2.13	1.20	2749.59	2746.14	3.45
2.13	1.30	2.13	1.30	2749.10	2745.53	3.57
2.13	1.40	2.13	1.40	2752.27	2748.74	3.53
2.13	1.50	2.13	1.50	2752.64	2749.11	3.53
2.13	1.60	2.13	1.60	2748.99	2745.45	3.54
2.13	1.70	2.13	1.70	2754.01	2750.48	3.53
2.13	1.80	2.13	1.80	2761.07	2757.52	3.55
2.13	1.90	2.13	1.90	2768.27	2764.70	3.56
2.13	2.00	2.13	2.00	2767.29	2763.75	3.54

Flow Rate: 0.28 cm³/min (5 ft/day)

Table G.2.9. M-04-H-2 – High permeability – Polymer flooding

M-04-H-2						
By Fluid		Total		Pressure Inlet	Pressure Outlet	Pressure Dif
% Oil Recovered	PV (unit)	% Oil Recovered	PV (unit)	PSI	PSI	PSI
0.00	0.00	0.00	0.00	2745.37	2742.48	2.89
1.22	0.10	1.22	0.10	2730.90	2727.87	3.03
6.69	0.21	6.69	0.21	2715.75	2712.50	3.26
27.36	0.27	27.36	0.27	2706.02	2702.61	3.41
50.46	0.37	50.46	0.37	2698.36	2694.97	3.39
52.58	0.51	52.58	0.51	2692.71	2690.16	2.55
54.71	0.62	54.71	0.62	2689.46	2686.38	3.08
57.75	0.71	57.75	0.71	2688.44	2685.29	3.15
57.75	0.81	57.75	0.81	2688.32	2685.13	3.19
57.75	0.87	57.75	0.87	2691.64	2688.61	3.03
58.05	0.96	58.05	0.96	2694.97	2691.55	3.42
58.97	1.13	58.97	1.13	2699.74	2696.61	3.13
60.18	1.20	60.18	1.20	2705.67	2702.53	3.15
63.72	1.30	63.72	1.30	2710.47	2707.52	2.95
65.78	1.40	65.78	1.40	2715.70	2712.75	2.95
65.78	1.50	65.78	1.50	2721.78	2718.29	3.49
65.78	1.60	65.78	1.60	2727.82	2724.68	3.14
65.78	1.70	65.78	1.70	2733.89	2730.76	3.13
65.78	1.80	65.78	1.80	2740.37	2737.46	2.91
65.78	1.90	65.78	1.90	2748.85	2745.91	2.94
65.78	2.00	65.78	2.00	2757.32	2754.75	2.57
65.78	2.00	65.78	2.00	2765.86	2763.12	2.74

Flow Rate: 0.06 cm³/min (1 ft/day)

Table G.2.10. M-04-H-2 – High permeability – Tertiary water flooding

M-04-H-2						
By Fluid		Total		Pressure Inlet	Pressure Outlet	Pressure Dif
% Oil Recovered	PV (unit)	% Oil Recovered	PV (unit)	PSI	PSI	PSI
0.00	0.00	65.78	2.00	2679.92	2676.80	3.13
0.00	0.10	65.78	2.10	2675.69	2672.54	3.15
0.00	0.21	65.78	2.21	2672.29	2669.17	3.12
0.00	0.27	65.78	2.27	2671.72	2668.61	3.11
0.00	0.37	65.78	2.37	2672.83	2669.72	3.12
0.59	0.51	66.37	2.51	2676.31	2673.16	3.15
0.59	0.62	66.37	2.62	2682.12	2678.84	3.28
0.59	0.71	66.37	2.71	2689.26	2685.99	3.27
0.59	0.81	66.37	2.81	2694.56	2691.25	3.31
0.59	0.87	66.37	2.87	2699.15	2695.88	3.26
0.59	0.96	66.37	2.96	2704.78	2701.50	3.28
0.59	1.05	66.37	3.05	2711.27	2708.00	3.27
0.59	1.13	66.37	3.13	2718.42	2715.15	3.27
0.59	1.20	66.37	3.20	2726.17	2722.88	3.29
0.88	1.30	66.67	3.30	2735.29	2732.01	3.28
0.88	1.40	66.67	3.40	2744.40	2741.12	3.28
0.88	1.50	66.67	3.50	2754.46	2751.17	3.29
0.88	1.60	66.67	3.60	2764.72	2761.43	3.29
1.18	1.70	66.96	3.70	2775.01	2771.71	3.30
1.18	1.80	66.96	3.80	2785.01	2781.68	3.33
1.18	1.90	66.96	3.90	2794.93	2791.61	3.32
1.18	2.00	66.96	4.00	2805.62	2802.30	3.32

Flow Rate: 0.28 cm³/min (5 ft/day)

Table G.2.11. D-94-L-1 – Low permeability – Secondary water flooding

D-94-L-1						
By Fluid		Total		Pressure Inlet	Pressure Outlet	Pressure Dif
% Oil Recovered	PV (unit)	% Oil Recovered	PV (unit)	PSI	PSI	PSI
0.00	0.00	0.00	0.00	2561.73	2517.53	44.20
0.00	0.10	0.00	0.10	2596.49	2558.41	38.09
0.00	0.21	0.00	0.21	2635.77	2584.00	51.78
0.00	0.27	0.00	0.27	2672.15	2628.36	43.79
2.42	0.37	2.42	0.37	2709.09	2664.25	44.85
2.42	0.51	2.42	0.51	2746.08	2703.67	42.41
7.25	0.62	7.25	0.62	2783.27	2739.72	43.55
19.32	0.71	19.32	0.71	2823.02	2777.10	45.92
19.32	0.81	19.32	0.81	2860.07	2830.78	29.29
19.32	0.87	19.32	0.87	2896.56	2866.50	30.06
19.32	0.96	19.32	0.96	2897.90	2866.50	31.41
20.29	1.13	20.29	1.13	2904.49	2875.47	29.02
20.29	1.20	20.29	1.20	2910.09	2878.00	32.10
21.74	1.30	21.74	1.30	2913.52	2884.61	28.91
21.74	1.40	21.74	1.40	2902.84	2873.63	29.21
21.74	1.50	21.74	1.50	2915.34	2886.09	29.25
24.15	1.60	24.15	1.60	2911.99	2882.58	29.41
29.95	1.70	29.95	1.70	2917.53	2888.06	29.47
41.55	1.80	41.55	1.80	2905.42	2870.19	35.24
43.96	1.90	43.96	1.90	2910.78	2881.94	28.84
44.44	2.00	44.44	2.00	2910.20	2881.59	28.61
44.44	2.00	44.44	2.00	2914.54	2885.99	28.55

Flow Rate: 0.28 cm³/min (5 ft/day)

Table G.2.12. D-94-L-1 – Low permeability – Polymer flooding

D-94-L-1						
By Fluid		Total		Pressure Inlet	Pressure Outlet	Pressure Dif
% Oil Recovered	PV (unit)	% Oil Recovered	PV (unit)	PSI	PSI	PSI
0.00	0.00	44.44	2.00	2782.58	2777.79	4.79
0.00	0.10	44.44	2.10	2779.19	2774.41	4.78
0.00	0.21	44.44	2.21	2778.23	2772.42	5.80
0.00	0.27	44.44	2.27	2779.26	2776.06	3.20
0.00	0.37	44.44	2.37	2781.67	2777.17	4.49
0.00	0.51	44.44	2.51	2785.41	2780.25	5.16
0.00	0.62	44.44	2.62	2790.03	2776.39	13.64
0.97	0.71	45.41	2.71	2795.33	2791.87	3.46
0.97	0.81	45.41	2.81	2801.65	2794.48	7.17
0.97	0.87	45.41	2.87	2807.83	2799.79	8.04
0.97	0.96	45.41	2.96	2813.80	2805.73	8.07
0.97	1.05	45.41	3.05	2819.51	2811.07	8.44
0.97	1.13	45.41	3.13	2825.47	2812.51	12.97
0.97	1.20	45.41	3.20	2831.84	2813.78	18.07
1.45	1.30	45.89	3.30	2837.91	2819.69	18.22
2.42	1.40	46.86	3.40	2844.22	2827.52	16.70
2.42	1.50	46.86	3.50	2850.44	2840.34	10.10
2.42	1.60	46.86	3.60	2857.03	2835.11	21.92
2.90	1.70	47.34	3.70	2864.50	2842.64	21.86
2.90	1.80	47.34	3.80	2871.50	2840.23	31.27
2.90	1.90	47.34	3.90	2878.20	2817.12	61.08
2.90	2.00	47.34	4.00	2884.32	2834.32	50.00

Flow Rate: 0.06 cm³/min (1 ft/day)

Table G.2.13. D-94-L-1 – Low permeability – Tertiary water flooding

D-94-L-1						
By Fluid		Total		Pressure Inlet	Pressure Outlet	Pressure Dif
% Oil Recovered	PV (unit)	% Oil Recovered	PV (unit)	PSI	PSI	PSI
0.00	0.00	47.34	4.00	2772.27	2768.87	3.40
0.00	0.06	47.34	4.06	2783.62	2780.32	3.30
0.00	0.17	47.34	4.17	2794.39	2790.99	3.40
0.00	0.24	47.34	4.24	2806.88	2802.88	4.00
0.00	0.33	47.34	4.33	2822.10	2818.60	3.50
0.00	0.54	47.34	4.54	2835.96	2831.26	4.70
0.00	0.59	47.34	4.59	2850.69	2846.49	4.20
0.00	0.69	47.34	4.69	2864.48	2860.68	3.80
0.00	0.84	47.34	4.84	2874.48	2871.08	3.40
0.00	0.90	47.34	4.90	2880.88	2877.38	3.50
0.00	1.00	47.34	5.00	2884.55	2881.45	3.10

Flow Rate: 0.28 cm³/min (5 ft/day)

Table G.2.14. D-94-L-2 – Low permeability – Secondary water flooding

D-94-L-2						
By Fluid		Total		Pressure Inlet	Pressure Outlet	Pressure Dif
% Oil Recovered	PV (unit)	% Oil Recovered	PV (unit)	PSI	PSI	PSI
0.00	0.00	0.00	0.00	2899.89	2896.33	3.56
0.00	0.10	0.00	0.10	2901.96	2888.44	13.52
1.76	0.21	1.76	0.21	2894.78	2891.20	3.58
13.53	0.27	13.53	0.27	2875.13	2859.87	15.25
18.82	0.37	18.82	0.37	2894.33	2887.93	6.40
27.65	0.51	27.65	0.51	2892.53	2876.23	16.30
44.12	0.62	44.12	0.62	2891.80	2876.61	15.20
45.88	0.71	45.88	0.71	2887.78	2877.78	10.00
45.88	0.81	45.88	0.81	2893.67	2885.11	8.56
47.06	0.87	47.06	0.87	2895.75	2891.43	4.32
48.82	0.96	48.82	0.96	2891.53	2887.41	4.12
48.82	1.13	48.82	1.13	2883.23	2878.75	4.48
48.82	1.20	48.82	1.20	2884.39	2869.39	15.00
48.82	1.30	48.82	1.30	2892.25	2887.95	4.30
48.82	1.40	48.82	1.40	2875.25	2871.15	4.10
48.82	1.50	48.82	1.50	2889.69	2884.89	4.80
48.82	1.60	48.82	1.60	2888.31	2883.31	5.00
48.82	1.70	48.82	1.70	2890.95	2877.05	13.90
48.82	1.80	48.82	1.80	2902.37	2888.17	14.20
48.82	1.90	48.82	1.90	2881.66	2877.16	4.50
48.82	2.00	48.82	2.00	2872.32	2857.62	14.70
48.82	2.00	48.82	2.00	2886.26	2881.36	4.90

Flow Rate: 0.28 cm³/min (5 ft/day)

Table G.2.15. D-94-L-2 – Low permeability – Polymer flooding

D-94-L-2						
By Fluid		Total		Pressure Inlet	Pressure Outlet	Pressure Dif
% Oil Recovered	PV (unit)	% Oil Recovered	PV (unit)	PSI	PSI	PSI
0.00	0.00	48.82	2.00	2862.64	2857.44	5.20
0.59	0.10	49.41	2.10	2857.77	2842.37	15.40
1.18	0.21	50.00	2.21	2858.00	2852.60	5.40
1.18	0.27	50.00	2.27	2862.63	2853.83	8.80
1.18	0.37	50.00	2.37	2864.81	2854.21	10.60
1.18	0.51	50.00	2.51	2863.94	2850.24	13.70
1.18	0.62	50.00	2.62	2864.09	2856.19	7.90
2.35	0.71	51.18	2.71	2864.37	2860.99	3.39
2.94	0.81	51.76	2.81	2866.29	2848.43	17.85
2.94	0.87	51.76	2.87	2867.79	2848.59	19.19
2.94	0.96	51.76	2.96	2868.69	2855.79	12.90
2.94	1.05	51.76	3.05	2869.67	2865.04	4.63
2.94	1.13	51.76	3.13	2870.38	2858.98	11.40
3.53	1.20	52.35	3.20	2871.72	2855.41	16.31
3.53	1.30	52.35	3.30	2873.78	2859.78	14.00
3.53	1.40	52.35	3.40	2875.40	2863.40	12.00
3.53	1.50	52.35	3.50	2877.97	2860.97	17.00
3.53	1.60	52.35	3.60	2881.67	2873.67	8.00
3.53	1.70	52.35	3.70	2878.97	2871.97	7.00
3.53	1.80	52.35	3.80	2874.57	2869.57	5.00
3.53	1.90	52.35	3.90	2866.73	2862.73	4.00
3.53	2.00	52.35	4.00	2872.59	2868.70	3.89

Flow Rate: 0.06 cm³/min (1 ft/day)

Table G.2.16. D-94-L-2 – Low permeability – Tertiary water flooding

D-94-L-2						
By Fluid		Total		Pressure Inlet	Pressure Outlet	Pressure Dif
% Oil Recovered	PV (unit)	% Oil Recovered	PV (unit)	PSI	PSI	PSI
0.00	0.00	52.35	4.00	2872.46	2869.06	3.40
0.00	0.06	52.35	4.06	2869.69	2866.39	3.30
0.00	0.17	52.35	4.17	2868.09	2864.69	3.40
0.00	0.24	52.35	4.24	2867.57	2863.57	4.00
0.00	0.33	52.35	4.33	2864.86	2861.36	3.50
0.00	0.54	52.35	4.54	2864.67	2859.97	4.70
0.00	0.59	52.35	4.59	2867.68	2863.48	4.20
0.00	0.69	52.35	4.69	2863.01	2859.21	3.80
0.00	0.84	52.35	4.84	2868.55	2865.15	3.40
0.00	0.90	52.35	4.90	2872.46	2868.96	3.50
0.00	1.00	52.35	5.00	2872.61	2869.51	3.10

Flow Rate: 0.28 cm³/min (5 ft/day)

Table G.2.17. M-04-L-1 – Low permeability – Polymer flooding

M-04-L-1						
By Fluid		Total		Pressure Inlet	Pressure Outlet	Pressure Dif
% Oil Recovered	PV (unit)	% Oil Recovered	PV (unit)	PSI	PSI	PSI
0.00	0.00	0.00	0.00	2648.34	2646.41	1.93
0.00	0.10	0.00	0.10	2656.25	2654.48	1.77
1.37	0.21	1.37	0.21	2663.72	2661.98	1.73
5.94	0.27	5.94	0.27	2671.78	2670.44	1.34
7.31	0.37	7.31	0.37	2679.98	2678.73	1.25
13.24	0.51	18.24	0.51	2688.44	2687.38	1.06
31.51	0.62	31.51	0.62	2697.78	2696.76	1.01
34.25	0.71	39.25	0.71	2706.33	2706.29	0.05
38.81	0.81	45.98	0.78	2714.79	2713.70	1.09
52.51	0.87	49.51	0.82	2723.73	2722.74	0.99
52.51	0.96	50.51	0.96	2732.75	2728.16	4.58
52.51	1.13	52.51	1.13	2741.76	2739.26	2.49
52.51	1.20	52.51	1.20	2750.63	2749.72	0.90
52.51	1.30	52.51	1.30	2759.72	2756.91	2.81
52.51	1.40	52.51	1.40	2768.87	2766.72	2.15
53.42	1.50	53.42	1.50	2778.02	2772.53	5.49
53.88	1.60	53.88	1.60	2788.24	2782.86	5.37
53.88	1.70	53.88	1.70	2797.68	2793.11	4.57
53.88	1.80	53.88	1.80	2807.07	2796.23	10.84
53.88	1.90	53.88	1.90	2816.34	2804.09	12.25
53.88	2.00	53.88	2.00	2826.25	2815.90	10.35

Flow Rate: 0.06 cm³/min (1 ft/day)

Table G.2.18. M-04-L-1 – Low permeability – Tertiary water flooding

M-04-L-1						
By Fluid		Total		Pressure Inlet	Pressure Outlet	Pressure Dif
% Oil Recovered	PV (unit)	% Oil Recovered	PV (unit)	PSI	PSI	PSI
0.00	0.00	0.00	0.00	2888.74	2879.52	9.22
0.00	0.10	0.00	0.10	2894.26	2884.44	9.81
0.00	0.21	0.00	0.21	2899.23	2889.69	9.55
0.00	0.27	0.00	0.27	2901.92	2893.93	7.99
0.00	0.37	0.00	0.37	2899.26	2891.12	8.14
0.00	0.51	0.00	0.51	2899.18	2891.06	8.12
0.00	0.62	0.00	0.62	2897.11	2890.46	6.65
0.46	0.71	0.46	0.71	2894.85	2884.70	10.15
0.46	0.81	0.46	0.81	2893.32	2885.07	8.25
0.46	0.87	0.46	0.87	2895.55	2887.26	8.29
0.46	0.96	0.46	0.96	2890.45	2882.31	8.14
0.46	1.05	0.46	1.05	2885.21	2877.23	7.98
0.46	1.13	0.46	1.13	2883.97	2875.92	8.05
0.46	1.20	0.46	1.20	2884.22	2876.50	7.72
0.46	1.30	0.46	1.30	2885.31	2876.83	8.48
0.46	1.40	0.46	1.40	2888.01	2879.74	8.28
0.46	1.50	0.46	1.50	2890.90	2882.41	8.49
0.46	1.60	0.46	1.60	2893.34	2884.57	8.77
0.46	1.70	0.46	1.70	2895.41	2888.04	7.37
0.46	1.80	0.46	1.80	2893.95	2886.95	7.00
0.46	1.90	0.46	1.90	2894.72	2887.92	6.80
0.46	2.00	0.46	2.00	2895.17	2888.07	7.10

Flow Rate: 0.28 cm³/min (5 ft/day)

Table G.2.19. M-04-L-2 – Low permeability – Polymer flooding

M-04-L-2						
By Fluid		Total		Pressure Inlet	Pressure Outlet	Pressure Dif
% Oil Recovered	PV (unit)	% Oil Recovered	PV (unit)	PSI	PSI	PSI
0.0	0.0	0.0	0.0	2616.5	2611.9	4.60
0.0	0.1	0.0	0.1	2627.3	2626.7	0.62
0.0	0.2	0.0	0.2	2637.7	2637.6	0.15
0.0	0.3	0.0	0.3	2648.2	2646.5	1.76
0.0	0.4	0.0	0.4	2658.8	2658.1	0.73
3.7	0.5	3.7	0.5	2669.5	2669.0	0.48
5.3	0.6	5.3	0.6	2680.8	2678.2	2.62
22.1	0.7	22.1	0.7	2691.5	2691.1	0.40
35.3	0.8	35.3	0.8	2702.3	2701.0	1.37
42.6	0.9	42.6	1.0	2713.2	2711.7	1.50
44.2	1.0	44.2	1.1	2724.1	2722.5	1.64
44.7	1.1	44.7	1.1	2735.9	2734.3	1.62
44.7	1.2	44.7	1.2	2746.9	2737.9	9.03
44.7	1.3	44.7	1.3	2757.8	2755.5	2.34
44.7	1.4	44.7	1.4	2768.8	2768.2	0.66
44.7	1.5	44.7	1.5	2779.8	2775.6	4.21
47.9	1.6	47.9	1.6	2791.4	2788.5	2.84
47.9	1.7	47.9	1.7	2802.3	2796.4	5.92
47.9	1.8	47.9	1.8	2813.2	2807.3	5.92
47.9	1.9	47.9	1.9	2824.0	2818.1	5.93
47.9	2.0	47.9	2.0	2835.0	2824.6	10.31

Flow Rate: 0.06 cm³/min (1 ft/day)

Table G.2.20. M-04-L-2 – Low permeability – Tertiary water flooding

M-04-L-2						
By Fluid		Total		Pressure Inlet	Pressure Outlet	Pressure Dif
% Oil Recovered	PV (unit)	% Oil Recovered	PV (unit)	PSI	PSI	PSI
0.00	0.0	0.0	0.0	2965.7	2956.2	9.49
0.00	0.1	0.0	0.1	2968.0	2957.4	10.64
0.00	0.2	0.0	0.2	2970.3	2958.1	12.18
0.00	0.3	0.0	0.3	2971.4	2958.2	13.24
0.00	0.4	0.0	0.4	2972.8	2959.3	13.56
0.00	0.5	0.0	0.5	2972.0	2958.8	13.21
0.00	0.6	0.0	0.6	2971.6	2960.9	10.64
0.00	0.7	0.0	0.7	2971.3	2969.9	1.33
0.53	0.8	0.5	0.8	2971.0	2968.2	2.84
1.58	0.9	1.6	0.9	2966.4	2959.0	7.46
1.58	1.0	1.6	1.0	2965.5	2957.6	7.85
1.58	1.1	1.6	1.1	2963.4	2952.5	10.87
1.58	1.1	1.6	1.1	2962.4	2953.2	9.19
1.58	1.2	1.6	1.2	2965.8	2961.7	4.14
1.58	1.3	1.6	1.3	2973.3	2966.9	6.48
1.58	1.4	1.6	1.4	2979.7	2972.9	6.78
1.58	1.5	1.6	1.5	2977.2	2969.8	7.46
1.58	1.6	1.6	1.6	2966.0	2959.6	6.32
1.58	1.7	1.6	1.7	2949.5	2939.1	10.38
1.58	1.8	1.6	1.8	2949.8	2940.0	9.80
1.58	1.9	1.6	1.9	2969.8	2959.0	10.79
1.58	2.0	1.6	2.0	2964.2	2954.4	9.80

Flow Rate: 0.28 cm³/min (5 ft/day)

APPENDIX H: Core flooding Material Balance Calculation

In this research was considered the core flooding material balance calculation methodology described in detail at Moayedi (2015), and adapted to the specific experimental conditions considered in Hebron Field experimental polymer flooding experimental sequence.

Considering Appendix B.1 results, D-94-A-1 composite core will be used as example in this section; based on this:

- Composite pore volume = $44.6 \pm 0.1 \text{ cm}^3$
- Outlet dead volume = $4.4 \pm 0.1 \text{ cm}^3$, this outlet dead volume is calculated considering the dead volume related to the experimental setup parts such as: tee, tubings, valves, spacers, BPR. This value is constant for the entire core flooding experiments performed using the setup assembled.

$$\mathbf{PV} = \text{Actual PV} + \text{Outlet Dead Volume} = (44.6 \pm 0.1) + (4.4 \pm 0.1) = 49 \pm 0.1 \text{ cm}^3 \quad \text{Eq. H.1}$$

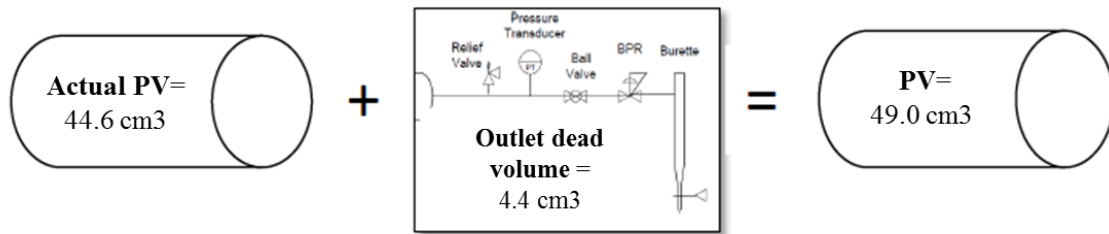


Figure H.1. Pore volume at Hebron field core flooding experiment #1(modified after Moayedi, 2015)

H.1. Experiment #1 core flooding sequence

H.1.1. Primary waterflooding (formation water)

H.1.2. Oil flooding

H.1.3. Secondary waterflooding (2 PV of injection water (seawater))

H.1.4. Polymer flooding (2 PV)

H.1.5. Tertiary waterflooding (1 PV)

H.1.1. Primary waterflooding (formation water)

Total volume of synthetic formation water inside the core = PV = $49 \pm 0.1 \text{ cm}^3$

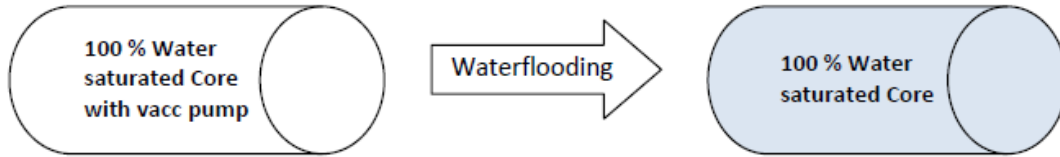


Figure H.2. Primary waterflooding (after Moayedi, 2015)

H.1.2. Oil flooding until no more water production

There were several times of burette drainage during oil flooding in experiment #1, and it can be summarized in the figure below:

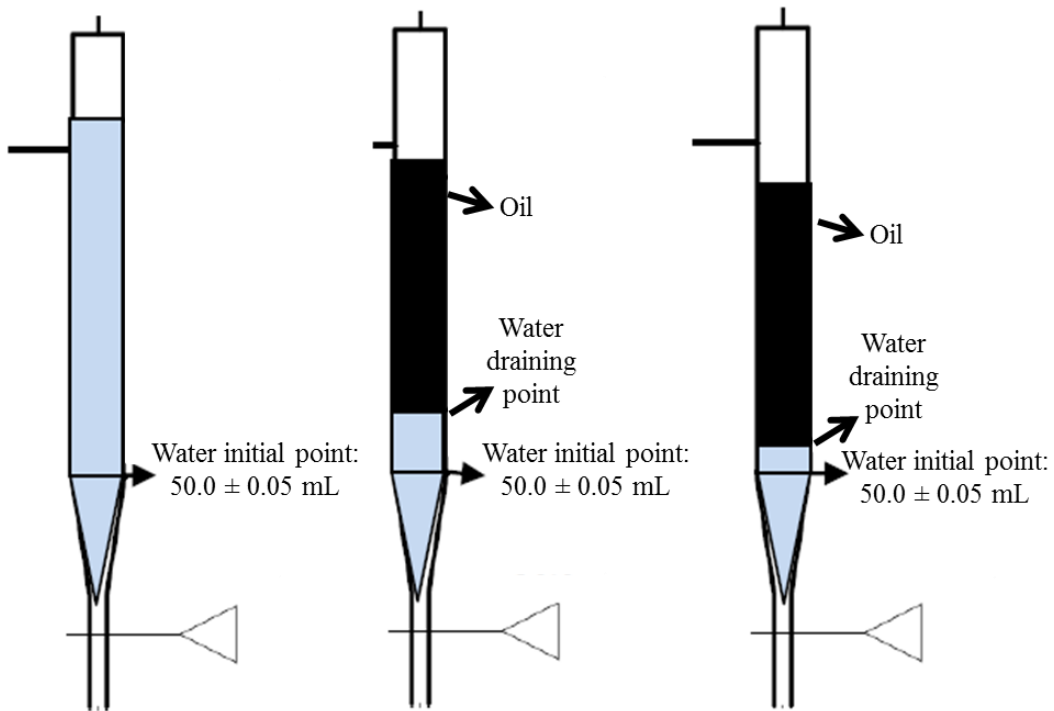


Figure H.3. Burette reading during oil flooding in experiment #1 (after Moayedi, 2015)

a) Produced water during oil flooding = $\sum(\text{water level at initial point} - \text{water level at draining point}) = 35.5 \pm 0.2 \text{ cm}^3$

b) Original oil in place, OOIP = Produced water during this step = $35.5 \pm 0.2 \text{ cm}^3$

c) Connate water saturation $S_{wc} = \frac{PV - OOIP}{PV} = \frac{49 - 35.5}{49} = 0.28 \pm 0.004 \text{ cm}^3$ Eq. H.2

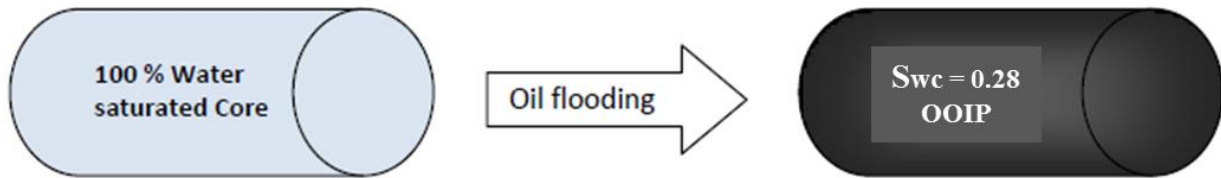


Figure H.4. Primary waterflooding (modified after Moayed, 2015)

H.1.3. Secondary waterflooding (2 PV of injection water (seawater))

a) Produced oil during secondary waterflooding, $O_1 = \sum(\text{water level at draining point} - \text{oil level at draining point}) = 20.6 \pm 0.09 \text{ cm}^3$ Eq. H.3

b) Residual oil in place, $ROIP = 35.5 \pm 0.2 \text{ cm}^3 - 20.6 \pm 0.09 \text{ cm}^3 = 14.9 \pm 0.2 \text{ cm}^3$ Eq. H.4

c) Residual oil saturation, $S_{or} = \frac{OOIP - O_1}{PV} = 0.30 \pm 0.004 \text{ cm}^3$ Eq. H.5

d) Secondary waterflood recovery = $\frac{O_1}{OOIP} \times 100 = 58.0 \pm 0.4 \%$ Eq. H.6

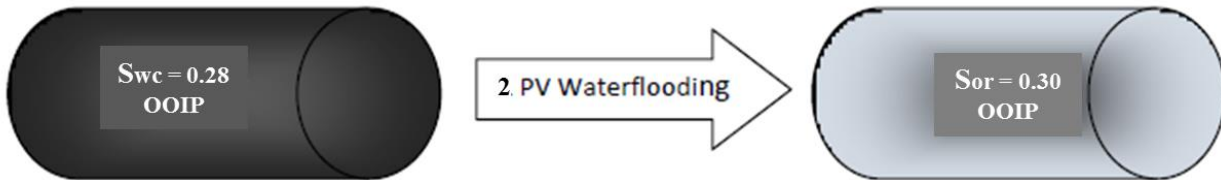


Figure H.5. Secondary waterflooding (modified after Moayed, 2015)

H.1.4. Polymer flooding (2 PV)

a) Total produced oil during polymer flooding (2 PV), $O_2 = \sum(\text{water level at draining point} - \text{oil level at initial point}) = 2.1 \pm 0.1 \text{ cm}^3$ Eq. H.7

b) Residual oil in place, $ROIP = 14.9 \pm 0.2 \text{ cm}^3 - 2.1 \pm 0.1 \text{ cm}^3 = 12.8 \pm 0.2 \text{ cm}^3$ Eq. H.8

c) Residual oil saturation, $S_{or} = \frac{OOIP - O_1}{PV} = 0.26 \pm 0.005 \text{ cm}^3$ Eq. H.9

d) Polymer flooding oil recovery = $\frac{O_1}{OOIP} \times 100 = 5.9 \pm 0.6 \%$ Eq. H.10

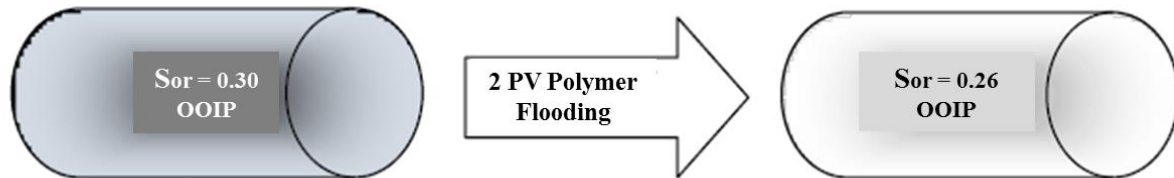


Figure H.6. Polymer flooding (modified after Moayedi, 2015)

H.1.5. Tertiary waterflooding (1 PV)

a) Total produced oil during tertiary waterflooding (1 PV), $O_3 = \sum(\text{water level at draining point} - \text{oil level at initial point}) = 0.5 \pm 0.1 \text{ cm}^3$ Eq. H.11

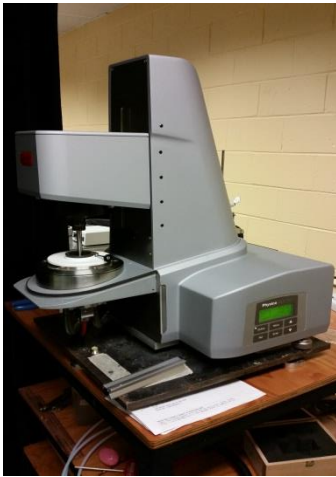
b) Total produced oil, $O_4 = \text{produced oil secondary waterflooding, } O_1 + \text{produced oil during polymer flooding (2 PV), } O_2 + \text{produced oil during tertiary waterflooding (1 PV), } O_3 = 23.2 \pm 0.1 \text{ cm}^3$ Eq. H.12

c) Total oil recovery = $\frac{O_4}{OOIP} \times 100 = 65.4 \pm 0.6 \%$ Eq. H.13



Figure H.7. Total oil recovery (modified after Moayedi, 2015)

APPENDIX H: Experimental set-up images



A) Anton-Paar Modular Compact Rheometer 300



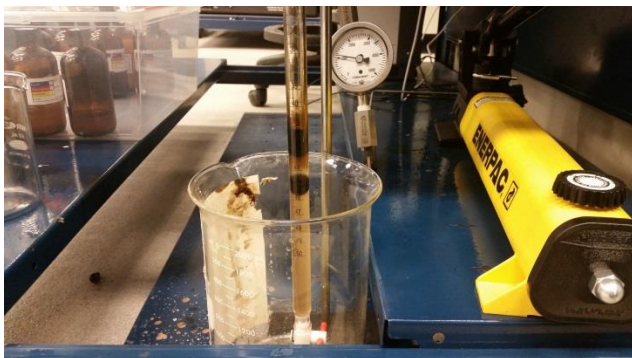
B) Polymer solution test preparation



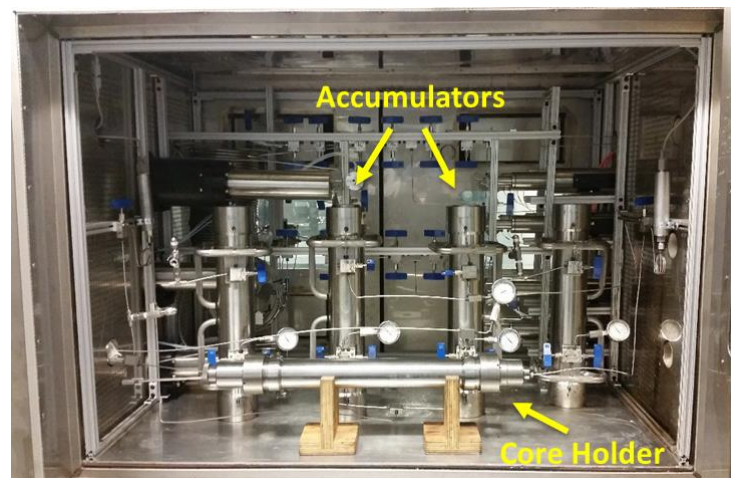
C) Polymer solution dilution



D) Polymer solutions in amber bottles



E) Oil displaced



F) Core flooding set-up